GEOLOGICA ULTRAIECTINA

Mededelingen van de
Faculteit Aardwetenschappen der
Rijksuniversiteit te Utrecht

No. 80

PROPERTIES OF PLIOCENE SEDIMENTARY GEOMAGNETIC REVERSAL RECORDS FROM THE MEDITERRANEAN

J.H. LINSSEN

GEOLOGICA ULTRAIECTINA

Mededelingen van de
Faculteit Aardwetenschappen der
Rijksuniversiteit te Utrecht

No. 80

PROPERTIES OF PLIOCENE SEDIMENTARY GEOMAGNETIC REVERSAL RECORDS FROM THE MEDITERRANEAN

X. XII. 26

CIP-GEGEVENS KONINKLIJKE BIBLIOTHEEK DEN HAAG

Linssen, Joannes Hubertus

Properties of Pliocene sedimentary geomagnetic
reversal records from the Mediterranean /
Joannes Hubertus Linssen
[Utrecht : Faculteit Aardwetenschappen der Rijksuniversiteit Utrecht]
(Geologica Ultraiectina, ISSN 0072-1026 : no. 80)
Proefschrift Utrecht. - Met lit. opg. - Met samenvatting in het Nederlands.
ISBN 90-71577-33-3
Trefw.: paleomagnetisme : sedimentologie : aardmagnetisme /
Middellandse Zee-gebied : onderzoek.

PROPERTIES OF PLIOCENE SEDIMENTARY GEOMAGNETIC REVERSAL RECORDS FROM THE MEDITERRANEAN

Eigenschappen van Pliocene sedimentaire registraties van geomagnetische polariteitsomkeringen

(met een samenvatting in het Nederlands)

PROEFSCHRIFT

TER VERKRIJGING VAN DE GRAAD VAN DOCTOR AAN
DE RIJKSUNIVERSITEIT TE UTRECHT, OP GEZAG VAN
DE RECTOR MAGNIFICUS, PROF.DR. J.A. VAN GINKEL,
INGEVOLGE HET BESLUIT VAN HET COLLEGE VAN DEKANEN
IN HET OPENBAAR TE VERDEDIGEN OP 6 MEI 1991
DES NAMIDDAGS TE 12.45 UUR

DOOR

JOANNES HUBERTUS LINSSEN

GEBOREN OP 7 OKTOBER 1959 TE 'S-GRAVENHAGE

1991

PROMOTOR : PROF. DR. J.D.A. ZIJDERVELD
CO-PROMOTOR : DR. C.G. LANGEREIS

aan Emilie

Contents

Samenvatting		1
Summary		5
I	Introduction	9
II	Preliminary results of a study of four successive sedimentary geomagnetic reversal records from the Mediterranean. (upper Thvera, lower and upper Sidufjall, lower Nunivak)	13
III	A succession of five early Pliocene geomagnetic reversal records from the Mediterranean.	49
IV	Rock magnetism of the magnetite and pyrrhotite bearing sediments from the Trubi formation (Italy)	89
V	The Mammoth and lower Kaena geomagnetic sedimentary reversal records of the Punta Piccola section	131
VI	Two lower Pliocene sedimentary geomagnetic reversal records from Corfu	163
VII	Conclusions	185
References		189
Appendices		203

Samenvatting

Het dipolaire aardmagneetveld is in de geschiedenis van de aarde veelvuldig van polariteit omgekeerd. Alhoewel deze eigenschap van het aardmagneetveld reeds aan het begin van deze eeuw ontdekt werd (Brunhes, 1906), is heden ten dage nog nauwelijks bekend hoe dit proces zich voltrekt en wat de oorzaak van de polariteitsomkeringen is. Het aardmagneetveld en dus ook veranderingen van het aardmagneetveld worden geregistreerd in de natuurlijke remanente magnetisatie (NRM) van gesteentes ten tijde van hun ontstaan. De bestudering van registraties van polariteitsomkeringen aan de hand van de NRM van sedimentaire gesteentes is het onderwerp van deze dissertatie.

Acht polariteitsomkeringen uit de Gilbert en Gauss chrons zijn bestudeerd aan de hand van vroeg en midden Pliocene mariene sedimentaire afzettingen uit het Middellandse Zee-gebied. De mariene mergels van de Trubi en Monte Narbone formaties uit Italie (Calabrië en Sicilië), waarin zich de registraties van alle acht onderzochte polariteits-omkeringen bevinden, bestaan uit een cyclische afwisseling van lithologische eenheden (0.1-1.0 m) met verschillende carbonaatgehaltes. De accumulatiesnelheid van de Italiaanse sedimenten is 5-9 cm per 1000 jaar. De vroeg Pliocene sedimenten op Corfu, waarin registraties van twee polariteitsomkeringen uit de Gilbert chron zijn bestudeerd, bestaan uit een snelle afwisseling van mariene klei en zandige turbidieten; de accumulatiesnelheid van de bemonsterde mariene klei is 70 cm per 1000 jaar. De exacte ouderdom en de bemonsteringslocatie van de geregistreerde polariteitsomkeringen waren eerder vastgesteld tijdens een magnetostratigrafisch onderzoek.

Gezien de accumulatiesnelheden en de gebruikte bemonsteringsmethode is het in principe mogelijk variaties van het aardmagneetveld aan te tonen die binnen 100-300 jaar hebben plaatsgevonden. Aangezien we echter naar een afbeelding - de registraties in gesteentes - en niet naar de werkelijke variaties van het aardmagneetveld kijken, zal er onvermijdelijk een zeker verlies aan detail optreden. Twee factoren bepalen of de registraties gebruikt kunnen worden om ze tot variaties van het aardmagneetveld te herleiden: de mogelijkheid om de oorspronkelijke remanente magnetisatie te isoleren en de wijze waarop de acquisitie van deze oorspronkelijke remanente magnetisatie tot stand is gekomen.

Properties of Pliocene sedimentary geomagnetic reversal records

Oorspronkelijke remanente magnetisaties zijn veelal niet de enige remanente magnetisaties in sedimenten. Zo ook niet in de bestudeerde sedimenten, waar drie of meer magnetisaties in één enkel monster aanwezig bleken te zijn. Van deze remanente magnetisaties bleken er één in het laboratorium (visceus) en één in de oorspronkelijke bemonsteringslocatie (secundair) in het huidige aardmagneetveld gevormd te zijn. In dit onderzoek is de scheiding van de oorspronkelijke remanente magnetisatie(s) enerzijds en de secundaire en visceuze magnetisaties anderzijds extra belangrijk, aangezien de intensiteit van het aardmagneetveld en dus de intensiteit van de oorspronkelijke remanente magnetisatie sterk daalt tijdens een polariteitsomkering, terwijl de intensiteiten van de secundaire en visceuze magnetisaties gelijk blijven. In de Italiaanse sedimenten zijn de remanente magnetisaties door een stapsgewijze wisselveld-demagnetisatie, maar vooral door stapsgewijze thermische demagnetisatie met succes gescheiden. De magnetisaties in de sedimenten uit Corfu konden echter met dezelfde methoden niet volledig gescheiden worden. De oorspronkelijke magnetisaties konden onder meer geïdentificeerd worden omdat de inclinaties een consistente inclinatiefout vertonen, veroorzaakt door compactie van het sediment. Tevens komen de declinaties van de oorspronkelijke magnetisaties overeen met een Pliocene regionale tektonische rotatie.

De wijze waarop de oorspronkelijke remanente magnetisatie verkregen is kon voor een groot deel worden afgeleid uit de resultaten van het gesteentemagnetisch en geochemisch onderzoek. In de Italiaanse sedimenten konden de dragers van de oorspronkelijke natuurlijke remanente magnetisaties worden geïdentificeerd als de ferrimagnetische mineralen magnetiet en pyrrhotien. In de sedimenten van Corfu is de drager hoogstwaarschijnlijk magnetiet. De korrelgroottes van de magnetiet en pyrrhotien bleken respectievelijk in het (pseudo) single domain en single domain bereik te liggen. Pyrrhotien komt vooral voor in de mergels met een laag carbonaatgehalte, terwijl magnetiet meer voorkomt in de mergels met hogere carbonaatgehaltes. Pyrrhotien wordt typisch gevormd in suboxische omstandigheden na accumulatie van het sediment. De overeenkomst tussen de richtingen van de magnetiet en pyrrhotien magnetisaties maakt het zeer waarschijnlijk dat beide mineralen gelijktijdig of kort na elkaar in het sediment gevormd zijn, en wel, gezien de sedimentatiesnelheid en op basis van de resultaten van andere onderzoekers, enige duizenden jaren na afzetting van het sediment. De natuurlijke remanente magnetisatie van magnetiet en pyrrhotien is dan ook een chemische remanente magnetisatie. Alhoewel er zonder twijfel sprake is van een vertraging tussen het sedimentatieproces en de acquisitie van remanente magnetisatie, moet, gezien de aanwezige inclinatiefout, de acquisitie echter

wel voor compactie van het sediment hebben plaatsgehad. De waarnemingen geven aanleiding om aan te nemen dat de vertraging in de acquisitie geen factor is die de kwaliteit van de registraties beinvloedt. Belangrijke factoren in het acquisitieproces die bepalen hoe de variaties in de registraties corresponderen met variaties van het aardmagneetveld, zijn de continuïteit van het acquisitieproces en de grootte van het sedimentaire interval waarbinnen de acquisitie gelijktijdig heeft plaatsgevonden, het zogenaamde lock-in interval. In dit onderzoek zijn geen aanwijzingen gevonden dat discontinuïteit in de acquisitie van de remanentie een rol heeft gespeeld, behalve in het geval van vroege remagnetisaties die zijn waargenomen bij lithologische grenzen. In de resultaten van een zeer recent onderzoek aan andere registraties van polariteitsomkeringen in soortgelijke sedimenten lijken deze aanwijzingen wel aanwezig te zijn (van Hoof en Langereis, submitted). Het was in het kader van het huidige onderzoek niet mogelijk meer zekerheid over dit aspect te verkrijgen. Derhalve moet gesteld worden dat bij de interpretatie van de kwalitatief zeer goede registraties ervan is uitgegaan dat het acquisitieproces continu is en dat de registraties de variaties van het aardmagneetveld nauwkeurig representeren.

De registraties laten zien dat de intensiteit van de oorspronkelijke remanente magnetisatie in het centrum van de omkering afneemt tot ongeveer 10% van de oorspronkelijke waarde. Dit is in overeenstemming met de resultaten van soortgelijke onderzoeken. Opmerkelijk daarentegen is de afgeleide korte tijdsduur van de vroeg Pliocene polariteitsomkeringen. Waar in andere onderzoeken van oudere en jongere registraties van polariteitsomkeringen veelal tijdsduren zijn vastgesteld van tienduizend(en) jaren, is een belangrijke uitkomst van dit onderzoek dat voor de grootste richtings- en intensiteitveranderingen vaak niet meer dan enige honderden tot duizenden jaren nodig zijn. De conclusies over de tijdsduur van polariteitsomkeringen worden in het huidige onderzoek ondersteund door waarnemingen aan verschillende registraties van een identieke polariteitsovergang. De omvang van de richtings- en intensiteitsveranderingen in de registraties geven aan dat de snelste geomagnetische veranderingen 0.2° per jaar en 5% van de oorspronkelijke intensiteit per jaar bedragen. Opgemerkt dient te worden dat bij de snelste veranderingen in de registraties de grens van het oplossend vermogen bereikt lijkt te zijn, hetgeen tot een speculatie over een nòg kortere duur aanleiding zou kunnen geven. Hieruit kan geconcludeerd worden dat de grootte van het lock-in interval beperkt is tot enige centimeters.

Naast polariteitsomkeringen komen excursies van richting en intensiteit in meerdere registraties voor. In een enkel geval is een volledige excursie met een duur van ongeveer 1500 jaar geregistreerd vlak boven een polariteitsomkering. De registraties laten zien dat

een polariteitsomkering meestal aanvangt met een toename van de inclinatie van 5-50° in 1000-10000 jaar. De polariteitsomkeringen geven geen eenduidig axisymmetrisch (zonaal) of niet-axisymmetrisch beeld, wel vertonen de zonale polariteitsomkeringen met een "eenvoudig" verloop een sterke overeenkomst met elders beschreven registraties van de jongste Matuyama-Brunhes polariteitsomkering. Tezamen suggereren deze waarnemingen, gedaan op verschillende locaties, dat zonale veldconfiguraties een belangrijk element vormen van polariteitsomkeringen. Voortgaande studies van wereldwijd bemonsterde registraties van de in deze dissertatie beschreven polariteitsomkeringen zullen samen tot een ruimtelijk beeld en dus tot een beter begrip van het omkeringsproces moeten kunnen leiden.

Summary

In the history of the Earth the dipolar geomagnetic field has frequently reversed polarity. Though this property was already known early this century (Brunhes, 1906), nowadays the characteristics and the origin of polarity transitions are still largely unknown. The geomagnetic field and its variations are recorded in rocks as a natural remanent magnetization (NRM) during the formation of these rocks. The study of the NRM in sedimentary reversal records is the subject of this dissertation.

Eight reversals from the Gilbert and Gauss Chrons were studied in early and middle Pliocene marine sedimentary sequences from the Mediterranean area. The marine marls of the Trubi and Monte Narbone sequences from Italy (Calabria and Sicily), containing the records of all eight reversals, are composed of a rhythmic alternation of high- and low-carbonate units (0.1-1.0 m). The accumulation rate of the Italian sediments is 5-9 cm/kyr. De early Pliocene sediments from Corfu, containing two reversal records from the Gilbert Chron, show a rapid alternation of marine clays and sandy turbidites. The accumulation rate of the sampled clays is 70 cm/kyr. The ages and sampling locations of all reversal records were established in a previous magnetostratigraphic investigation.

In theory, the accumulation rates of the sediment and the applied sampling methods make it possible to demonstrate geomagnetic field variations which occurred in 100-300 year. However, since we examined the *records* and not the *actual* variations of the geomagnetic field, some loss of detail will certainly be present. Two aspects determine if the records can be related to the *actual* geomagnetic field variations: the characteristics of the remanence acquisition process and the extent to which the original remanent magnetization can be isolated from younger magnetizations.

To start with the latter aspect, in most sediments the original remanent magnetization is not the only magnetization type present. In the studied sediments three and sometimes even more remanent magnetic components were present in a single sediment specimen. One of these magnetizations was introduced in the laboratory (viscous magnetization) and one was introduced in the original sampling location in the present-day field (secondary magnetization). The separation of the original magnetization from the viscous and secondary magnetizations is specially important in the present study since the intensity of the geomagnetic field, and thus the intensity of the original remanent magnetization,

decreases during a polarity transition, whereas the intensities of the viscous and secondary magnetizations remain relatively constant. In the Italian sediments the remanent magnetizations have been removed by stepwise alternating field demagnetization, but more successfully by stepwise thermal demagnetization. The original remanent magnetizations could be distinguished from the younger magnetizations by their inclination error, which was introduced during early compaction of the sediment. Furthermore, the declinations of the original magnetization correspond to a Pliocene regional tectonic rotation.

The investigation of the remanence acquistion process has been performed with rockmagnetic and geochemical methods. The carriers of the original remanent magnetization in the Italian sediment were identified as the ferrimagnetic minerals magnetite and pyrrhotite. In the Corfu sediments the carrier of the original magnetization is most probably magnetite. The grain sizes of magnetite and pyrrhotite are in the (pseudo) single domain size range. In the Italian sediments, pyrrhotite occurs predominantly in the marls with a low carbonate content, whereas magnetite is somewhat more abundant in the marls with a high carbonate content. Typically, pyrrhotite is formed in sub-oxic environments after accumulation of the sediment. The correspondence between the directions of magnetite and pyrrhotite indicates that both minerals are formed (almost) simultaneously in the sediment. On the basis of the results of other investigations and the accumulation rate of the sediment it is concluded that magnetite and pyrrhotite are formed a few thousand years after deposition of the sediment. The inclination error indicates that the formation of the minerals and the remanence acquisition took place before compaction of the sediment. As a consequence, the natural remanent magnetization can be further defined as a chemical remanent magnetization. The results indicate that the delay in remanence acquisition with respect to the accumulation process has not affected the quality of the records. The extent to which the variations in the records correspond to variations of the geomagnetic field is determined by the continuity of the acquisition process and the size of the sedimentary interval in which the remanence acquisition occurred, i.e. the lock-in interval. In the present study no evidence has been found that discontinuity of remanence acquisition has played an important role; only close to lithological boundaries some early remagnetizations were observed. The results of a very recent investigation of other reversal records indicate that discontinuous remanence acquisition processes may occur (van Hoof en Langereis, submitted). It was not possible to acquire more conclusive evidence concerning this aspect. In this context, the interpretation of the high-quality reversal records partly relies on the assumption that the acquisition process is continuous and the

records give an accurate representation of the geomagnetic field.

At the centre of the polarity reversal the records show a decrease of the original remanent magnetization to 10% of the typical non-transitional values. This is in correspondence with the results of other investigations. Remarkable is the very short duration of the Pliocene reversals: the major directional and intensity changes occur in a few hundred or thousand years, whereas the results of other investigations indicate durations of ten thousand years or even longer. In the present study the conclusions on the durations are supported by observations on different records of an identical polarity transition. The magnitudes of the most rapid directional and intensity variations in the records are 0.2° per year and 5% of the typical non-transitional intensity per year. The most rapid variations are very close to the resolution of the record, which indicates that the actual durations of the reversals may even be shorter. It may therefore be concluded that the size of the lock-in interval is limited to a few cm's.

In a single record a full excursion with a duration of approximately 1.5 kyr has been recorded above a reversal. The reversal records indicate that the onset of a polarity transition concurs with a decrease of the intensity and an increase of the inclination of 5-50° in 1-10 kyr. The reversal records are not uniformly axisymmetrical (zonal) or non-axisymmetrical. The simple "zonal" records correspond with records of the youngest Matuyama-Brunhes polarity transition. These observations from remote sites indicate that zonal transitional fields are an important aspect of reversals. Continuation of the study of globally distributed records of the reversals described in this study will lead to a further understanding of the reversal process.

Chapter I

Introduction

Natural remanent magnetizations in rocks are the only witnesses of geomagnetic field reversals. During the last decade the number of well documented descriptions of geomagnetic reversal records has significantly increased. However, a detailed understanding of the reversal process has not been accomplished yet. A characteristic of the transitional field which is now generally accepted, is the low intensity equal to 10-20% of typical non-transitional values. Properties of reversals which are still a subject of dispute are the durations - believed to be in the range 2-30 kyr - and the transitional field geometry.

Reversals may be recorded in intrusive, extrusive and sedimentary rocks. High quality extrusive and intrusive reversal records are extremely sparse. In the present study, the emphasis is on marine sedimentary records since these are more abundant and, in contrast to extrusive and igneous rocks, provide a continuous image of the reversal process and an appropriate time control. It would be auspicious to study a single geomagnetic reversal from many globally distributed records. Despite the fact that sedimentary reversal records occur more frequently than any other type, the number of known records of one and the same geomagnetic reversal is limited mainly to the Matuyama-Brunhes reversal and the reversals of the Jaramillo and Olduvai subchrons. Records of these young reversals are typically sampled from deep sea cores, which require delicate sampling and error-prone analysis techniques. Rather than searching for globally distributed records of the same reversal, land-based sedimentary sequences within a restricted area - The Mediterrenean - containing many subsequent reversal records were preferred for this study. Although this approach will not result in a global image of the reversal process, it has the advantage that the time-dependent behaviour of the geodynamo during multiple reversals can be studied.

A total of 10 records of 8 different reversals were obtained from sections in Pliocene marine sedimentary sequences situated in the Mediterranean area (Calabria, Sicily and

Corfu). All reversal records had been accurately correlated to the geomagnetic polarity time-scale in previous magnetostratigraphic studies. The 5 Calabrian records correspond to the upper Thvera, lower and upper Sidufjall, lower and upper Nunivak reversals from the Gilbert Chron. The 3 Sicilian records are the lower and upper Mammoth and the lower Kaena reversals from the Gauss Chron. The 2 Corfu records correspond to the upper Thvera and lower Sidufjall reversals. The marine marls sampled in Calabria and Sicily are part of the same Trubi formation and have average accumulation rates of 5-9 cm/kyr (fig.1). The rapidly accumulated (~70 cm/kyr) marine clays from Corfu have been sampled to acquire a very high resolution record of geomagnetic field variations. Since the Calabrian and Corfu sections are separated by only a moderate distance, one may expect the corresponding reversal records to reflect the same regional characteristics of the geomagnetic field variations.

Fig. 1. Overview of the Monte Singa section in Calabria (Italy).

Introduction

During the course of this study it became evident that there many complexities and difficulties are involved in the analysis of the reversal records. Although there is little doubt that the Mediterranean sediments have accurately recorded the *long term* geomagnetic field variations, the extent to which the records represent *rapid* geomagnetic field variations, associated with polarity reversals, was largely unknown at the beginning of this study. At that time knowledge of this aspect did not appear to be essential since reversals were generally believed to proceed rather slowly (10-30 kyr). However, the first examinations of the Calabrian reversal records learned that rates of change could be much higher (0.2-2 kyr). In this context - records of rapid geomagnetic variations - the almost classical phrase "primary magnetization" acquires a special meaning. Usually, in paleomagnetic research primary magnetizations are identified by the most stable characteristic directions which are then argued to represent the "primary" or original magnetization. An important difference is that in these "classical" studies there must be a consistency in the observed directions, whereas in reversal studies this consistency is absent by definition. In that situation magnetic components may be separated using specific parts of the blocking temperature spectrum or the coercive force spectrum of the carriers of the magnetization. A contribution to the knowledge of the geomagnetic reversal process is therefore best served by an additional study of the characteristics of remanence acquisition, the carriers of the natural remanent magnetization, and the processes affecting the original remanence. This objective is accomplished by rockmagnetic and geochemical investigations of the carriers of the remanent magnetization.

This thesis has been written as a series of 5 papers, which discuss different aspects of the Mediterranean reversal records. Chapter 2 has already been published (Linssen, 1988) and discusses the preliminary results of a study of the four oldest Calabrian reversal records. All five reversal records from the Calabrian sediments (chapter 3) and the rockmagnetic properties of these sediments (chapter 4) were investigated in more detail at a later stage. Most of the conclusions from the preliminary 1988 paper could be confirmed, new and important details were found, and in a few cases slightly deviating conclusions were drawn. The results of the Sicilian and the Corfu reversal records are presented in chapter 5 and 6. A final chapter (7) discusses the conclusions from the previous chapters. Data of the reversal records have been included in the appendices.

Chapter II

Preliminary results of a study of four successive sedimentary geomagnetic reversal records from the Mediterranean. (upper Thvera, lower and upper Sidufjall, lower Nunivak)[1]

Abstract

The results of a study of four successive Early Pliocene geomagnetic reversal records are presented. The polarity transitions have been recorded in the Trubi formation of Calabria (S.Italy) which is composed of alternating carbonate-poor and carbonate-rich marly layers with moderately high (>5 cm/kyr) accumulation rates. The multicomponent NRM contains a well-defined primary component in which two dominant magnetic phases can be recognized: a magnetite and a low-temperature (LT; i.e. removed at moderate temperatures) phase. Most probably the low-temperature phase is pyrrhotite. The combined presence of pyrrhotite and magnetite in the sediment restricts the validity of a X_{ARM}/X test for paleointensity studies. The magnetite magnetizations reveal a more smoothed record relative to the records of the LT phase magnetizations. Between the two phases, no significant delay in the moment of remanence acquisition is observed. The durations of the major directional changes for the reversals are estimated to be in the range 0.3-3.0 kyr. The VGP path of the upper Thvera record follows a great-circle 90°W of the site meridian, indicating a clearly non-zonal transitional field, whereas the VGP paths of the other reversal records are close to the site meridian, indicating a mainly zonal transitional field. The lower Sidufjall and lower Nunivak records are nearly identical and have a zonal harmonic content similar to records reported for the Matuyama-Brunhes polarity transition.

(1) Published in Physics of the Earth and Planetary Interiors, Volume 52 (1988), Page 207-231.

1. Introduction

One of the most outstanding physical properties of the earth is that its magnetic field reverses polarity at irregular intervals. This feature was not known until the beginning of this century; at that time it was noticed that certain extrusive rocks contain remanent magnetizations with opposite directions. These reversed magnetizations were proved to be caused by the normal or reversed geomagnetic fields that existed during the formation of these rocks. The recordings in rocks of past reversals are probably the only source of information concerning this phenomenon. In recent years, geomagnetic reversal records in various kinds of rocks have been the subject of extensive studies (e.g. Valet, 1985; Prevot et al.,1985; Mankinen et al.,1985). A review of recent developments is provided by Bogue and Hoffman (1987).

So far, the only generally accepted conclusion to be drawn concerning geomagnetic field behaviour during a polarity transition, is that the dipole field disappears. This conclusion was first suggested after the observation of diverging Virtual Geomagnetic Pole (VGP) paths calculated from data of two Matuyama-Brunhes polarity transition records located at remote sites on the earth's surface (Hillhouse & Cox,1976). Meanwhile, many other similar observations have confirmed the validity of this conclusion (see e.g. Hoffman, 1977).

Various studies have revealed characteristics of reversal records which may well be properties of the transitional geomagnetic field. For instance, it has been observed that directional and intensity variations in successive reversals records at a single site are not always identical (Valet, 1985; Valet et al., 1988). This may indicate that the mechanism which causes the observed transitional magnetic field directions and intensities changes with time.

The reversal process appears to be fast relative to the geological time scale. The various observations suggest that the durations of reversals are not always identical. For instance, the results from the Steens Mountain record of a Miocene reversal (Mankinen et al., 1985) indicate that main directional changes associated with the reversal take place in about 0.7 kyr, whereas results from a sedimentary record of the upper Olduvai reversal indicate a duration of about 11.1 kyrs (Clement and Kent, 1985). The period in which anomalous intensities associated with the reversals occurs is a multiple of the duration of the directional changes.

At first sight, diverging data of different reversals suggest that the transitional field cannot be generalized. However, we are dealing with a geometrical problem; a geomagnetic reversal may give different effects at distant sites on earth. The standing field model (Hillhouse & Cox, 1976) and the flooding model (Hoffman, 1977,1979), which are essentially phenomenological, predict the transitional geomagnetic field at spatially distributed sites on the earth's surface as well as between successive reversals at the same site.

The study of similarities and dissimilarities in reversal records at geometrically distributed sites may shed light on the physical origin of the reversal process. The strategy of systematically studying geographically distributed records of the same reversal, or of studying successions of reversal records at one site has been followed by some investigators (e.g. Valet, 1985; Clement and Kent, 1986). However, most of their conclusions have been of a different tenor. Some successions of reversal records suggest a mainly zonal transitional field geometry (Bogue and Coe, 1982,1984); others indicate significant non-zonal field components (Clement and Kent, 1984).

The harmonic content of reversal records with zonal transitional field geometries is also subject to some discussion. For instance, Bogue and Coe (1982,1984) suggested that a specific reversal started with an octupolar transitional field, whereas near the termination of the reversal a quadrupolar zonal harmonic component dominated.

In some successions of reversal records antipodal transitional fields have been observed (Valet and Laj, 1984). Another succession of reversal records provided evidence that the transitional field was invariant (Clement and Kent, 1985). These observations suggest different types of reversal mechanisms (Bogue and Hoffman, 1987); this idea has also been suggested on theoretical grounds (Olson, 1983).

The fact that these extreme speculations are based on a limited number of (sequences of) reversal records illustrates the need for more data from reversal records.

Reversals of the geomagnetic field have been recorded in sediments and in intrusive and extrusive igneous rocks. Although the high quality spot readings of the geomagnetic field in extrusive igneous rocks can be successfully used in the study of reversal records, it should be realized that high flow rate sequences of lavas with reversal records are seldom found (Bogue and Coe, 1982,1984; Prevot et al., 1985; Mankinen et al., 1985).

Preliminary results of a study of four sedimentary geomagnetic reversal records

Geomagnetic reversals are most successfully studied in sedimentary records since they are widespread.

Sediments that are used in reversal studies have to satisfy certain conditions: the sedimentary reversal record must reveal the major directional and intensity variations of the transitional geomagnetic field. For instance, this implies that the accumulation rate for the sediment must be at least 1 cm/kyr. The accumulation rate near the reversal record is usually extracted from the boundary ages of the underlying and overlying polarity intervals and the stratigraphic lengths of the recorded polarity intervals. If temporal information is to be extracted from the record, the variation in the accumulation rate on the scale of the reversal record must be small.

Sediments often contain a variety of magnetic minerals (Freeman,1986). The origin of these minerals may be depositional, authigenic or secondary. Each of these minerals may contribute in a different degree to the NRM. As a result the total (multicomponent) NRM may be very complex. Reversal records in red beds (Herrero-Bervera and Helsley, 1983; Tauxe and Badgley, 1984) suggest that backtracking, i.e. the varying predominance of components acquired at slightly different times in a rapidly evolving transitional field, may occur. In order to study a sedimentary reversal record properly one needs to try and isolate the remanence directions of all primary magnetic minerals with progressive demagnetization techniques and to determine the relative timing of the magnetic remanence.

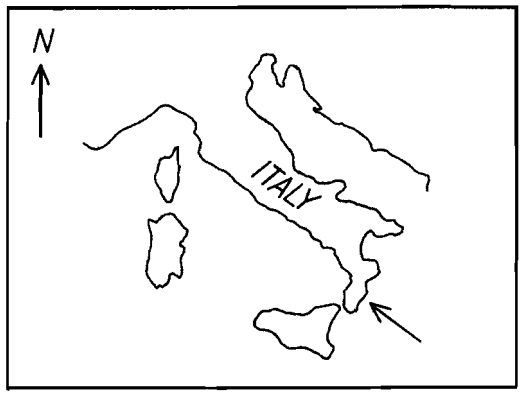

Fig. 1. Location of Lower Pliocene Trubi formation sampled for this study.

Investigators from the Utrecht paleomagnetic laboratory have been able to identify a great number of reversal records in the late Miocene marine deposits of Crete (Langereis, 1984). Detailed studies have been made of the rockmagnetic properties of the sediment (Langereis, 1984; Linssen, 1984; Valet, 1985; Chang and Kirschvink, 1985). The reversal records were extensively and successfully investigated at the paleomagnetic laboratory in Gif-sur-Yvette (Valet, 1985). The magnetostratigraphically well-defined (Zijderveld et al., 1986) Lower Pliocene marine deposits of southern Italy (38°15'N,16°12'E; See fig. 1), known as the Trubi formation (see e.g. Cita, 1973; Hilgen, 1987), appeared to be very suitable for making a study of a succession of undisturbed, well-dated reversal records. The sediments from the Trubi formation have rockmagnetic properties quite similar to those of the Cretan sediments.

In this paper we present the results of four successive reversal records from the Gilbert chron sampled in the Trubi formation: the upper Thvera, lower and upper Sidufjall and the lower Nunivak. Before discussing the reversal records the magnetic minerals which contribute to the NRM are discussed. In the general discussion an attempt will be made to determine more accurately the accumulation rate of the sediment in which the reversals are recorded.

2. Geology

The Trubi formation consists of alternating layers of marine marls with high and low carbonate contents; these layers are denoted as High Carbonate Units (HCU) and Low Carbonate Units (LCU) respectively. The well-defined unit boundaries facilitate the recognition of the few minor faults. The thickness of the individual units is laterally constant (on the scale of the exposure: a few hundred metres), the layer thickness of different units ranges from 0.1 to 1.3 m. Each of the four reversals are recorded within a single unit, none of them at a boundary. The bedding plane of the sediment at the site dips 6.5° to E.

Magnetostratigraphic results (Zijderveld et al.,1986) show that between the upper Thvera and the lower Nunivak the mean accumulation rate in the part of the section sampled for this study increased from 4.9 to 7.6 cm/kyr.

3. Sampling

The sampling equipment consisted of a portable generator, electric drilling machines and water-cooled brass drills with diamond cutting edges. The drills have a diameter of 2.54 cm. Planes were cut perpendicular to the bedding plane at least 20 cm deeper than the shallowest fresh rock surface. In the upper Thvera and lower Nunivak records sampling levels were marked on these planes at stratigraphic intervals ranging from 2.5 to 5.0 cm; at each level 3 to 5 cores were drilled in a direction parallel to the bedding plane. The lower and upper Sidufjall records and a part of the upper Thvera record were sampled using a slightly different method: the number of cores per level was 1 to 2, the spacing between the levels was varied from 0.5 to 2.5 cm. A few additional vertically drilled samples were obtained from the lower Sidufjall record. For this purpose, special drills were used with a length of 20 cm.

4. Instrumentation

Thermal demagnetizations were performed in tunnel furnaces with mu-metal shielding. The alternating field demagnetizations were applied to the specimens in stationary holders. Most of the magnetization measurements were performed with a 2G-Enterprises cryogenic magnetometer having a sensitivity of 10^{-11} Am^2; a small number of samples were measured with a modified Jelinek spinner magnetometer having a sensitivity of 10^{-10} Am^2. The reproducibility of both magnetometers is better than 1° for magnetizations exceeding 10^{-9} Am^2.

5. NRM components

5.1 Magnetic phases of the NRM components.

The demagnetization diagrams and derived decay curves of figure 2 show rockmagnetic characteristics that are representative for the sediment. The components which point to the origin of the diagrams have near reversed axial dipole field (RADF) directions, these components are therefore almost certainly primary ones (see also Zijderveld et al., 1986).

Figures 2a,c are demagnetization diagrams of two specimens from nearly the same horizon in a sedimentary interval above the upper Thvera reversal record. Specimen

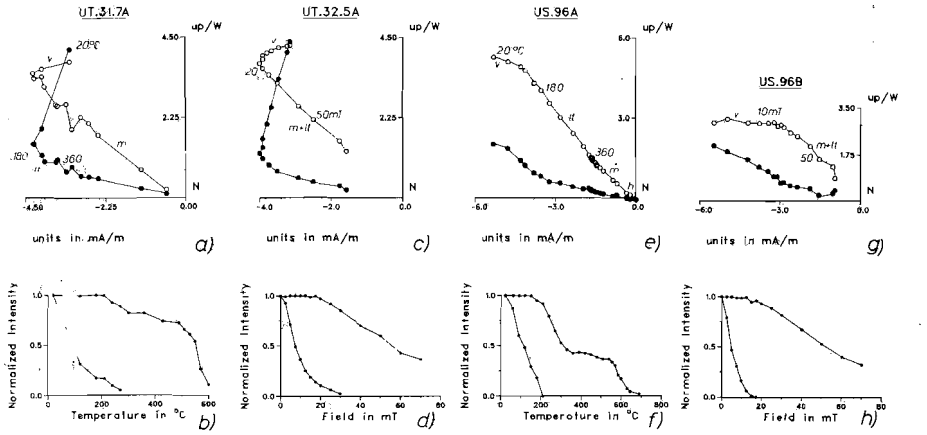

Fig. 2. Orthogonal projection diagrams (Zijderveld,1967) and corresponding decay curves. In the demagnetization diagrams the closed (open) symbols denote the projection on the horizontal (vertical) plane. Specimens are from levels above the upper Thvera (UT) and upper Sidufjall (US) reversal records. Figure a) and e) are thermal demagnetization diagrams and c) and g) are alternating field demagnetization diagrams. "m", "lt" and "v" denote respectively: the magnetite phase, the low-temperature (LT) phase and the viscous component. The normalized decay curves (b,d,f,h) show the decay of the viscous component and the primary component (m+lt).

UT.31.7A has been subjected to a thermal demagnetization and specimen UT.32.5A to an alternating field (AF) demagnetization treatment. Both demagnetization diagrams show a primary component and a viscous component. The viscous component is shallow and westward directed. The latter component is an artifact since its direction is highly correlated with the drilling direction. Similar viscous components, although generally with a lower magnitude, are observed in the demagnetization results of many specimens. The normalized decay curves (figs. 2b,d) show that the viscous component is removed in an alternating field of 15 mT and at a temperature of 240 °C.

The primary component has a unimodal decay when demagnetized in an alternating field and a bimodal decay when thermally demagnetized. Apparently, the primary component is carried by a low temperature (LT) magnetic phase of which the remanence is removed below 360 °C and by a high temperature (HT) magnetic phase of which the remanence is removed just below 600 °C. It is also clear from figure 2b that the thermal decay curves of the viscous component and of the LT phase overlap to a significant extent. The overlap of the decay curve of the viscous component and of the primary component in the AF decay curve (fig. 2d) is less significant.

Figures 2e,g show demagnetization diagrams of two specimens from neighbouring sites from an interval above the upper Sidufjall reversal record. Specimen US.96A has been subjected to a thermal demagnetization and specimen US.96B to an AF demagnetization treatment. The demagnetization diagrams and the decay curves (figs. 2f,h) also show a primary and a viscous component. A few other characteristics distinguish them from the previous examples: the thermal demagnetization diagram has a primary component with a trimodal decay due to the presence of a third magnetic phase, the remanence of which is removed just below 700 °C. The LT phase has a slightly higher inclination than the phases whose remanences are broken down at higher temperatures. Table 1 gives the directions of the phases with near RADF directions from figure 2. Note that the inclination of the primary component from the upper Sidufjall specimens obtained with AF demagnetization is intermediate to the directions of the LT and HT phases obtained with thermal demagnetization. Note also that the decay of the primary component in the AF decay curves (figs. 2d,h) is unimodal. Apparently the LT and HT phases have (almost) completely coinciding coercive force spectra in the range 20-70 mT.

Primary components with a similar decay are common in marine marls (Langereis, 1984; Valet, 1985). The two magnetic phases whose remanences are broken down just below 600 and 700 °C are most probably magnetite (Curie temperature : 578 °C) and hematite (Neël temperature : 680 °C). The magnetite phase is observed in all thermally treated specimens. The hematite phase is observed occasionally and always has a low intensity; therefore, the hematite phase is not discussed in the following sections. The determination of the LT phase is discussed in section 6.

5.2 Directions of NRM components outside the reversal records

The study of viscous and primary NRM components outside the reversal records provides a tool for distinguishing these components in the reversal record where we are looking for primary components with unknown transitional directions.

Throughout the sedimentary intervals above and below the reversal records it was observed that the directions of the primary component obtained with thermal demagnetization comprise two linear segments that make an angle of 0-20°. The linear segments correspond to the LT phase and the magnetite phase. Often the angle between the linear segments is only visible in the projection on the vertical plane. Generally, the

Table 1
Least-squares declination and inclination values of the primary components from the demagnetization diagrams depicted in figure 2.

	Total		LT component		HT component	
Specimen	Decl.	Incl.	Decl.	Incl.	Decl.	Incl.
UT.31.7A			194.1	-38.5	192.3	-36.2
UT.32.5A	190.7	-40.1				
US.96A			190.4	-51.2	187.8	-40.1
US.96B	192.3	-45.3				

Column 1: demagnetization data points exceeding 240 °C or 15 mT.
Column 2: the demagnetization data between 240 and 360 °C.
Column 3: the demagnetization data after 360 °C.

magnetite phase has inclinations that are about 10° lower than the local axial dipole field inclination (52°). The LT phase has inclinations that are intermediate to the inclinations of the magnetite phase and to the axial dipole field inclination. The systematic inclination error of the magnetite phase was suggested to be caused by compaction of the sediment (Laj et al., 1982; Langereis,1984).

The inclination error of magnetic phases with near normal axial dipole field (NADF) directions allows them to be distinguished from secondary magnetizations. Secondary magnetizations cannot be distinguished from an LT phase with an NADF direction (without an inclination error). The observation that 1) the sedimentary interval which contains such phases is unaltered and rockmagnetically homogeneous and 2) a neighbouring rockmagnetically similar sedimentary interval contains LT phases that carry near RADF directions demonstrates that the component with the NADF direction is a primary one.

Viscous components are easily recognized by the strong relation between their directions and the storage orientation of the specimens. The observed viscous components have relaxation times exceeding a few days. An example of a viscous component has been given in section 5.1. The thermal decay curves of the viscous component and the LT phase of the primary component have a significant overlap. Consequently, the relative

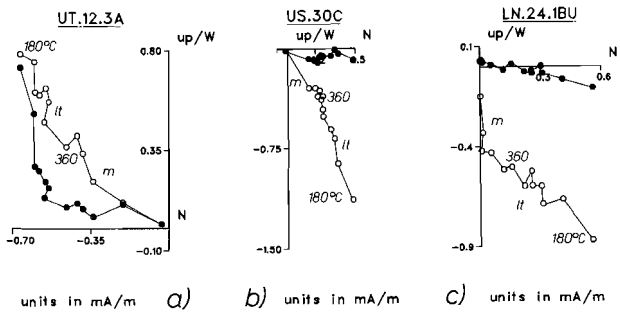

Fig. 3. Thermal demagnetization diagrams of specimens from the upper Thvera (a), upper Sidufjall (b) and lower Nunivak (c) transition records. The demagnetization data for temperatures below 180 °C were omitted. All diagrams show linear segments corresponding to the LT and the magnetite phase (denoted as "lt" and "m" respectively).

magnitudes of the LT phase and the viscous component determine how well the direction of the magnetization of the LT phase can be determined. Fortunately, viscous component with high intensities and LT phases with very low intensities were never observed in the same specimens.

5.3 Directions of NRM components in the reversal records.

Within the reversal records an anomalous direction of a remanent magnetization is defined as a part of a primary component when 1) its thermal decay is identical to the decay of the LT or the magnetite phase (see fig. 2), 2) when it is found in other specimens from approximately the same stratigraphic level, or 3) it is part of a directional variation of identical phases as a function of stratigraphic height.

In the sedimentary intervals outside the reversal records the magnetizations of the LT phase and the magnetite phase can have different directions. This characteristic is more extremely encountered in specimens from the reversal record; figure 3 shows three examples. The difference in direction between the LT and magnetite phase can be caused 1) by different lock-in depths of these phases or/and 2) by different lock-in intervals of these phases. The implication of the first possibility is a backtracking of the local geomagnetic field directions recorded by the two phases. In that case, there will be two

identical records of the geomagnetic field behaviour during its reversal between which an apparent time-lag exists. The latter possibility that the two phases have different lock-in intervals will result in two records which are smoothed to different extents. Only the study of the directional and intensity variations with time (stratigraphic distance) of the LT and magnetite phase can indicate to what degree these possibilities reflect the real remanence acquisition processes.

6. Bulk-rockmagnetic investigation of the sediment

A detailed study has been made of the bulk-rockmagnetic properties of the Trubi sediment (Linssen, in prep.). The relevant information is given below.

Specimens of the four studied reversal records were subjected to bulk-rockmagnetic experiments so that the nature and the grain sizes of the LT and magnetite phases which carry the primary component could be examined. Rockmagnetic information about the minerals in the sediment contributes to the interpretation of accumulation rate variations and of the continuity of sedimentary deposition. It should also indicate whether it is feasible to relate remanent magnetizations and/or rockmagnetic parameters to paleointensities.

6.1 Continuous thermal demagnetization and low temperature treatment

We subjected representative specimens from the sampled reversal records to successive thermal treatments in order to investigate alteration effects upon heating. Prior to each heating or cooling cycle the specimens were given an Isothermal Saturation Remanence (ISR) in a 2 T DC field. The term ISR is used for convenience although it will demonstrated in section 6.2 that the specimens are not completely saturated in 2 T.

The first heating cycle for specimen US.109.1B shows (fig. 4a) that the ISR is dominated by two magnetic phases the remanence of which is completely removed at 360 and 580 °C respectively. Since these break-down temperatures are similar to those of the primary component of the NRM, one must conclude that they are carried by the same phases. During the second heating cycle applied to the same specimen (fig. 4a), it is demonstrated that the LT phase is absent and that the ISR which is left after 360 °C has decreased. Obviously, during the first heating cycle the LT phase was physically removed.

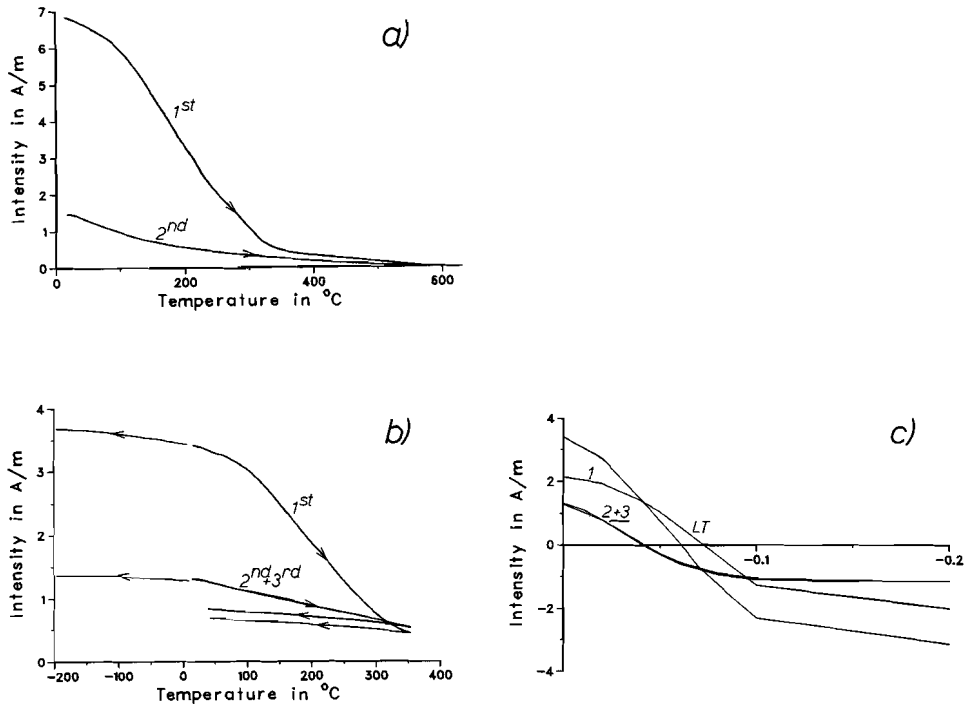

Fig. 4. (a,b) Continuous thermal treatments of specimens from the upper Sidufjall reversal record. The specimen acquired an ISR in a 2 T field before each thermal treatment. The heating cycles are numbered. (c) Remanent hysteresis curves determined before each of the thermal treatments of fig. 4b. Magnetite and the LT phase contribute to curve 1, original and newly formed magnetite contribute to curve 2 and 3. The curve denoted "LT" remains after subtraction of curve 1 and 2. It represents the contribution of newly formed magnetite and the LT phase.

The decreased ISR left after 360 °C points to a partial alteration of magnetite. There is no evidence that new magnetic minerals have been produced as a result of the alterations.

Figure 4b depicts the results of a similar experiment. However, in this case the specimen (US.113B), which acquired an ISR, is successively cooled to -190 °C, re-heated to room temperature, re-given an ISR and heated to 360 °C. The latter heating step is assumed to cause a complete alteration of the LT phase on the basis of the results for the similar specimen US.109.1B. It should be noted that the remanence increased significantly with cooling. Afterwards, the same specimen is twice subjected to the identical experimental procedure. The results for these experiments confirm that the LT phase was altered during the first thermal treatment. The significant remanence increase that occurred upon

cooling has now disappeared; apparently, this remanence increase is a characteristic of the LT phase. The second and the third heating curves are identical and have a slightly higher ISR left at 360 °C than the first heating curve. Apparently, during the first heating cycle, a new magnetic mineral was produced. The fact that the second and the third heating curves are identical suggests that they represent true demagnetization behaviour and are not affected by alteration.

The remanent hysteresis curves of specimen US.113B determined prior to each heating step show (fig. 4c) lower H_{CR} values after the first heating cycle. The first remanent hysteresis curve represents the LT and magnetite phase, the second curve represents the magnetite phase and the new magnetic phase that was produced during the first heating cycle to 360 °C. Subtraction of the second from the remanent hysteresis curve, produces an estimate of the remanent hysteresis curve of the LT phase; it is an estimate since the curve is slightly biased by the contribution of the new magnetic material.

The initial susceptibilities (X_i) of other specimens, similar to specimen US.113B, show a slight (<5%) increase during a stepwise thermal demagnetization treatment up to 300 °C. The X_i decreases significantly after heating the specimen to 360 °C (>20%). Further heating causes the X_i to increase again to values that are 2-4 times above the X_i of the non-heated specimen.

Heating experiments with specimens from sediments with similar rockmagnetic contents (Linssen, 1984) suggested that with increasing temperature magnetite was produced from the non-magnetic matrix. Hysteresis experiments provided evidence that the grain size of the newly formed magnetite increased (due to growth) from superparamagnetic (SP) grain size ranges, to the single-domain (SD) grain size range and subsequently to the pseudo-single-domain (PSD) or even the multi-domain (MD) grain size range. In these sediments the transition of the magnetite through the SD grain size range always occurred at 450 °C and caused a maximum of ISR (which was 2-10 times greater than the ISR of the non-heated specimen). Heating the specimens to temperatures above 500 °C caused the old and new magnetite to alter to hematite.

In summary, it is concluded that the observed break-down of the remanence carried by the LT phase (magnetite) is in the main (partly) due to alteration of these minerals

rather than to their demagnetization. The LT phase alters completely below 360 °C, the magnetite alters partly between 360 and 600 °C. There is evidence that magnetite is produced below 360 °C and that some magnetite is altered after the specimens are heated to 600 °C. Low temperature treatment shows (1) a significant remanence increase of the LT phase with cooling and (2) hardly any effects for the remanence of magnetite. The last observation indicates a small grain size (< 5 micrometer) for magnetite since the loss of remanence upon cooling to the isotropic point of magnetite decreases with grain size (Hartstra, 1982).

The LT phase in specimen US.113B has an H_{CR} value of about 72 mT; this value is slightly biased by the production of the newly formed fine grained magnetite. Since fine grained magnetite has an H_{CR} lower than 70 mT (Hartstra, 1982), the true H_{CR} value of the LT phase will probably be in excess of 72 mT.

6.2 ARM and ISR characteristics

It was investigated whether Anhysteretic Remanent Magnetization (ARM) and ISR characteristics allowed a more quantative determination of the contribution of the LT and magnetite phase to the NRM. The specimens for the ISR and ARM experiments have been selected from the same sedimentary interval as those from the previous section. In figure 5a the thermal decay curves are depicted of (1) an ARM acquired in an alternating field (AF) of 100 mT, (2) an ARM acquired in an AF field of 350 mT, (3) an ISR acquired in a 2 T field and (4) a primary component of an NRM. The ARM inducing direct field was 0.036 mT. Since the previous sections provided evidence that the main magnetic phases are an LT and a magnetite phase, a bimodal decay is expected. The bimodality is evident in the thermal decay of the NRM and ISR. The thermal decay curves of ARM are only slightly bimodal. The decay curve of ARM acquired in 350 mT shows hardly a more pronounced bimodality than the decay curve of the ARM acquired in 100 mT. The thermal decay of the NRM is not identical to the thermal decay of the ARM or the ISR. The thermal decay curves show that, with respect to the NRM, the LT phase acquires less ARM and more ISR.

The normalized ISR and ARM acquisition curves (figs. 5b,c) demonstrate that specimens from this sediment are not completely saturated respectively in 2 T DC fields and 350 mT AF fields. The ISR and ARM acquisition curves show, in spite of the presence of the LT and the magnetite phase, no sign of bimodality.

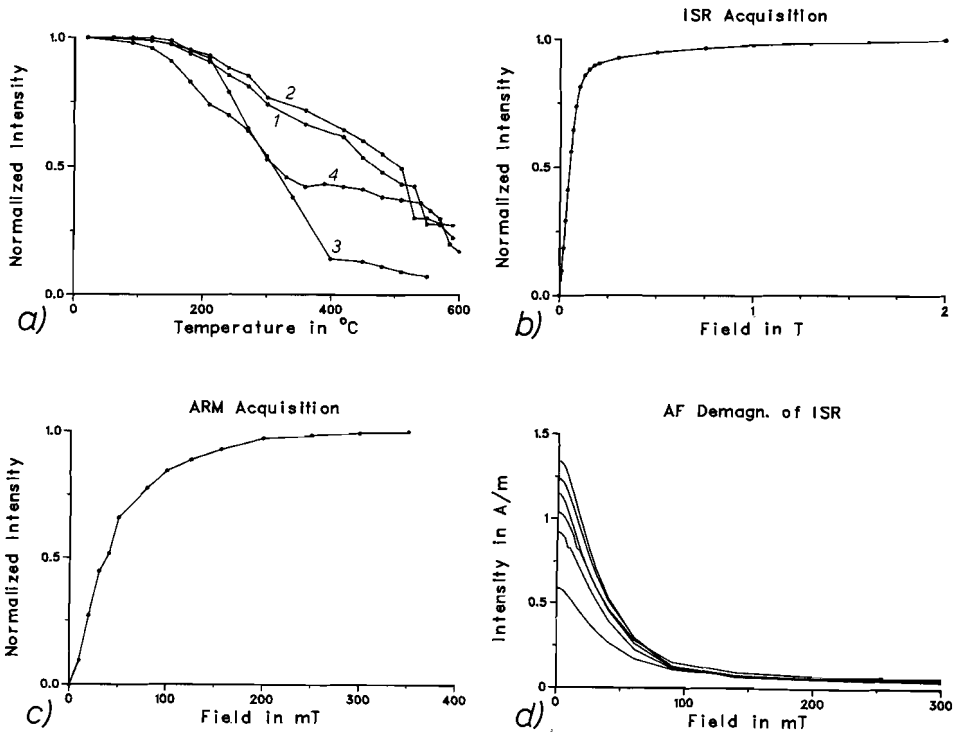

Fig. 5. (a) thermal decay curves of specimens from the US reversal record with (1) ARM acquired in an AF field of 100 mT, (2) ARM acquired in an AF field of 350 mT, (3) ISR acquired in 2 T, (4) primary component of the NRM. (b) ARM acquisition curve (c) ISR acquisition curve (d) AF demagnetization curves of ISR. Continuous thermal treatment (with exact temperature readings) of specimens from the same sedimentary intervals as the specimens of figure 5a-d demonstrated that the magnetizations of all specimens is entirely removed at 600 °C.

In some sedimentary intervals the intensities of the primary component show a major variation. A closer examination demonstrates that this intensity variation often is caused by a change in rockmagnetic properties in either the magnetite or the LT phase.

This is illustrated by the AF decay curves (fig. 5d) of specimens from such a sedimentary interval. The specimens acquired an ISR in a 2 T field. The figure shows that the high coercive fractions have equal intensities, unlike the low coercive fractions.

Thermal demagnetization of other specimens from the same sedimentary interval

showed that an acquired ISR was entirely removed below 600 °C. These observations suggests that the observed NRM variation is due to rockmagnetic changes of magnetite and is not caused by the geomagnetic field. A minor contribution to the high-coercive fraction of small amounts of high-coercive minerals other than the LT phase (e.g. hematite) cannot be excluded.

In summary, the thermal demagnetization of ARM shows only a small contribution of the LT phase, although this contribution increases slightly with the applied alternating field. The contribution of the LT phase to the ARM is lower than to the NRM, whereas its contribution to the ISR is higher than to the NRM.

The sediment under study, containing a LT and a magnetite phase, does not give bimodal ARM and ISR acquisition curves. The LT phase is not saturated in 2 T DC fields. Variations in the intensity of the magnetite correlate with variations in the low coercive fraction of the ISR, whereas they do not correlate with the high coercive fraction of the ISR.

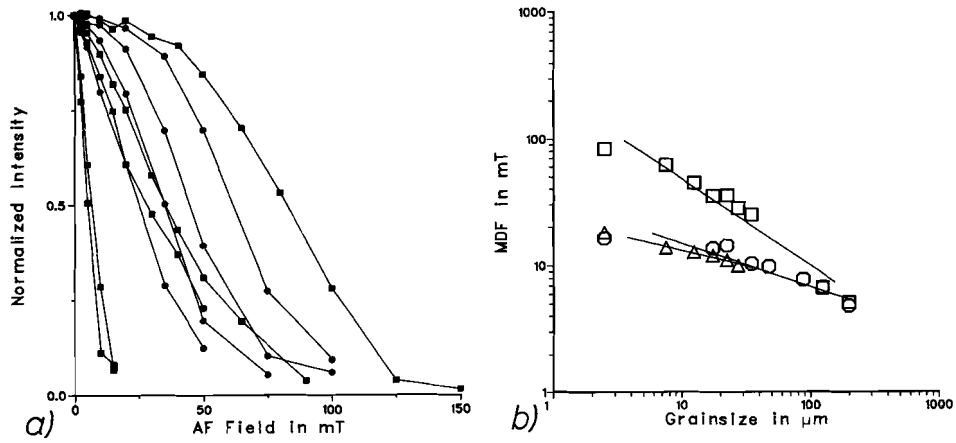

Fig. 6. (a) AF decay curves of ARM in synthetic specimens containing natural pyrrhotite of various grain size ranges. Closed circles denote EOR pyrrhotite, closed squares denote TTE pyrrhotite (See Dekkers, this volume). (b) Median destructive field of ARM. Squares denote natural pyrrhotite (TTE,EOR; see fig. 6a), circles denote natural magnetite (HM4T; Hartstra, 1982), triangles denote natural maghemite (DKA, Dankers, 1978).

6.3 Determination of the LT phase

The fact that the LT phase alters completely upon heating to 360 °C points to pyrrhotite (Schwarz,1975) and maghemite (Dankers, 1978). In figure 6a the results of the AF demagnetization of the ARM of some natural pyrrhotites is shown (Dekkers, Unpublished data). Figure 6b depicts the grain size variation of the Median Destructive Field of ARM ($H_{1/2A}$) for natural magnetite, maghemite and pyrrhotite. All minerals show increasing $H_{1/2A}$ values with decreasing grain sizes. The magnetite and maghemite behaviour is similar; the $H_{1/2A}$ increase for pyrrhotite is more significant. Considering the $H_{1/2A}$ data for maghemite it is expected that an ARM acquisition in an alternating field of 350 mT will saturate or nearly saturate small (say 1-5 micrometer) grains of this mineral.

The thermal demagnetization data of ARM (fig. 5a) indicate otherwise; a pronounced bimodal thermal decay would be expected if the LT phase is maghemite. With regard to figure 6b, the quoted thermal demagnetization data of ARM makes sense if the LT phase is pyrrhotite. The ISR results for pyrrhotite (Dekkers, 1988) resemble the experimental results presented in the previous sections (High H_{CR}, ISR not completely saturated at 2T). Finally, in the studied specimens we observed a typical pyrrhotite characteristic: spurious remanences are produced when >80% of the remanence of the pyrrhotite phase is demagnetized with alternating fields (Schwarz, 1975).

Given the present information, pyrrhotite is considered to be the most likely carrier of the LT phase. This mineral (most probably) is produced authigenically; chemical characteristics of sea water are such that it would oxidize detrital pyrrhotite. Post sedimentary or early diagenetic processes in the presence of organic matter encourage the formation of sulphidic minerals, which indeed are abundant in the sediment (Linssen, 1984). Therefore, it is tentatively concluded that the LT phase is pyrrhotite. Low temperature characteristics and H_{CR} suggest that the grain size of the pyrrhotite and magnetite in the sediment is <5 micrometer.

6.4 Implications

King et al. (1983) developed a rockmagnetic test to discover whether magnetic remanence of a sediment can be related to paleointensity. Although this test is used by investigators working on sediments which are rockmagnetically similar to the sediment of the Trubi formation the experiments suggest that its use is not really justified because in

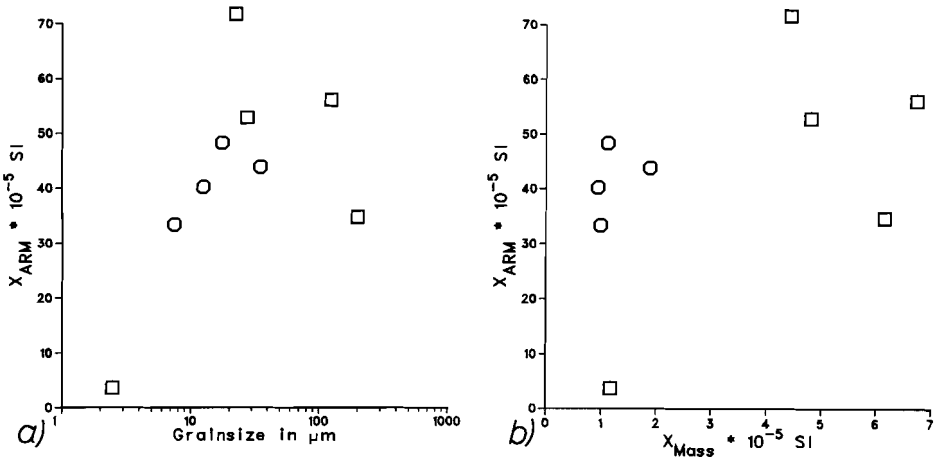

Fig. 7. (a) X_{ARM} of EOR (circles) and TTE (squares) natural pyrrhotites versus grain size. (b) X_{ARM}-X diagram according to King et al. (1983) of EOR (circles) and TTE (boxes) natural pyrrhotites. For susceptibility data of pyrrhotite see Dekkers (1988).

our view the first condition of this test, namely that the dominant magnetic mineral should be magnetite, is not satisfied.

In the range 2-20 um, the X_{ARM} of natural pyrrhotite tends to increase with grain size (fig. 7a). A maximum may be present near 20-30 um. This trend is opposite to the trend observed for magnetite (King et al. 1983). In figure 7b the susceptibility data for pyrrhotite (Dekkers, 1988) and the above ARM data are combined in an X_{ARM}-X plot according to King et al. (1983). When these data are compared to the magnetite data of King it becomes clear that the presence of pyrrhotite biases the grain size of magnetite interpreted from the X_{ARM}-X diagram to lower values. The apparent variations in the concentrations of magnetite that are interpreted from the X_{ARM}-X plot can easily be influenced by variations in pyrrhotite content of the sediment.

The obvious way to solve this problem would be to determine X_{ARM} and X_i after the alteration of pyrrhotite upon heating the specimens to 360 °C. However, the experiments also provided evidence that small-grained magnetite has already been produced at this temperature. Kings' model may only be used when the contribution to X_{ARM} and X_i by the newly formed magnetite can be calculated or is proven to be minor. The correction for the presence of the newly formed small grained (say .01-5 um) magnetite is problematical

since the grain size variation of the X_{ARM} carried by this magnetite is large (King et al., 1983).

The non-uniformity of mineral contents in this type of sediment prevents the successful use of standard tests for determining the paleointensities in sediments. Alternatively, to test whether one of the two phases is suitable for representing the ancient geomagnetic field intensity, one has to use rockmagnetic methods with which one can discriminate the two magnetic phases. Neither X nor ARM has such characteristics.

7. Demagnetization procedures and analysis of demagnetization data

Viscous behaviour of thermally treated specimens, due to the production of small SD magnetite grains with relaxation times of <100 seconds (Section 5.3; Linssen, 1984), was successfully suppressed by heating specimens for no longer than the time necessary to create a homogeneous (<5 °C) temperature distribution in the specimen and to cool the specimens rapidly with air. Heating times varied from 30 minutes at 100 °C to 20 minutes at 600 °C. A homogeneous temperature distribution in a specimen is required to prevent unwanted smoothing effects in the demagnetization results caused by the removal of remanent magnetizations with different directions and thermal decay. Heating experiments with thermocouples in dummy specimens demonstrated that a temperature inhomogeneity in the specimens, at all temperatures, is never in excess of 5 °C after 20 minutes heating time. Furthermore, the temperature of the specimens as a function of the heating time was determined. At heating times of 20-30 minutes, the results of the experiments showed a maximum bias of 0-20 °C to lower temperatures (relative to the temperature indication of the furnace).

Partial thermal remanent magnetization (PTRM) can be produced during cooling of the newly formed "sensitive" small SD magnetite in a non-zero (<25 nT) magnetic field. The recognition of such a PTRM is important in this study since we are looking for (small) remanences with anomalous (transitional) directions. This PTRM could be recognized and accounted for since the position of the specimens in the furnace was varied and registered at each heating step. The magnitude of a PTRM in a specimen was never in excess of 0.05 mA/m.

The large number of demagnetization data have been analyzed with an in-house developed interactive computer program that makes use of graphical projection routines. In

this program linear segments are "least-squares fitted" to data points selected by the operator. The directions of these linear segments are employed to construct (Zijderveld, 1967) and calculate intensities. The interactive computer program displays demagnetization diagrams and decay curves and facilitates the calculation of the directions and intensities.

The minor but indefinite viscous and laboratory induced remanences exceed the small measurement error of the cryogenic and spinner magnetometers. For this reason the demagnetization data were not weighted with the measurement error. The statistical error which was determined is the maximum angular deviation (MAD;Kirschvink, 1980).

8. Reversal records

The thermal demagnetization results are presented for the upper Thvera (UT), lower and upper Sidufjall (LS and US) and the lower Nunivak (LN) reversal records. The demagnetization results for the LS and LN records comprise the directions and intensities of the magnetite phase, whereas the results for the UT and the US records also include the demagnetization results for the LT phase. The LT phase records for the LS and LN reversals have not yet been determined. The AF results will not be discussed in this paper. One should note that the magnetite and the LT phase records have inclination errors relative to NADF or RADF directions (section 5.2). The inclination error is about 10° for magnetite and probably less for the LT phase. The LT phase has a decay curve with a small temperature interval of non-overlap with either the viscous component and the magnetite phase. Relative to the magnetite results, a high statistical error is produced if the limited number of demagnetization data points are least-squares fitted.

For lack of a better method, the intensities of the magnetite and LT phase are compared with an ISR acquired in a 2 T field and beside, for the UT and US records, with the remanence which remains after a 300 mT AF demagnetization of the ISR (ISR_{AF}). The ISR and ISR_{AF} are considered to be related with the contribution to the primary component of respectively: LT phase+magnetite and LT phase (Section 5 and 6). The ISR_{AF} records must be considered with caution since locally minerals with high coercive forces (e.g. hematite) may contribute to the ISR_{AF}. One should also notice that the ISR fraction which remains after an AF demagnetization in a 300 mT field is small (<10%) relative to the initial ISR.

The demagnetization results of specimens from sedimentary intervals near the boundaries between the HCU's and LCU's often do not answer to the criteria of section

5.3. For this reason they were omitted.

The accumulation rate variation will be discussed in section 10. Prior to this discussion the duration of the observed directional and intensity variations will be given in cm. Table 2 provides an overview.

Table 2 Durations of reversal features

Reversal	UT		LS		US		LN	
	a	b	a	b	a	b	a	b
1.Anom. Intensities	26.0	26.0	1.3	1.9	5.0	7.7	2.1	4.0
2.Anom. Directions	17.0	17.0	2.5	3.8	10.0	15.4	4.1	8.0
3.Major declinations	1.0	1.0	0.6	1.0	0.5	0.8	0.3	0.7
4.Major inclinations	3.0	3.0	1.3	1.9	2.0	3.1	2.1	4.0

Table 2. Durations (in kyr) for observed changes (row 1-4) in the studied reversal records. Columns (a) denote durations relative to the accumulation rates from this study. Columns (b) denote durations calculated with accumulation rates from Zijderveld et al. (1986).

8.1 upper Thvera polarity transition

The length of the sampled and investigated sedimentary interval is 250 cm. It comprises two LCU's, one complete HCU and a lower part of another HCU. Figures 8a,b show the thermal demagnetization results for the magnetite and the LT phases respectively. Transitional magnetite and LT phase magnetizations related to the upper Thvera N-R reversal are observed in the lower HCU (43 cm) and in the upper LCU (78 cm). It should be noted that the directional changes in the LT phase record have higher amplitudes than those in the magnetite record. For both records similar directional changes seem to take place at identical sedimentary levels. Starting at the base of the lower LCU, the directional changes are as follows: the record starts with near NADF directions showing a slight oscillation. At the base of the lowermost HCU the directional changes observed in the declination record intensify. They are accompanied by a gradual steepening of the inclination in the interval from 55 to 75 cm. Subsequently, the inclination decreases to near-zero values in the interval from 75 to 95 cm. Above this interval the inclination returns to near NADF directions before it changes to negative values at the 106 cm level. Above the 106 cm interval the declination and inclination show a damped oscillation

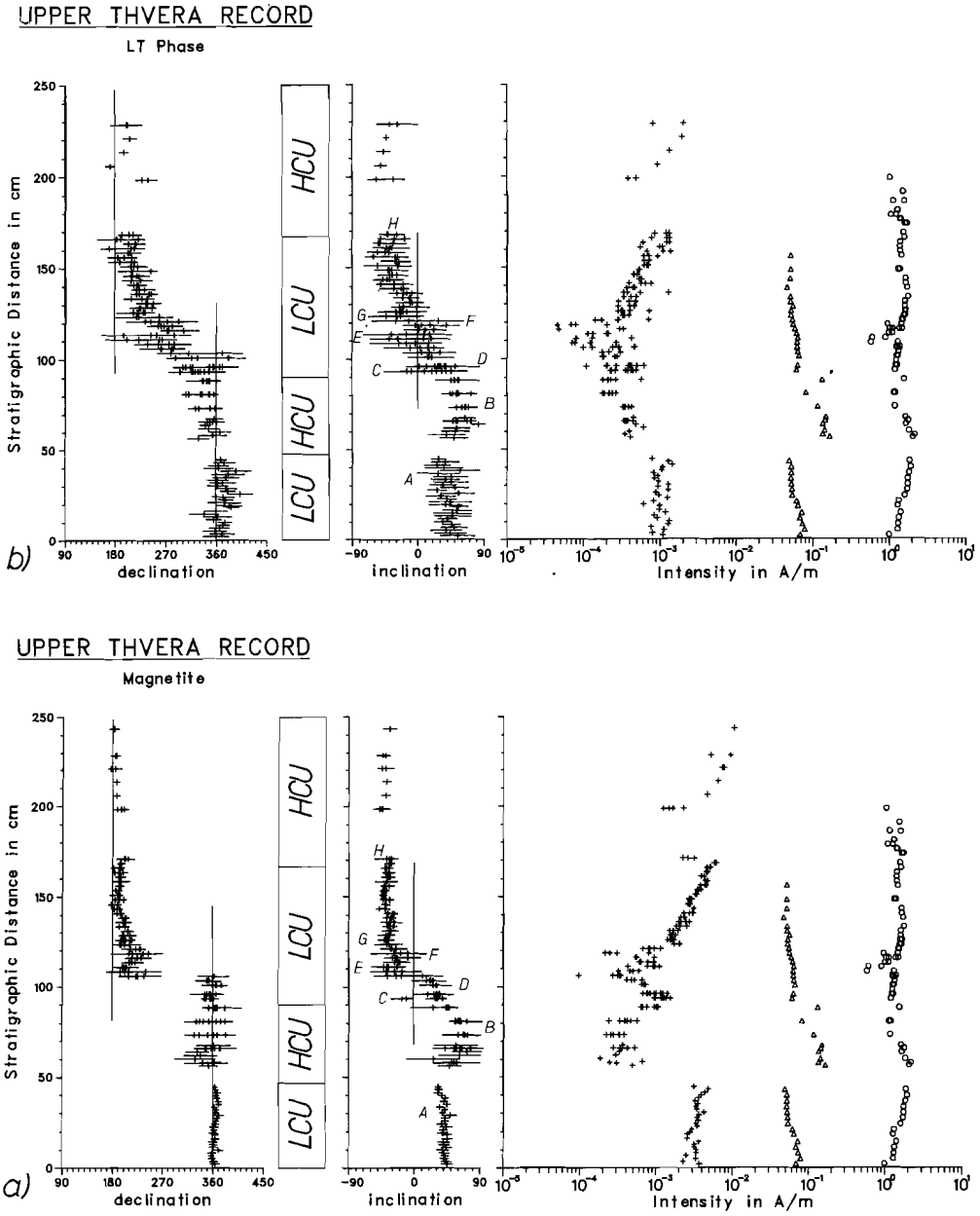

Fig. 8. upper Thvera reversal records for the magnetite (a) and LT phase (b). The error bar represents the maximum angular deviation (Kirschvink, 1980). The circles denote the ISR, the triangles denote the ISR_{AF}. Characters refer to virtual geomagnetic poles in figure 12.

which almost disappears at the 150 cm level. Above the 150 cm level only near RADF directions are observed.

The magnetite and LT phase intensity records show lowered values between the 50 cm and the 170 cm levels. A minimum intensity is present at the 106 cm level in the magnetite record and at 118 cm in the LT phase record. Both minima do not correlate with the ISR minimum at 110 cm. The records demonstrate that the minimum intensity is ~5% of the maximum intensity. The LCU unit between 93 cm and 158 cm is characterized by fairly constant ISR_{AF} values. The experiments which underlie figure 5d (AF decay curves of ISR) are made with specimens from the interval near the ISR minimum at the 110 cm level. The constant ISR_{AF} values in this interval suggest that the minimum is caused by bulk-rockmagnetic changes (in concentrations and/or grain sizes) of magnetite. The intensity variation of the magnetite and LT phase in the lowermost HCU unit is somewhat obscured by bulk-rockmagnetic changes. Since the ISR_{AF} values in this interval are high relative to the ISR values, one is led to the assumption that this maximum is caused by bulk-rockmagnetic changes of the LT phase. This correlates with the observation that the intensity decrease in the lower HCU is more significant for the magnetite record than for the LT phase record.

8.2 lower Sidufjall polarity transition

The sedimentary interval, containing the lower Sidufjall R-N reversal record, has a length of 50 cm. The record comprises the lowermost part of an HCU (fig. 9). A preceding investigation already ascertained the fact that the reversal is recorded in a small sedimentary interval. Therefore, this interval was sampled closely both with horizontally and vertically drilled cores. Figure 9 shows the thermal demagnetization results for magnetite. The demagnetization results for specimens (slices with a thickness of 0.9 cm) from the vertical core are connected by straight lines.

The reversal is recorded as follows. In the interval between the 10 and 18 cm levels the inclination slightly steepens (from -40° to -60°) whereas the intensity increases ~20%. At the 18 cm level the intensity starts to decrease. From the 20 cm to the 23 cm level the intensity decrease is accompanied by a change to eastward and steeply downward directed magnetizations. From the 23 cm to the 27 cm interval the intensity increases whereas the declinations and inclinations turn to near NADF directions. The intensity at the 10 and 27 cm level are nearly identical. The intensity minimum at the 23 cm level is 20% of the

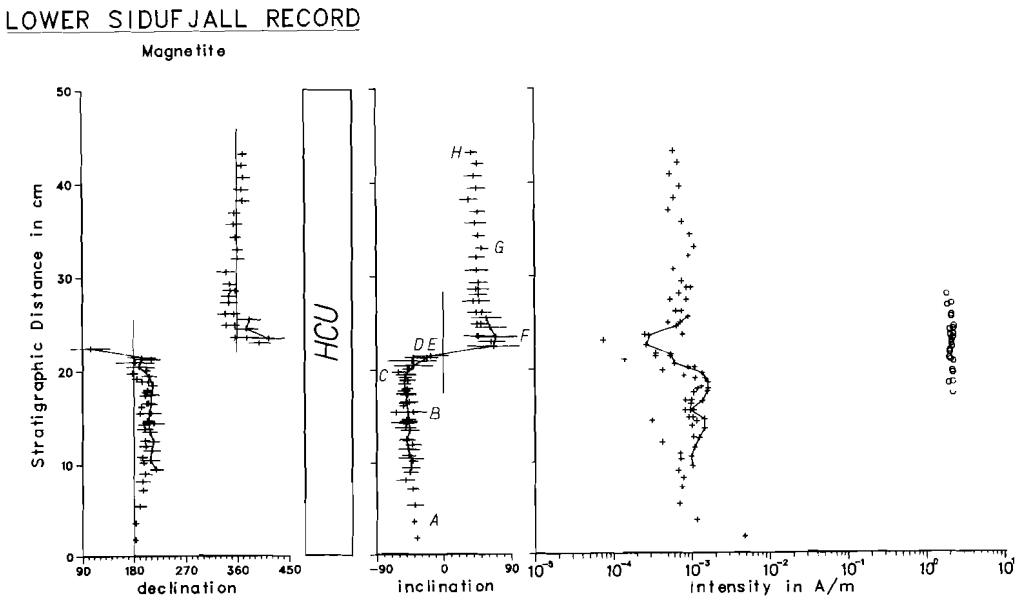

Fig. 9. lower Sidufjall reversal record for the magnetite phase. See also caption figure 8.

intensities at the 10 and 27 cm levels whereas it is 15% of the intensity at the 18 cm level. The ISR is constant in the interval from the 17 to the 28 cm level. Note that the minimum intensity coincides with steeply downward directed magnetizations.

8.3 upper Sidufjall polarity transition

The investigated sedimentary interval has a length of 150 cm, containing an HCU (104 cm) and an overlying LCU (46 cm). The upper Sidufjall N-R reversal is recorded in the HCU. The thermal demagnetization results of the magnetite and the LT phase are depicted in figures 10a,b respectively.

The reversal proceeds as follows. The record starts with near NADF directions. After an initial increase, the inclinations shallow near the 20 cm level. Low inclinations are recorded in the interval between the 20 cm and the 40 cm level. The lowered inclination values are accompanied by an intensity increase.

Near the 40 cm level the intensities decrease. The decrease is sudden and sharp in the LT phase record whereas it is gradual in the magnetite record. At the level where the intensities starts to decrease the magnetizations become more steeply downward directed. Again the change is rapid in the LT phase record and gradual in the magnetite record. Up to the 44 cm level the declination values show an increasing rate of variation. At the 44 cm level the declinations swing to near-south (magnetite record) and south-west (LT phase record). The declination returns to north near the 60 cm level. The sense of movement of the declination near the 40 and the 60 cm level suggests that the first swing is eastward directed, whereas the return is westward directed.

The interval between the 42 cm and the 87 cm level is characterized by low intensities, steep downward directed magnetizations and a major variation of the declination. Concurrently with high inclinations, declinations are of course always poorly defined. In the interval between the 42 and the 87 cm level the variation of the inclination in the magnetite record is between 35 and 80°, whereas it is between 50 and 85° in the LT phase record.

Between the 87 cm and 93 cm level the inclinations and declinations change to near RADF directions in both the magnetite and the LT phase records. However, in the interval from the 93 cm to 100 cm level the inclination again shallows. In the LT phase record the shallowing of inclination is accompanied by an intensity high. The intensity high is hardly observed in the magnetite record. At the 100 cm level the magnetization becomes steep upward directed. This change is more rapid in the LT phase record than it is in the magnetite record. In the LT phase record the steepening of inclination is accompanied by an intensity low.

Above the hiatus in the record of demagnetization results the directions are close to the RADF, whereas the intensities tend to increase.

The intensity records of the magnetite and the LT phase in the HCU are accompanied by constant or gradually changing ISR and ISR_{AF} records. The ISR_{AF} record of the LCU shows constant values, whereas the ISR record of the LCU shows strong variations (>10x). The ISR variations at the top of the LCU somewhat obscure the observed intensity increase in that part of the magnetite record. However, the nearly constant ISR_{AF} values of the LCU and the intensity increase in the LT phase record suggest that the increased intensities in the magnetite record are not (only) caused by bulk-rockmagnetic changes.

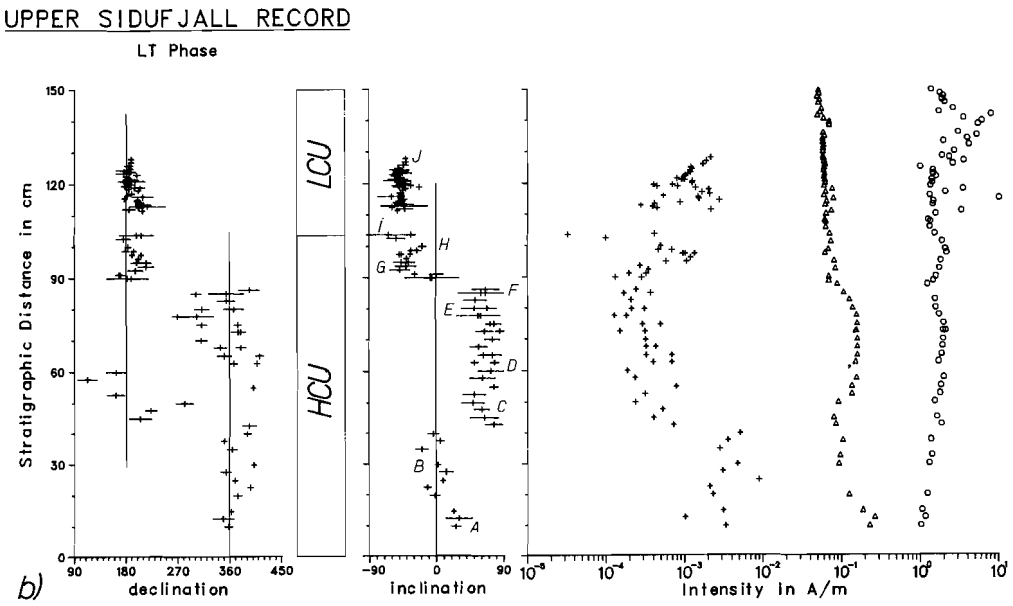

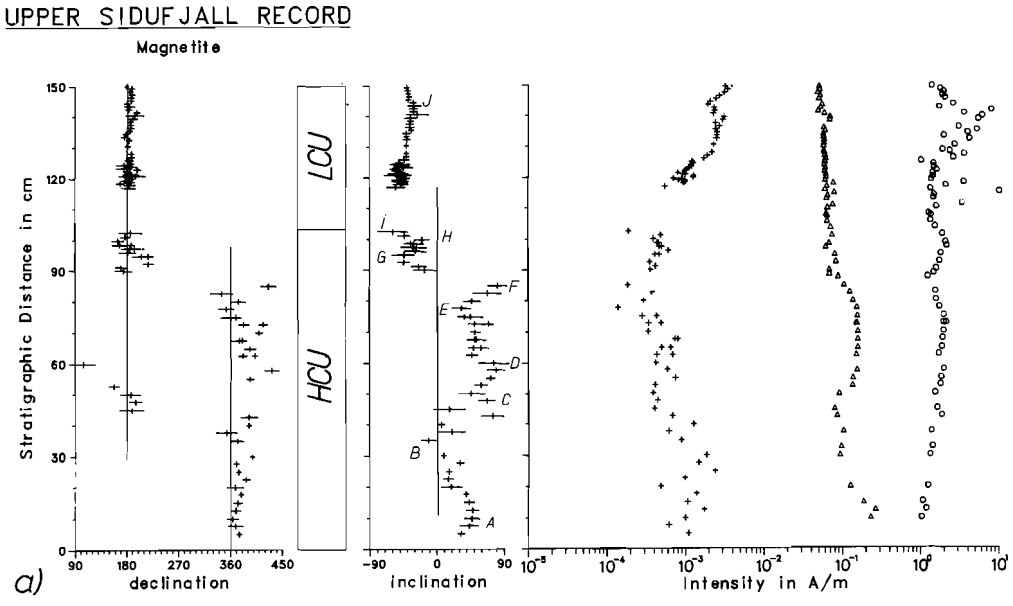

Fig. 10. upper Sidufjall reversal records for the magnetite (a) and LT phase (b). See also caption figure 8.

8.4 lower Nunivak polarity transition

The sedimentary interval which was investigated has a length 150 cm. It contains an HCU (73 cm) and an LCU (87 cm). The lower Nunivak R-N reversal is recorded in the HCU. Figure 11 shows the thermal demagnetization results for the magnetite phase.

The directional and intensity changes which accompany the reversal are as follows. From the base of the record, where near RADF directions are observed, the magnetization becomes gradually more steeply upward directed (up to 50°). At the 42 cm level the inclination starts shallowing. Near the 53 cm level the inclination is zero. Between the 53 cm and the 60 cm interval the magnetization becomes progressively more steeply downward directed. At the 60 cm level the mean inclination value is >70°.

Above the 60 cm level the inclination shallows to near NADF directions. Near the 60 cm level the declination record shows only one sudden change with no intermediate directions. The level at which this change occurs nearly coincides with the level at which the inclination becomes steep downward directed. The intensity record shows a "V" shaped intensity low. The intensity minimum is near the 56 cm level. The nearly constant ISR record from the 40 to the 80 cm level suggests that the intensity low is not caused by bulk-rockmagnetic changes. The minimum intensity is ~10% of the intensity prior to and after the reversal.

9. Virtual Geomagnetic Poles

Figures 12 show the virtual geomagnetic poles (VGP's) for the demagnetization results from section 8. One should note that the results have an inclination error. As a result of this error the VGP's of the near RADF or near NADF directions are respectively near- and far-sided. The corresponding characters in the projections of the VGP's and in the records of demagnetization results relate specific directional features.

Respectively, the VGP's of the upper Thvera record move: from a far-sided location

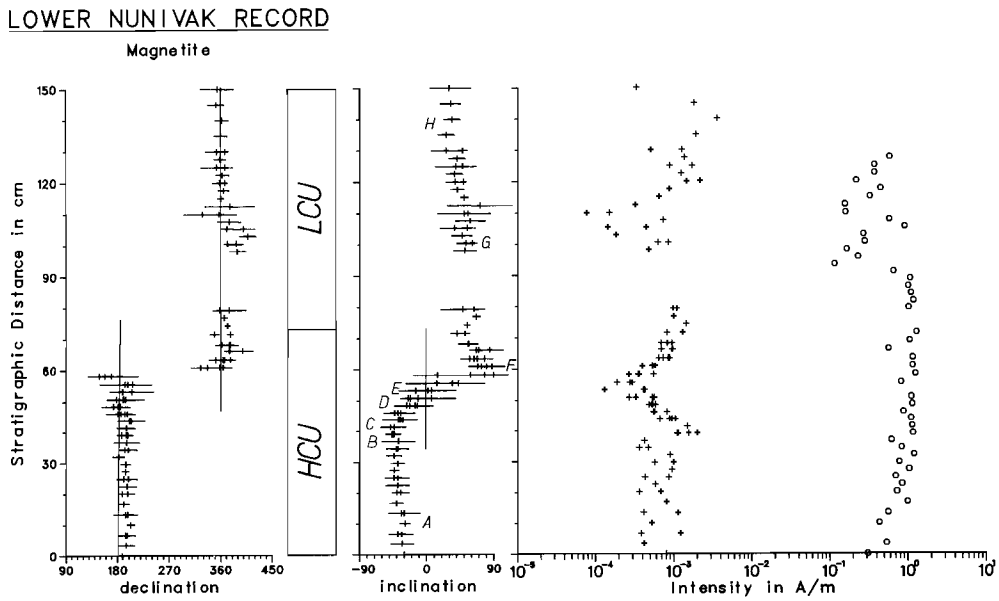

Fig. 11. lower Nunivak reversal record for the magnetite phase. See also caption figure 8.

at 80°N (A), to the geographic pole (B), to a far sided location at 70°N (C) and back to the far sided location at 80°N (D). The westward declinations between the directional features (D) and (E) cause the VGP's to be confined to a great-circle ~90° west of the site meridian. The oscillation (E-F-G) proceeds along the same great-circle. The directions become stable at a near-sided location at 70°S (H).

The VGP's of the lower Sidufjall and the lower Nunivak record move: from a near-sided location at 70°S (A), to the geographic pole (B), to a near-sided location at 70°S (C), along a path 30°E of the site meridian (LS) or along the site meridian (LN) (D,E), to a location at the latitude of the site (F), to the geographic north pole (G) and at last to a far-sided location at 80°N (H).

The VGP's of the upper Sidufjall move: from a far-sided location at 80°N (A), to a far sided location at 60°N (B), near a location on the site meridian at 30°S (C), to a location near the equator (D), back to a far-sided location at 80°N (E), to a near-sided location at the latitude of the site (F), to a near-sided location at 60°S (G), to a near-sided location on the site meridian at 60°S (H), to a location near the antipodal site (I), and at last to a near-sided location at 70°S (H).

10. Discussion

Sedimentary reversal records are formed during a period of high geomagnetic field variation per unit time. Reports on depositional realignment (Tucker,1980) and smoothing (Hoffman and Slade,1986) provide valuable information about the acquisition of remanence in sediments. The synthetic records in these reports have been actually observed. For instance, Tauxe and Badgley (1984) found four magnetic phases in red beds

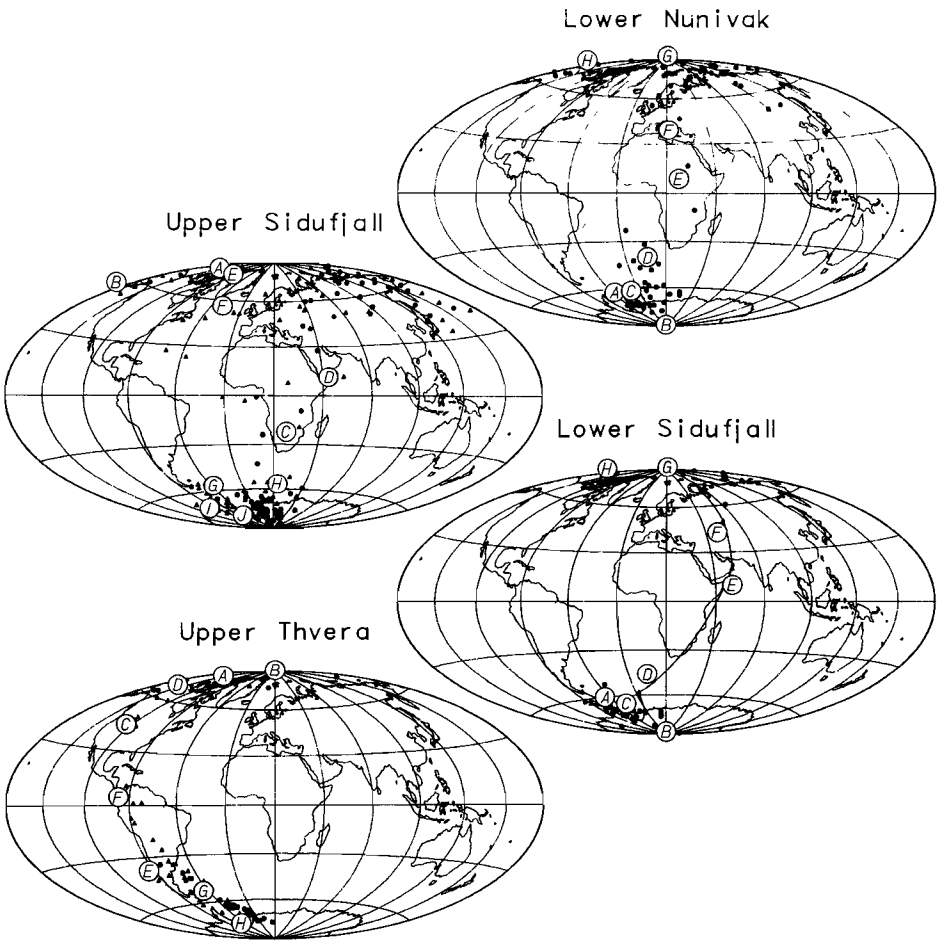

Fig. 12. Virtual geomagnetic poles of the reversal records in Aitoff projections of the earth centred around the site meridian. Character refer to corresponding labeled directions in the reversal records (fig. 8-11).

each with a different timing of remanence acquisition giving delayed transitional paths for these phases.

In the present study we observed a different behaviour for the two magnetic phases that comprise the primary component (Section 5.2, 5.3, 8.1 and 8.3). Different directions are observed during periods of stable polarity and of polarity reversal. In view of the directional records of magnetite and the LT phase of the same reversal in which corresponding directional changes occur at the same sedimentary level, one is led to the conclusion that these phases do not produce significantly delayed records.

However, the same records demonstrate convincingly that the directional variations of the LT phase exceed those of the magnetite phase. It is therefore tentatively concluded that the remanences of the LT phase produce a less smoothed record of geomagnetic field behaviour than the remanences of the magnetite phases.

Each of the sampled polarity transition records resides for the greater part in a specific HCU or LCU. In order to make a more realistic estimate of the duration of the sampled polarity transitions one needs to have knowledge of the accumulation rates of the HCU's and LCU's separately. The accumulation rates were estimated by comparing the accumulated thicknesses of the HCU's and LCU's (provided by Zijderveld and corrected by the author for the exact location of each reversal record) with the known durations of the adjacent polarity intervals. In this section, the mean accumulation rate for a polarity interval gradually decreases with increasing age. One can calculate mean accumulation rates for the HCU's and LCU's in adjacent polarity intervals if the assumption is made that the accumulation rates of the HCU's and of the LCU's are constant (two equations and two unknowns). If this method is performed on all neighbouring polarity intervals, the result is a moving average of the accumulation rate.

Minor variations in the accumulation rate will be smoothed in the moving averages of the accumulation rate. However, an overall trend in the accumulation rate will be unaffected. The method has not been used with the Sidufjall subchron and the overlying reversed polarity interval since the mean accumulation rates in these polarity intervals are too distinct to yield realistic estimates.

The results are depicted in figure 13. It appears that the increase in the accumulation rate from 4.9 to 7.6 cm/kyr is due to an increase in carbonate influx. This caused the accumulation rate of the HCU to dominate the increase of the accumulation rate of the

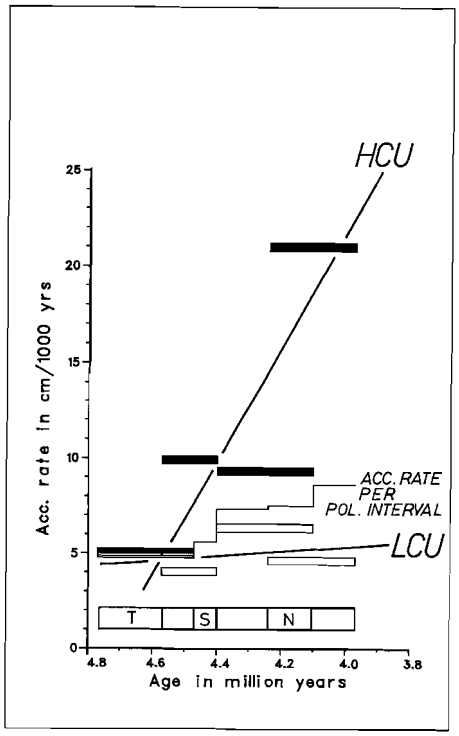

Fig. 13. Accumulation rates for 6 successive polarity subzones from the Gilbert Chron (thin solid line). The normal polarity intervals are indicated (in the inset) as T (Thvera), S (Sidufjall) and N (Nunivak). The calculated mean accumulation rates for the HCU (closed boxes) and the LCU (open boxes) in two successive polarity intervals have been least-squares fitted (thick solid lines).

LCU by a factor 3 during the time interval between the UT and the LN reversal. The accumulation rates of the sediment containing the reversal records were obtained from a least-squares fit of the calculated HCU and LCU accumulation rates; although these values will probably not be absolutely accurate they are thought to be more realistic than those corresponding to the duration of the polarity intervals and total (HCU+LCU) sediment thicknesses.

This approach is supported by the fact that the lengths of the quite similar lower Sidufjall and the lower Nunivak reversal records, which are both recorded in a HCU, are different by a factor three. The durations of these reversal records are identical if the above-described method is used to calculate the accumulation rates.

The durations of the directional and intensity changes related to the reversals records (section 8) are produced in table 2. The durations which were calculated from the accumulation rates of Zijderveld et al. (1986) as well as the durations calculated from the above described method are given. It should be noted that the duration of the major directional changes that give rise to a change in magnetic polarity take place in very short time intervals. This time interval is shortest for the change in declination for the three youngest reversals.

A comparison of the four studied reversal records demonstrates the high degree of similarity between the two R-N reversals records (LS and LN). The points of differences between the LS and LN reversal are the moment at which the intensity minimum is observed and the sense of movement in the declination records. The LS record suggests an intensity low at the moment when the inclination is nearly vertical, whereas the LN suggests an intensity low at the moment when the inclination is near zero. It is hoped that further investigation (e.g. production of LT phase records and ISR_{AF} records) will provide information that indicates whether this effect is real or is produced during the remanence acquisition. The declination record of the LS reversal suggests an eastward sense of movement (rapid and late in the record) whereas no intermediate declinations are observed in the LN record.

The UT reversal record shows a number of directional oscillations. During these oscillations there is an intensity low. A second short-period intensity low is observed at the level where the inclination changes sign. It is not clear whether this second intensity low is real or is caused by rockmagnetic changes.

The US reversal record seems to be most complicated. The record shows a characteristic phenomenon: a shallowing of the inclination accompanied by an intensity high and a subsequent steepening of the inclination accompanied by an intensity low. This feature is also observed above the major directional change (actual reversal?). There seems to be some kind of symmetry between these directional and intensity changes.

When the dipole field is absent for a long period of time, as seems to be the case in the upper Sidufjall transition, the record of the (steeply downwards directed) remaining field suggests a westward trend.

The projections of the VGP's calculated from the intermediate directions demonstrate that all directional changes in the reversals, including the rebounds, are confined to a path along a specific great-circle. For the UT reversal this path is along a great-circle ~90°W of the site meridian implying a non-zonal transitional field. The LS reversal is zonal with a minor contribution of non-zonal terms. The US reversal shows major directional changes in the vertical plane but the directional changes in the horizontal plane are either near south or near north; it indicates a mainly zonal transitional field behaviour. The LN reversal is clearly confined (within 30°) to the site meridian and again suggests the presence of a zonal transitional field geometry. One is led to the conclusion that there is a trend in the dominance of the zonal field. The zonal field seems to be less significant in the UT record whereas it is most dominant in the LN record.

The rebounds from the UT and US reversals are quite similar to the "stop and go" movements observed in the Steens Mountain record (Mankinen et al., 1985; Prevot et al., 1985).

The phenomenological "standing field" model of Hillhouse and Cox (1976) and the "flooding" model of Hoffman (1977,1979) provide transitional field geometries. The standing field model is based on the assumption that the dipole field decays and is subsequently rebuild in the opposite sense while a standing field remains. The standing field may be zonal and/or non-zonal. In the flooding model it is assumed that the reversal process is initiated at localized point in the fluid core and then floods through the rest of the core. The flooding model assumes zonal transitional fields although moderate non-zonal terms can also be incorporated. The standing field model predicts identical VGP paths for successive polarity transitions from the same site.

Identical VGP paths for successive reversal records in the flooding model imply that, 1) in case of an octupolar transitional field, the reversal process in one of the two identical transitions is simultaneously initiated in different hemispheres of the core or, 2) in case of a quadrupolar transitional field the reversal process is initiated in one region but in different hemispheres of the core.

Regarding the sequence of four reversal records as a whole, neither the flooding model nor the standing field model easily fits the results. The flooding model does not fit the results since the UT reversal seems to be dominated by non-axisymmetric terms.

The standing field model only fits the results if it can be assumed that the standing field changed from zonal to non-zonal between the upper Thvera and the lower Sidufjall.

The descriptive zonal harmonic model of the Matuyama-Brunhes (R-N) reversal provided by Williams and Fuller (1981) fits the LS and LN (R-N) reversal records. For the latitude of Calabria the model predicts 1) a "V" shaped intensity low which is ~10% of the original field and 2) high inclinations late in the reversal (after the inclination changed sign). Clement and Kent (1984,1985,1986) report records of the upper Olduvai (N-R) and lower Jaramillo (R-N) reversals. The records are from sedimentary deep-sea cores from southern and northern latitudes. They suggested that during these reversals a standing field was present with a harmonic content which was slightly different compared to the Matuyama-Brunhes reversal. Actually, the energy distribution to the different zonal terms was identical, they merely changed the signs of the zonal G_2 and G_4 terms. No reversal of the zonal G_3 term was observed. In doing so, the inclination record for different hemispheres mirrors with respect to the horizontal plane. The observation in the present study of a set of older reversals with a harmonic content nearly identical to the Matuyama-Brunhes reversal leads to the speculation that one or more of the low-order even zonal terms reverses polarity on a time scale larger than the dipole field. The above quoted reversal records span a period of ~3 million years. It should be noted that the zonal harmonic contents of the upper Olduvai and lower Jaramillo reversal records provided by Theyer et al. (1985) and Herrero-Bervera and Theyer (1986) are different from the records provided by Clement and Kent. Within the context of the zonal harmonic approach there is no explanation for these differences.

It is expected (Bogue and Coe, 1984) that a zonal reversal process which is dominated by quadrupolar terms gives records in which the intensity decrease is strongly latitude dependent (near 45% of the original field at 0° latitude and near 35% at 35° : the latitude of Calabria). The relation between latitude and paleointensity in a reversal is nearly absent when octupolar terms dominate the reversal process (near 20% of the original field intensity for all latitudes).

The observed intensity minima in the studied reversal records range from 5 to 15% of the intensities that are observed at the onset of the reversal. If we consider that the relative intensity decreases are related to the paleointensities, then the records argue for a dominating presence of octupolar or even higher-order terms.

Bogue and Coe (1982,1984) report results of a study of two successive (R-N-R) reversal records in lavas from Kauai, Hawaii, with a K-Ar age of 4.5 to 5.6 Myr for the R-N transition. This age corresponds either to the succession lower Thvera, upper Thvera transitions or to the succession formed by the last normal subchron of Chron 5. Since the K-Ar dating method may easily yield errors of 0.1 Myrs for these ages (Mankinen & Dalrymple, 1979), the Kauai results may also correspond to the lower and upper Sidufjall successions.

The Kauai results strongly suggest near-sided axisymmetric geomagnetic field behaviour during both polarity transitions. The Calabrian upper Thvera reversal is non-axisymmetric and consequently does not fit the Kauai results. The Calabrian lower Sidufjall reversal has a slight offset from an axisymmetric transitional field, whereas the upper Sidufjall reversal is, on the whole, axisymmetric. On the base of this information, the Kauai records might fit the Calabrian LS and US records. However, the paleointensity study for the Kauai R-N reversal, which provides evidence for a two stage intensity decrease, does not fit the Calabrian LS results.

Since the studied reversal records appear to have intrinsic features which are unique, it seems worthwhile considering whether they can be used as dating tools for this region. If more remote records of these reversals become available and if they can be generalized, it might be possible to use reversal records as dating tools on a world-wide scale.

Acknowledgements

Prof.Dr. J.D.A.Zijderveld, Dr. F.Heller and Dr. C.G.Langereis are thanked for their criticism, Dr. K.A.Hoffman for his suggestions and Mrs. McNab for the linguistic corrections. T.A.T.Mullender and H.K.Thio are thanked for their assistance in the field. The author is much indebted to H.J.Meijer for the enormous numbers of measurements he

Chapter III

A succession of five early Pliocene geomagnetic reversal records from the Mediterranean.

1. Introduction

A detailed magnetostratigraphic study of the Lower Pliocene Trubi formation correlated the sedimentary succession exposed in the Monte Singa composite section (fig. 1; 38°15'N, 16°12'E) to the geomagnetic polarity time-scale (Zijderveld et al., 1986). It was shown that the base of the Monte Singa composite section starts at the Miocene-Pliocene boundary, just below the Thvera subzone and that the top of the section extends to the reversed polarity zone above the normal Cochiti subzone. The ages of the lowermost and uppermost part of the section are 4.9 and 3.9 Ma.

The preliminary results of the lower four successive geomagnetic reversal records exposed in the Monte Singa section have been reported earlier (Linssen, 1988): the oldest reversal in this succession is the upper Thvera, the overlying reversals are respectively the lower and upper Sidufjall and the lower Nunivak. The reversals occur in the Gilbert chron and cover a time-span of 0.33 Ma. The four successive reversal records show that the major directional changes of the polarity transitions occur within a short time span of 0.5-2.5 kyr (Linssen, 1988).

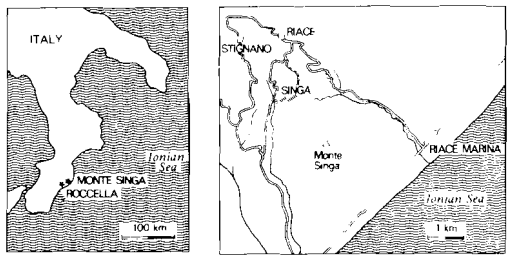

Fig. 1 Location of the Monte Singa section in Calabria (S.Italy).

In the present paper the results of the upper Nunivak reversal record from the same Monte Singa section are reported. In addition, the four preceding reversal records (Linssen, 1988), including some new data, are reviewed and discussed.

2. Geology and sampling

The marine sediments from the Monte Singa section are part of the Lower-Pliocene Trubi formation. The sedimentary succession is composed of rhythmic alternating layers of marls with high- and low-carbonate contents which are denoted as high- and low-carbonate units (HCU and LCU) respectively. The base of a rhythmite is placed at the base of a LCU (Hilgen, 1987). The layer thickness of the individual units is laterally constant on the scale of the exposure and the layer thickness of the different units varies from 0.1 to 1 meters. The bedding tilt in the Monte Singa section is uniform: 6° SSE.

On the basis of the magnetostratigraphic data from Zijderveld et al. (1986), the accumulation rate of the sediment in the Monte Singa section was shown to increase from

Table 1. Accumulation rates of sediment near the geomagnetic reversal records

Reversal	Unit	MgnStr	Precession	
			(1)	(2)
lower Thvera	HCU&LCU	4.8	3.4	3.7
upper Thvera	LCU	5.1	5.8	5.2
lower Sidufjall	HCU	5.0	6.3	5.4
upper Sidufjall	HCU	6.3	8.3	9.6
lower Nunivak	HCU	7.6	10.1	7.5
upper Nunivak	HCU	8.1	9.2	8.4

Table 1. Accumulation rates for the sediment from the Singa section near the geomagnetic reversal records. The column "Unit" denotes whether the main part of the reversal is recorded in a HCU or LCU. The accumulation rates in the "MgnStr" column are calculated with the magnetostratigraphic data of Zijderveld et al. (1986) and are corrected for the exact location of each reversal record (Linssen, 1988). The accumulation rates from the "MgnStr" column are calculated by taking the average accumulation rate of the underlying and overlying polarity zones. The "precession" column results if it is assumed that the deposition of each HCU and LCU pair took place in 21.7 kyr, the average precession cycle. In the latter calculation two values are given since it is unknown with which of the neighbouring units the 21.7 kyr set is formed; column 1 (2) represents the combination with the lower (upper) unit. Lower Thvera data are obtained from unpublished data of the author.

5.0 cm/kyr for the Thvera subzone to 8.6 cm/kyr for the topmost part of the section. For the Nunivak subzone and the reversed subzone above the Nunivak the average accumulation rates are respectively 7.5 and 8.6 cm/kyr. The average value of 8.1 cm/kyr is a straightforward approximation of the accumulation rate of the upper Nunivak reversal record. The origin of the rhythmites is believed to be related to the precession cycle of the Earth's orbit (Zijderveld et al., 1986; Hilgen, 1987; Hilgen and Langereis, 1989), which has an average periodicity of 21.7 kyr. According to this hypothesis the accumulation rate of the HCU sediment enclosing the upper Nunivak reversal record is in the range 8.4-9.2 cm/kyr (table 1).

The upper Nunivak reversal record was sampled twice: in 1986 and 1987. The 1986 and 1987 sampling tracks are separated by a distance of 2 metres and have a stratigraphic length of respectively 80 and 25 cm. The position of the 1986 and 1987 records with respect to the lithology of the sediment is depicted in figure 10 and 11. The results of the 1986 sampling accurately located the upper Nunivak reversal. The actual reversal was shown to occur in a sedimentary interval of approximately 10 cm in a HCU with a thickness of 1.04 cm. The purpose of the 1987 sampling was to obtain more details of the upper Nunivak reversal record and special care was taken to acquire a high resolution and accurate stratigraphic control in the short reversal record.

Methods

Before sampling, the weathered surface of the sediment was removed in order to obtain fresh (blue coloured) sediment. The sampling equipment consisted of a water cooled electric drill powered by a generator and brass drilling cores, one inch in diameter. Both records were sampled from a grid of lines parallel to the bedding plane. The grid was marked on a plane which was cut nearly perpendicular to the bedding plane. The 1986 record was sampled with 3 or 4 cores per sampling level with a spacing of 2.5-5 cm. The 1987 record was sampled with 1 core per sampling level with a spacing of 1 cm. The cores were cut to specimens with a standard length of 22 mm. In order to obtain a better resolution of the reversal record, some of the cylindrical specimens were split into halves approximately parallel to the bedding plane. The exact position of each specimen was calculated incorporating both the orientation of the core and the bedding plane, the width

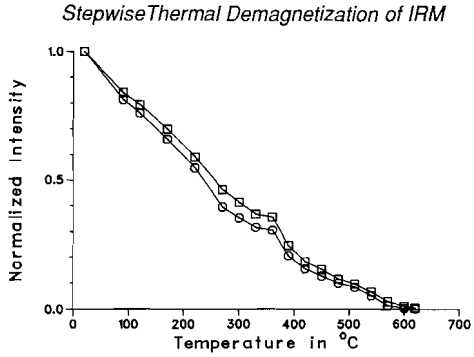

Fig. 2 Stepwise thermal decay curves of IRM acquired in a 2 T field. Demagnetization takes place just below 600 °C which indicates that magnetite is the dominant carrier of the IRM.

of the saw and the position of the specimen in the original core. The accuracy in sample position is better than 1 cm in the 1986 record and better than 0.5 cm in the 1987 record.

Stepwise progressive thermal demagnetizations were performed in tunnel furnaces with mu-metal shielding; the alternating field demagnetizations were done using a stationary holder (Zijderveld, 1967; Dankers and Zijderveld, 1981). Thermal demagnetization procedures were focussed on the suppression of laboratory induced viscous magnetizations due to the growth of superparamagnetic magnetite during heating to temperatures above 360 °C (Linssen, 1988, chapter 4). In addition, a partial thermo-remanent magnetization (PTRM) may be acquired by newly formed (pseudo) single domain magnetite in the low intensity magnetic fields ambient in the furnace, but minimizing the heating and cooling times of the specimens is successful in suppressing these effects to a large extent (Linssen, 1988). In the present study, the magnitude of a laboratory induced PTRM component was never in excess of 0.05 mA/m.

All measurements of the natural remanent magnetization (NRM) were made with a 2G-Enterprises cryogenic magnetometer having a sensitivity of 10^{-11} Am^2; the reproducibility of the measurements is better than 1° for magnetizations exceeding 10^{-9} Am^2. Analysis of the considerable amount of demagnetization data was done with the help of an in-house developed interactive and graphics-based computer program. Directions of the remanent magnetizations were calculated by means of least squares analysis (Kirschvink, 1980).

Continuous measurements of magnetization during heating were performed with a fluxgate spinner magnetometer; the temperatures of the specimens are controlled in a water-cooled furnace. Susceptibility measurements have been determined using an AC bridge (KLY-1).

3. Rock magnetism of the upper Nunivak record

The magnetomineralogy of the Monte Singa Trubi sediment has been investigated in detail and is the subject of a separate paper (Linssen, 1988; chapter 4). It was found that the characteristic remanent magnetization (ChRM) and IRM are carried by pyrrhotite and cation-deficient (CD) magnetite. The remanence of pyrrhotite is removed below 360 °C and the remanence of CD magnetite is removed below 580-620 °C (Heider and Dunlop, 1986). The (pseudo) single domain magnetite grains are 0.1-0.2 micrometer in the HCU's and less than 0.1 micrometer in the LCU's. The single domain pyrrhotite grains are smaller than 2 micrometer; no evidence has been found that the grain size of pyrrhotite is substantially deviant in the HCU or LCU. The average concentration of magnetite is approximately 5 ppm in the LCU and 20 ppm in the HCU, the average concentration of pyrrhotite is approximately 40 ppm in the HCU and 670 ppm in the LCU.

Above the upper Nunivak (N-R) reversal record the intensities of the natural remanent magnetization (NRM) rapidly decrease to values which are more than an order of magnitude lower than the intensities in the underlying sedimentary interval (Zijderveld et al., 1986). The origin of this decrease of the NRM intensity and the homogeneity of the magnetomineralogy in the upper Nunivak reversal record are the subjects of the present rockmagnetic investigation.

3.1 Thermal demagnetization of IRM

Specimens obtained from a HCU on either side of the level at which the NRM rapidly decreases have a maximum blocking temperature of 580°C (figs. 2,3). This indicates that magnetite is the dominant magnetic mineral in the HCU. The specimens obtained from the interval below the NRM drop level show a component with T_B~150 °C during a continuous thermal demagnetization cycle to 360 °C (fig. 3). This component is absent in the results of a second heating cycle of the same specimen with a new IRM_{2T}, indicating that its carrier is altered below 360 °C. A likely carrier of this component is

goethite (see Dekkers, 1988). The same component is not observed in the levels above the NRM drop level, nor was it observed in the lower part of the Monte Singa section (Linssen, 1988; chapter 4).

The contribution of pyrrhotite to the IRM_{2T} in HCU specimens from the lower part of the Monte Singa section has been assessed at 10%. However, in samples from the upper Nunivak record an increased decay between 330-360 °C, attributed to the presence of pyrrhotite (chapter 4), is not observed (figs. 2,3). Apparently, in that HCU interval the pyrrhotite contribution to the IRM_{2T} is below the detection limit.

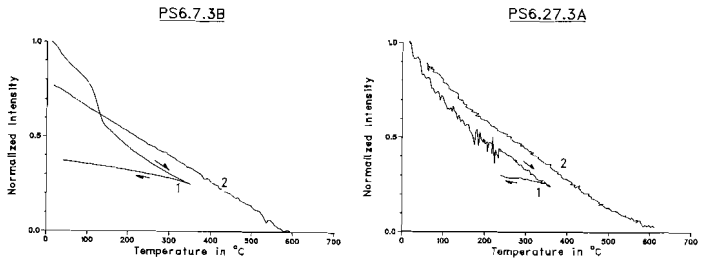

Fig. 3 Continuous thermal demagnetization of IRM in a two-step procedure. First the specimen acquires IRM in 2 T and is demagnetized at a maximum temperature of 360 °C (curve denoted "1"). Then the specimen again acquires an IRM and it is heated until no significant remanence is left (curve denoted "2"). All intensities have been normalized with respect to the initial IRM before the first heating cycle. Specimen PS6.7.3B (level 17.3 cm) and PS6.27.3A (level 48.4 cm) were obtained on either side of the stratigraphic level at which the NRM intensity drops. The decay curve of the first heating cycle shows no evidence for the presence of pyrrhotite. Magnetite (T_B~578°C) is the dominant magnetic mineral carrier of IRM in these specimens.

3.2 Records of rockmagnetic parameters

Records of rockmagnetic parameters provide insight in the origin of the ChRM intensity changes, i.e. they help to determine whether these intensity changes are introduced by rockmagnetic changes or by paleointensity variations. The variations of the susceptibility, IRM_{2T} and the related remanent coercive force (H_{CR}) in the 1986 and 1987 upper Nunivak records are shown in figure 10e and 11e.

The initial susceptibility shows virtually no variation (fig. 10e). The Monte Singa

Trubi consists of calcite, clay minerals (predominantly kaolinite and illite) and quartz. The estimated concentration of these minerals is respectively 55, 35 and 10% by weight (chapter 4). This mix of minerals produces a susceptibility of at least 80.10^{-6} SI (e.g. Collinson, 1983), predominantly determined by the clay minerals. Hence, the matrix susceptibility is 67% of the average susceptibility of 120.10^{-6} SI. As a consequence, the rockmagnetic variations in the sediment will not be fully expressed by the susceptibility. Of course, the buffering effect of the clay-mineral matrix also affects the validity of rock-magnetic methods which make use of the susceptibility parameter. For instance, the X/IRM (Dankers, 1978) and X/X_{ARM} (King et al.,1982) ratios characterize the grain size distribution of dispersed magnetite. However, the values of these parameters in marine sediments may not be compared to experimentally derived values without correcting for the unknown variation of the clay-mineral susceptibility. It follows that for the present sediment the remanent magnetic parameters provide a more solid basis for the interpretation of ChRM intensity changes.

The IRM_{2T} and H_{CR} values of LCU samples heated at 360 °C are virtually identical to the corresponding values of the unheated samples (fig. 10e). The absence of the typical IRM_{2T} and H_{CR} decrease, due to the alteration of pyrrhotite at 360 °C, indicates a small contribution of pyrrhotite remanence in the LCU. This is in contrast to the LCU's of the lower parts of the Monte Singa section (Linssen, 1988; chapter 4). It is concluded that magnetite is the dominant magnetic mineral in the upper Nunivak record, both below and above the NRM drop level and in the HCU and LCU.

The IRM_{2T} maximum below the NRM drop level and the decrease of IRM_{2T} and H_{CR} are related to the lithological change at the HCU/LCU boundary (fig. 10e). The NRM drop level at 45 cm is not only characterized by a ChRM decrease of an order of magnitude, but also by an IRM_{2T} intensity increase of an order of magnitude. The coincidence of the ChRM intensity decrease and the IRM_{2T} increase indicates that the origin of the ChRM intensity change is not related to a variation of the paleomagnetic field intensity, but rather to a rockmagnetic change of magnetite. However, variations in either grain size or concentration of magnetite affect the ChRM and IRM in the same sense, which is incompatible with the observations. A possible, but tentative explanation for this discrepancy is that above the NRM drop level, in contrast to the interval below this level, the IRM and ChRM are carried by different parts of the magnetite grain size spectrum.

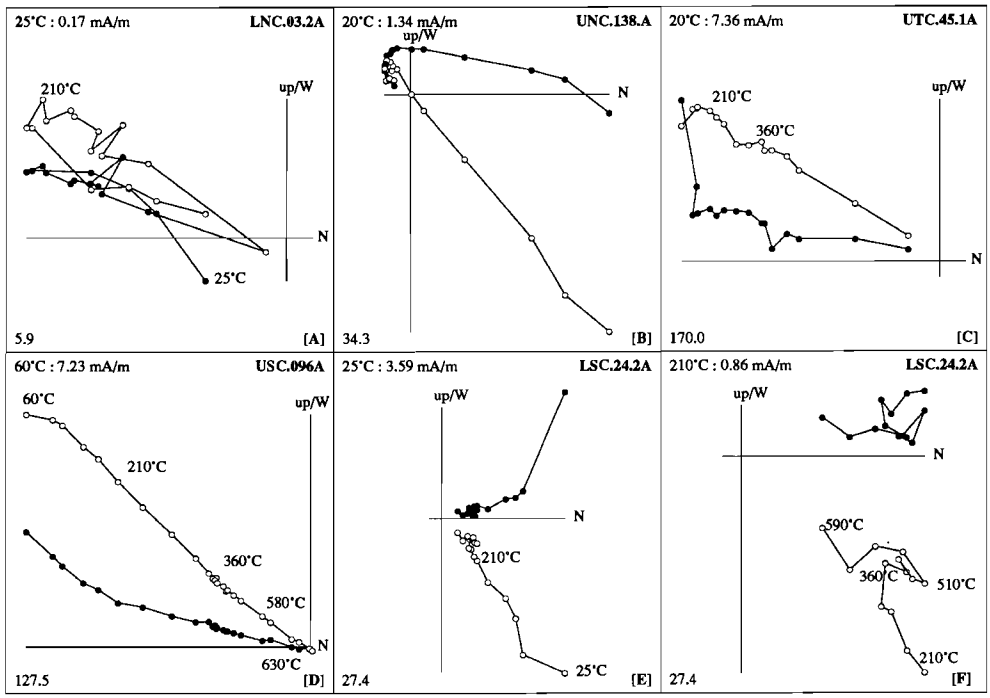

Fig. 4 Thermal demagnetization diagrams (orthogonal projections, Zijderveld, 1967) for specimens from various reversal records from the Monte Singa section. Open (closed) symbols denote projections on the vertical (horizontal) plane. The stratigraphic level of the specimens is indicated in the lower left corner of each diagram. The intensity at the first step is indicated in the upper left corner of each diagram. The last step is 590 °C unless indicated otherwise. Normal step sizes are 30 °C in the range 90-510 °C and 20 °C for temperatures above 510 °C. **[A]** Specimen LNC.03.2A comes from an HCU interval below the lower Nunivak reversal record (cycle 30, Hilgen and Langereis, 1988). The thermal demagnetization diagram shows the removal of a viscous component (20-120 °C), a secondary component (120-210 °C) and the composite ChRM component (>210 °C). **[B]** Specimen UNC.138.A comes from an HCU interval above the upper Nunivak reversal record. The diagram shows a large secondary and viscous component and a small ChRM component. **[C]** Specimen UTC.45.1A comes from an HCU interval above the upper Thvera reversal record (cycle 16). The composite ChRM component is dominated by the high-temperature magnetite component. **[D]** Specimen USC.096A comes from an LCU interval above the upper Sidufjall reversal record (cycle 23). The composite ChRM component consist of a low-temperature component (210-360 °C) and a high-temperature (cation-deficient) magnetite component (480-640 °C). **[E,F]** Specimen LSC.24.2A comes from an HCU interval in the lower Sidufjall reversal record (cycle 20). The enlargement [F] of the demagnetization diagram shows the medium-temperature component (360-480 °C) with, what appears to be, a reversed direction.

4. Demagnetization and directions of the stable ChRM

The NRM of specimens from the lower part of the Monte Singa section reflect two components with a characteristic remanent magnetization: Between 210 and 360 °C a pyrrhotite (low-temperature, LT) component is demagnetized and above 480 °C a magnetite (high-temperature, HT) component is demagnetized (fig. 4; Linssen, 1988; chapter 4). The secondary and viscous components are removed below 210 °C. The intensity of the secondary component demagnetized below 210 °C is small in the lower part of the Singa section (fig. 4 [A]; Linssen, 1988), but is relatively large for the sediment enclosing the upper Nunivak reversal (fig. 4 [B]). The ChRM components are easily distinguished from the secondary and viscous components by their maximum blocking temperature, but also by the fact that the ChRM direction is subject to an inclination error of 15 to 20° (See also Zijderveld et al., 1986; Linssen, 1988).

An additional medium-temperature (MT) component may sparsely be observed in the temperature trajectory between 360 and 480 °C. The MT component is only recognized as an additional component if its direction is clearly different from those of the LT and HT components. In a few cases the MT component has reversed directions at levels where the LT and HT components have normal directions (fig. 4 [E and enlargement F]). In this study, the presence of the MT component could only be demonstrated in small HCU intervals of the lower and upper Sidufjall reversal records. The presence of multiple deviant ChRM directions at a single stratigraphic level can be explained by a delay between the timing of remanence acquisition of the magnetic minerals. An alternative explanation for the presence of the MT component comes from the observed increase of IRM_{2T} between 360 and 480 °C (chapter 4), attributed to magnetite production during heating. The increase of the intensity of remanence carried by magnetite may yield an artificial reversed component. As a result of the sparse occurrence of the MT component in the Monte Singa section and the inconsistent relations between the MT component on the one hand and the pyrrhotite (LT) and magnetite (HT) components on the other hand, insufficient information is available to conclude about the origin of the MT component, or to conclude about the relation between the MT component and the other components.

To avoid problems with the interpretation of the intensities of the LT, MT and HT components the demagnetization data have been split in three groups of *quasi* blocking spectra with fixed start- and end-points: The demagnetization data between 210 and

360 °C, supposed to represent the ChRM carried by pyrrhotite (if present); the demagnetization data between 360 and 480 °C, supposed to represent the magnetization carried by the medium temperature component (rarely present) and the demagnetization data above 480 °C, supposed to represent the ChRM component carried by magnetite (always present). The linear components present in the three temperature trajectories, whether or not representing true LT, MT or HT components, have been determined and reported for all five reversal records.

The non-transitional directions of the ChRM carried by magnetite for the complete Monte Singa section are depicted in figure 5 and listed in table 2. The inclination error with respect to the local geocentric axial dipole field (57°) corresponds to $\tan I_o = 0.52 \, . \, \tan I_f$ (King et al., 1955; Verosub, 1977; Blow and Hamilton, 1978; Anson and Kodama, 1987), in which I_o and I_f are respectively the ChRM inclination and the geocentric axial dipole field inclination. The stable normal and reversed ChRM directions for the complete Monte Singa section, respectively 4.2° and 191.0°, yield an average declination of 7.6°. This deviation indicates that the sedimentary succession has rotated 7.6° clockwise after its deposition. Furthermore, the stable directions of the ChRM are not antiparallel; i.e. a 6.8° offset is present. This offset is attributed to non-zonal geomagnetic field components.

The average reversed non-transitional ChRM direction in the upper Nunivak record is statistically identical to the corresponding direction reported for the other reversal records (table 2). The average normal non-transitional direction is different: it is steeper and more northward directed. Hence, it is concluded that the onset of the upper Nunivak reversal is not completely recorded in the sampled interval.

Table 2 ChRM directions

	Polarity	Decl.	Incl.	a_{95}
Complete section	reversed	191.0	-38.5	1.3
	normal	4.2	39.9	1.7
upper Nunivak record	reversed	194.4	-43.9	7.6
	normal	359.6	52.1	1.8

Table 2. Average ChRM directions of magnetite in the sedimentary intervals adjacent to the upper Thvera, lower and upper Sidufjall and lower Nunivak records and the average non-transitional ChRM directions in the sedimentary intervals adjacent to the upper Nunivak record. The correction for the bedding tilt has been applied. The average directions were calculated with Fisher (1957) statistics.

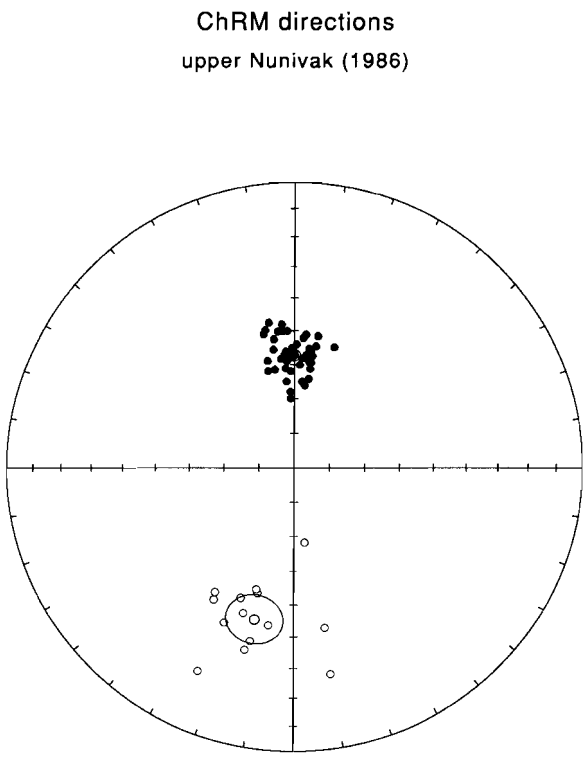

Fig. 5 Non-transitional ChRM directions of the upper Nunivak record in equal area projection. The thin ovals represent the angles of confidence calculated according to Fisher (1957).

5. Five sequential reversal records

5.1 The upper Thvera, lower and upper Sidufjall and lower Nunivak reversal records revisited

The preliminary results of the upper Thvera, lower and upper Sidufjall and lower Nunivak reversal records have been reported previously (Linssen, 1988). An extension of the data set, the subdivision in quasi blocking temperature spectra and a recalculation of the stratigraphic position of the specimens incorporating the position of all specimens in the original drilling core have provided a more detailed picture of these

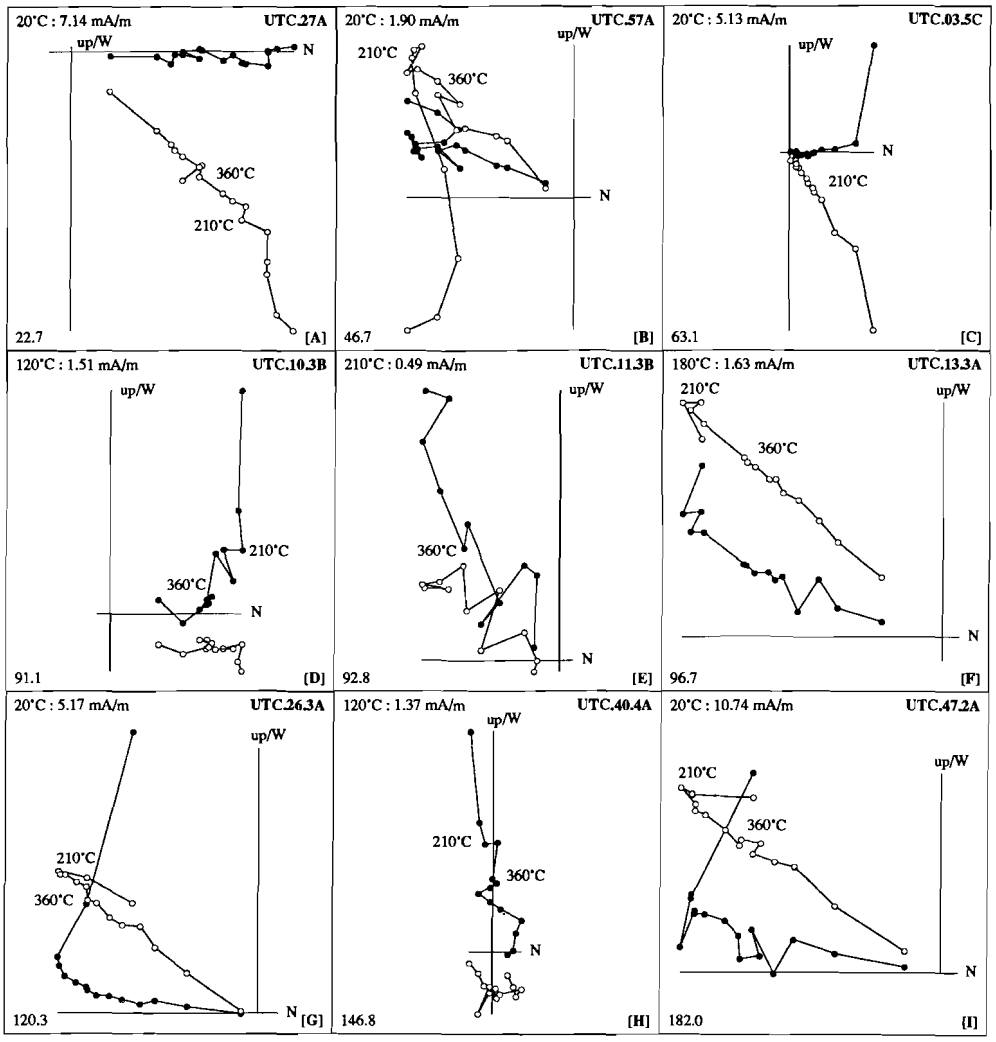

Fig. 6a Thermal demagnetization diagrams for specimens from the upper Thvera reversal record. See also caption fig. 4.

reversals (figs. 6,7,8,9; table 3).

The upper Thvera N-R record has been sampled in a sedimentary interval of 200 cm, enclosing two LCU/HCU alternations. The HT (magnetite) and the LT (pyrrhotite) components are both well defined in the upper Thvera record (fig. 6a). The 360-480 °C

component has the direction of the HT magnetite component (fig. 6d); probably this component corresponds to the 360-480 °C temperature range in the blocking spectrum of the HT component, rather than to an additional MT component.

The multiple lithological changes in the upper Thvera record complicate the observation of transitional directions of the reversal. Each of the lithological changes may introduce anomalous directions which are not directly related to the reversal. For instance, the reversed directions and the rapid intensity decrease of the LT and HT components close to the 48 cm unit boundary indicate an early remagnetization (fig. 6a [B],b,c,d), the normal directions and the rapid intensity decrease at the 146 cm level indicate a late, possibly secondary, remagnetization (fig. 6a [H],b,c,d). The changes are most prominent in the record of the HT component, although they are also noticeable in the record of the LT components.

Transitional directions of the upper Thvera reversal are observed immediately above the lithological change at the 48 cm level and continue to the 120 cm level. The actual upper Thvera reversal has its centre between the 90 and 100 cm levels; in this interval the largest directional changes are observed. Apart from the directional changes at the actual reversal, additional oscillations are present below (inclination: 60-80 cm) and above (declination, inclination: 100-120 cm) the actual reversal. Close to the lithological boundary at the 90 cm level the LT and HT components have different directions, i.e. the HT magnetite component is biased to present-day field directions, whereas the LT component shows transitional directions. It is plausible that these differences are caused by rockmagnetic changes of the carrier of the HT component accompanying the lithological change at the unit boundary.

The lower Sidufjall R-N reversal record is one of the least complicated records in the Monte-Singa section. It is recorded in the middle of a HCU and shows no significant variation of rockmagnetic parameters (fig. 7), or geochemical parameters (chapter 4). The MT and the LT component are not well developed in the lower Sidufjall record; the 210-480 °C temperature trajectory is dominated by the corresponding interval in the blocking temperature spectrum of the HT component (fig. 7a,c). Above the reversal a few specimens with low intensity MT components and reversed directions are observed (see also fig. 4 [E,F]).

Properties of the actual lower Sidufjall reversal (fig. 7b,c) are the very rapid directional transition, the slightly increasing inclinations prior to the reversal and the steep inclination maximum after the reversal. Furthermore, the intensity minimum, down to 10%

upperThvera - 480-620°C component

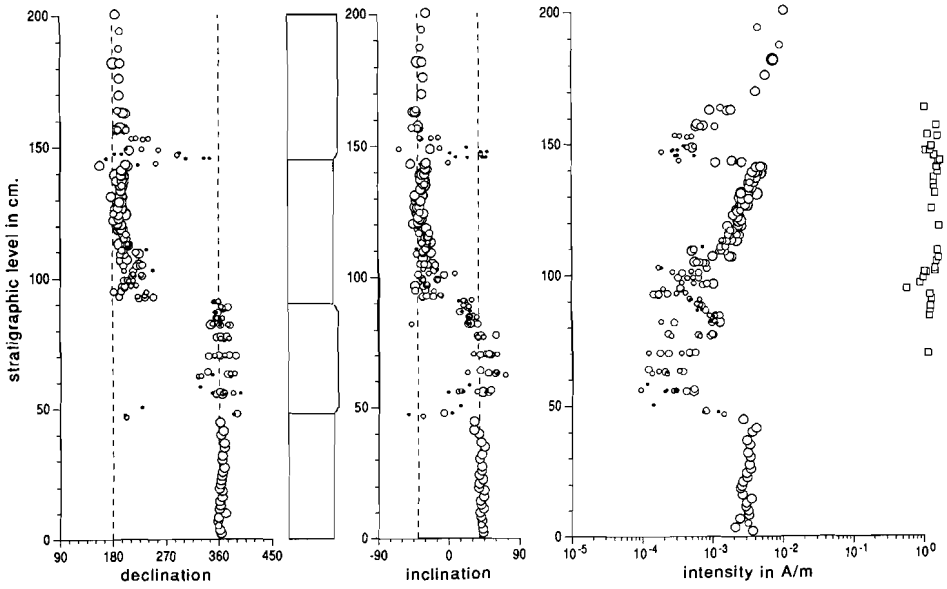

upperThvera - 210-360°C component

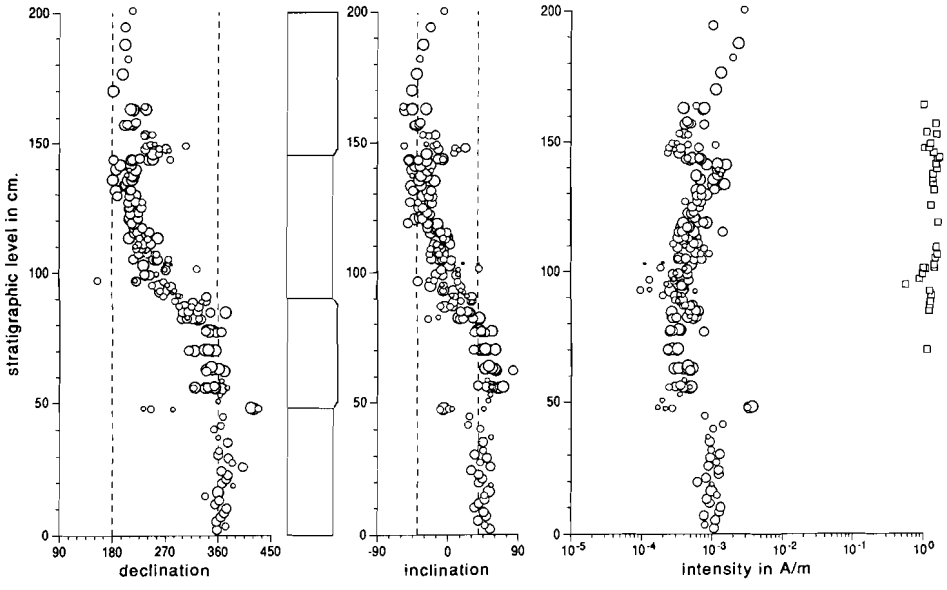

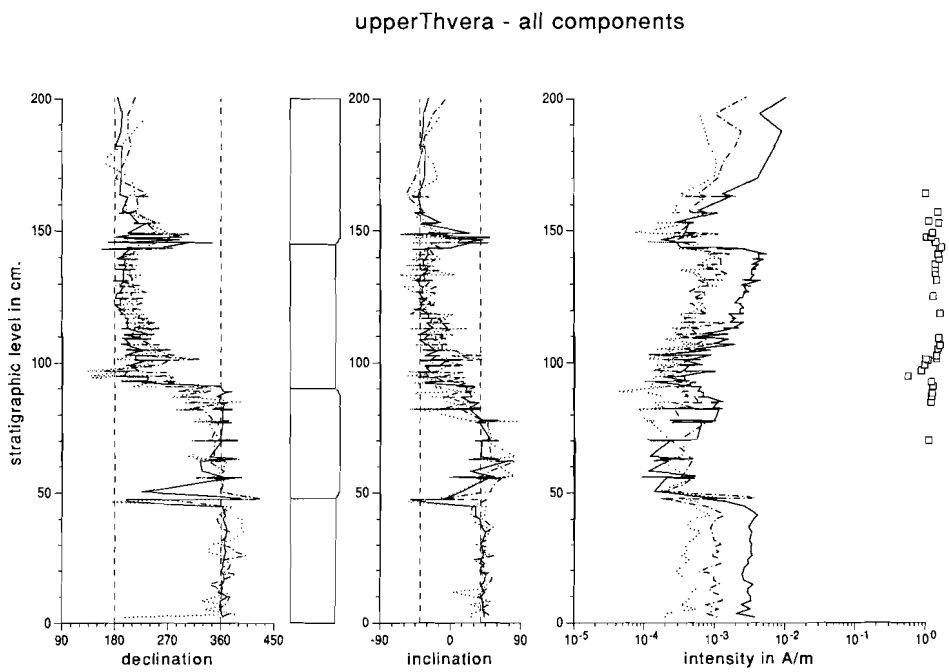

Fig. 6 upper Thvera reversal record of **(b, left below)** LT component, **(c, left above)** HT components and **(d, above)** of all (LT, MT and HT) components. Directions and intensities of the components are represented by circles in five different sizes related to quality of the demagnetization; the largest size corresponds to an excellent quality component, the smallest size corresponds to a low quality component. The vertical dashed lines in the declination and inclination records indicate the geocentric axial dipole field directions (including an inclination error $\tan I_o = 0.52 \cdot \tan I_f$). The column between the inclination and declination record represent the lithology; the indurated part represents the HCU, the less-indurated part represents the LCU. In the intensity record the squares denote the IRM acquired in 2 T, diamonds denote H_{CR} values ($*10^2$) and triangles denote initial susceptibilities (in 10^{-2} SI). The corresponding bold symbols denote the values of the rockmagnetic parameters which were determined after the same specimens were heated at 360 °C. The 210-360 °C components are connected by a dash-dot line, the 360-480 °C components by a dotted line and the 480-620 °C components by a solid line.

of the pre-transitional intensities, completely encloses the major directional changes of the reversal. The intensity after the reversal is approximately 70% of the pre-reversal intensity. The uncomplicated nature of the lower Sidufjall reversal records and the absence of any relation to the lithology indicates that the lithology has not, or only to a minor extent, affected the geomagnetic record.

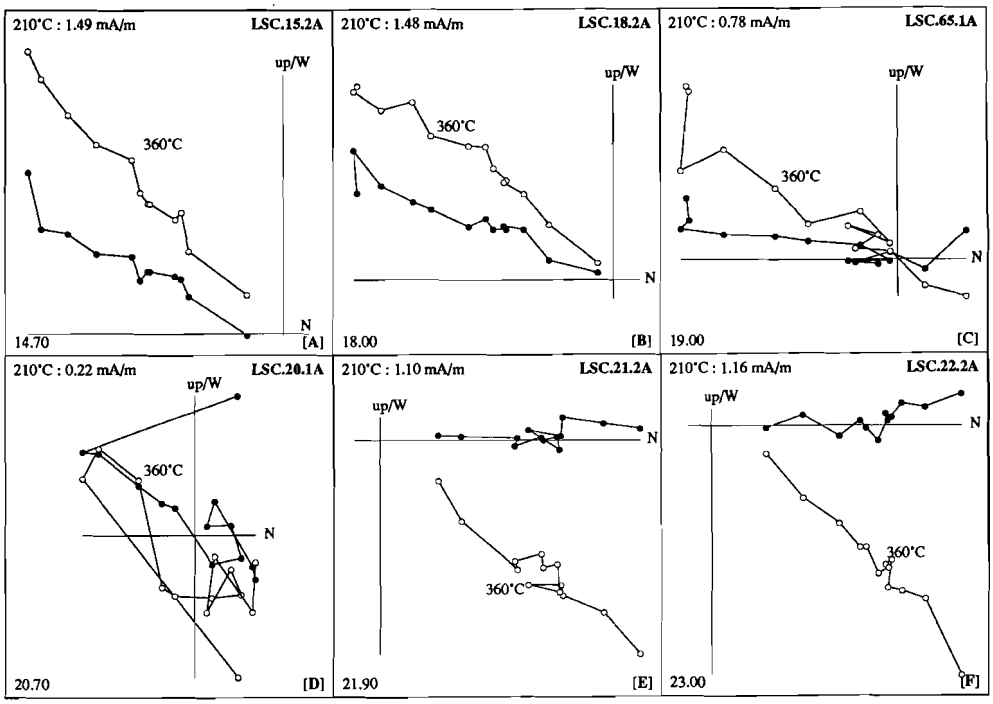

Fig. 7a Thermal demagnetization diagrams for specimens from the lower Sidufjall reversal record. See also caption fig. 4.

The upper Sidufjall N-R reversal record was sampled in a HCU (1.04 m) and part of an overlying LCU (0.96 m). The HT and LT components are well developed in this record (fig. 8a,b,c,d), a low intensity MT component is recognized in a few samples in the 50-60 cm interval (fig. 8a [B],d). Close to the HCU/LCU unit boundary at the 1.04 cm level secondary magnetizations occur, most prominently in the record of the HT component (fig. 8a [E]). An additional hematite-like component, demagnetized between 620-680 °C, shows up near the HCU/LCU unit boundary (fig. 8a [D], fig. 8d). The hematite-like component is of secondary origin, regarding its near present-day field directions.

Fig. 7 lower Sidufjall reversal record of **(b, right below)** HT component and **(c, right above)** all (LT, MT and HT) components. See also caption fig. 6.

Lower Sidufjall - all components

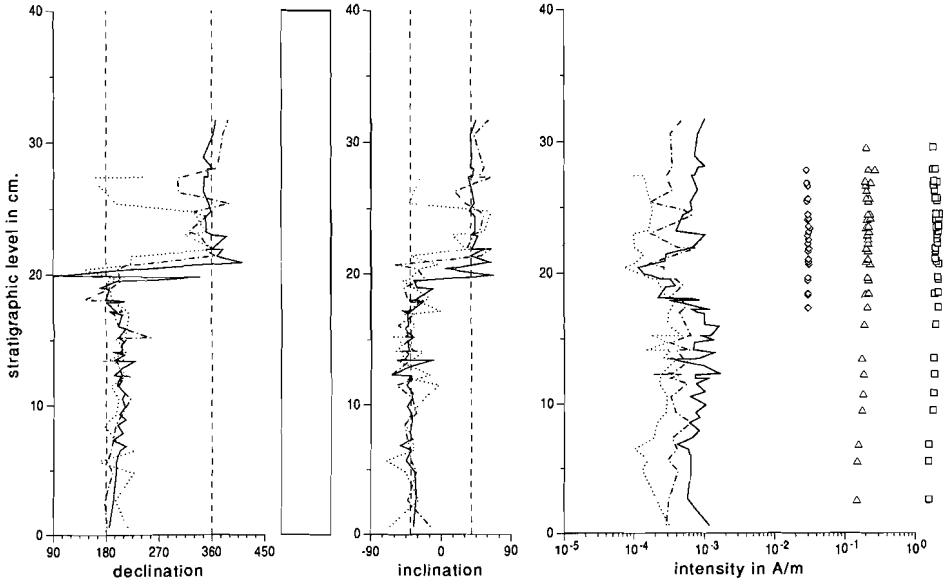

Lower Sidufjall - 480-620°C component

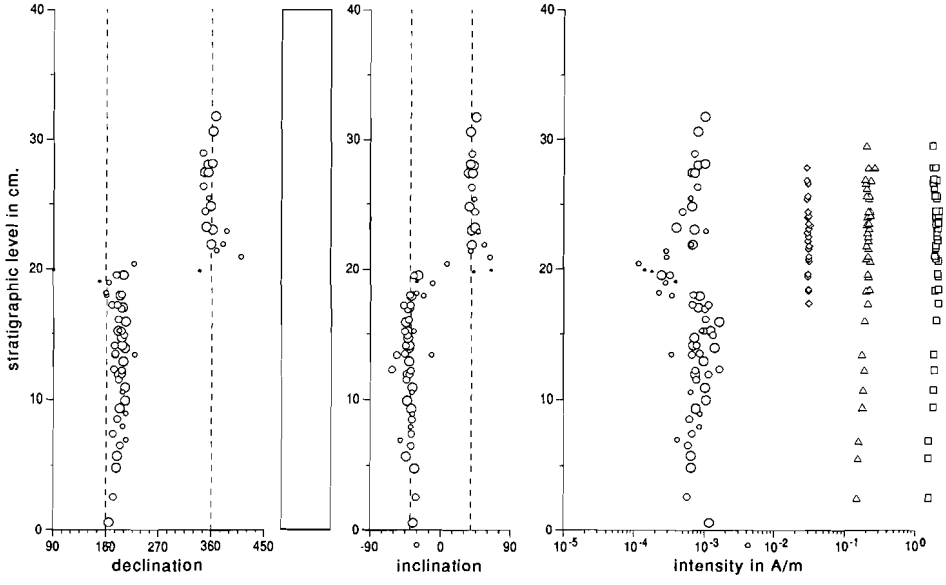

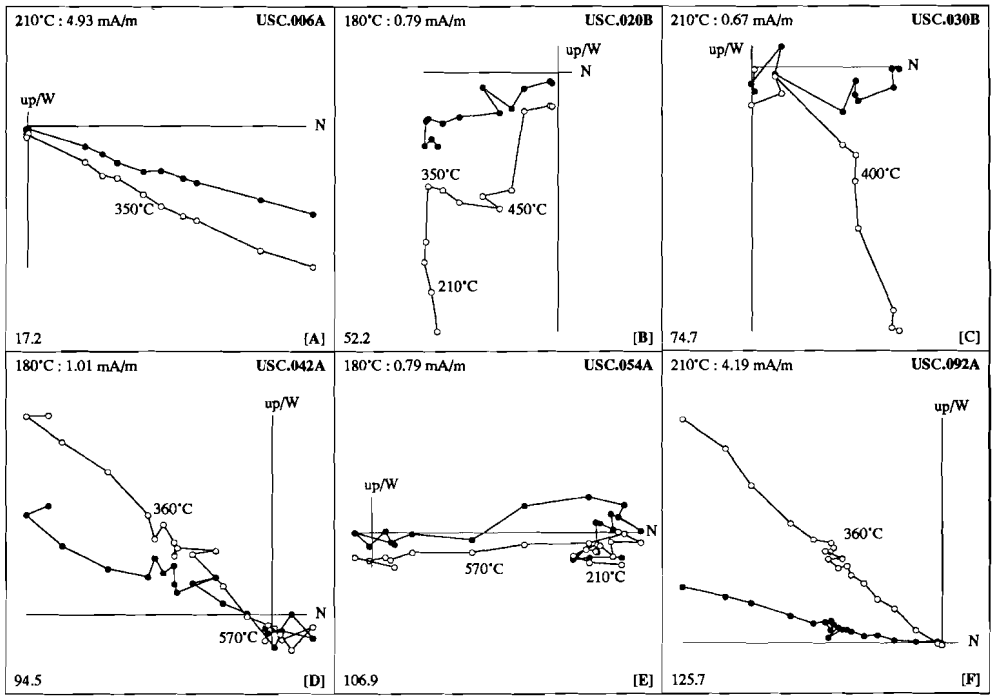

Fig. 8a Thermal demagnetization diagrams for specimens from the upper Sidufjall reversal record. See also caption fig. 4.

In the upper Sidufjall reversal record shallow (transitional) inclinations occur in the interval 0-20 cm, whereas the actual reversal occurs close to the 90 cm level. The declinations and intensities are stable in this part of the record. The decrease of the inclination is followed by a rapid inclination increase close to the 40 cm level. The long interval (40-80 cm) of very steep inclinations (75-90°), accompanied by scattered declinations and low intensities, preludes the actual reversal. The interval with decreased intensities (approximately 40-140 cm) encloses most of the reversal related directional variations. Generally, the LT component shows more transitional directions than the HT component. The firm variations of the intensity of the LT component in the LCU above the actual reversal are related to rockmagnetic changes of pyrrhotite, as is demonstrated by the corresponding variations in the IRM_{2T} record.

The lower Nunivak R-N reversal record has been sampled in a HCU (74 cm) and an overlying LCU (76 cm). The MT and the LT component are not well developed in this

record. As a result, an overprint of the HT component, and, at the low-intensities near the actual reversal (45-65 cm), of the remaining high temperature fraction of a secondary component is present (fig. 9a,b,c,d). The overprint of the LT component by a secondary component is further illustrated by the absence of a clear intensity minimum and secondary directions near the actual reversal resulting in an artificial shift of the reversal to lower levels. This shift does not correspond to a time lag in remanence acquisition of the LT and HT components as is illustrated by the similarity of the inclination records in the same sedimentary interval. Above the 100 cm level some unidentified components occur in the 240-480 °C trajectory (fig. 9a [B]), possibly related to early magnetized carriers of LT or MT components.

Conform the results of Linssen (1988), it is concluded that the R-N lower Sidufjall and R-N lower Nunivak reversal records are very similar, both with regard to their transitional field geometry and with regard to the durations of the various reversal features. Characteristics of the actual lower Nunivak reversal (fig. 9b,c) are the very rapid directional transition, the slightly increasing inclinations prior to the reversal and the steep inclinations immediately above the reversal. Furthermore, the intensity minimum, down to 10% of the pre-transitional intensities, completely encloses the major directional changes of the reversal. The intensity minimum corresponds to the level at which the declinations reverse. At this level the inclination has already reversed and is steeply downward directed. The intensity of the IRM_{2T} is nearly constant in the interval in which the transitional directions and intensities variations of the HT component occur.

The reversal records demonstrate that the HT and LT components have very similar transitional directions and intensities in the intervals in which both components are well developed. A detailed examination indicates that in those intervals the LT component shows a larger number of transitional directions. Furthermore, the LT component, compared to the HT component, is less biased to secondary directions near lithological boundaries.

With respect to the geometry of the transitional field, the upper Thvera inclination record is symmetrically related to the lower Sidufjall and lower Nunivak records. The main difference between the lower Sidufjall and lower Nunivak records and the upper Thvera record is the duration of the reversal. In the lower Sidufjall, upper Sidufjall and lower Nunivak reversal records the main directional and intensity changes are rapid, resp. 0.3-4.0 and 1.3-7.7 kyr (table 3). The reversal-related intensity changes of the

Upper Sidufjall - 480-620°C and 620-680°C components

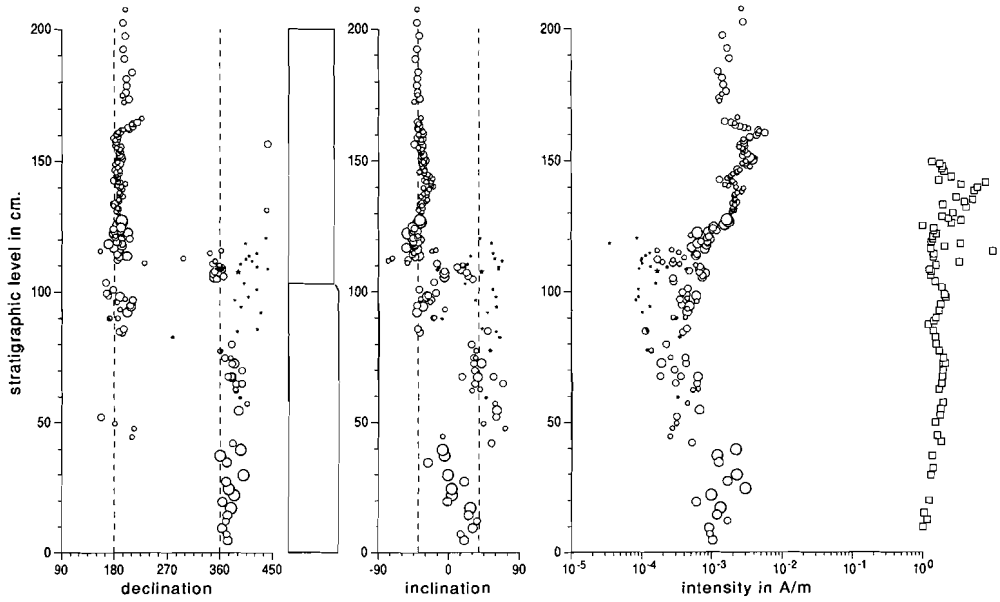

Upper Sidufjall - 210-360°C component

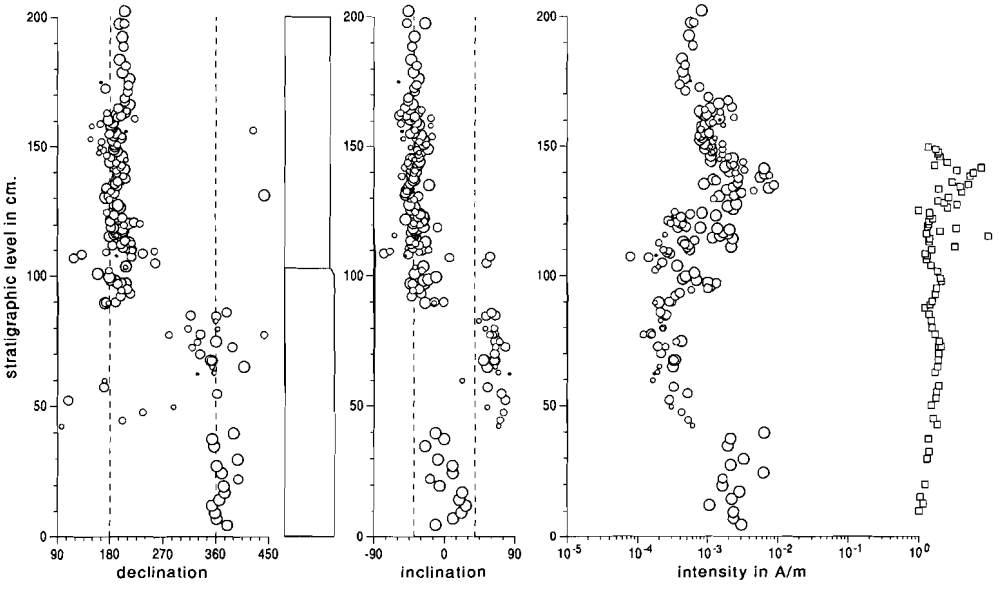

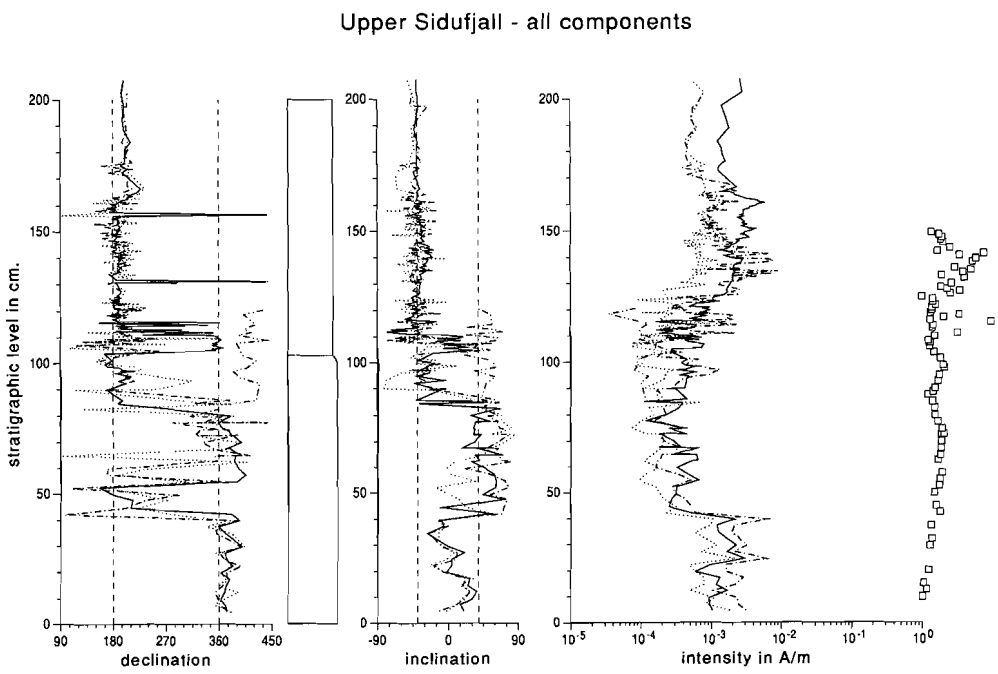

Fig. 8 upper Sidufjall reversal record of **(b, left below)** the LT component, **(c, left above)** the HT component and **(d, above)** all (LT, MT, HT) components. The asterisks represent hematite components. See also caption fig. 6.

upper Thvera reversal record seem to occur in a period of 26 kyr. The upper Thvera record shows an oscillating and purely non-zonal transitional field, whereas the other records exhibit more or less zonal transitional fields. The VGP path of the upper Thvera reversal record is confined to a meridian 90°W of site. The VGP paths of the lower Sidufjall, upper Sidufjall and lower Nunivak reversal records follow a path close to the site meridian (Linssen, 1988).

The upper Sidufjall record suggests a reversal process in which geomagnetic field changes were interspersed with long periods of transitional but stationary directions and intensities. More reversals of this type have been reported, a typical one being the Steens Mountain record (Mankinen et al., 1985, Prevot et al., 1985).

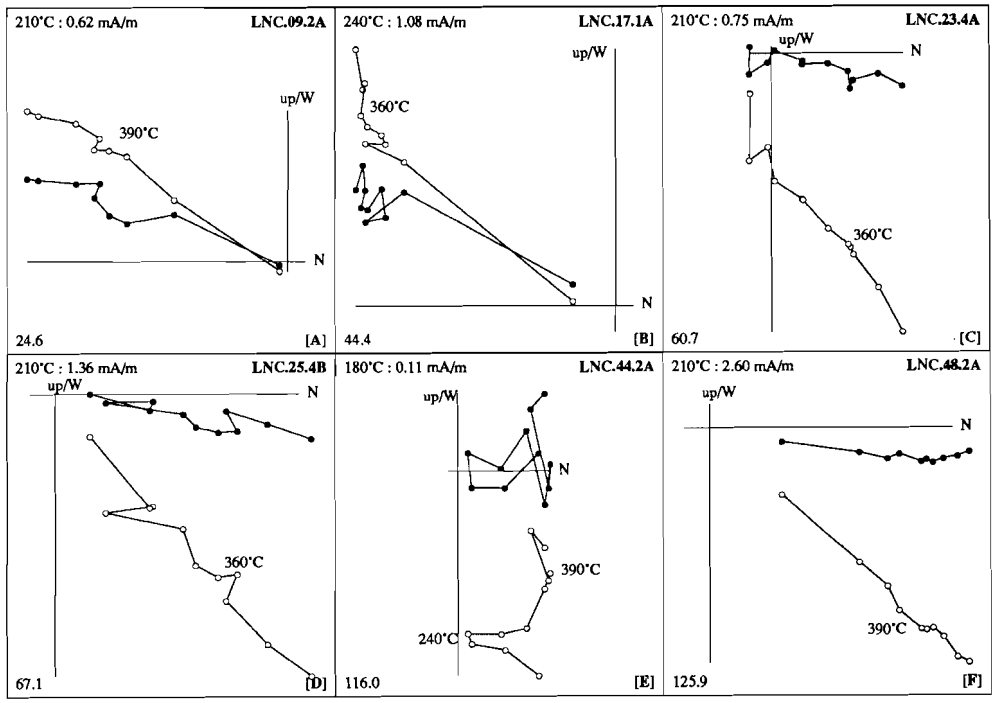

Fig. 9a Thermal demagnetization diagrams for specimens from the lower Nunivak reversal record. See also caption fig. 4.

5.2 The upper Nunivak reversal records

The 1986 upper Nunivak N-R reversal record of the HT magnetite component (480-620 °C, fig. 10d) shows that the actual reversal occurs in the upper half of the HCU (thickness of 1.04 m). The record starts with anomalously steep downward directed magnetizations. The major directional changes of the upper Nunivak reversal record occur in a sedimentary interval with a length of approximately 10 cm. The LT and MT components are not well developed in the upper Nunivak record (fig. 10a,b,c and fig. 11a,b,c). Furthermore, demagnetization in the 210-360 °C trajectory near the centre of the reversal does not completely isolate the low intensity magnetite component from the large remaining secondary magnetization (fig. 10a [C], fig. 11a [E,F]). An artificial shift of the N-R reversal record of the LT component to higher levels results. In this respect, a comparison with the R-N lower Nunivak reversal record, with a similar shift to lower

levels, is illustrative. Hence, the ChRM of the low intensity LT component could not be determined with sufficient accurracy.

The details of the actual reversal are best shown in the high resolution 1987 record (fig. 11d,e). This record shows that the HT reversal occurs near the 28 cm level and proceeds rapidly for the inclination; the declination values already start to change near the 20 cm level. The declinations align to reversed values approximately at the 40 cm level (see 1986 record). The intensity record shows an asymmetric minimum in the 16-33 cm interval. The minimum ChRM intensities (~10^{-4} A/m) occur at the 27 cm level and are approximately 10% of the pre-reversal ChRM intensities and 15-20% of the post-reversal intensities. The IRM_{2T} record in the 16-33 cm interval shows a maximal (random) variation of a factor 2-3. These IRM variations are dominated by changes in the concentration of magnetite, rather than by grain size changes, as demonstrated by the minor variation in the grain size dependent H_{CR}.

The interval in which the major directional change of the inclination takes place has a length of 5 cm. The gradually changing declination and intensity records have a length of approximately 20 cm. This length has to be extended to at least 40 cm if the anomalous steep inclination values preceding the reversal are considered to be part of the reversal. The various features in the reversal record have been converted to durations using the minimum

Table 3 Durations of reversal features

Reversal:	UT		LS		US		LN		UN	
	I<	>I	I<	>I	I<	>I	I<	>I	I<	>I
Anm. Int.	26.0	26.0	1.3	1.9	5.0	7.7	2.1	4.0	2.2	2.5
Anm. Dir.	17.0	17.0	2.5	3.8	10.0	15.4	4.1	8.0	4.3	4.9+
Maj. Dec.	1.0	1.0	0.6	1.0	0.5	0.8	0.3	0.7	2.2	2.5
Maj. Inc.	3.0	3.0	1.3	1.9	2.0	3.1	2.1	4.0	0.5	0.6

Table 3. Durations (in kyr) for observed reversal related variations of the HT magnetite component in the upper Thvera (UT), lower Sidufjall (LS), upper Sidufjall (US), lower Nunivak (LN) and the upper Nunivak (UN) reversal records. The estimated minimum (I<) and maximum (>I) durations have been given for the period with anomalous directions, anomalous intensities, major declination change and the major inclination change (Linssen, 1988). The "+" for the upper Nunivak denotes that the duration value given is probably underestimated.

Lower-Nunivak - 480-620°C component

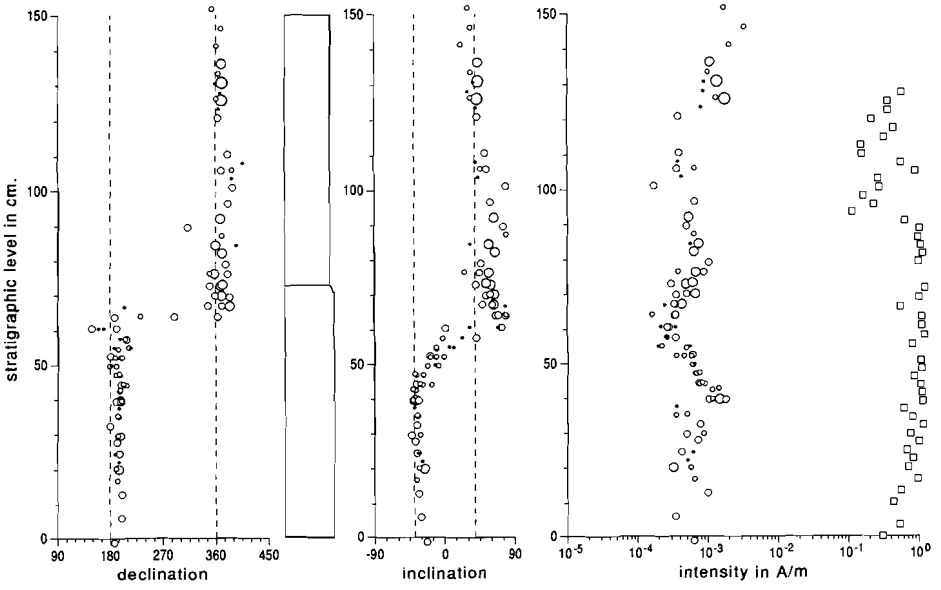

Lower-Nunivak - 210-360°C component

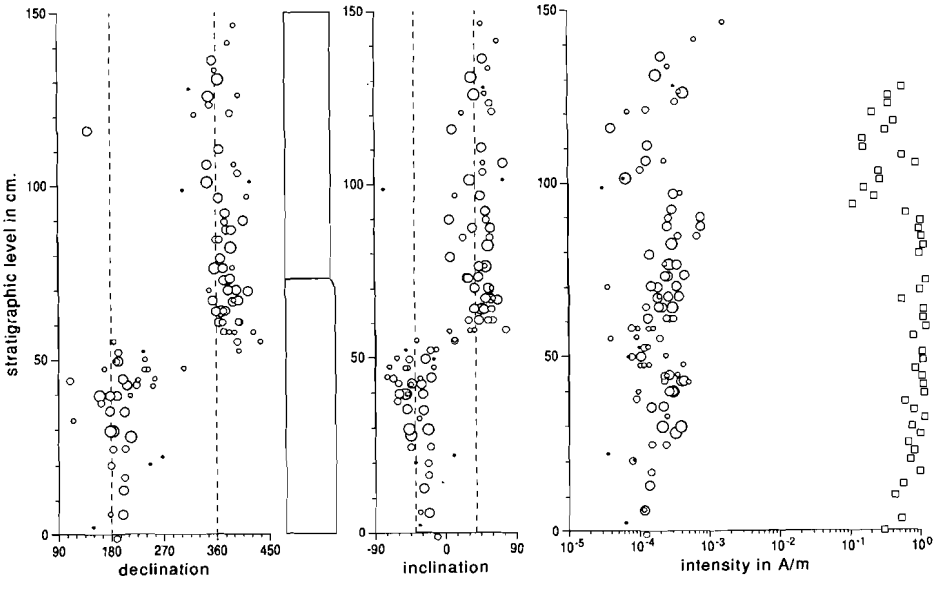

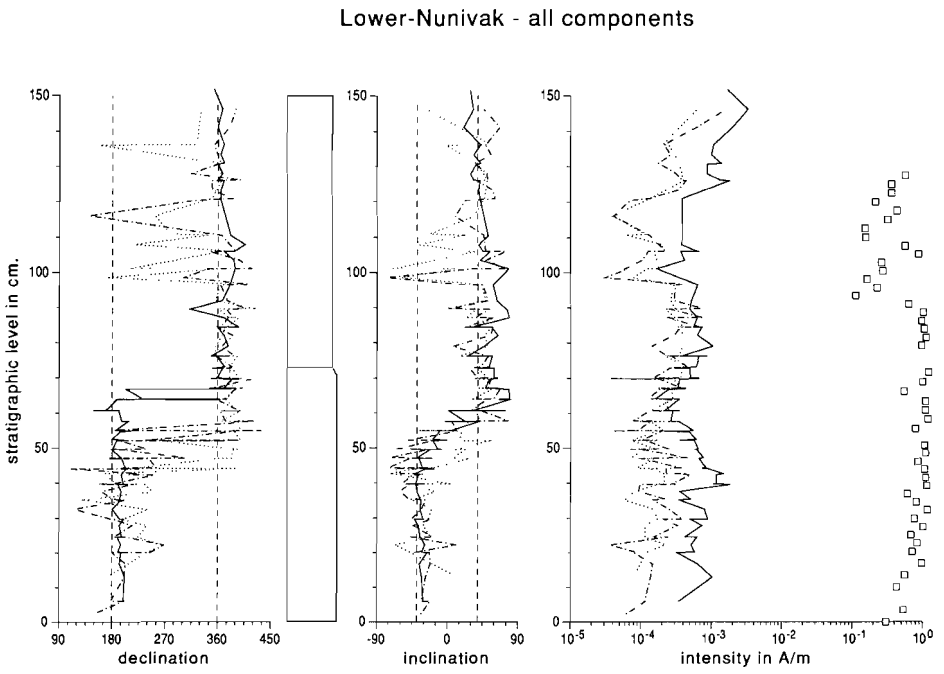

Fig. 9 lower Nunivak reversal record of **(b, left below)** the LT component, **(c, left above)** the HT component and **(d, above)** all (LT, MT, HT) components. See also caption fig. 6.

and maximum values for the accumulation rates (table 1). The duration of the period with anomalous directions of the upper Nunivak reversal is in the range 4.3-4.9 kyr, or longer, if the named anomalous directions at the low-end of the record are considered. The duration of the period with anomalous intensities is in the range 2.2-2.5 kyr and the durations of the periods with major declination and inclination changes are in the ranges 2.2-2.5 and 0.5-0.6 kyr (table 3).

The virtual geomagnetic poles (VGP's) have been calculated from the directions of the (HT) magnetite component in the 1987 upper Nunivak reversal record (fig. 12). The VGP projections are given both before and after correction for the inclination error (f=0.52). The gradual N-W-S change of declination results in a VGP path which is located at nearly 90°W of the site meridian passing the Americas.

The upper Nunivak N-R reversal record bears a major resemblance to the

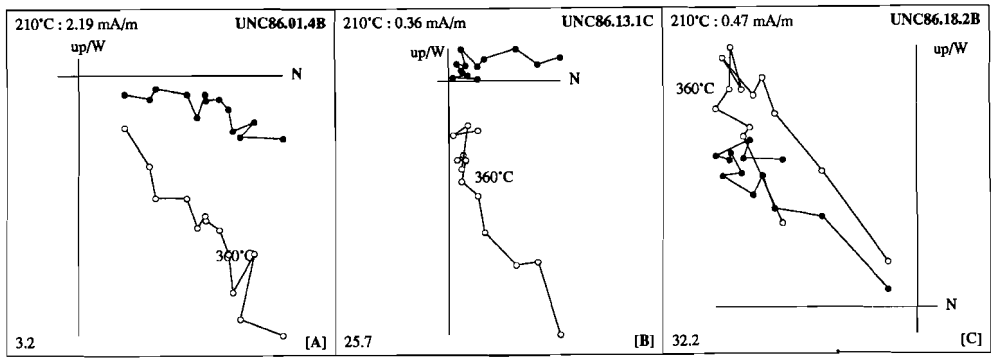

Fig. 10a Thermal demagnetization diagrams for specimens from the upper Nunivak 1986 reversal record. See also caption fig. 4.

upper Thvera N-R reversal record from the same section. The steep inclinations before the actual reversal and the gradual N-W-S change of the declinations (causing the VGP path 90°W of the site meridian) are similar aspects of the two reversal records. Furthermore, both records show directional oscillations prior to the actual reversal. Different aspects of these records are that a) the upper Thvera record shows a longer duration of the intensity low (26 kyr) than the upper Nunivak reversal record (2-3 kyr) (table 3) and that b) the period during which transitional directions occur in the upper Thvera record, in contrast to the upper Nunivak, is less than the period of transitional intensities. However, the difference in duration may be uncharacteristic considering the possible absence of the lowermost interval in the upper Nunivak reversal record.

6. Discussion

The analysis of ChRM components in the investigated marine marls is even more complicated than suggested previously (Linssen, 1988). It was shown that the HT and the LT components occur in all sedimentary intervals, but the intensity of the LT component varies considerably with the lithology (chapter 4). Generally, the intensity of the LT component is less in the HCU units than in the LCU units. As a result, the intensity of the LT

Fig. 10 upper Nunivak 1986 N-R reversal records of **(b, right below)** 210-360 °C component, **(c, right above)** 360-480 °C component, **(d, next page below)** 480-620 °C component and **(e, next page above)** gives all components. See also caption fig. 6.

Upper Nunivak (86) - 360-480°C component

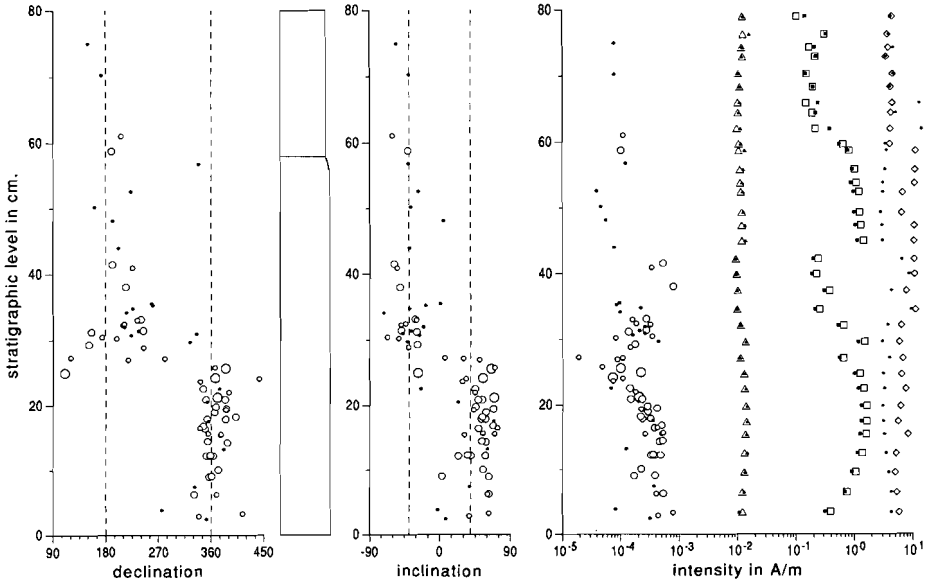

Upper Nunivak (86) - 210-360°C component

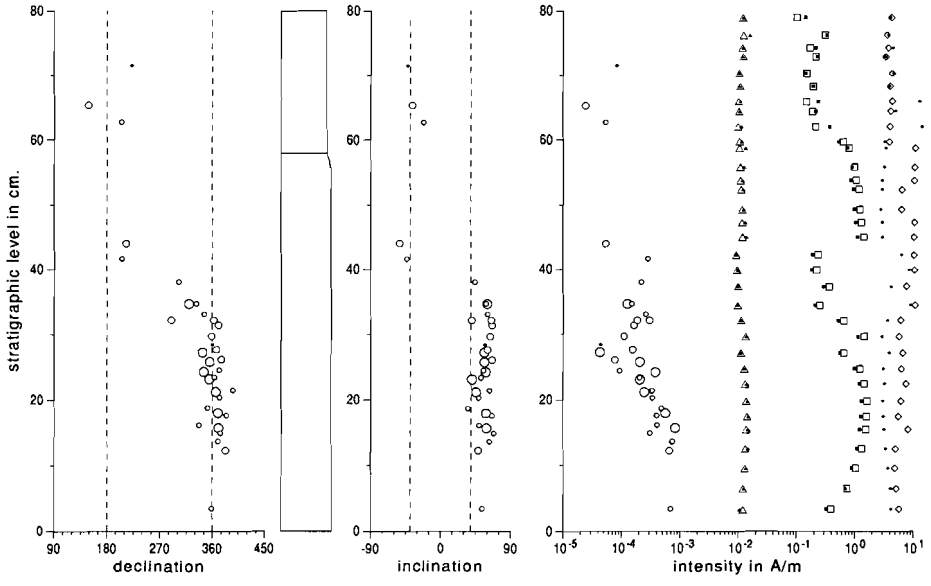

Upper Nunivak (86) - all components

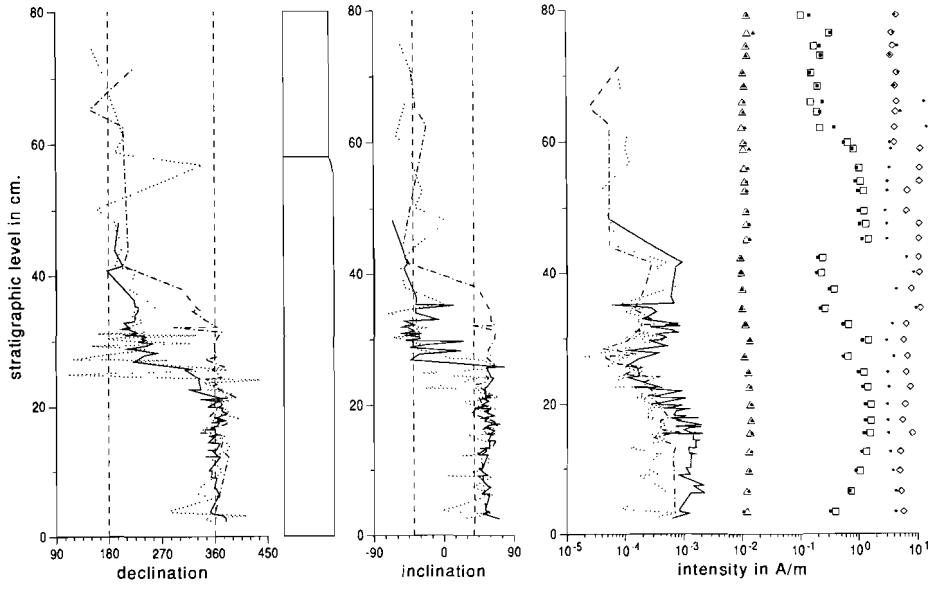

Upper Nunivak (86) - 480-620°C component

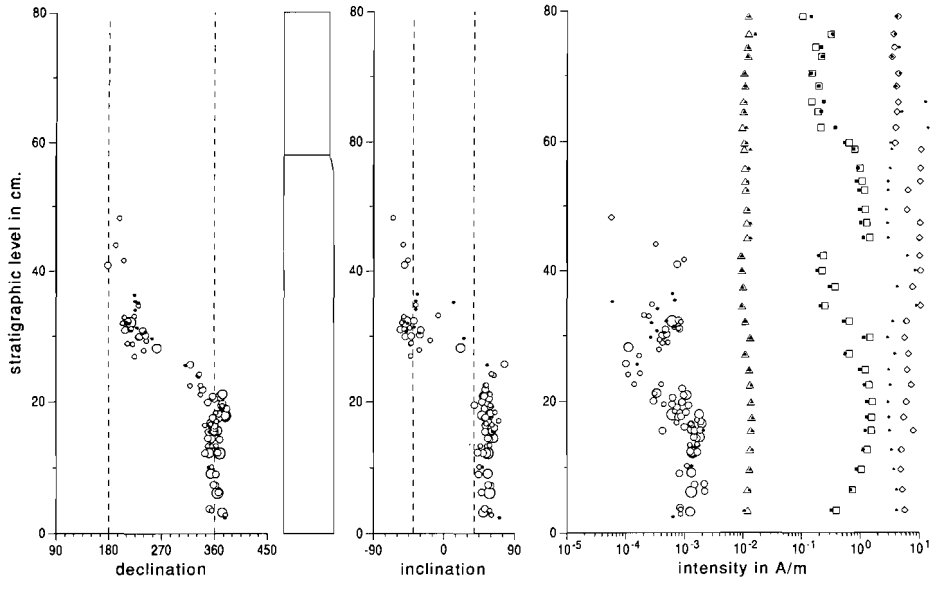

component in the HCU samples is low and it is more difficult to obtain reliable LT records. Moreover, approaching the top of the Monte Singa section, i.e. in the lower and upper Nunivak reversal records, the magnitude of the LT component decreases and a significant overprint of a secondary component is present. The HT component is partly remagnetized in the intervals close to the lithological (HCU-LCU) boundaries. For all records the intervals in which these suspicious remanences occur could be isolated. In this discussion it is further assumed that the other principal features of the reversal records are accurate images of the geomagnetic field.

A comparison of the investigated records learns that the the upper Thvera reversal record has a clearly non-zonal transitional field geometry, a moderately rapid (3 kyr) inclination change and a long duration of the intensity low, whereas the Sidufjall and lower Nunivak reversal records have rapid inclination and intensity changes. The upper Nunivak record shows intermediate characteristics. Although the duration of the upper Nunivak reversal record appears to be shorter than the upper Thvera record, the other characteristics, such as the transitional field geometry and the oscillating directions, are very similar to the upper Thvera.

If one assumes that the frozen-in flux approximation (Gubbins and Roberts, 1983) is applicable to the present reversals, one may also expect, for a fluid-driven reversal process initiated at a single location and producing significant outer core toroidal velocity fields (Hoffman, 1986; Hide, 1981), that an increased duration for a reversal process also introduces more zonal transitional fields at remote sites. However, the observed relation between duration of the major directional and intensity changes and zonal contents of the symmetrically related reversal records (e.g. upper Thvera, lower Sidufjall, lower Nunivak) is contrary to the features of the described reversal mechanism. In the next paragraphs alternative explanations are examined. For this purpose, the reversal records from the Monte Singa section are compared with other reversal records.

There is a striking similarity between the lower Sidufjall and the lower Nunivak reversal records and many records reported for the Matuyama-Brunhes (MB) reversal from nearly the same latitude (Williams and Fuller, 1981; Theyer et al., 1985; Clement and Kent, 1986). Most of the MB reversal records from mid-northern latitudes are characterized by a gradual shallowing of the inclinations before reversing sign. These reversals are rapidly followed by steep and downward directed inclinations. Also, the intensity records of all of these reversal records show minima down to 10% of the typical non-transitional field intensity.

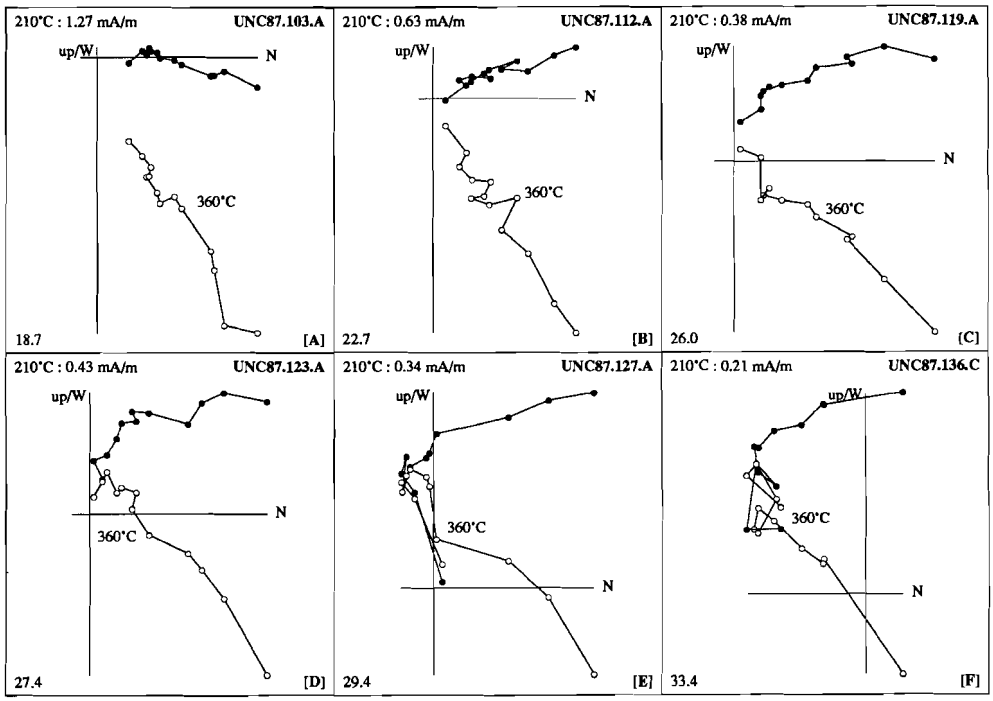

Fig. 11a Thermal demagnetization diagrams for specimens from the upper Nunivak 1987 reversal records. See also caption fig. 4.

Hoffman (1981) and Williams and Fuller (1981) developed phenomenological models which well described many of the available and spatially distributed MB reversal records. Hoffman concluded that non-zonal quadrupole and zonal octupole components dominated the MB transitional field. In Hoffman's model the zonal octupole changed polarity during the reversal (cf. Merrill and McElhinny, 1977).

In the zonal harmonic model of Williams and Fuller (WF model) it is assumed that during the reversal process the time evolution of the intensity is similar to the one derived for the Tertiary intrusive Tatoosh reversal record (Dodson et al., 1978). It is assumed that during the latter reversal 75% of the energy lost by the dipole field source is partitioned

Fig. 11 upper Nunivak 1987 N-R reversal records of **(b, right below)** 210-360 °C component, **(c, right above)** 360-480 °C component, **(d, next page below)** 480-620 °C component and **(e, next page above)** gives all components. The stratigraphic levels correspond to those of the upper Nunivak 1986 record. See also caption fig. 6.

Upper Nunivak (87) - 360-480°C component

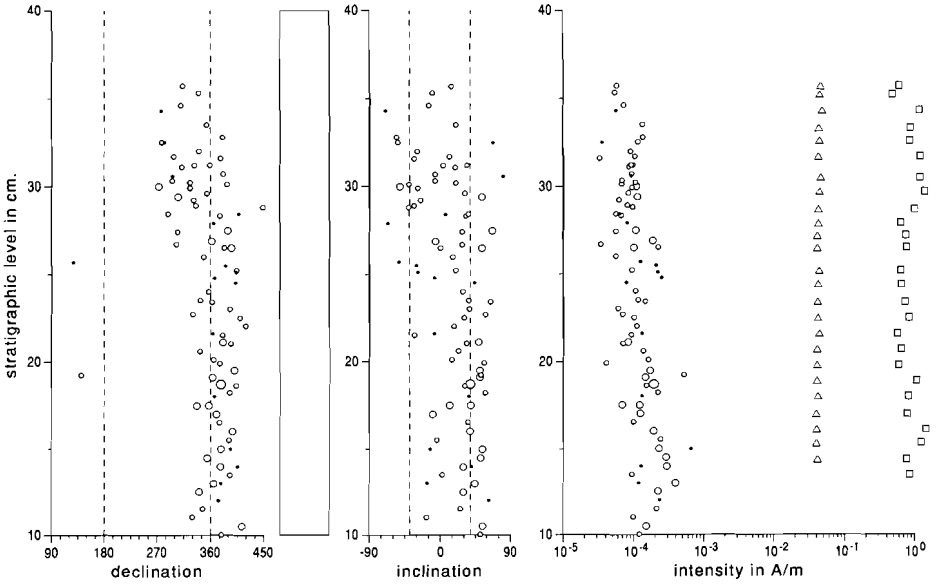

Upper Nunivak (87) - 210-360°C component

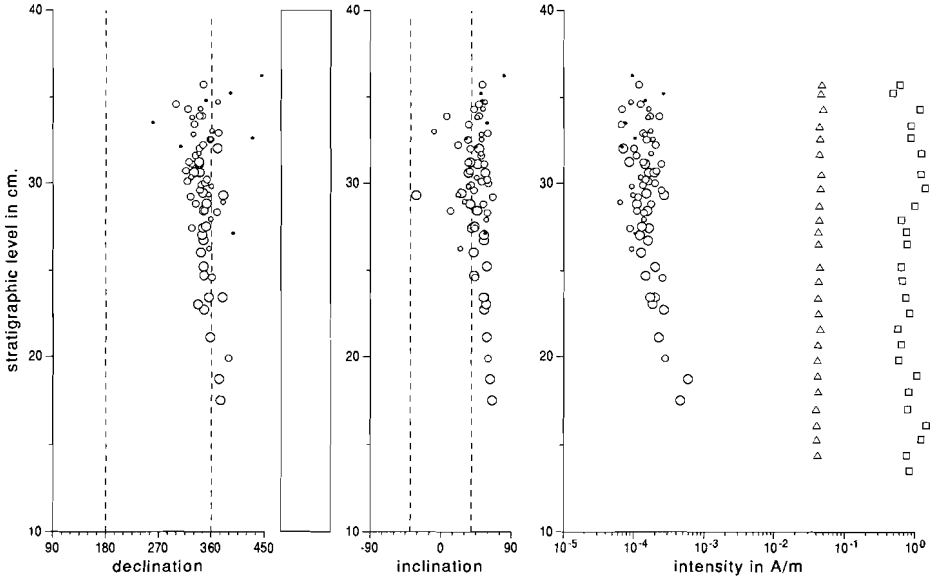

Upper Nunivak (87) - all components

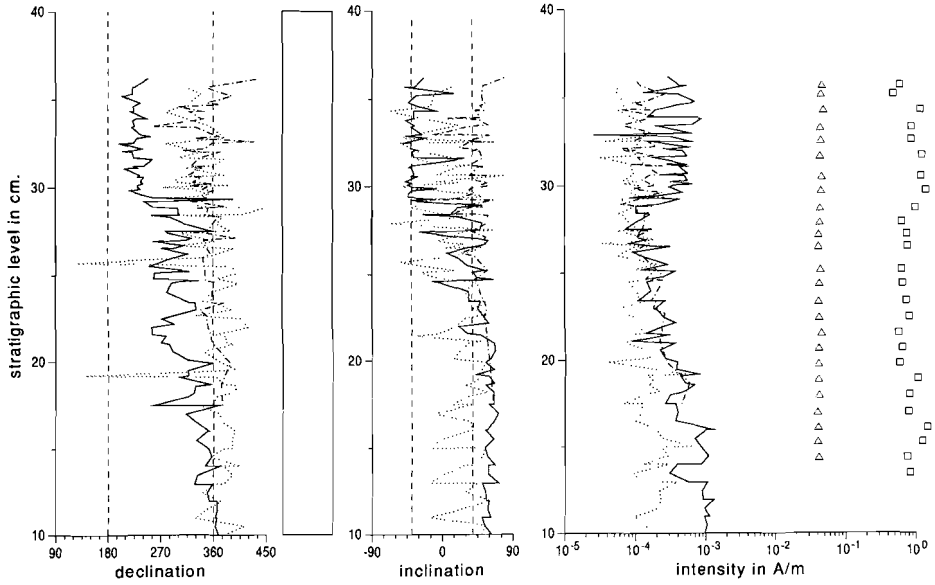

Upper Nunivak (87) - 480-620°C component

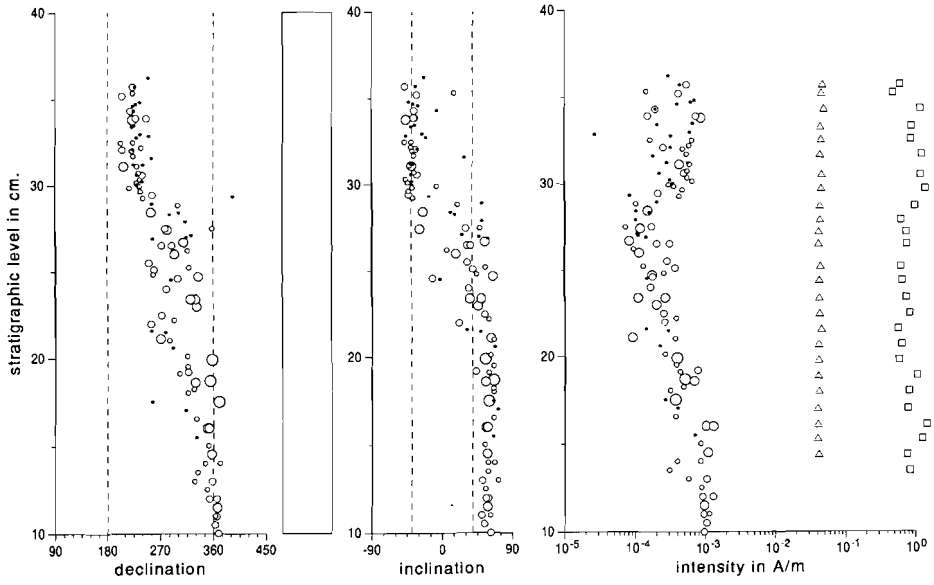

between the low-order harmonics of the zonal geomagnetic field, i.e. g_2, g_3 and g_4. This assumption is based on a study of historical observations of the geomagnetic field (Verosub and Cox, 1971). For the MB reversal the WF model fits if the energy transfer ratio to g_2, $-g_3$ and g_4 terms is 2 : 3 : 5. The adjusted WF model (Clement, 1987), having a different time-evolution based on a theoretical study of helicity fluctuations in the core (Olson, 1983), was not used. The minimum reversal duration of 7.5 kyr predicted by the adjusted WF model (based on conductivity values for the outer core; Gardiner and Stacey, 1971) does not agree with the durations of the presently discussed records.

Figure 13a, b and d show the inclination and intensity records of respectively the upper Thvera, lower Sidufjall and lower Nunivak reversals and the records predicted by the WF model. The fit of the WF model to the lower Sidufjall and lower Nunivak records is reasonably good. The observation of high inclination values (>70°) in the non-zonal upper Thvera record, prior to the actual polarity transition followed by shallow inclinations is in general agreement with the zonal WF model. Figure 13c shows the inclination record of the upper Sidufjall reversal record. Although, as a whole, the complex upper Sidufjall record is not in agreement with the WF model, the interval in which the last and major inclination change occurs does show some similarities.

A bias between the WF model and the reversal records is caused by the shallow inclination increase prior to the reversal (5-10°), as can be seen in the lower Sidufjall and lower Nunivak records. This bias is even larger in the upper Sidufjall and upper Nunivak reversal records, in which long periods of steep inclinations prior to the actual polarity transition are observed.

The standing field theory (Hillhouse and Cox, 1976) predicts identical zonal harmonic contents for successive reversal records from northern and southern hemispheres and as such is thought to give a possible explanation for the observed WF transitional field geometry of remote reversal records. However, the only available MB-like records of identical reversals from northern and southern hemispheres, the upper Olduvai and lower Jaramillo reversals have different zonal harmonic contents (Theyer et al., 1985; Clement and Kent, 1984, 1985, 1986). Partly this may be attributed to the fact that the records are too complex to be unambiguously fitted by the WF model and partly there may be an over-interpretation of the smoothed data for which no error estimates are available.

Obvious is the gross anti-symmetrical relationship between the high quality results from the southern hemisphere RC14-14 DSDP core and the other (northern hemisphere) MB-like results. For instance, the southern hemisphere lower Jaramillo reversal record

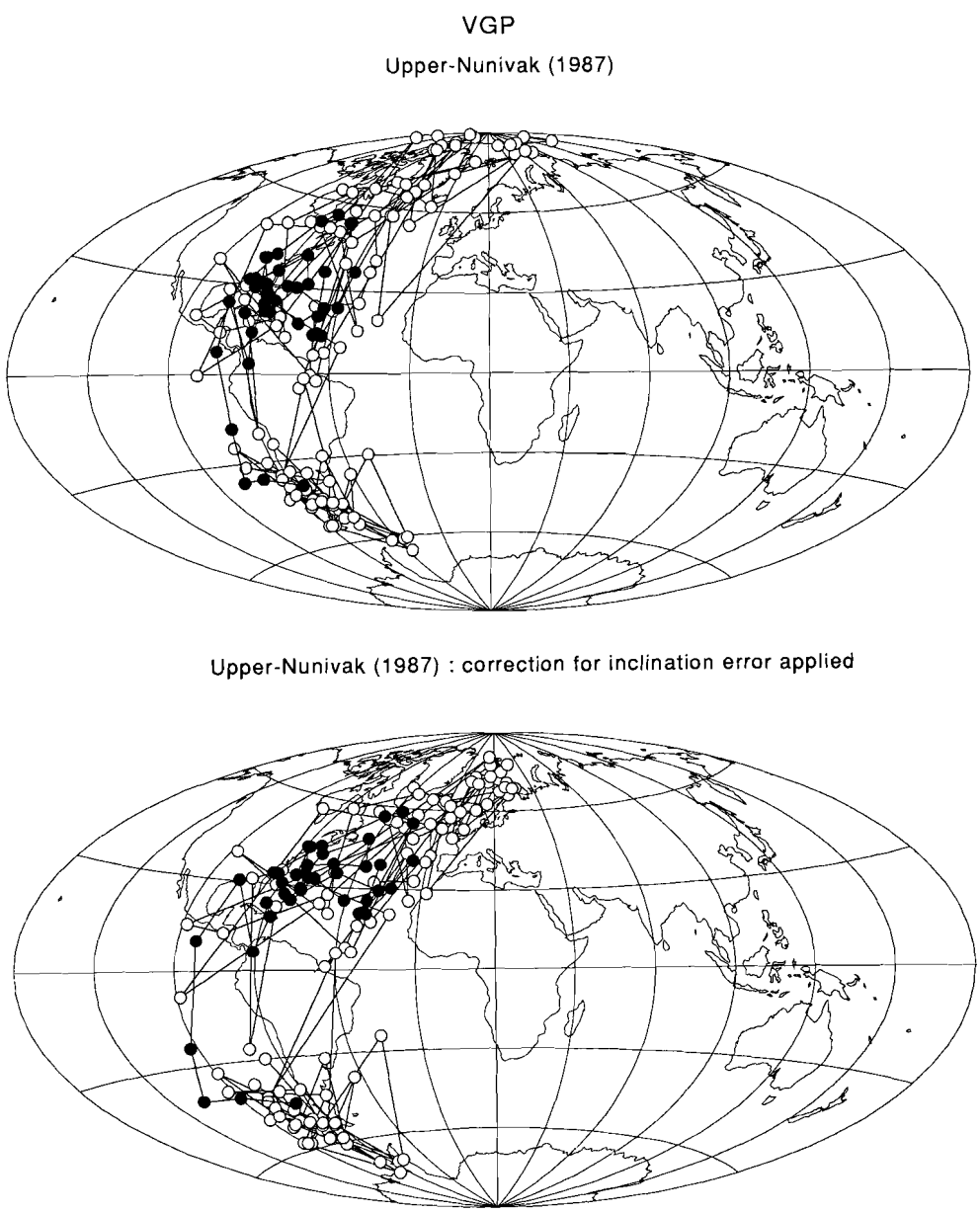

Fig. 12 Aitoff projections of the earth centred around the site meridian. The open circles correspond with the locations of the virtual geomagnetic poles of ChRM from the 1987 upper Nunivak reversal record. The projections are given before and after (f=0.52) correction for the inclination error. The closed symbols correspond to a five-point running average of the reversal record (20-30 cm interval).

unambiguously fits to a WF model in which the energy partitioning to non-dipole zonal harmonics is changed to $-g_2 : -g_3 : -g_4 = 2 : 3 : 5$. This anti-symmetrical relationship is in direct conflict with the standing field theory.

It is possible to reproduce the observed MB-like reversal records using a more simple transitional field geometry than the one used in the WF model. However, in that case one should abandon the WF model assumption that about 75% of the dipole source energy is partitioned between the quadrupole and octupole harmonics. The fit between the reversal records and the modified WF model is optimized by changing the energy transferred from the dipole source energy to either quadrupole or octupole harmonics (fig. 14). In fact, this modified WF model constrains the possible dynamic changes due to reversal initiating perturbations somewhere in the fluid core as is geometrically elaborated in the flooding model (Hoffman, 1977; Hoffman, 1979). The remaining part of the dipole-field energy is assumed to be dissipated, for instance in high-order field components. With only 2-4% of the dipole energy transferred to either the zonal quadrupolar ($+g_2$, curve B) or the octupolar ($+g_3$, curve C) harmonic terms, inclination and intensity records for the Calabrian site latitude are produced that are almost identical to the WF model (curve A). Within the accuracy limits of the data there are no differences between the various synthetic records.

In contrast to the WF model, this modified WF model with either a quadrupolar ($-g_2$, curve D for R-N) or an octupolar ($+g_3$, curve E for R-N) transitional field reproduces the available northern and southern hemisphere records (Clement and Kent, 1986) (curve F). In the modified model the signs of the octupolar transitional fields for the northern and southern hemisphere MB-like reversal records are identical. This argues for an octupolar transitional field model if one supposes a single reversal process to be responsible for the MB-like reversals occurring in the last 5 Ma.

To explain the inclination increase prior to and immediately after the lower Sidufjall and lower Nunivak reversals in the dynamic reversal mechanism, one requires reversing and non-reversing non-dipole field components (Merrill and McElhinny, 1977) which decay more slowly than the dipole field.

However, unless the reversing non-dipole field components find their origin at the core mantle boundary, they are assumed to decay more rapidly than the dipole field during a reversal (e.g. LeMouël, 1984). Indeed, the fact that the transitional fields of the lower Sidufjall and lower Nunivak records do not show the non-zonal component observed in the stable geomagnetic field (causing the 6.8° declination offset between the non-anti-

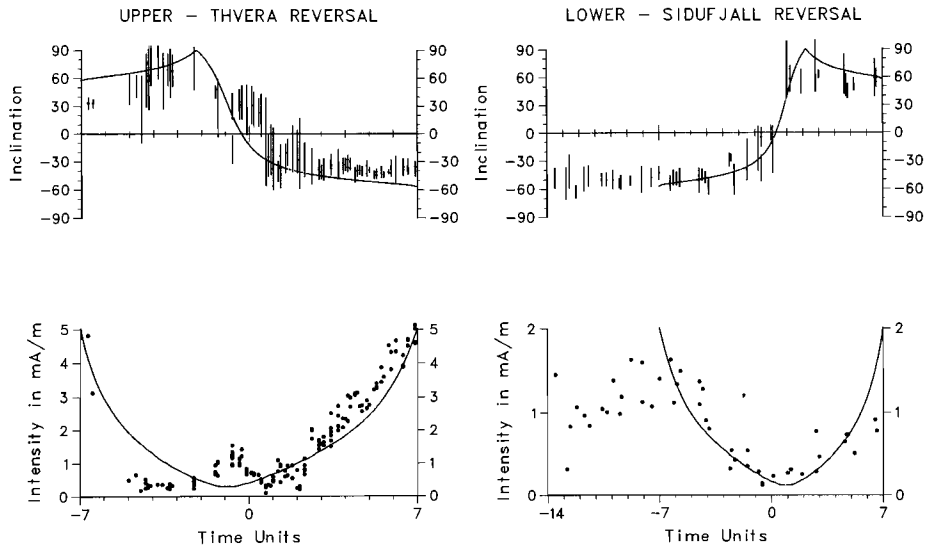

Fig. 13 Inclination and intensity record of (**a**) the Upper Thvera (N-R, 4.57 Ma), (**b**) lower Sidufjall (R-N, 4.47 Ma), (**c, right page**) upper Sidufjall (N-R, 4.40 Ma) and (**d, right page**) Lower Nunivak (R-N, 4.24 Ma) reversal records (single data points) and synthetic records (bold lines) as a function of time units (TU, Williams and Fuller, 1981). The model develops between -7 and 7 TU. The reversal records represent the primary components carried by magnetite (Linssen, 1988) and include some new data. The inclination data are not corrected for the compaction induced inclination error (Anson and Kodama, 1987). The error bar is conform the maximum angular deviation (Kirschvink, 1981). The synthetic record is produced with the zonal harmonic model of Williams and Fuller (1981). The synthetic intensities have arbitrary units. The model fits best to the zonal R-N reversal records. The lower Sidufjall and lower Nunivak inclination records show an initial inclination increase relative to the reversed near axial dipole field inclination values (-38.5° with $a_{95} = 1.3°$).

parallel ChRM directions; section 4) provides evidence that this non-dipole component decays faster than the dipole field. Furthermore, the non-zonal component of the stable geomagnetic field is restored after completion of all reversals. It follows that the source of the non-zonal geomagnetic field components survives geomagnetic reversals.

The observed initial inclination increase need not be in conflict with the modified WF model. If it is assumed that the reversal is initiated in a specific region in the fluid core. Before the reversal floods (longitudinally and/or latitudinally) to the other parts of the core there will be a period in which the magnetic disturbance of reversed flux (Gubbins, 1987) grows while the dipole field is still relatively stable. In the ideal case the geomagnetic field will be comprised of two components, one introduced by the dipole field and one introduced by the growing region of reversed flux. The locations of the region of

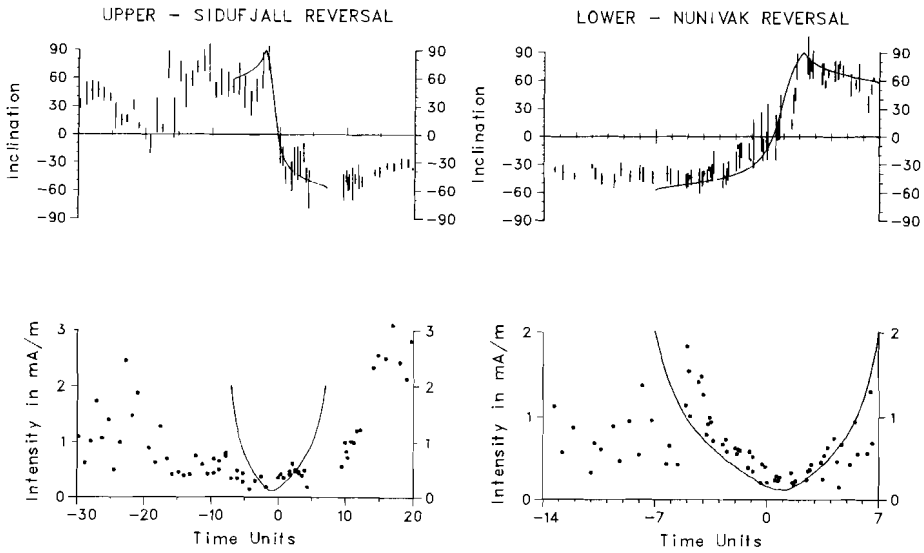

reversed flux and the site will then determine the magnitude of geomagnetic field deflection prior to the actual reversal (fig. 15).

Gubbins (1987) proposed that reversals are initiated by local lower-mantle temperature anomalies related to mantle convection and most probably occurring at mid-latitudes (i.e. at the latitude of maximal toroidal fields). Essentially his theory constrains the flooding model of Hoffman (Hoffman, 1977; Hoffman, 1979). The physical consequences of the model are quadrupole dominated transitional fields exhibiting similar characteristics for reversals occurring within the life-time of the temperature anomalies.

On the one hand, this approach is attractive as it provides a reason why the reported MB-like reversals are found over long periods of geological time. Moreover, both Gubbins and the proposed modified WF model do not require frozen-in flux conditions during the reversal. On the other hand, there is some evidence that the reported transitional fields are not dominated by quadrupolar fields (RC14-14 records, Clement and Kent, 1984; Clement and Kent, 1985, and figs. 14) and that the reported initial inclination increase in the lower Sidufjall and lower Nunivak records, if related to reversed flux features, is more easily produced by a perturbation located at low latitudes (fig. 15). As a result, we cannot constrain the modified WF model in terms of Gubbins physical model.

If the flooding process is dominated by latitudinal rather than by longitudinal fluid

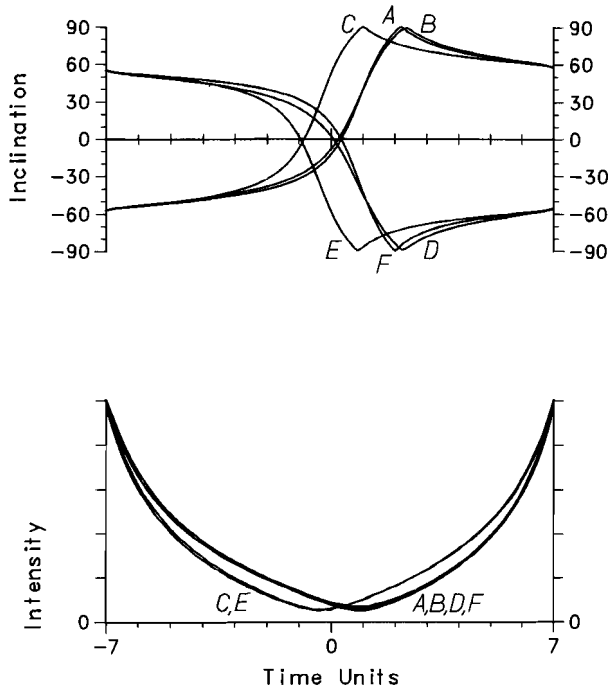

Fig. 14 Descriptive models for reversed to normal polarity transitions at 38°N (A-C) and 36°S (D-F). TU denotes time unit (Williams and Fuller, 1981). Curve A is the original WF model. Curve B, C, D and E results after partitioning 2% of the dipole source energy to respectively g_2, g_3, $-g_2$ and g_3. Curve F is the WF model for which $-g_2 : -g_3 : -g_4 = 2 : 3 : 5$. For comparison, the WF model time evolution has been used for all curves.

motions, the rapidly evolving reversals (lower Sidufjall, lower Nunivak) exhibiting zonal transitional field geometries are explained by an initiation location somewhere on or near the site meridian. The non-zonal upper Thvera and upper Nunivak records are then explained by an initiation somewhere between 286° and 196°E. The initiation longitude of the youngest (lower Sidufjall, lower Nunivak) reversals corresponds well to the longitude at which today reversed fluxes are observed (Gubbins, 1987).

The resemblance of the strongly non-zonal upper Thvera and upper Nunivak reversal records, in between of which three zonal reversal records are present, indicates that different types of reversals were not restricted to different epoches in the outer-core history. In

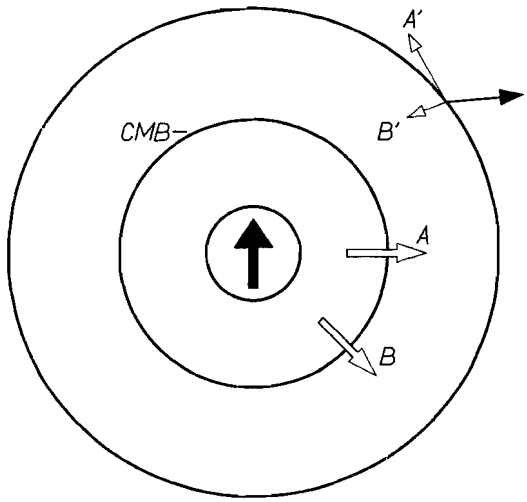

Fig. 15 Illustration of the deviations from the geocentric dipole field directions that are introduced by a small eccentric reversed flux source superimposed on a still unaffected geocentric dipole field. The figure gives a cross section of the earth with the inner-outer core boundary and the core mantle boundary (CMB). As a simplification the flux is considered to be caused by a reversed dipole perpendicular to the CMB at the equator (A) or at mid southern-latitudes (B). The closed and open vectors (with arbitrary lengths) at the earth's surface respectively denote the magnetic field directions caused by the geocentric dipole field and the eccentric reversed flux sources (A',B').

terms of Gubbins (1987) model this implicates that an initiation of successive reversals in the geomagnetic history may have taken place at different locations at the core-mantle boundary.

Acknowledgments

Both H.K.Thio and T.v.Hoof are thanked for their assistance during collection of the samples. H.J.Meier is gratefully thanked for his assistance in the laboratory. Prof.Dr.J.D.A.Zijderveld and Dr.C.G.Langereis are thanked for their critical reading of the manuscript. The investigations were supported by the Netherlands Foundation for Earth Science Research (AWON) with financial aid from the Netherlands Organization for the Advancement of Pure Research (Z.W.O., now N.W.O.).

Chapter IV

Rock magnetism of the magnetite and pyrrhotite bearing sediments from the Trubi formation (Italy)

1. Introduction

Magnetostratigraphic research of Neogene marine marls in the Central Mediterranean at the paleomagnetic laboratory "Fort Hoofddijk" yielded the information to identify a sequence of 25 reversals with an age ranging from 7.5 to 1.5 Ma. The oldest marine marls are of late Miocene age and are located on Crete (Langereis, 1984; Langereis et al., 1984). Pliocene marine marls are located in Calabria (Zijderveld et al., 1986) and on Sicily (Hilgen and Langereis, 1988; Zachariasse et al., 1989, 1990). These sedimentary sequences have been and still are the source for extensive studies of geomagnetic reversal records (See e.g. Valet et al., 1988; Linssen, 1988).

Both magnetostratigraphic and geomagnetic reversal studies rely entirely on the analysis of the direction and intensity of the primary component of the natural remanent magnetization (NRM), i.e. the magnetization induced by the geomagnetic field and recorded by the sediment during or shortly after deposition. During the life-time of a sediment new NRM components may have been introduced. For instance, this may occur as a result of the magnetic viscosity of the original magnetic minerals and by the production of magnetic minerals in the sediment after its consolidation. Hence, the identification of the carriers of the primary, but also of the younger secondary and viscous components of the NRM, and the distinction of their rockmagnetic properties is of crucial importance for the reliability of the results of magnetostratigraphic and geomagnetic reversal studies. The Lower Pliocene sediments from Calabria, known as the Trubi marls, are the subject of the present study. However, the significance of this study stretches itself beyond the sediment from the Trubi formation only; for instance, the Miocene marine marls of western Crete (Langereis et al., 1983, 1984; Valet et al., 1985) and the Pliocene marls from Sicily (Hilgen and Langereis, 1988) show many similar characteristics.

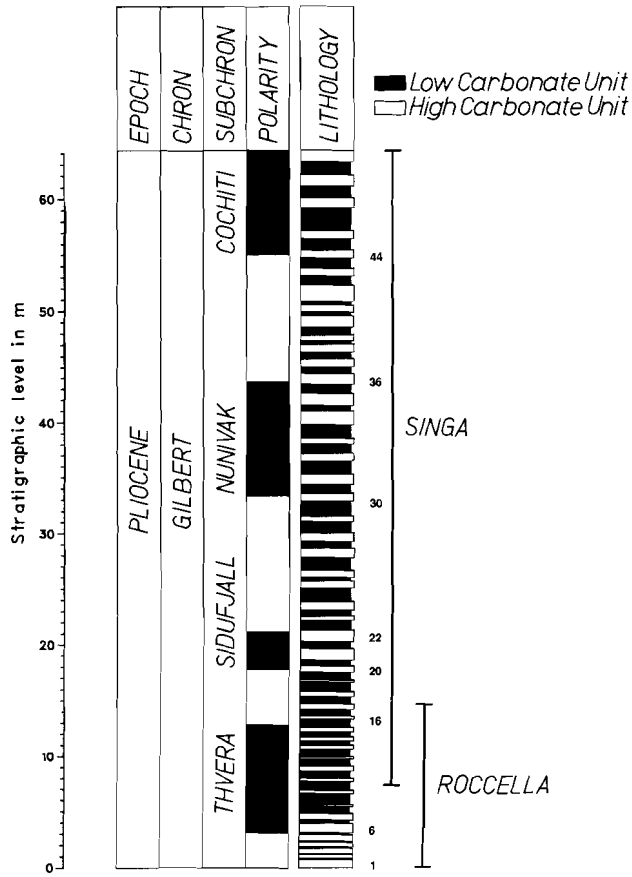

Fig. 1 Magnetostratigraphy and lithostratigraphy of the Monte Singa and Rocella sections (Zijderveld, 1986) The base of the sedimentary succession coincides with the Miocene/Pliocene boundary (4.84 Ma). Ages of the polarity boundaries are: lower Thvera: 4.77 Ma; upper Thvera: 4.57 Ma; lower Sidufjall: 4.47 Ma; upper Sidufjall: 4.40 Ma; lower Nunivak: 4.24 Ma; upper Nunivak: 4.10 Ma and lower Cochiti: 3.97 Ma (Berggren et al., 1985). The HCU units are indurated with respect to the LCU units. The small-scale cycle numbering is indicated (Hilgen and Langereis, 1988; Hilgen, 1987). The HCU of small-scale cycle 20 and the LCU of cycle 21 have been used for magnetic separation (section 6).

Some of the rockmagnetic characteristics of the Trubi marls have already been investigated during a study of geomagnetic reversal records (Linssen, 1988). This study showed the multi-component nature of the NRM of the Trubi marls. It was shown that two

ChRM components exist in the sediment, which become subsequently removed by progressive thermal demagnetization. Pure magnetite (T_B=580 °C) and cation deficient magnetite (T_B>580 °C) are the carriers of the high blocking temperature ChRM component. The identification of the ChRM component with the low blocking temperature was less straightforward. Rockmagnetic experiments showed that the remanent coercive force (H_{CR}) of the carrier of the low temperature component is considerably higher (70 mT) than the H_{CR} of the magnetite component (40 mT). The carrier of the low blocking temperature component was demonstrated to become largely altered near 360 °C. These observations, related to the available literature data suggested monoclinic pyrrhotite (Fe_7S_8) to be the carrier of the low temperature part of the ChRM component (Schwarz and Harris, 1970; Dunlop, 1986; Dekkers, 1988; Argyle and Dunlop, 1990). However, the identification of pyrrhotite remained tentative, principally since little is known about the paleomagnetic and rockmagnetic properties of fine grained sedimentary pyrrhotite (e.g. Kligfield and Channel, 1981; Freeman, 1986).

In the present study of the Trubi sediment substantial effort was put in a detailed investigation of the carriers of the characteristic remanent magnetization (ChRM) with geochemical and rockmagnetic methods. The purpose of this study is to provide insight in the identity and properties of the carriers of the ChRM component. The rockmagnetic part of this study includes the determination of isothermal remanent magnetization, hysteresis characteristics and susceptibility. The geochemical methods include X-ray diffraction, scanning electron microscopy, microprobe analysis, reflected and transmitted light microscopy. In contrast to rockmagnetic methods, geochemical methods have a relatively high detection limit and are not fit to be applied to the sediments directly; the estimated concentration of the magnetic minerals in the sediment is <<1%. Therefore, the geochemical methods were applied on magnetic extracts from the sediment.

2. Geology and magnetostratigraphy

The Lower Pliocene Trubi formation consists of a rhythmic sequence of marine marls and is widespread in the Calabrian and Sicilian sedimentary basins. The magnetostratigraphy of the Trubi formation was established in the Monte Singa section in Calabria (fig. 1, Zijderveld et al., 1986) and in the Punta Piccola section in Sicily (Zachariasse et al., 1989). The present study, related to a study of detailed reversal records (Linssen, 1988), was performed on sediments from the Monte Singa section.

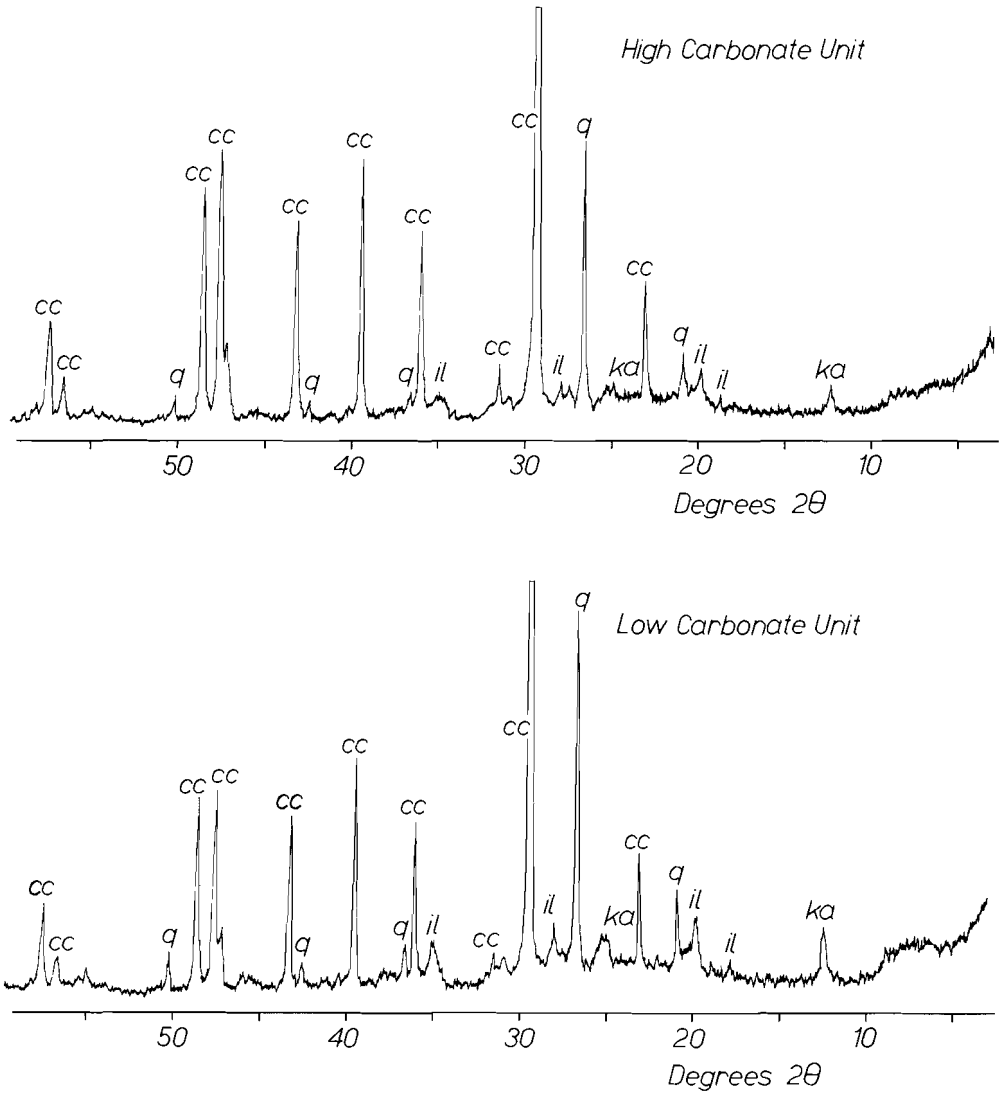

Fig. 2 X-ray diffractograms (Cu K_{alfa} radiation) of the high- and low carbonate units from the Calabrian Trubi formation. Predominant minerals are calcite (cc, $CaCO_3$), quartz (q, SiO_2), kaolinite (ka, $Al_4Si_4O_{10}[OH]_8$) and illite (il, $KAl_4Si_7AlO_{20}[OH]_4$). Calcite and quartz are abundant in the LCU's and HCU's. The clay minerals (illite, kaolinite) are somewhat more abundant in the LCU's than in the HCU's.

The Trubi sediment exposed in the Monte Singa section is undisturbed. No evidence exists that the sediment exposed in the Singa section was ever subjected to important thermal effects. The rhythmites of the sediment consist of alternating carbonate-poor and carbonate-rich marls; which are designated as Low Carbonate Units (LCU) and High Carbonate Units (HCU) respectively. The lithology of the Calabrian Trubi is different from the Sicilian Trubi. Within the Sicilian HCU three subunits can be distinguished: the central portion of the HCU is less calcareous and less indurated (Zachariasse et al., 1989; De Visser et al., 1989). The layer thickness of the individual units is laterally nearly constant at the scale of the exposure and ranges from 0.1 to 1.0 metres. The origin of the rhythmic sedimentation is believed to be related to the earth's average precession cycle of 21.7 kyr (Zijderveld et al., 1986; Hilgen, 1987).

The Monte Singa section magnetostratigraphically extends from the Thvera subzone to the Cochiti subzone. The geomagnetic reversal studies and present rockmagnetic investigations were restricted to the sedimentary interval enclosing the upper Thvera and upper Nunivak reversal records. Within this interval high (2-20 mA/m) NRM intensities occur (Zijderveld et al., 1986).

The sediment used for magnetic extraction and subsequent geochemical and rock-magnetic investigation was obtained from a sedimentary interval near the lower Sidufjall reversal record (fig. 1). This interval includes both a HCU and a LCU (cycle 20; Hilgen and Langereis, 1988). The rapidly proceeding lower Sidufjall reversal is present in a HCU (Linssen, 1988). The occurrence of the reversal and the distinctive properties of the HCU and LCU make this interval very suitable for the purpose of the present investigation.

3. Instrumentation for the magnetic measurements

Stepwise thermal demagnetizations were performed either in a Schönstedt tunnel furnace with mu-metal shielding or in a laboratory built furnace of the same type. Stationary alternating field demagnetization was applied in three orthogonal directions. Remanent magnetization measurements were accomplished with a laboratory built digital spinner magnetometer and with a 2G-Enterprises cryogenic magnetometer. Measurements of the initial susceptibility were performed with an AC bridge (KLY-1). Continuous measurements of the remanent magnetization during low-temperature cycling and continuous thermal demagnetization were carried out with the laboratory built HALT spinner. Essentially the HALT spinner is a fluxgate spinner magnetometer mounted in a

Helmholtz system. The specimen holder can be placed either in a water-cooled furnace for continuous thermal demagnetization or a dewar vessel in which aliquots of liquid nitrogen can be sprayed for low-temperature experiments (Dankers, 1978). Hysteresis loops were determined by measuring the imbalance in a pair of coils in an AF field; one of the coils contains the specimen. For this study the hysteresis device was equiped with a digital storage-scope and a microcomputer.

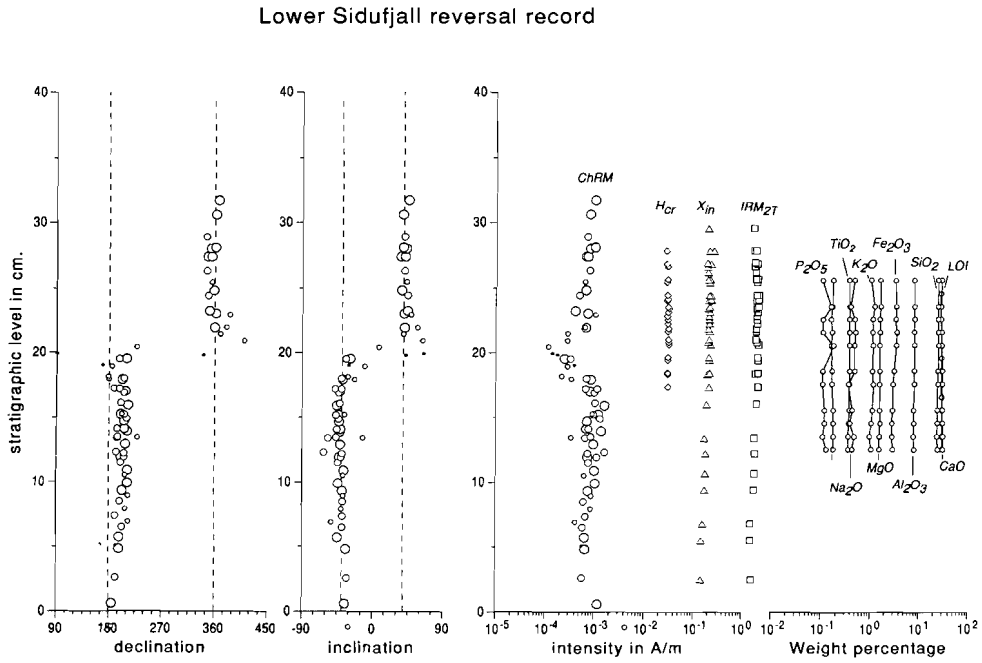

Fig. 3 lower Sidufjall reversal record (Linssen, 1988; chapter 3) and weight percentages of the major element oxides for specimens from the lower Sidufjall reversal record. Analysis was performed with X-ray fluorescence; the error is less than 5%. LOI (loss on ignition) was determined by measuring the weight of the samples before and after heating; the weight percentages of the major element oxides have been corrected for the LOI. The reversal record shows the magnetite components demagnetized between 480 and 620 °C. Largest (smallest) circles indicate most (least) reliable magnetizations.

4. Mineralogy and chemistry of the marls

The mineralogy and chemical composition of the marls was studied in the sedimentary interval enclosing the lower Sidufjall reversal record (Linssen, 1988). The principal mineral constituents of the HCU and LCU have been inferred from X-ray diffraction (XRD) analysis (fig. 2).

The main group of minerals occurring in the HCU and LCU proved to be calcite, quartz and the clay minerals kaolinite, illite and minor clay-mineral-like chlorite. No reflections of magnetic minerals were observed. Apparently, the amount of magnetic minerals in the marls is below the detection limit of the XRD device (1-5%).

The major element oxides have been determined in the HCU in which the lower Sidufjall reversal record is present. The concentrations of the element oxides are fairly constant across the actual reversal (fig. 3). CaO, SiO_2 and the volatile compounds make up approximately 85% of the sediment's weight. The volatile compounds (LOI) include CO_2 (from calcite) and H_2O. Usually, H_2O is present in sediment as interstitial water (2-4%) and as mineral water, (e.g. in clay minerals about 5-10%).

The concentrations of the major elements and the ideal stoichiometry of the minerals (Deer et al., 1977), which were identified with XRD analysis, yield an estimation of the concentration of the main mineral constituents of the HCU. The calculated calcite concentration is approximately 52-56% by weight. Clay minerals (predominantly kaolinite and illite) and quartz make up respectively 29-33% and 7-11% of the sediment's weight. The weight percentage of interstitial and loosely held mineral water is approximately 5-10%.

The observed calcite content (52-56%) is less than reported by de Visser et al. (1989) for the corresponding beige units in the Sicilian Trubi, in which it is reported to be 65%. Probably this difference in carbonate content is caused by the less indurated nature of the Monte Singa Trubi. De Visser et al. (1989) further demonstrated a variation of kaolinite (less in the LCU layers) and no variation of the illite or chlorite concentration. According to De Visser et al. (1989) these data point to a rhythmic variation between cool and arid (HCU) and warm and humid (LCU) periods.

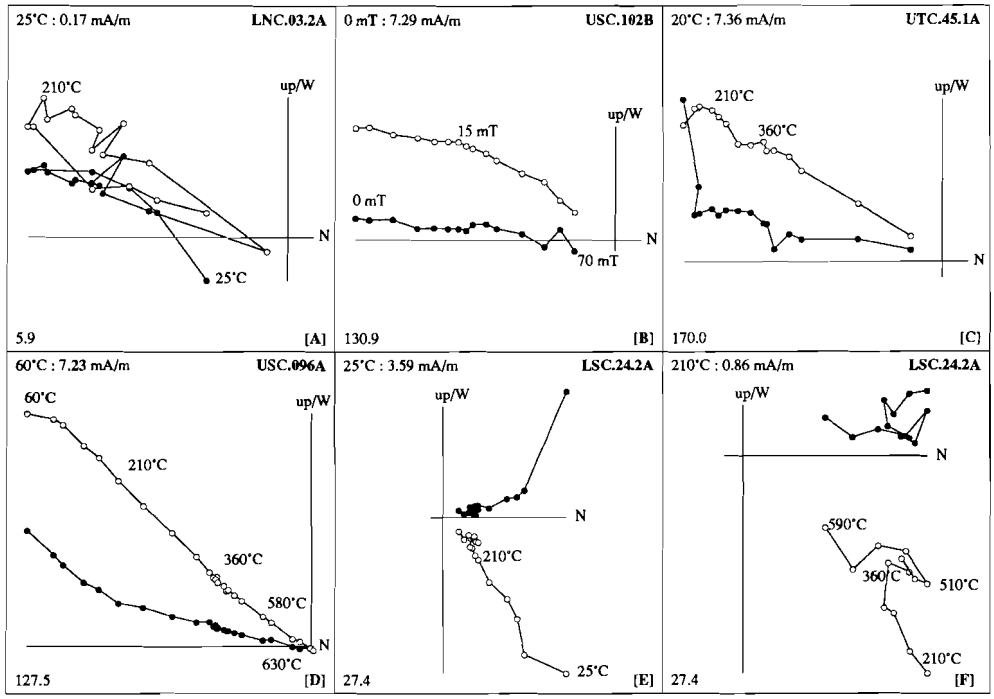

Fig. 4 Thermal and AF demagnetization diagrams (orthogonal projections, Zijderveld, 1967) for specimens from the Trubi sediment (after Linssen, 1988). Open (closed) symbols denote projections on the vertical (horizontal) plane. The stratigraphic level of the specimens is indicated in the lower left corner of each diagram. The intensity at the first step is indicated in the upper left corner of each diagram. Normal demagnetization steps in the range 90-510 °C are 30 °C, steps above 510 °C are 20 °C. The AF demagnetization was performed with 2.5 mT increments in the range 0-20 mT, additional steps are taken at 25 and 30 mT, above 30 mT the increment is 10 mT. **[A]** Specimen LNC.03.2A is from a HCU interval below the lower Nunivak reversal (cycle 30, see also fig. 3). The thermal demagnetization diagram shows the removal of a viscous component (25-120 °C), a secondary component (120-210 °C) and the composite ChRM component (>210 °C). **[B]** Specimen USC.102B is from a LCU interval above the upper Sidufjall reversal (cycle 23). The alternating field demagnetization diagram shows an apparently single ChRM component (>15 mT), which is in fact a composite component. Note that high fields (>80 mT) tend to produce scattered results. [C] Specimen UTC.45.1A is from a HCU interval above the upper Thvera reversal (cycle 16). The composite ChRM component is dominated by the high-temperature magnetite component. **[D]** Specimen USC.096A is from a LCU interval above the upper Sidufjall reversal (cycle 22). The composite ChRM component consist of a low-temperature component (210-360 °C) and a high-temperature (cation-deficient) magnetite component (480-640 °C). **[E,F]** Specimen LSC.24.2A is from a HCU interval above the lower Sidufjall reversal record (cycle 20). The enlargement **[F]** of the demagnetization diagram shows a medium-temperature component (360-480 °C) with what appears to be a reversed direction.

5. Natural remanent magnetization

The natural remanent magnetization (NRM) of the sediment from the Trubi formation is composed of a ChRM, a viscous and a secondary magnetization (fig. 4a). The viscous and secondary components are small compared to the ChRM component. The ChRM component is supposed to have a primary origin (Zijderveld et al., 1986; Linssen, 1988).

The viscous and secondary components in the Trubi sediment have largely overlapping blocking temperature and coercive force spectra. As a result the viscous and secondary components show up as a smoothly curved trajectory in the demagnetization diagram, or occasionally even as an apparently single (linear) component with a direction intermediate to the laboratory field and the present day field of the sediment in-situ. During thermal demagnetization the viscous/secondary component is removed at a temperature of 210 °C (figs. 4a,c). The maximum alternating field required to remove the viscous/ secondary component is 15 mT (cf. fig. 4b).

A closer investigation of the thermal demagnetization diagrams demonstrate that the ChRM components are composed of a low temperature and a high temperature ChRM (sub-)component (figs.4c,d). The maximum blocking temperatures of the carriers of the two ChRM components are 360 °C and between 580-620 °C. The high-temperature component is cation-deficient (CD) magnetite (e.g. Heider and Dunlop, 1986), the low-temperature component was suggested to be pyrrhotite (Linssen, 1988). The low-temperature component is most prominent in the LCU (compare fig. 4c and d). The succession of demagnetization diagrams in figure 5 obtained from the rapidly proceeding lower Sidufjall reversal record (Linssen, 1988), demonstrates that the two ChRM components have the same direction in all specimens, and hence almost synchronously recorded the same geomagnetic field. Records of the low-temperature component show slightly more detailed variations than the high-temperature magnetite component (Linssen, 1988, chapter 3).

In the AF decay curves the ChRM component appears to be composed of a single magnetic phase. Obviously, the two magnetic phases of the ChRM component have only slightly different and largely overlapping coercive force spectra (fig. 4b). The maximum alternating field required to demagnetize the entire composite ChRM component is near 120 mT, although it is difficult to determine this value accurately since high alternating fields (>80 mT) tend to produce scattered demagnetization results.

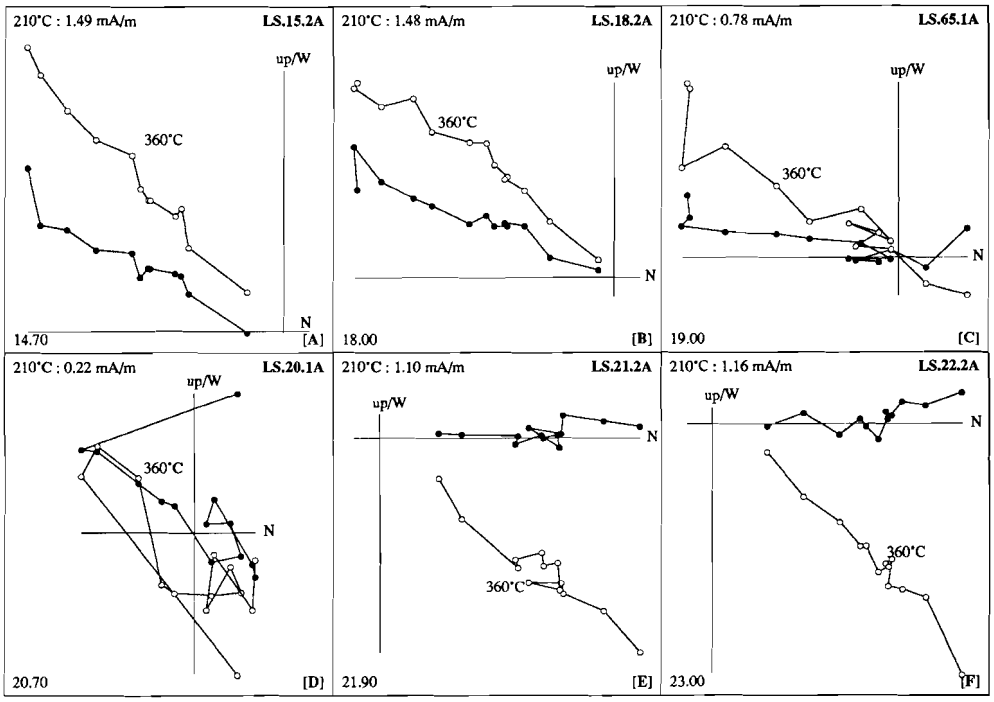

Fig. 5 Thermal demagnetization diagrams (orthogonal projections, Zijderveld, 1967) of the NRM from specimens from the lower Sidufjall reversal record (Linssen, 1988; chapter 3, see also fig. 3). Open (closed) symbols denote projections on the vertical (horizontal) plane. The stratigraphic level of the specimens is indicated in the lower left corner of each diagram. The demagnetization starts at 210 °C, the last step is 570 °C, the 360 °C demagnetization step is indicated in each diagram. The intensity at the first step is indicated in the upper left corner of each diagram. The succession of diagrams shows that the low temperature component (210-360 °C) and the high-temperature magnetite component (480-620 °C) rapidly and (almost) simultaneously change direction.

Rarely a low intensity component shows up during thermal demagnetization between 360 and 480 °C (figs.4e and enlargement 4f). Since consistent records of these medium temperature components are absent in the Monte Singa section it was not possible to conclude whether this component is an additional component, or an artificial component introduced during the alteration of the sediment upon heating. The origin of the medium temperature component will not be elaborated in this study.

6. Geochemical investigation of the magnetic extracts

In spite of the high resolution of rockmagnetic methods, the identification of magnetic minerals of micron and sub-micron size is complicated with these methods. This is largely due to the fact that information on magnetic properties of these fine-grained, and preferably stress-free minerals is only sparsely available and for a limited number of minerals such as magnetite (e.g. Dunlop, 1986; Argyle and Dunlop, 1990). Other methods which may assist to identify magnetic minerals are microprobe analysis, scanning electronic microscopy and X-ray diffraction analysis. However, these geochemical methods fail to identify magnetic minerals occurring in low concentrations (see section 4). With the purpose to identify the magnetic minerals which are dispersed in the Trubi sediment, the magnetic mineral content was separated with magnetic methods and subsequently investigated with geochemical and rockmagnetic methods.

6.1 Experimental procedures

The HCU and LCU samples used for the magnetic separation were obtained from a large number of small and fresh samples taken throughout the sedimentary intervals enclosing the lower Sidufjall reversal record (fig. 1). Prior to the magnetic separation the marls were dispersed in distilled water to produce a slurry of low viscosity (400 grams of sediment in 2 litre of water per batch). The dispersion of the unconsolidated marls was easy. Dispersion, in contrast to crushing, preserves the original grain size and internal stress conditions of the magnetic minerals. Ascorbic acid was added to the suspension to achieve slightly reducing conditions, thus preventing oxidation of the magnetic compounds.

The slurry was slowly pumped around in a closed circuit of plastic tubes (inner diameter 0.7 cm) passing the magnetic poles of a Franz Isodynamic Separator which was set at maximum strength (2.5 Amps.~0.8 T). The Franz Isodynamic Separator removes paramagnetic and ferrimagnetic grains from the suspension. A centrifugal pump (Eheim) was used to avoid magnetic interference and contamination of the suspension. The vessel holding the bulk of the suspension was put into a cooled ultrasonic bath during circulation in order to preserve the homogeneity of the suspension.

The circulation time for a complete 2 litre suspension batch was 5-15 minutes. Every

six to eight hours the pumping was stopped and the magnetic extract was removed. This procedure was repeated until no significant yield was gained (total pumping time approximately 50 hrs.). To obtain a semi-quantitative separation of high and low susceptibility fractions two additional separation steps were performed on the magnetic extracts with stepwise increasing field strengths of 0.25 and 0.5 Amps. The fractions obtained at currents of 0.25 Amps. for the LCU and those at currents of 0.5 Amps. and 2.5 Amps for the HCU did not yield significant amounts of material and were added to the nearest fraction. The fractions which were used in this study are:

- Fraction 1 : Original sediment from LCU
- Fraction 2 : Residual sediment from LCU
- Fraction 3 : Extract obtained with I=0.25 Amps. (+ 0.5 and 2.5 Amps.) from HCU
- Fraction 4 : Extract obtained with I=0.5 Amps. (+ 0.25 Amps.) from LCU
- Fraction 5 : Extract obtained with I=2.5 Amps. from LCU

For the preparation of synthetic specimens known weight quantities of the magnetic extracts were dispersed in a quartz/bassanite matrix. This quartz/bassanite matrix (CM Löt soldering investment for dental metal work) is hardly magnetic and withstands temperatures up to 1700 °C.

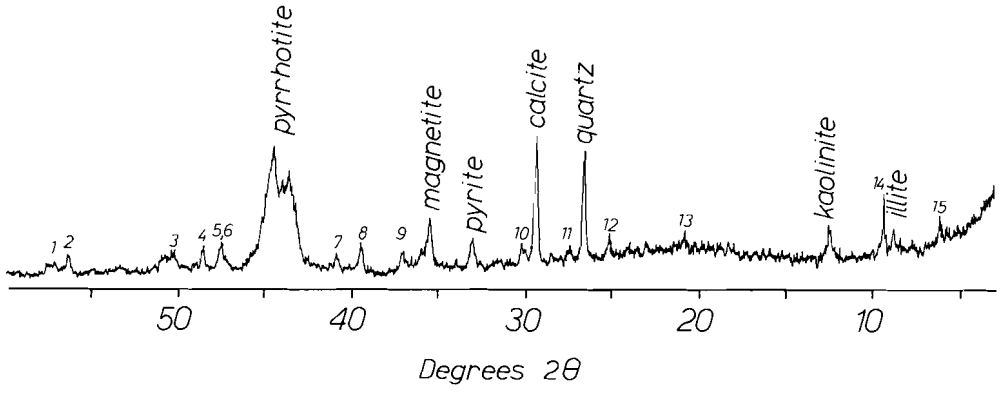

Fig. 6a X-ray diffractogram (Cu K_{alfa} radiation) of the magnetic extract obtained from a HCU (fraction 3). The main reflections of the identified minerals are shown by the mineral names. The main mineral is pyrrhotite which is present with a complex spectrum of reflections; the peaks are at d=2.035, d=2.060 and d=2.078 Å. Pyrrhotite reference data : 4C-Pyrrhotite, JCPDS-ICDD, (290723), 85% [-1,2,2] at 2.979 Å, 55% [2,0,4] at 2.069 Å, 90% [3,2,2] at 2.064 Å, 100% [-5,2,2] at 2.054 Å, 35% [3,1,3] at 2.046 Å, 80% [0,4,0] at 1.718 Å. Significant reflections but of lower intensities for magnetite are denoted 1,10; for pyrite: 2,6,7,9; for calcite: 4,5,8 and for quartz : 3,13. Non-identified phases are denoted 11,12,14 and 15.

6.2 X-ray diffraction

X-ray diffraction of fraction 3 (HCU, fig. 6a) reveals the presence of magnetite, pyrrhotite and (non-magnetic) pyrite. The main reflections near d=2.035 Å, d=2.060 and d=2.078 Å are characteristic for monoclinic (ferrimagnetic) 4C-pyrrhotite. The observation of monoclinic pyrrhotite and magnetite reflections confirm the suggestion (Linssen, 1988) that these minerals are the important magnetic mineral constituents of the Trubi sediment. The presence of (non-magnetic) pyrite in the magnetic extract indicates that pyrite is physically attached or intergrown with magnetite and/or pyrrhotite. A comparison of the X-ray diffractogram with the diffractograms of the original sediment (fig. 2) shows that a

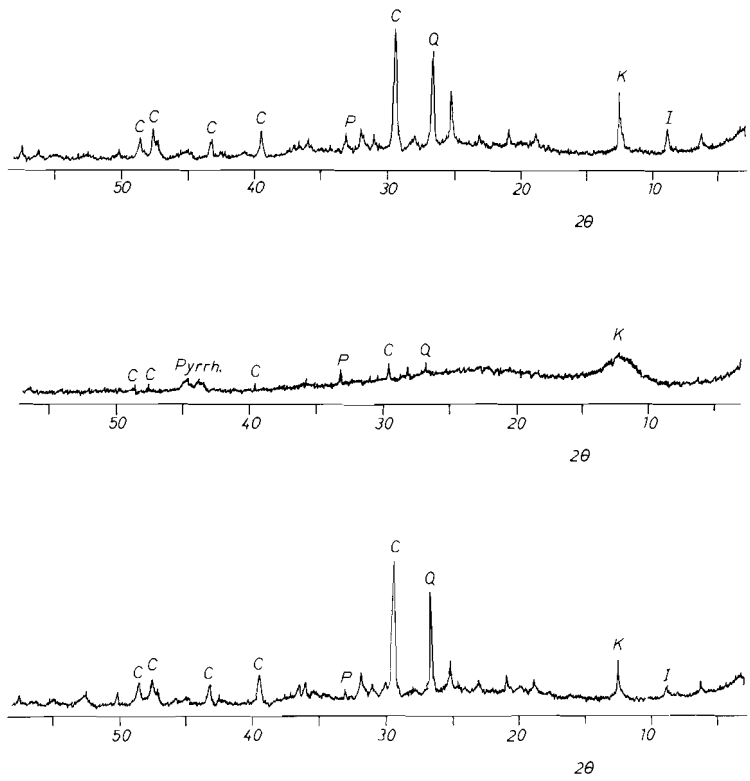

Fig. 6 X-ray diffractogram of (**b, below**) fraction 4 (LCU), (**c, middle**) fraction 3 (HCU) heated at 360 °C and (**d, above**) fraction 4 (LCU) heated at 360 °C. Little material of heated fraction 3 was available for the XRD. Minerals are denoted (Pyrrh)otite, (P)yrite, (C)alcite, (Q)uartz, (K)aolinite, (I)llite. See also caption fig. 6a.

significant amount of calcite, quartz and clay minerals is still present in the extract.

In the diffractograms of fractions 4 and 5 (LCU, fr.4 in fig. 6b) reflections from the same non-magnetic minerals are present. Reflections of pyrrhotite and magnetite do not show up. Again, the presence of non-magnetic pyrite in the magnetic extract indicates that this mineral is physically attached or intergrown with magnetic minerals.

The magnetic content of the extract is expected to change significantly after heating at 360 °C due to the alteration of pyrrhotite at this temperature (Linssen, 1988). The pyrrhotite alterations during heating are known to proceed by oxidation and sulphur-loss, although most prominently above 400 °C (Schwarz and Harris, 1970; Bennett et al., 1972). X-ray diffractograms of the heated (360 °C) fractions 3 and 4 were made to study this phenomenon (fig. 6c,d); not enough material from fraction 5 was left to be included in this experiment. The diffractogram of the heated fraction 3 still reveals pyrrhotite reflections, although the intensities have decreased relative to the diffractogram of the non-heated specimen. Both in fraction 3 and 4 the reflections of pyrite gained intensity, suggesting a pyrrhotite to pyrite alteration during heating.

It is remarkable that the specimens, after being heated to 360 °C, still show the reflections of monoclinic (ferrimagnetic) pyrrhotite, whereas it was demonstrated (Linssen, 1988) that the carrier of the low temperature pyrrhotite component loses its remanent magnetic properties after being heated at this temperature. There is no unambiguous explanation for this observation. However, it is shown (Clark, 1984; Dekkers, 1988) that the remanence and susceptibility of pyrrhotite rapidly decreases for grains smaller than 15 micrometer. This decrease likely extends to grain sizes below the single domain threshold size of pyrrhotite. Hence, a speculative explanation might be that at 360 °C, due to an alteration of monoclinic pyrrhotite, the average grain size of pyrrhotite has decreased to a (still single domain) size at which the remanence (and susceptibility) is small. An alternative and perhaps supplementary explanation for these observations is that less magnetic anti-ferromagnetic hexagonal pyrrhotite, to which phase monoclinic ferrimagnetic pyrrhotite reverts at 254 °C, is quenched during cooling (Kissin and Scott, 1982 and references therein).

6.3 Optical and microprobe investigation of the magnetic extracts

6.3.1 Optical microscopy

Observation of polished thin sections of the magnetic extracts demonstrated no more than 10% opaque minerals in fraction 3 (HCU), less than 5% in fraction 4 (LCU) and less than 1% in fraction 5 (LCU). The unambiguous microscopic determination of the magnetic minerals in the extracts was not possible due to the small grain sizes of the opaque minerals (<2 micrometer). However, the yellowish reflection of some grains in the extracts indicated that sulphidic minerals, such as pyrite and pyrrhotite, are present. Sporadically rather large (10 micrometer) lamellar grains were observed in fraction 3 (HCU, fig. 7a). Microprobe analysis identified these grains as FeTi-oxides (section 6.3.2).

6.3.2 Microprobe and scanning electron microscope observations

The composition of the magnetic extracts has been investigated with a scanning electron microscope (SEM) and a JEOL microprobe with SEM facility (fig. 7b-e). The optical resolution of the microprobe and both SEM facilities is slightly better than 1 micrometer, as is the effective spot size for microprobe analysis. As a consequence, only the grains of 1 micrometer and larger could be analyzed with the microprobe. The investigated samples consist both of polished grains from the magnetic extracts dispersed in Bakelite or Araldite and of unpolished grains distributed on the glass plate without any adhesive or matrix.

Microprobe analysis of the magnetic extracts indicate the presence of quartz, calcite and clay minerals. In none of the magnetic extracts a single magnetite grain was spotted, although the rockmagnetic investigations unambiguously demonstrated the occurrence of this mineral in the sediment. Most probably magnetite was not observed due to the limited resolving power of the microprobe.

The SEM analysis of the samples confirm that the majority of the sulphidic grains is smaller than 2 micrometer, whereas a minority is in the 2-10 micrometer range.

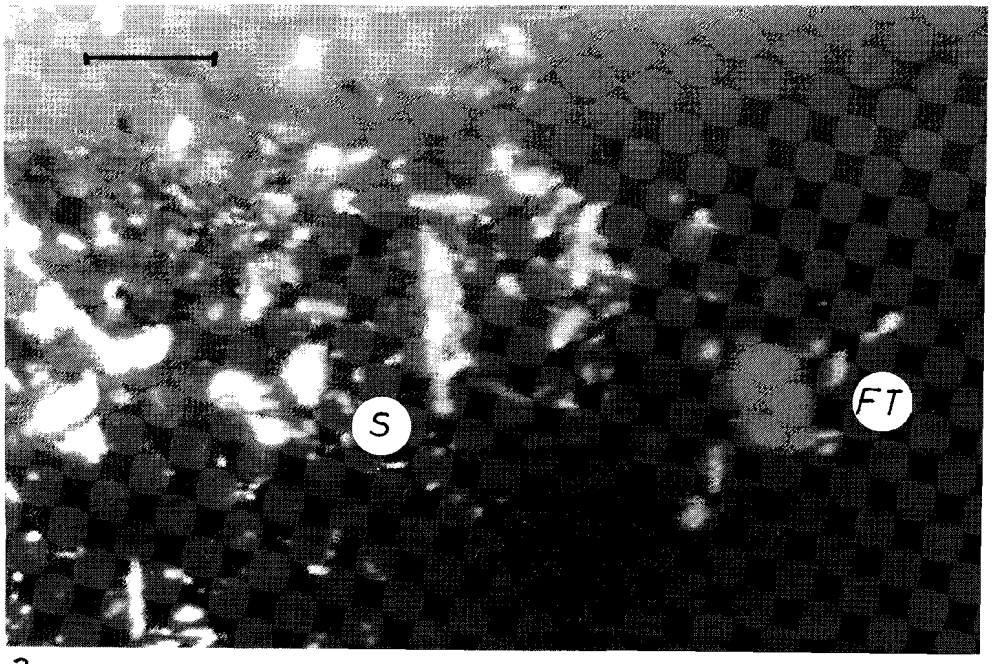

a

b

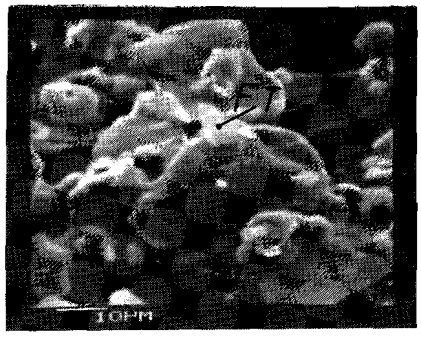

c

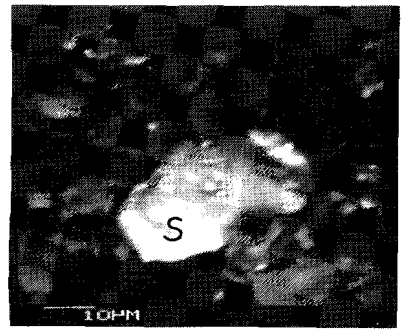

Fig. 7 Photographs from optical studies of the magnetic extract from an HCU sample (I=0.25 Amp., fraction 3). a) reflection microscope photo of an assemblage of sulphide grains (S) and a FeTi-oxide (FT) (the bar corresponds to 20 micrometer), b) SEM image of FeTi-oxide, c) and d) SEM and backscatter images of large sulphidic grains. Note the numerous high intensity reflections from small (<2 micrometer) sulphidic grains.

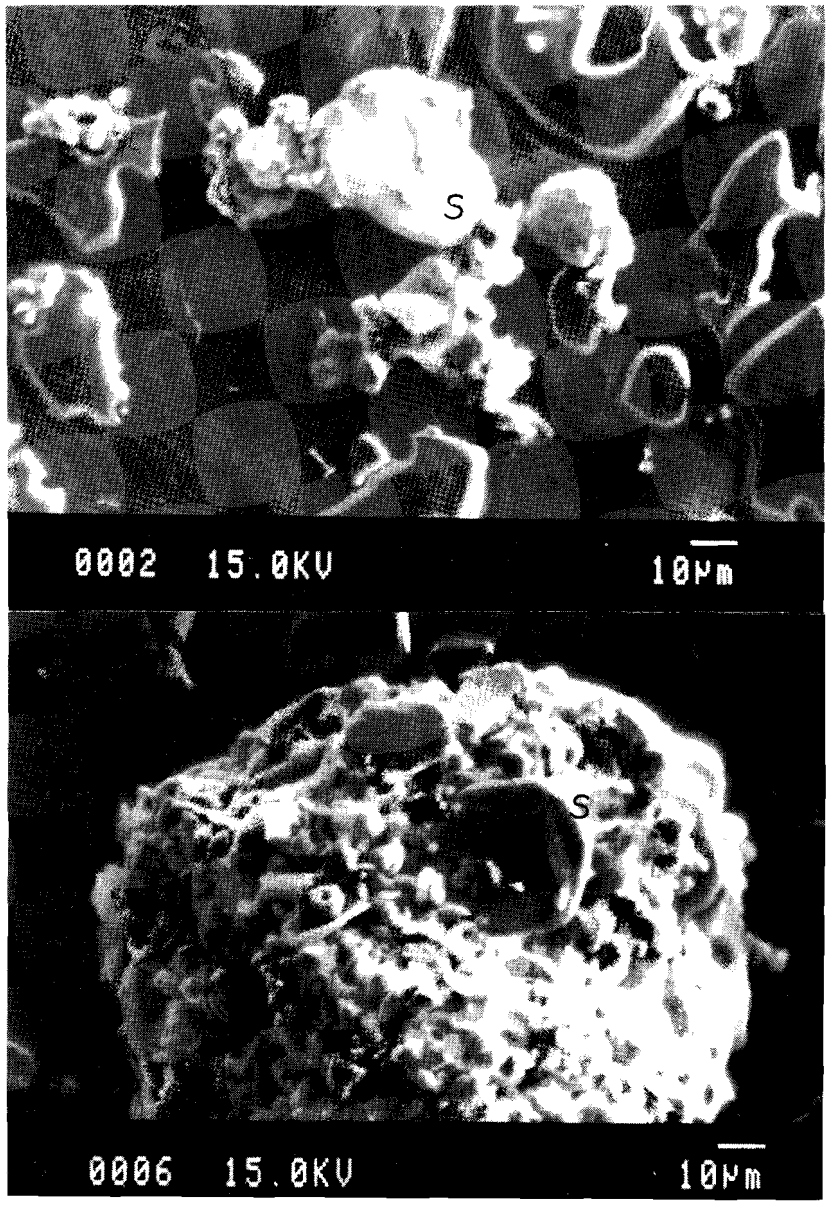

The latter SEM images show sulphidic grains which are rather rounded and have irregular marks on the surface corresponding to characteristic biogenic morphologies (Blakemore et al., 1981; Vali et al., 1987), e) SEM image of a sulphidic grain which is embedded in clay mineral grains and carbonate fragments of organic origin. The SEM semi-quantitative analysis of the sulphidic grains does not allow a distinction between pyrite and pyrrhotite

Table 1. *Quantitative microprobe analysis of a sulphidic grain*

	(1)		(2)		(3)		(4)	
	Wt.%	At.%	Wt.%	At.%	Wt.%	At.%	Wt.%	At.%
Fe	54.94	45.77	54.75	45.33	45.99	37.04	46.42	38.63
Cu	0.00	0.00	0.16	0.12	0.00	0.00	0.00	0.00
As	0.00	0.00	0.00	0.00	0.00	0.00	0.00	0.00
S	36.70	53.25	36.18	52.76	44.13	61.89	41.97	60.84
Al	0.00	0.00	0.00	0.00	0.18	0.31	0.00	0.00
Si	0.38	0.63	0.54	0.90	0.43	0.69	0.25	0.42
Ca	0.30	0.34	0.33	0.39	0.06	0.07	0.09	0.11
Total	92.32	100.00	91.77	100.00	90.79	100.00	88.73	100.00

Table 1. Spots (1-4): Weight and normalized atom percentages of four spots in a sulphidic grain as determined with a JEOL Microprobe with SEM facility. Commonly associated elements have been included in the analysis of the Fe sulphides. ZAF correction has been applied. Operating conditions 15 kV, 40 Degs. In pyrrhotite the weight percentage of Fe:S~60:40, the atom percentages are Fe:S~47:53; in pyrite the weight percentage of Fe:S~47:53 and atom percentages are Fe:S~33:67. Analysis of the total ED spectrum showed that no other elements are present. None of the weight percentages add up to 100%. The analysed spots (1) and (2) give a near pyrrhotite stoichiometry, whereas spots (3) and (4) in the same grain give a near pyrite stoichiometry.

Sporadically larger grains (10-20 micrometer) are observed (fig. 7b,d,e). Only the largest grains could be analysed properly with the microprobe. The analysis of a large number of sulphidic grains revealed weight deficiencies of 8% and more (see e.g. table 1). The weight deficiency is present in the small grains and in grains which are many times larger than the microprobe spot size. Hence, a contribution of matrix material to the analysis may be excluded as the origin of the weight deficiency.

Microprobe elemental distribution maps of Fe and S of an unpolished and a polished sulphidic grain (figs.8a,b) demonstrate that the Fe distribution is constant, whereas the S distribution is not. The uneven distribution of S is lamellar; the individual lamellae have a width of approximately 1 micrometer. The normalized atom percentages of the brightest lamellae in the polished grains reveal a near pyrrhotite stoichiometry (table 1, spot 1 and 2), whereas the somewhat darker lamellae have a stoichiometry closer to that of pyrite (table 1, spot 3 and 4). The origin of the lamellae is not clear; they may be formed by secondary processes. The lamellar structure in the small (<<10 micrometer) sulphidic grains can have important effects on the magnetic properties of pyrrhotite: The effective grain size diminishes resulting in a considerable lower remanence and susceptibility (Clark, 1984; Dekkers, 1988).

The opaque and rather large (10 micrometer) lamellar grains, observed with reflection microscopy (fig. 7a), were identified as FeTi-oxides. The FeTi-oxide was sparsely observed in fraction 3 (HCU) and was never observed in fraction 4 and 5 (LCU), nor did it show up in the XRD analysis of any of the fractions (XRD detection limit 1-5%). The FeTi-oxide contains almost equal quantities of both Fe and Ti and shows small (<1 micrometer) exsolution lamellae which could not be analyzed individually. The FeTi-oxide grains are sharp edged, relatively large and occur in a narrow grain size range ($10^{+}/_{-}$ 3 micrometer) (fig. 7b). No crystalline habitus was observed enabling the determinative discrimination between a trigonal (Ti-hematite) and a cubic (Ti-magnetite, Ti-maghemite) crystal structure. Titano-magnetites have a Curie temperature between the Curie temperature of magnetite (580 °C) and ulvöspinel (-153 °C). Thermal demagnetization revealed maximum blocking temperatures at 580 °C (magnetite), 360 °C and 210 °C. The FeTi-oxide is only observed in the HCU, whereas the 360 °C component is typical for the LCU. Hence, the FeTi-oxide is very unlikely to correspond to the 360 °C component. More likely the remanent magnetic contribution of the FeTi-oxide, if any, is limited to the viscous/secondary component of the NRM removed at 210 °C.

7. Rock magnetism of the magnetic extracts

Application of XRD and microprobe analysis to the magnetic extracts demonstrated the presence of magnetite, pyrrhotite and a FeTi-oxide in the sediment. However, with these geochemical methods it is not possible to adequately determine the concentrations and grain sizes of the magnetic minerals, nor can these methods help to determine the contributions of the magnetic minerals to the remanence. It is the latter contribution of the magnetic minerals to the remanence in which we are particularly interested from a paleomagnetic point of view. Yet, the established identities of the contributing magnetic minerals enables one to relate the rockmagnetic observations to grain size dependent rockmagnetic parameters.

There are several rockmagnetic methods which provide facilities to determine grain size or concentration of dispersed magnetic minerals. However, the specific capability and/or accuracy of these methods to establish these rockmagnetic parameters varies considerably. In order to increase the reliability and accuracy of the results more than one rockmagnetic method has been applied. The continuous and stepwise thermal

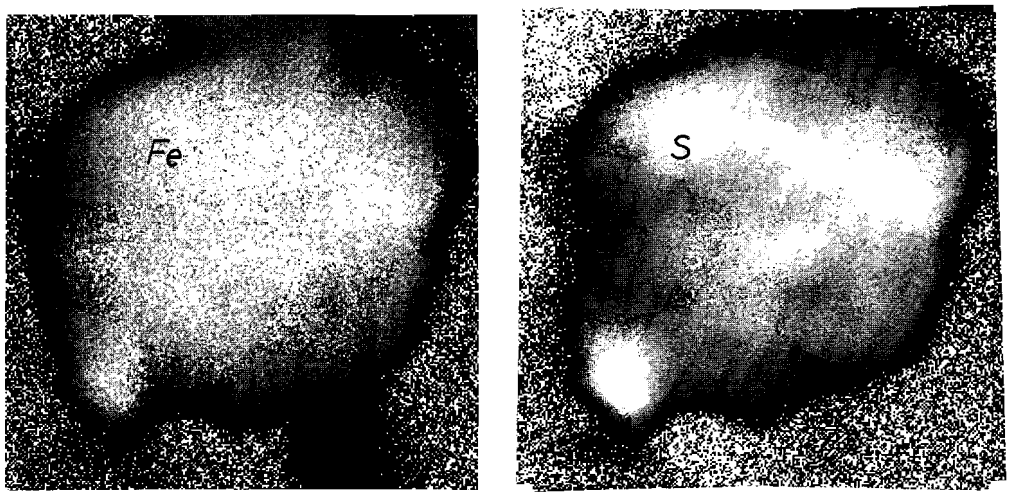

Fig. 8 JEOL microprobe images of magnetic extracts. (a, above) Fe and S distribution for an unpolished sulphide grain and (b, right page) backscatter image and S distribution for another polished sulphide grain. Mark that the Fe distribution in (a) is uniform whereas the distribution of S is not. The backscatter intensity is proportional to the mean atom number at the analyzed spot. Hence, the brightest areas indicate pyrrhotite, the darkest areas indicate hydrous Fe,S compounds or S rich Fe,S compounds (pyrite).

demagnetization methods (section 7.2) were applied to determine the contributions of magnetite and pyrrhotite to the remanence, but also to determine the effects of the alteration process which takes place upon heating. Since the remanence of pyrrhotite is completely removed at 360 °C (Linssen, 1988), it was possible to isolate the (grain size dependent) IRM characteristics of both magnetite and pyrrhotite (section 7.3). The alternating field demagnetization results of ARM (section 7.4) yield median destructive fields, the values of which are also grain size dependent (Dekkers, 1988; Linssen, 1988). The determination of in-field hysteresis parameters provides information on the domain state and grain size of magnetite and pyrrhotite (section 7.5). The low temperature treatments (section 7.6) were performed to establish the average grain sizes of magnetite and pyrrhotite. Finally, the various rockmagnetic results have been compiled and re-calculated to properties of magnetite and pyrrhotite in the HCU and LCU (section 7.7). The experiments have been conducted on fractions 3 (HCU), 4 and 5 (LCU, see section 6.1 for details).

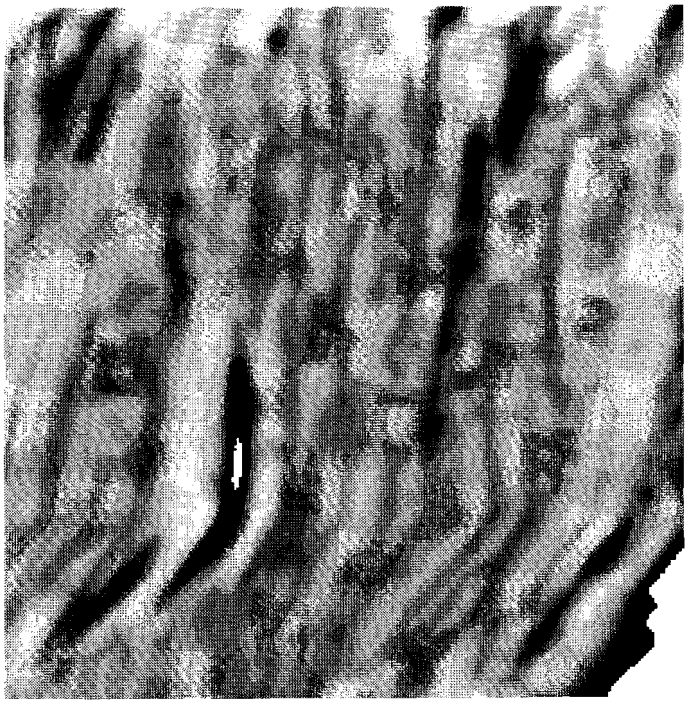

Backscatter

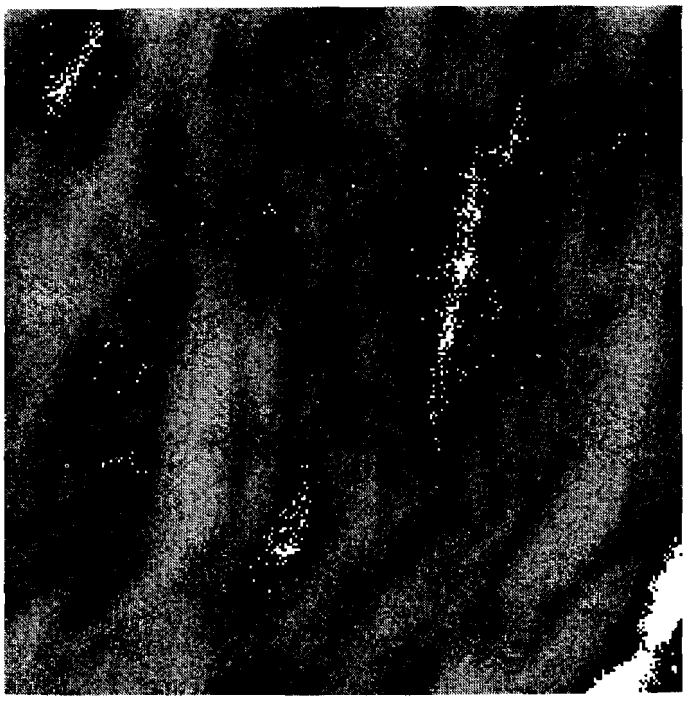

S

1 micrometer

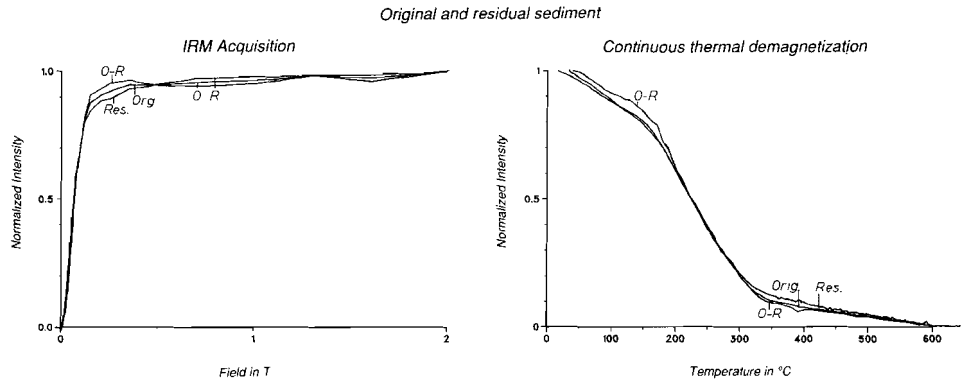

Fig. 9 (a, left) Normalized IRM acquisition curves for an original LCU sample and its residue after separation of magnetic minerals. The curve denoted O-R theoretically represents the extracted magnetic minerals and is obtained by subtraction of the (non-normalized) acquisition curves of the residue from that of the original sediment sample. **(b, right)** The continuous thermal decay curves of the original LCU sediments, the residue after the separation procedure and the difference curve (O-R) theoretically representing the extracted magnetic minerals (see a). The bulb in the decay curve between 150 and 220 °C is due to a matrix effect: i.e. a gypsum to anhydrite reaction (Dekkers, 1989).

The separation of dispersed magnetic minerals from sediments has been performed before (e.g. Løvlie et al., 1971, and references therein; Kent and Lowrie, 1974; Karlin and Levi, 1985; Chang and Kirschvink, 1985). The reported separation techniques were successful in removing not more than 50-70% of the magnetic material from the sediment. In the present study the results of the separation procedure are more or less similar.

For a full appreciation of the geochemical and rockmagnetic results it is important to establish the differences between the original sediment and the investigated magnetic extracts. For this reason, the side effects of the separation process have been paid special attention in the first part of this section.

7.1 Efficiency of the magnetic separation process

IRM acquisition shows that an amount of magnetic minerals has been removed from the original LCU sediment carrying 51% of the IRM acquired in a 2 T field (IRM_{2T}). The corresponding figure in the HCU is 75% (table 2).

IRM acquisition characteristics of the original and residual sediment of the LCU are very similar (fig. 9a), which implicitly indicates that the IRM characteristics of the

removed fraction (the magnetic extracts) and the original sediment are similar. This is illustrated by the difference curve that results after subtraction of the IRM acquisition curves of the residual and original sediment (fig. 9a), and by the IRM acquisition curve of the magnetic extract (fig. 13).

The continuous thermal demagnetization curves of IRM_{2T} for the original and residual sediment give a similar result: the difference curve and the continuous thermal demagnetization curves of the magnetic extracts are in close correspondence (fig. 9b, fig. 11). The curves show the two maximum blocking temperatures of pyrrhotite and magnetite, respectively near 360 °C and 580 °C. Backward extrapolation of the magnetite branch of the decay curves to room temperature indicates that the $IRM_{MAGNETITE/2T}$: $IRM_{PYRRHOTITE/2T}$ ratio is approximately 0.1-0.2 : 0.8-0.9. As an illustration, the corresponding $ChRM_{MAGNETITE}$: $ChRM_{PYRRHOTITE}$ in the same LCU and HCU from which the extracts have been obtained are respectively 0.5 : 0.5 and 0.9 : 0.1.

Although the differences between the three decay curves in figure 11 are small, the intensity of the high temperature branch of the residual sediment is evidently a few percent higher compared to the original LCU sediment. This implies that, with respect to the original sediment, the residue has a slightly higher $IRM_{MAGNETITE/2T}$: $IRM_{PYRRHOTITE/2T}$ ratio. Consequently, the $IRM_{MAGNETITE/2T}$: $IRM_{PYRRHOTITE/2T}$ ratio for the magnetic extracts is a few percent lower than for the original sediment.

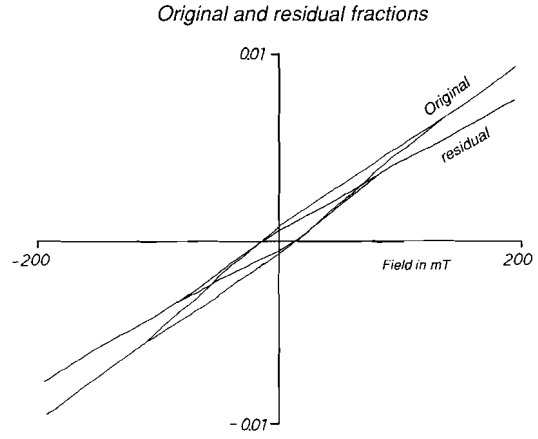

Fig. 10 Hysteresis curves for the original and residual sediment from the LCU after the magnetic separation. Intensities in Am^2.

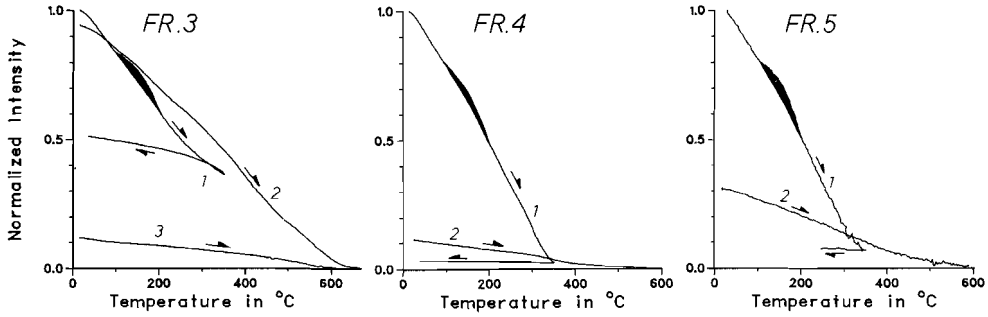

Fig. 11 Successive continuous thermal decay curves (denoted "1", "2" and "3") of IRM_{2T} in the magnetic extracts from a HCU (fraction 3) and from a LCU (fraction 4,5). The intensities are normalized with respect to the IRM_{2T} acquired at room temperature before the first heating cycle. The arrows indicate heating and cooling curves. The bold area on the first heating curve indicates the temperature lag induced by dehydration of the gypsum matrix (Dekkers, 1989).

In-field hysteresis of the original and residual fraction (fig. 10) of the LCU shows that the high field susceptibility (HFS) of the residual fraction is approximately 80% of the HFS of the original fraction (table 2). Since the residual sediment contains about half of the remanent magnetic material of the original sediment, the HFS of the residual sediment is relatively high. The high HFS of the residual sediment demonstrates that it is enriched in grains contributing most to the HFS, i.e. typically (small) superparamagnetic grains. Apparently, the separation process caused a bias of the grain size distribution in the magnetic extracts to larger grain sizes. However, the observed bias must be very small for the remanent magnetic minerals as it is hardly represented by the remanent coercive force (H_{CR}) of the original and residual fractions (table 2). It may therefore also be concluded that the original and residual sediments, and hence the original sediment and the magnetic extracts have a very similar remanent magnetic mineral content. Regarding the similarity between the original and residual fractions, it is concluded that an important part of the remanent magnetic minerals in the sediment (approximately 50% for the LCU, and 25% for the HCU), of similar type and grain size as found in the magnetic extracts, is tightly attached to relatively large non-magnetic minerals, thus inhibiting their extraction with magnetic methods.

Table 2. *Rockmagnetic characteristics of the various magnetic fractions obtained after extraction*

			.....Magnetic extracts.....		
	(1) (LCU) Original fraction	(2) (LCU) Residual fraction	(3) (HCU) I=0.25A	(4) (LCU) I=0.5A	(5) (LCU) I=2.5A
Weight (gr)	400	399	0.05	0.33	0.48
IRM (10^{-4}.Am^2)	6.00	2.87	2.312	2.926	0.148
IRM (Am^2/kg)	$1.50.10^{-3}$	$0.72.10^{-3}$	4.625	0.878	0.031
HFS (10^{-6}.m^3/kg)	0.58	0.46	28.06	5.89	0.60
J_{RS}/J_S			0.37	0.66	0.68
H_C (mT)			15	34	30
H_{CR} (mT)	62	63	27	61	60
H_{CR}/H_C			1.8	1.8	2.0
H_{CR}' (mT)			38	76	78
H_{CR}' 360 (mT)			40	47	59
H_{CR}' 360 d (mT)				80	83
MDF (mT)			19	54	67
X (10^{-6}.m^3/kg)			208.92	14.09	0.14
X/IRM (10^{-6}.m/A)			45.17	16.05	4.52

Table 2. Rockmagnetic parameters for sediment samples from an LCU (1), its residue after extraction of magnetic minerals (2) and the magnetic extracts obtained from this sediment with I=0.5 Amps. (4) and I=2.5 Amps. (5) and the same rockmagnetic parameters for an extract obtained with I=0.25 Amps. from an HCU (3). The rockmagnetic parameters include IRM (acquired in 2 T), J_{RS}'/J_S' determined in 0.2 T , High field susceptibility (HFS), H_C, H_{CR}, H_{CR}', H_{CR}' 360 (after the specimens were heated at 360 °C), H_{CR}' 360 d (derived H_{CR}' for pyrrhotite after the specimens were heated at 360 °C), MDF (the median destructive field of the ARM), X and X/IRM. For details see text. For comparison with original and residual LCU sediment: the original (400 grams) and residual (399 grams) HCU sediment have an IRM_{2T} of respectively $0.77.10^{-3}$ and $0.19.10^{-3}$ Am^2/kg (or $3.07.10^{-4}$ and $0.76.10^{-4}$ Am^2).

7.2 Behaviour of isothermal remanent magnetization and susceptibility during continuous and stepwise thermal demagnetization.

Successive continuous thermal demagnetization cycles imposed on the HCU and LCU extracts (fraction 3,4,5; fig. 11) demonstrate the alterations in the magnetic material which occur upon heating. Prior to each heating cycle the specimens acquired an IRM_{2T}. The first heating cycle up to 360 °C shows that the LCU fractions 4 and 5 have lost 90% of their remanence. Fraction 3, obtained from a HCU sediment sample, has lost 65% of its

remanence at 360 °C. During the second heating cycle the same specimens were heated to 650 °C. The corresponding heating curve illustrates the alterations which occurred during the first heating cycle: It does not show the typical blocking temperature of pyrrhotite; apparently the remanent magnetic properties of pyrrhotite were lost during the first heating cycle up to 360 °C. Magnetite is the only remanent magnetic mineral present during the second heating cycle. Hence, the contributions of pyrrhotite and magnetite to the IRM_{2T} can be calculated from the differences between the IRM_{2T} acquired prior to the first and second heating cycle. The results demonstrate that approximately 90% of the IRM_{2T} of the HCU extract is carried by magnetite and approximately 90% of the IRM_{2T} of the LCU extract is carried by pyrrhotite (table 3).

The alteration of pyrrhotite during the first heating cycle causes a decrease of the IRM_{2T} intensity at the onset of the second heating cycle. However, the heating curves show that the IRM_{2T} decrease is slightly compensated by a small IRM_{2T} increase: For all magnetic extracts the remanence at 360 °C during the second heating cycle has increased a few percent relative to the remanence at 360 °C during the first heating cycle (fig. 11, table 3).

***Table 3.** IRM_{2T} carried by magnetite and pyrrhotite*

	magnetite		*pyrrhotite*		*IRM increase*
	%	Am^2/kg	%	Am^2/kg	Am^2/kg
Fr. 3 (HCU)	85-95	3.931-4.393	5-15	0.231-0.694	0.462
Fr. 4 (LCU)	9-12	0.079-0.105	88-91	0.773-0.799	0.026
Fr. 5 (LCU)	25-30	0.007-0.009	70-75	0.022-0.023	0.001
Fr. 4+5 (LCU)	10-13	0.037-0.049	87-90	0.330-0.342	

Table 3. IRM_{2T} carried by magnetite and pyrrhotite calculated from the continuous thermal demagnetization results of the magnetic extracts. The IRM_{2T} carried by magnetite+pyrrhotite is given by the IRM_{2T}, acquired prior to the first heating cycle, the fraction of the IRM_{2T} carried by magnetite (denoted *"magnetite"*) is determined after the first and prior to the second heating cycle, the fraction of the IRM_{2T} carried by pyrrhotite (denoted *"pyrrhotite"*) follows. The range of values indicates the uncertainty with respect to the origin of the small IRM_{2T} increase noticed during the second heating cycle. The estimated IRM_{2T} increase at room temperature is denoted *"IRM increase"*. The actual percentages for magnetite dispersed in the sediment may be a few percent higher and/or the percentages for pyrrhotite may be a few percent lower due to the slight biasing effect on the grain size distribution introduced during the magnetic separation (section 7.1).

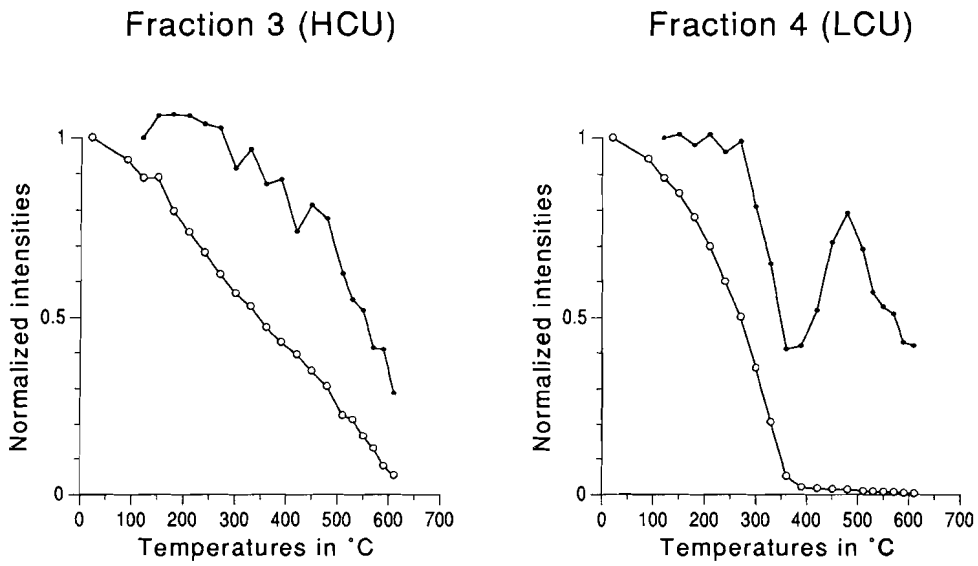

Fig. 12 Progressive stepwise thermal demagnetization of IRM_{2T} (open circles) induced in the magnetic extracts from a HCU (fraction 3) and a LCU (fraction 4) and the corresponding initial susceptibilities (closed circles) measured after each heating step. The IRM and the initial susceptibility are normalized to their initial values at room temperature (see table 2 for non-normalized values). The continuous (fig. 11) and stepwise demagnetization curves are virtually identical. Apparently the temperature dependency of the IRM carried by magnetite and pyrrhotite is small.

After the second heating cycle the fresh IRM_{2T} of fraction 3 (HCU) decreased by approximately 90% relative to the initial IRM_{2T} (fig. 11). Since most of the IRM_{2T} is carried by magnetite (table 3) the 90% decrease predominantly results from magnetite alteration. The third heating cycle of fraction 3 further illustrates the alteration process which took place during the second heating cycle. The curve shows a somewhat lower blocking temperature (580 °C) compared to the second heating cycle (620 °C). This demonstrates the presence of pure magnetite (T_B: 580 °C) during the third heating cycle, whereas CD magnetite (T_B> 580 °C) is present during the second heating cycle and in the original sediment (Linssen, 1988).

The IRM_{2T} of fraction 4 and 5 (LCU) decreased by more than an order of magnitude after the second heating cycle. Due to the sensitivity of the HALT spinner these magnetic extracts could not be subjected to a third heating cycle.

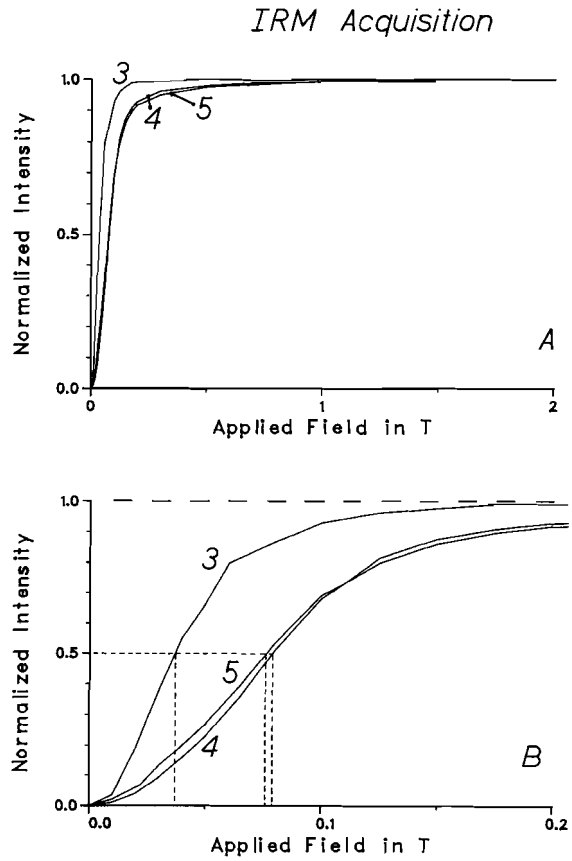

Fig. 13 IRM acquisition curves for magnetic extracts from a HCU (fractions 3) and from a LCU (fraction 4,5); (A) gives the complete curve, (B) is an enlargement of the low-field part of (A). The individual data are connected by straight lines. The intensity is normalized with respect to the maximum IRM value (listed in table 2). The dashed lines in (B) indicate the $H_{CR'}$.

The results of the stepwise thermal demagnetization experiments are in line with the results of the continuous thermal demagnetization: Most of the IRM_{2T} of fraction 3 is carried by CD magnetite with a maximum blocking temperature somewhat above 600 °C, whereas most of the IRM_{2T} of fraction 4 is removed near 360 °C and is carried by pyrrhotite (fig. 12).

Rock magnetism of the magnetite and pyrrhotite bearing Trubi formation

During the stepwise thermal demagnetization procedure the initial susceptibility of the magnetic extracts was determined after each demagnetization step (fig. 12). The monitored susceptibility changes reflect the magnetomineralogic changes that occur during the course of the demagnetization procedure. The initial susceptibility of fraction 3, predominantly containing magnetite, decreases after the specimen is heated to temperatures at and above 250 °C. The decrease of the susceptibility becomes more pronounced above 475 °C: 50% of the initial susceptibility is removed between 500 and 600 °C. The decrease of susceptibility indicates that magnetite alters to a non- or less magnetic phase in this temperature interval.

The initial susceptibility of fraction 4, predominantly containing pyrrhotite, shows a decrease between 270 and 360 °C, apparently related to the alteration of pyrrhotite in the same temperature interval. This observation is in concert with the speculative suggestion (section 6.2) that either (a) below 360 °C, or more specifically between 270 and 360 °C, pyrrhotite grains are decreased to a size at which they are not capable to carry significant remanence, nor have significant susceptibilities, or (b) hexagonal anti-ferromagnetic pyrrhotite, stable above 254 °C, is quenched upon cooling.

At 360 °C, the temperature above which the magnetic properties of pyrrhotite are no longer noticeable, the susceptibility starts to increase rapidly. Close to 475 °C a susceptibility maximum is observed similar to one observed by Valet (1986), Linssen (1988) and Dekkers (1990). Dekkers' (1990) experiments with pure pyrrhotite of known grain sizes in the range 5-150 micrometer demonstrated the alteration of pyrrhotite during heating to hematite via the magnetite phase, producing a susceptibility maximum near 500 °C (see also Schwarz and Harris,1970; Bennett et al.,1972; Linssen, 1988). Most likely the susceptibility maxima at approximately 475-500 °C (fraction 4 and specimens from Dekkers, 1990) and the temperature of increased decay at 475 °C in fraction 3 correspond to the characteristic temperature at which magnetite becomes altered to hematite. The XRD analysis (section 6.2) indicated an increase of the pyrite content in the magnetic extracts after being heated at 360 °C. This suggests that in the chain of reactions, the alteration of pyrrhotite to magnetite proceeds via the pyrite phase. The details of this reaction are not completely understood.

The IRM increase at 360 °C, observed in the second continuous thermal demagnetization cycle, is related to the original amount of magnetite in the magnetic extract, rather than to the amount of remanent magnetic pyrrhotite (table 3). Consequently, it is very unlikely that the IRM increase at 360 °C is due to an alteration of pyrrhotite to

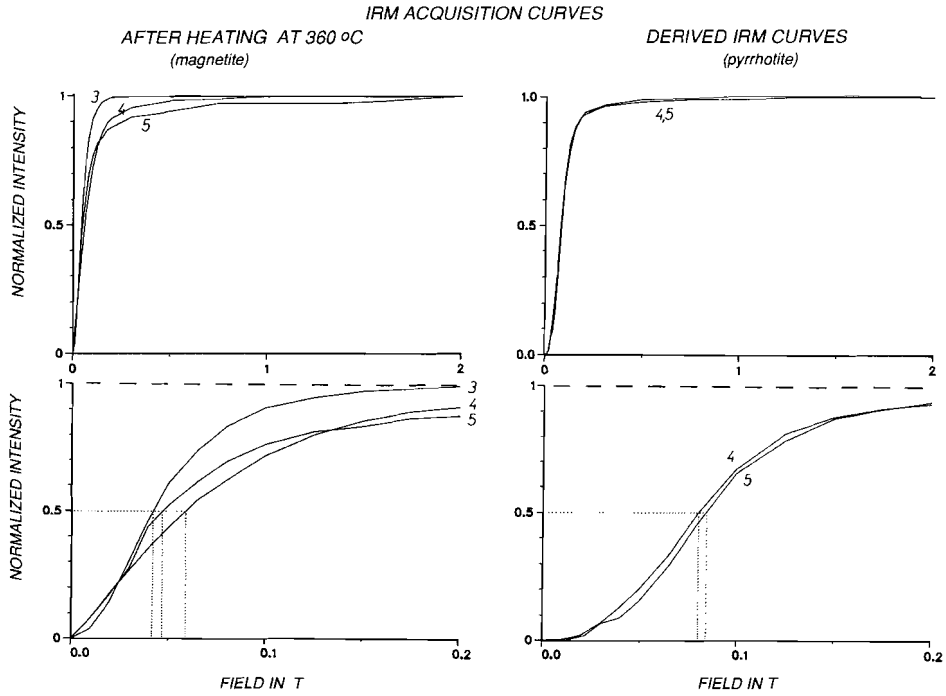

Fig. 14 Left : IRM acquisition curves after heating to 360 °C for fractions 3, 4 and 5 (see caption fig. 13) representing the magnetite fraction. Right : the derived IRM curves (see text) represent the pyrrhotite fraction. The upper figures give the complete IRM curves, the lower figures are an enlargement of the low-field part. The data points (not shown separately) are connected by straight lines. The intensity is normalized to the IRM_{2T} at room temperature values. The dotted lines in the lower figures indicate the H_{CR}'. Prior to the IRM acquisition the magnetic extracts were demagnetized in an alternating field of 300 mT in order to remove any remanence remaining after the first heating cycle to 360 °C.

magnetite (compare Linssen, 1988). Moreover, the IRM increase at 360 °C cannot be explained by an increase of the magnetite content, since the susceptibility of the specimens decrease rather than increase below 360 °C. The IRM increase at 360 °C can be tentatively explained by the magnetic interaction between magnetite and pyrrhotite: Magnetite grains which are physically attached to the pyrrhotite grains enhance the maximum unblocking temperature of pyrrhotite and, as a result of domain closure, decrease the IRM. Alternatively, the alteration of pyrrhotite to a non or less magnetic phase removes the source for magnetic interaction with magnetite, causing the observed IRM increase at 360 °C.

7.3 IRM acquisition

The IRM acquisition curves show that fraction 3 (HCU) predominantly containing magnetite (table 3), is already saturated at 0.2 T (fig. 13). Fractions 4 and 5 (LCU) are saturated at higher fields (0.5-1.0 T), reflecting the higher content of pyrrhotite. For corresponding grain sizes the H_{CR}, of pyrrhotite is significantly above the H_{CR}, of magnetite. For instance, the H_{CR}, of SD magnetite with a magnetotactic origin is in the range 24.1-48.5 mT (Moskowitz et al., 1990), whereas the H_{CR}, of a high-temperature SD pyrrhotite is 85 mT (EOR <5 micrometer: Dekkers, 1988). The H_{CR}, of fraction 3 is nearly half the H_{CR}, of fraction 4 and 5 (table 2), reflecting the differences in pyrrhotite and magnetite contents. Although the H_{CR}, values for fraction 4 and 5 are in the same range, the H_{CR}, of fraction 5 is slightly lower than fraction 4, which is in agreement with the slightly higher magnetite and lower pyrrhotite content of fraction 5 (table 3).

The remanent magnetic properties of pyrrhotite in the extracts are removed at 360 °C. Hence, IRM acquisition curves determined after the magnetic extracts were heated to 360 °C show the characteristics of the magnetite only (fig. 14). The H_{CR}, of the heated fraction 3 hardly changes relative to the original IRM acquisition curve (table 2). In contrast, the H_{CR}, values of fraction 4 and 5 drop some 20-30 mT to respectively 47 and 59 mT (fig. 14; table 2). The subtraction of the IRM curves acquired before and after heating yield the "derived" acquisition curves and H_{CR}, values of pyrrhotite (fig. 14, table 2). The "derived" H_{CR}, values for pyrrhotite in fraction 4 and 5 are respectively 81 and 83 mT.

7.4 Alternating field demagnetization of ARM

The median destructive fields (MDF) of ARM are well described for magnetite and pyrrhotite (Dekkers, 1988; Linssen, 1988; Hartstra, 1982). The MDF is considerably higher for pyrrhotite than for magnetite of an identical grain size. Consequently the MDF can be used to distinguish these minerals. In the present study the ARM was induced with a direct field of 0.035 mT and an alternating field of 300 mT.

The ARM carried by fraction 3 (HCU) is easily demagnetized (MDF=19 mT), which may be expected regarding its high magnetite contents. The ARM demagnetization curves for fractions 4 and 5 (LCU) show much higher MDF values (54+67 mT, fig. 15, table 2), which is attributed to the presence of pyrrhotite.

Pyrrhotite is known for its erroneous behaviour during alternating field

demagnetizations. This behaviour is caused by the electrical conductivity properties of pyrrhotite (Schwarz, 1975). The AF decay curves show that fraction 5 is not completely demagnetized with the maximal AF field of 310 mT, which is erratic since the ARM was acquired in a lower (300 mT) AF field. This erratic behaviour is typically observed during high field (>100 mT) demagnetization of the NRM. Apparently AF demagnetization results from sediments with high pyrrhotite contents (LCU units) have to be interpreted conservatively.

7.5 In-field hysteresis

The J_{RS}/J_S ratio is a domain state dependent parameter and thus suited to determine average grain sizes for assemblages of magnetic minerals. Theoretically, the maximal J_{RS}/J_S ratios for randomly oriented and non-interacting assemblages of single domain magnetite and pyrrhotite grains are respectively 0.5 and 0.75 (e.g. Dunlop, 1971).

The hysteresis loops of the fractions 3 (HCU), 4 and 5 (both LCU) were acquired in a 200 mT alternating field (fig. 16), which is sufficiently high to saturate magnetite. However, fine-grained pyrrhotite may require fields up to 5 T in order to be saturated

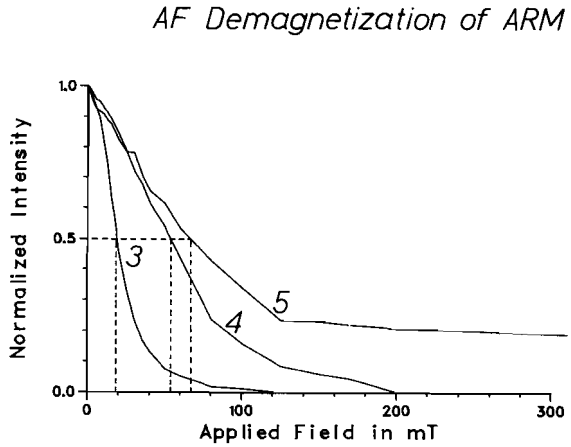

Fig. 15 Alternating field demagnetization of ARM carried by the magnetic extracts from a HCU (fraction 3) and a LCU (fraction 4,5). The dashed line indicates the median destructive field (MDF).

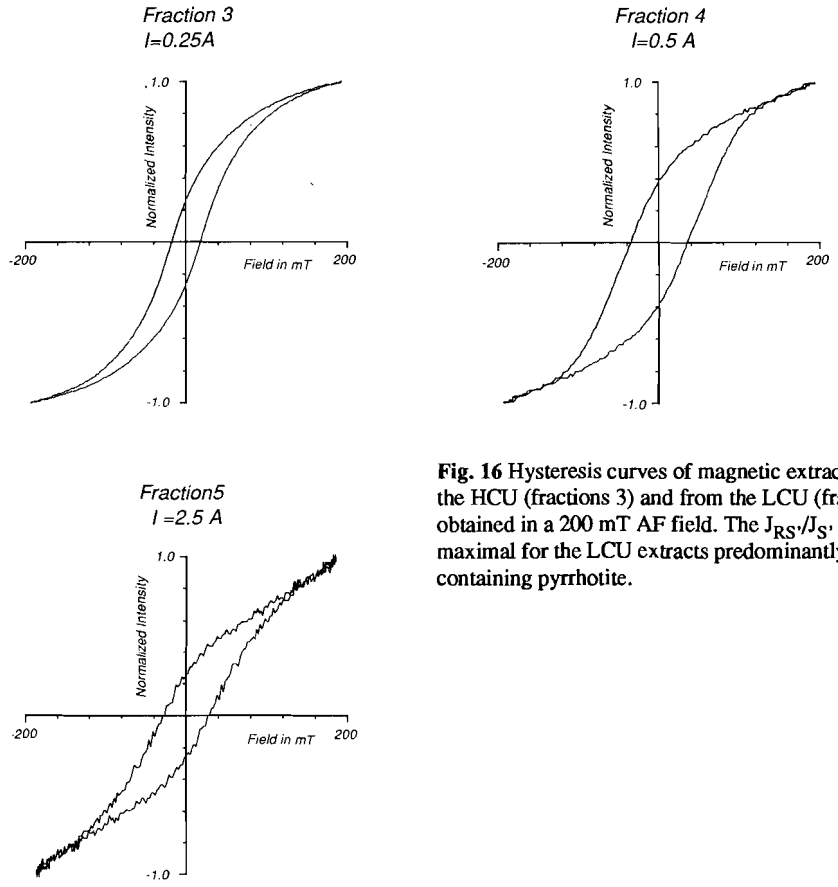

Fig. 16 Hysteresis curves of magnetic extracts from the HCU (fractions 3) and from the LCU (fraction 4,5) obtained in a 200 mT AF field. The $J_{RS'}/J_{S'}$ ratio is maximal for the LCU extracts predominantly containing pyrrhotite.

completely. Hence, the observed J_{RS}/J_S ratio for the pyrrhotite-rich fractions (LCU, fraction 4 and 5) is significantly above the true values, whereas the derived H_C value will be lower than the true value. To indicate the difference with true J_{RS}/J_S parameters the currently used parameter is denoted $J_{RS'}/J_{S'}$. The high field susceptibility (HFS) components introduced by pyrrhotite and the paramagnetic components in the sediment have been subtracted from the hysteresis loops before the $J_{S'}$ value was calculated.

Fraction 4 and 5 produce high $J_{RS'}/J_{S'}$ ratios (0.66 and 0.68) and H_C values (34 and 30 mT) compared to fraction 3 ($J_{RS'}/J_{S'}$=0.37 and H_C=15 mT) due to the high pyrrhotite contents. A correction for the presence of ~10% pyrrhotite in fraction 3 and ~10%

magnetite in fraction 4 (table 3) is necessary to calculate the J_{RS}/J_S of magnetite and $J_{RS'}/J_{S'}$ of pyrrhotite (using : $100/[0.66]_{LCU}=90/[J_{RS}/J_S]_{PYRRH.}+10/[J_{RS}/J_S]_{MAGN.}$ and $100/[0.37]_{HCU}=10/[J_{RS}/J_S]_{PYRRH.}+90/[J_{RS}/J_S]_{MAGN.}$). Assumptions in the calculation are that the differences in the pyrrhotite and/or magnetite properties which may exist between the HCU and LCU are not important and that there is no significant magnetic interaction in the sample. Because of the high concentrations of magnetite in the HCU and pyrrhotite in the LCU, the error in the calculated parameters for these dominating minerals in the HCU and LCU will be small. The pyrrhotite contribution to the J_{RS}/J_S, i.e. the $J_{RS'}/J_{S'}$, is 0.73. As a result of the non-saturation of pyrrhotite, it is not meaningful to calculate the grain size of pyrrhotite from this $J_{RS'}/J_{S'}$ value. The J_{RS}/J_S ratio for magnetite is 0.35, corresponding to a grain size of 0.1-0.2 micrometer (Dunlop, 1986; Argyle and Dunlop, 1990; Heider et al., 1987; Worm and Markert, 1987).

7.6 Low-temperature treatment

The low-temperature behaviour of IRM_{2T} carried by magnetite and pyrrhotite is grain size dependent (Hartstra, 1982; Dekkers, 1989). The low-temperature cycle of fraction 3 shows (fig. 17), after an initial small and gradual remanence increase of 5%, a minor remanence decrease at the Verwey transition of magnetite (Chikazumi, 1976; Yoshida and Iida, 1977) equal to 5%. The remanence does not recover on warming, but instead further decreases, yielding a remanence at room temperature which is approximately 6% lower than the initial IRM. The remanence loss of magnetite at the Verwey transition was studied by Hartstra (1982) for well defined grain size ranges from <5 to 100-150 micrometer. The remanence loss was shown to decrease with decreasing grain size. A comparison of extrapolated data from Hartstra (1982) and a correction for the pyrrhotite contribution to the IRM (~10%; table 3) yields a magnetite grain size of 0.1-0.5 micrometer. Mark that the crushed magnetite used by Hartstra is not completely stress free (Hartstra, 1984), which may result in a slight bias of the estimated grain size (e.g. Argyle and Dunlop, 1990). A second low-temperature cycle, applied to fraction 3 immediately after the first cycle without acquisition of a new remanence, is completely reversible. This result is conform similar experiments on magnetite (Hartstra (1982).

The low-temperature cycles of fraction 4 and 5 show a slight and continuous 4% remanence increase during cooling. The curves do not reveal the remanence maximum at -70 °C reported for pyrrhotite (Dekkers, 1989). On warming the remanence decreases; the

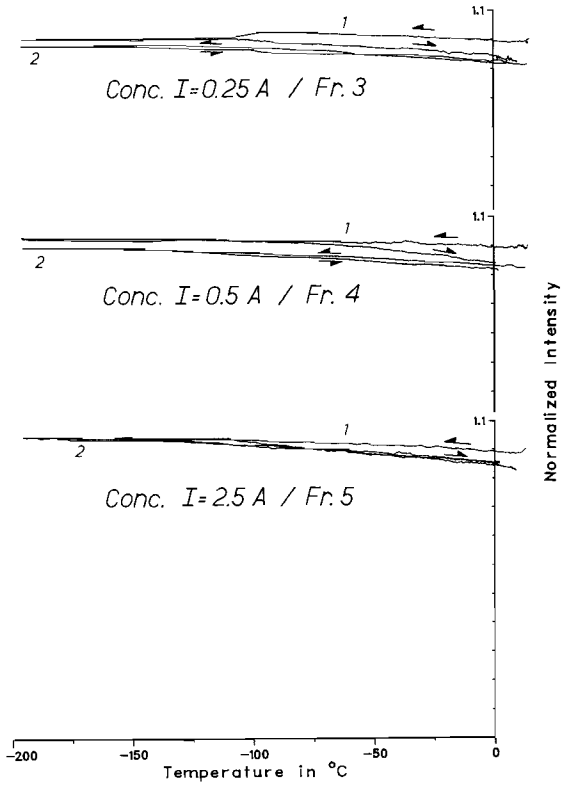

Fig. 17 Successive low-temperature cycles (denoted "1" and "2") to liquid nitrogen temperature of magnetic extracts from a HCU (fraction 3) and from a LCU (fraction 4,5). The magnetization is normalized with respect to the IRM_{2T} the specimens acquired prior to the first run at room temperature (table 2). The second low-temperature cycle was performed immediately after the first cycle (without acquiring a new magnetization). The arrows indicate the cooling and the warming curves unless these could not be resolved (Fraction 3, second run). The temperatures readings below -100 °C are subject to an erratic error as can be observed for the first cooling curve of fraction 3: the Verwey transition of magnetite is observed at -110 instead of -154 °C at which temperature the transition actually occurs (Chikazumi, 1976).

intensity at room temperature is 5-7% lower than the initial IRM, which is characteristic for pyrrhotite grains smaller than 15 micrometer (Dekkers, 1989). During the second low-temperature cycle the IRM intensity continuously increases 3-9%. The high degree of reversibility of the second low-temperature cycles concurs with experimental data (Dekkers, 1989).

7.7 Properties of magnetite and pyrrhotite in the sediment

The contributions of pyrrhotite and magnetite to the IRM_{2T} (table 3) and the rock-magnetic properties of the HCU and LCU extracts (table 2) have been re-calculated to properties of pyrrhotite and magnetite. If rockmagnetic parameters could not be measured directly the calculation proceeded conform the method of J_{RS}/J_S calculation in section 7.5. The results are listed in table 4.

The $H_{CR'}$ of the LCU was determined before and after alteration of pyrrhotite, thus allowing the $H_{CR'}$ of magnetite and pyrrhotite in the LCU to be determined directly (section 7.3). The results demonstrate that $H_{CR'}$ of magnetite is higher in the LCU than in the HCU (table 4). This difference points to a lower average grain size for magnetite in the LCU than in the HCU. The H_C, H_{CR} and grain size of magnetite in the LCU can directly be calculated from the $H_{CR'}$ using the grain-size independent relation between $H_{CR'}$ and H_{CR} (e.g. Hartstra, 1982; Argyle and Dunlop, 1990) and the H_{CR}/H_C ratio, which is known to decrease with grain size (Gaunt,1960; Stacey and Banerjee, 1974; Argyle and Dunlop, 1990). The resulting H_{CR} value of LCU magnetite (27.7 mT) indicates that H_C>15.3 mT, provided that H_{CR}/H_C<1.8. A H_C>15.3 mT points to a grain size below 0.08 micrometer (Argyle and Dunlop, 1990), which puts the grain size of magnetite in the LCU near the upper single domain grain size threshold. The magnetite in the HCU (0.1-0.2 micrometer) is pseudo single domain.

The observed MDF, H_{CR} and H_C values indicate an average pyrrhotite grain size of 5-10 micrometer (Dekkers, 1988; Linssen, 1988) , which is slightly too high regarding the microscopic and SEM observations of the extracts.

The concentration of the magnetite and the pyrrhotite properties in the extracts can be calculated from the rockmagnetic properties listed in table 4. The necessary scaling is provided by the hysteresis properties of magnetite and pyrrhotite. For magnetite the accepted value of J_S=93 Am^2/kg has been adapted (e.g. Collinson, 1983), which, together with the established J_{RS}/J_S ratio and IRM_{2T}, provides a sound basis for the calculation of the concentration. However, this method is not applicable to pyrrhotite since the determined J_{RS}/J_S ratio for pyrrhotite is too high and the J_S of fine-grained pyrrhotite seems to be grain size dependent (e.g. Dekkers, 1988). The preferred method for the determination of pyrrhotite concentration was the usage of experimentally determined

***Table 4.** Properties of magnetite and pyrrhotite in the Trubi sediment*

	LCU		HCU	
	Magnetite	Pyrrhotite	Magnetite	Pyrrhotite
Grain size in microm.	<0.1(1)	<2	0.1-0.2	<2
IRM_{2T} extr.(10^{-4}.Am^2)	0.35	2.73	2.08	0.23
IRM_{2T} sedm.(10^{-4}.Am^2)	0.69	5.35	2.77	0.31
J_{RS}/J_S	(>0.35)	<0.73	0.35	(<0.73)
H_C (mT)	>15.3(1)	<36.6	12.9	(<36.6)
H_{CR} (mT)	27.7(1)	65.7	23.1	(65.7)
H_{CR}/H_C	<1.8(1)	>1.8	1.8	(>1.8)
$H_{CR'}$ (mT)	48.0	81.0	40.0	(81.0)
MDF (mT)	(14.1)	59.5	14.1	(59.5)
Weight in extract (mg)	1	140	6	12
Conc.in sediment (ppm)	5	670	21	40

Table 4. Properties of pyrrhotite and magnetite in the Trubi sediment (400 gr sediment samples). The rockmagnetic parameters include grain sizes, IRM (acquired in 2 T) for the extract (IRM_{2T} extr.) and the sediment (IRM_{2T} sedm.), H_{CR}, H_C, median destructive field of the ARM (MDF), etc. The parameters of pyrrhotite in the HCU and magnetite in the LCU, which could not be inferred directly, and hence may be less accurate, are between brackets. For the calculation of the concentrations of magnetite J_S=93 Am^2/kg has been used (e.g. Collinson, 1983), and for fine-grained pyrrhotite IRM_{2T}~2 Am^2/kg (Dekkers, 1988). The parameters marked (1) have been calculated using the existing relations between $H_{CR'}$, H_{CR}, H_C and grain size.

IRM_{2T} intensities of fine-grained stress-free pyrrhotites. It was decided to use the experimental results of Dekkers (1988; IRM_{2T}~2 Am^2/kg), although the skarn pyrrhotites of Dekkers have a different origin than the pyrrhotites in the Trubi sediment. The IRM_{2T}~2 Am^2 /kg is significantly below maximal values reported for J_{RS}~15-17 Am^2/kg (Schwarz and Vaughan, 1972; Halgedahl and Fuller, 1981a). However, the prominent decrease of J_{RS} with decreasing grain size below 15 micrometer is supported by other, independent observations (e.g. Clark, 1984). The results demonstrate (table 4) that the concentrations of pyrrhotite in the HCU and LCU exceed the concentration of magnetite with respectively a factor 2 and two orders of magnitude. One of the puzzling outcomes is the incompatibility between the calculated concentration of pyrrhotite in the HCU and the LCU (table 4) and the results of the X-ray diffraction (section 6.2). Although the presence of pyrrhotite in the HCU extracts was clearly demonstrated with X-ray diffraction, we failed to do so in the LCU extracts. However, the high J_{RS}/J_S ratio and H_{CR} value indicate

that pyrrhotite is indeed present in the LCU. It is not likely that the observed discrepancy is caused by the fact that pyrrhotite is extremely small grained in the LCU since this would also affect the remanent magnetization of pyrrhotite, which in contrast is very high in the LCU. Furthermore, the concentration of pyrrhotite in the HCU and LCU extracts was well above the detection limit of 1-5%. Obviously this feature needs further investigation.

The thermal demagnetization characteristics suggest that interaction phenomena exists between the magnetizations of magnetite and the (non-homogeneous) pyrrhotite (section 7.2). Low temperature monoclinic pyrrhotite may contain 1% magnetite equivalents at most (Graham et al., 1987). Although this amount appears to be too small to explain the observed magnetite remanence, it might explain the observed magnetic interaction phenomena. Furthermore, the occurrence of magnetite equivalents in pyrrhotite may explain the slightly enhanced blocking temperature of pyrrhotite in the Trubi sediment (e.g. Onufrienok and Zvegintsev, 1981).

8. Origin of the magnetic minerals

The origin of the magnetic minerals in the sediment is of major interest to paleomagnetism as it gives information on the timing of the natural remanent magnetization. The geochemical and rockmagnetic investigations of this study have revealed the presence of magnetite, pyrrhotite and a FeTi-oxide, as well as some of their properties, such as grain size and concentration. The identification of the magnetic minerals and the assessment of their rockmagnetic properties provide a basis for a discussion on their origin.

The occurrence of pyrrhotite in the Trubi sediment excludes a detrital origin of this mineral; pyrrhotite is not the stable phase during the accumulation of marine sediments, rather pyrite will precipitate from even the most reducing aqueous solution (Hall, 1986). Hence, any pyrrhotite present in the sediment must have been formed in a suboxic or anoxic environment by authigenic processes in the early stages after sediment deposition (e.g. Karlin and Levi, 1985). Indeed, recent studies indicate that biogenic processes may introduce pyrrhotite which can carry a remanent magnetization (Farina et al., 1990; Mann et al., 1990).

The study of reversal records showed that magnetite and pyrrhotite acquired their magnetization at approximately the same moment or at least within a narrow time interval (Linssen, 1988; chapter 3). This observation makes it very unlikely that the ChRM compo-

nent carried by magnetite has a detrital origin, but instead it indicates that not only pyrrhotite, but also magnetite has an authigenic origin. Chang and Kirschvink (1985) found isolated biogenic magnetite grains smaller than 0.1 micrometer in sediments with similar rockmagnetic characteristics (see also Karlin, 1987; Moskowitz et al, 1990). This grain size is in close correspondence with the observations in the present study (table 4).

It is most likely that the observed FeTi oxides originate from wind-blown volcanic material. This origin is conform the unimodal grain size distribution of the grains, the texture, the high Ti content and the sharp edged habitues. The fact that the FeTi oxides were not observed in the LCU suggest a relation between the HCU/LCU rhythmites and volcanic activity or wind-blown African input (De Visser et al, 1989). It would be of great interest to further investigate the FeTi-oxide occurrence in the HCU and LCU and see if such a relation really exists. The presence of the FeTi oxide was not readily visible in the rockmagnetic results, or it should be that this mineral is the carrier of (a part) of the magnetite magnetization. However, since the FeTi mineral probably has a volcanic origin and the authigenic magnetite and pyrrhotite magnetizations were acquired below the sediment surface, it is very unlikely that a substantial part of the ChRM is carried by very fine-grained, not-observed, magnetite inclusions in the FeTi oxide.

The reliability of reversal records of authigenic origin depends on the complex relations between the thickness of the sedimentary reaction layer in which the authigenic minerals are produced and the rates at which the reversal proceeds and the sediment accumulates (Hoffman and Slade, 1986; Weeks et al., 1988; Rochette, 1990; deMenocal et al., 1990). The dependencies are such that the reliability increases if the reaction layer decreases in thickness, the reversal proceeds more slowly and the accumulation rate is increased. For the Trubi sediment it has been established that the accumulation rate is 5-10 cm/kyr (Zijderveld et al., 1986), which is well above suspected values (e.g. Rochette, 1990, deMenocal et al., 1990). On the other hand, the sedimentary intervals in which the major geomagnetic variations are observed are small (5-20 cm): the durations of the main reversal features are less than approximately 3 kyr (Linssen, 1988). In theory, the high pace of the reversals makes the (sparse) transitional directions less reliable. Moreover, the authigenic origin of the minerals carrying the ChRM indicates that some smoothing effects will undoubtly be present in the record, and probably be proportional with the thickness of the reaction zone. However, the observation of consis-

tent and rapid (1-3 kyr) variations below, in and above the reversal record (e.g. Linssen, 1988; chapter 3,5) provide evidence that the important directional features of the reversal are accurately recorded in the sediment (e.g. Rochette, 1990; Constable, 1990). The size of the reaction zone, acting as the primary filter cq. smoothing window (Lund and Karlin, 1990), can be estimated by the assessment of the duration of the most rapid variations which occur in the record. Important variations were demonstrated to occur in less than 3 cm (Linssen, 1988; chapter 3,5). The resolution of the recording process is estimated at 0.2°/yr and an intensity variation of 5% of the initial intensity per year.

9. Conclusions

Separation of the magnetic minerals in the Trubi sediment and their geochemical and rockmagnetic investigation has shown to be a useful method to identify assemblages of magnetic minerals with a small average grain size (<2 micrometer) and low concentration (5-700 ppm). The sub-optimal effectiveness of the separation process (51-75%) was demonstrated to have a very limited biasing effect on the results. The average grain size of remanent magnetic minerals in the magnetic extracts is slightly higher than in the original sediment.

The rockmagnetic and geochemical experiments on the magnetic extracts demonstrated the presence of magnetite, pyrrhotite, pyrite and a FeTi-oxide in the Trubi sediment. The various minerals are not uniformly distributed in the sediment, but follow the natural alternation of LCU and HCU units in the Trubi formation.

The presence of pyrrhotite was demonstrated with X-ray diffraction, but only in the HCU. Further evidence for the presence of pyrrhotite in the HCU and LCU comes from rockmagnetic observations on J_{RS}/J_S and (remanent) coercivities. Pyrrhotite was demonstrated to be most abundant in the LCU units and in coexistence with pyrite (section 6.2). The concentration of pyrrhotite in the investigated LCU and HCU samples is approximately 670 and 40 ppm respectively. Reflected light microscopy and SEM investigation of the magnetic extracts have shown that the average grain size of pyrrhotite is below 2 micrometer, i.e. within the single domain grain size range (Soffel, 1977, 1981; Halgedahl and Fuller, 1981; Clark, 1984; Dekkers, 1988). The visually observed grain size range of pyrrhotite and the average grain size calculated from grain size dependent rock-magnetic parameters such as H_{CR}, and MDF agree reasonably, although the rockmagnetic parameters show a slight bias to higher values (5-10 micrometer). Apparently, the present

authigenic pyrrhotites have a lower coercive force than the skarn pyrrhotites which were used as a reference.

The physical alteration of pyrrhotite was demonstrated to proceed between 270 and 475 °C. Between 270 and 360 °C the remanence and susceptibility of pyrrhotite decrease below the detection limit. Between 360 and 475 °C the pyrrhotite is altered to fine-grained magnetite. Probably the alteration of pyrrhotite to magnetite proceeds via the pyrite phase, although the details of this alteration are not completely understood. Above 475 °C the magnetite is altered to a less- or non-magnetic phase, believed to be hematite (Linssen, 1988; Dekkers, 1990). The reactivity of magnetite and pyrrhotite during thermal demagnetization proves to be complex and may be a source for magnetic contamination of the NRM directions and intensities. This is specially true for the pyrrhotite bearing sedimentary units (LCU) from which magnetite is produced between. The newly formed magnetite, produced between 360 °C and 475 °C in a near zero field, easily picks up laboratory induced remanent magnetizations (Linssen, 1988).

The presence of magnetite was demonstrated with X-ray diffraction and continuous and stepwise thermal demagnetization. Magnetite was not observed directly. The J_{RS}/J_S of magnetite is 0.35 in the HCU and >0.35 in the LCU, the H_{CR}=27.7 mT in the LCU and 23.1 mT in the HCU, the H_C>15.3 in the LCU and 12.9 mT in the HCU. The calculated grain size of magnetite in the HCU units is in the range 0.1-0.2 micrometer (PSD size range), in the LCU units less than 0.1 micrometer (SD-PSD size range). The calculated concentration of magnetite in the LCU and HCU is respectively 5 and 20 ppm.

Regarding the origin of magnetite and pyrrhotite it is concluded that both minerals were formed more or less simultaneously in a biogenic or authigenic environment. It is tentatively suggested that magnetite is (partly) intergrown with pyrrhotite, causing the presumed magnetic interactions between remanences of pyrrhotite and magnetite.

The total concentration of magnetite plus pyrrhotite was shown to be considerably higher in the LCU (680 ppm) than in the HCU (60 ppm) indicating a higher biogenic or authigenic activity or lower input of matrix material during periods of LCU deposition.

Small amounts of FeTi-oxide grains with equal amounts of Fe and Ti were observed with microprobe and reflected light microscope investigations. The FeTi-oxide grains were only observed in the HCU units. The grains have a uniform size (~10 micrometer) and a lamellar texture. Probably the FeTi-oxide grains have a volcanic origin. No indication has been found that this mineral contributes to the remanence, either IRM or ChRM.

Acknowledgments

This rockmagnetic investigation would have been impossible without the assistance of H.J.Meijer who accurately performed many of the measurements and T.A.T.Mullender who developed the hysteresis equipment and took care after the condition and improvement of the other equipment. Prof.Dr.J.D.A.Zijderveld and Dr.M.J.Dekkers are thanked for critically reading the manuscript and their helpful suggestions. The investigations were supported by the Netherlands Foundation for Earth Science Research (AWON) with financial aid from the Netherlands Organization for the Advancement of Pure Research (Z.W.O., now N.W.O.).

Chapter V

The Mammoth and lower Kaena geomagnetic sedimentary reversal records of the Punta Piccola section

1. Introduction

Sediments and extrusive igneous rocks are commonly used for the study of geomagnetic reversal records. The reversal records obtained from sediments, in contrast to extrusive igneous rocks, have an advantage of being continuous and of possessing a well defined time control. Moreover, a magnetostratigraphic investigation of the sedimentary sequence including the reversal records provides an accurate timing of the reversal with respect to the geomagnetic polarity time scale.

Sediments acquire their natural remanent magnetization (NRM) in a complex process over longer periods of time. In this respect, the ability to derive a reliable reversal record from a sedimentary sequence depends mainly on the accumulation rate of the sediment and on its magnetic properties.

Magnetostratigraphic research of marine sediments in the central Mediterranean by the paleomagnetic laboratory "Fort Hoofddijk" yielded the information to identify a continuous sequence of 25 reversals from 7.5 to 1.5 Ma. The Miocene reversal records from this sequence are located on Crete (Langereis, 1984; Langereis et al., 1984; Valet et al., 1988) and the Pliocene reversal records are located in Calabria (Zijderveld et al., 1986; Linssen, 1988) and on Sicily (Hilgen and Langereis, 1988; Zachariasse et al., 1989, 1990; Langereis and Hilgen, in press).

The presently discussed records of the lower Mammoth (N-R), upper Mammoth (R-N) and lower Kaena (N-R) reversals were obtained from Sicily (Italy). The results of the overlying upper Kaena reversal record are reported elsewhere (van Hoof and Langereis, submitted).

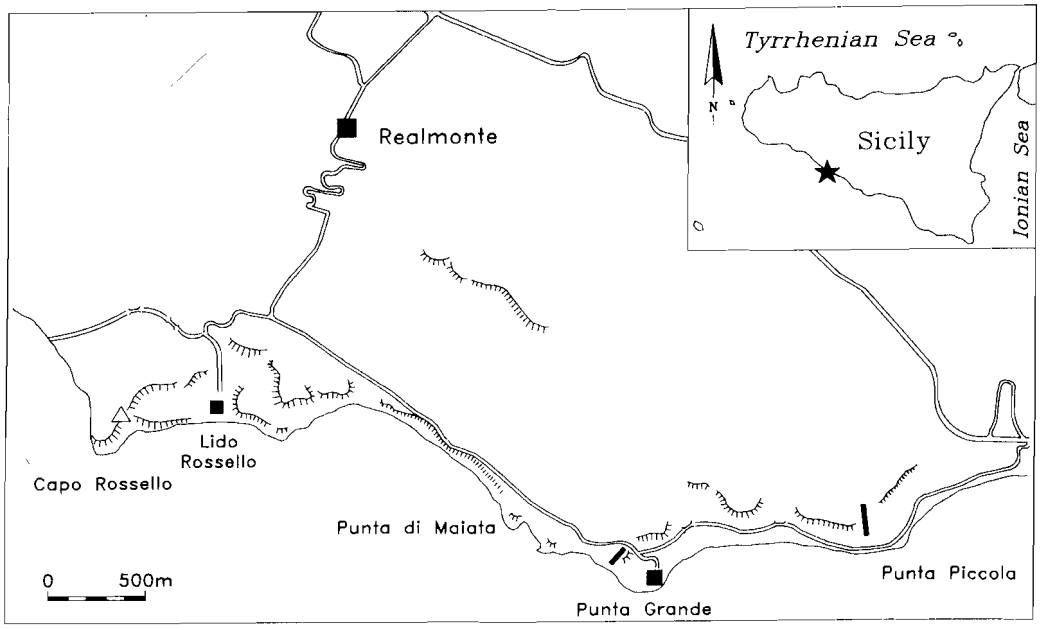

Fig. 1 Location of the Punta Piccola section in SW Sicily (Italy).

2. The Punta Piccola section

The reversal records were sampled in the Punta Piccola section (Brolsma, 1978; Spaak, 1983; Hilgen 1987; Zachariasse et al., 1989) situated in the Caltanisetta basin of southern Sicily (fig. 1). The Punta Piccola section consists of middle Pliocene sediments from the Trubi and Monte Narbone formation (Cita and Gartner, 1973; Brolsma, 1978; Spaak, 1983; Rio et al., 1984). The Trubi and Monte Narbone sediments are widespread in the Neogene basins of Sicily and Calabria (see e.g. Hilgen, 1987).

The magnetostratigraphy, biostratigraphy (Zacheriasse et al., 1989) and lithostratigraphy (Hilgen, 1987) of the Punta Piccola section has been investigated in detail and is shown in figure 2. The recorded reversals are the Gilbert-Gauss, lower and upper Mammoth, the lower and upper Kaena and the Gauss/Matuyama (Zachariasse et al., 1989).

The Mammoth and lower Kaena reversal records of the Punta Piccola section

The rhythmically bedded marls of the Trubi and Monte Narbone formation consist of carbonates (55-80%), clay minerals and minor amounts of quartz. The variation in the concentration of these minerals has introduced the rhythmic nature of the sediment (Hilgen, 1987; chapter 4; De Visser et al., 1988; Hilgen and Langereis, 1989).

A distinctive lithological feature of the Sicilian Trubi sediment is the detailed partitioning of the rhythmites. Single rhythmites in Sicily are quadripartite consisting of a grey, white, beige and white coloured bed and are denoted quadruplets (Hilgen, 1987). Single rhythmites in Calabria are bipartite and consist of a high carbonate unit (HCU) and a low carbonate unit (LCU). The LCU units correspond to the grey beds in the Sicilian quadruplets, the HCU units correspond to the white-beige-white beds in the quadruplets.

The Mammoth reversal records are located in the uppermost part of the Trubi formation, whereas the overlying lower Kaena reversal record is located just above the base of the Monte Narbone formation. The sedimentary interval enclosing the Mammoth reversal records is more indurated than the interval enclosing the overlying lower Kaena record. No further lithological differences between the sedimentary interval enclosing the lower Kaena reversal record and the underlying Trubi sediment have been observed (Hilgen, 1987).

The sediment exposed in the section shows a slight and almost uniform dip; near the sampling sites of the Mammoth reversal records the bedding tilt is 5° to ENE (N62°E). The bedding tilt near the lower Kaena reversal record is somewhat higher (11°). Due to the rhythmically bedded nature of the sedimentary sequence, any small fault can be easily recognized. At the location of the sampled records no faults are present.

The paleomagnetic results (Zacheriasse et al., 1989; Scheepers and Langereis, in prep.) indicate a Pliocene rotation of approximately 35° for the sedimentary sequence exposed in the Punta Piccola section.

The accumulation rate of the sediment is approximately 5 cm/kyr. The variation of the accumulation rates in the subsequent polarity subzones is low, although a slight decrease with decreasing age appears to be present (table 1). The accumulation rates used for the reversal records are the average accumulation rates of the under- and overlying polarity zones; i.e. 5.0, 4.7 and 4.6 cm/kyr for respectively the lower Mammoth, upper Mammoth and lower Kaena reversal records.

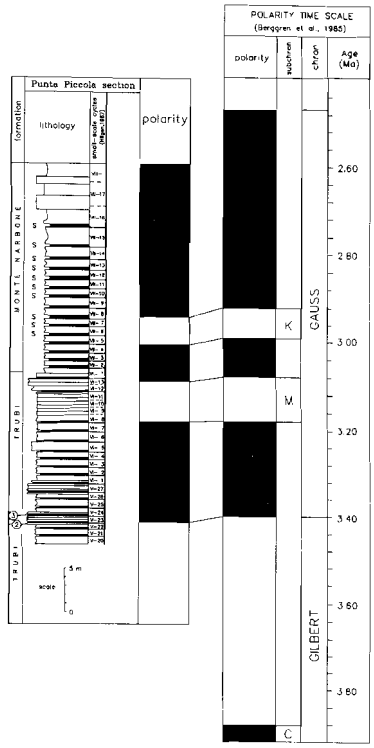

Fig. 2 Polarity sequence recorded in Punta Piccola section and lithology. 'K' denotes Kaena subchron, 'M' denotes Mammoth subchron (Berggren et al., 1985).

3. Methods

Prior to sampling, planes were cut perpendicular to the bedding plane (fig. 3). Considerable effort was put in removing the weathered surface in order to obtain fresh (dark grey and blue coloured) sediment.

Sampling equipment consisted of a portable generator, electric drilling machines and water-cooled brass drills with diamond cutting edges. Cores of 25 mm diameter were drilled parallel to the bedding plane and at least one core per sampling level was taken. Since the sampling levels were spaced 1 cm, a multiple coverage of specimens for all stratigraphic levels was obtained. In the laboratory, the cores were cut into standard specimen of 22 mm height. In order to obtain a better resolution of the reversal record, a number

Table 1 Accumulation rates of the Trubi sediment exposed in Punta Piccola section

Polarity intervals		Acc.rates cm/kyr
Gilbert/Gauss	- lower Mammoth	5.3
lower Mammoth	- upper Mammoth	4.7
upper Mammoth	- lower Kaena	4.7
lower Kaena	- upper Kaena	4.4

Table 1. Accumulation rates of the Trubi sediment exposed in the Punta Piccola section based on magnetostratigraphic data (Zachariasse et al., 1989). The ages of the geomagnetic reversals are : Gilbert/ Gauss 3.4 Ma; lower Mammoth 3.18 Ma; upper Mammoth 3.08 Ma; lower Kaena 2.99 Ma; upper Kaena 2.92 Ma (Berggren et al., 1985).

of specimens were split into halves approximately parallel to the bedding plane. The stratigraphic position of each specimen was calculated using the bedding plane, drilling orientation and width of the saw cut. The accuracy in the determination of the stratigraphic level is better than 0.5 cm.

Stepwise progressive thermal demagnetizations were performed in tunnel furnaces with mu-metal shielding; the alternating field (AF) demagnetizations were done using a stationary holder (Zijderveld, 1967; Dankers and Zijderveld, 1981). Thermal demagnetization was carried out with temperature increments of 30 °C up to 510 °C, and of 20 °C increments at higher temperatures. For AF demagnetizations generally 15-18 demagnetization steps were used up to a maximum field of 100 mT. All measurements of the remanent magnetization were made with a 2G-Enterprises cryogenic magnetometer having a sensitivity of 10^{-11} Am^2; its reproducibility is better than 1° for magnetizations exceeding 10^{-9} Am^2.

Thermal demagnetization procedures were focussed on the suppression of laboratory induced viscous magnetizations due to the production of superparamagnetic magnetite during heating at temperatures above 360 °C (Linssen, 1988; chapter 4). In addition, a partial thermo-remanent magnetization (PTRM) may be induced by the very small fields ambient in the furnace. Minimizing the heating and cooling times for the specimens is successful in suppressing these effects to a large extent (Linssen, 1988). In the present study the magnitude of a laboratory induced PTRM component was never in excess of 0.05 mA/m.

Analysis of the demagnetization data was done with the help of an in-house

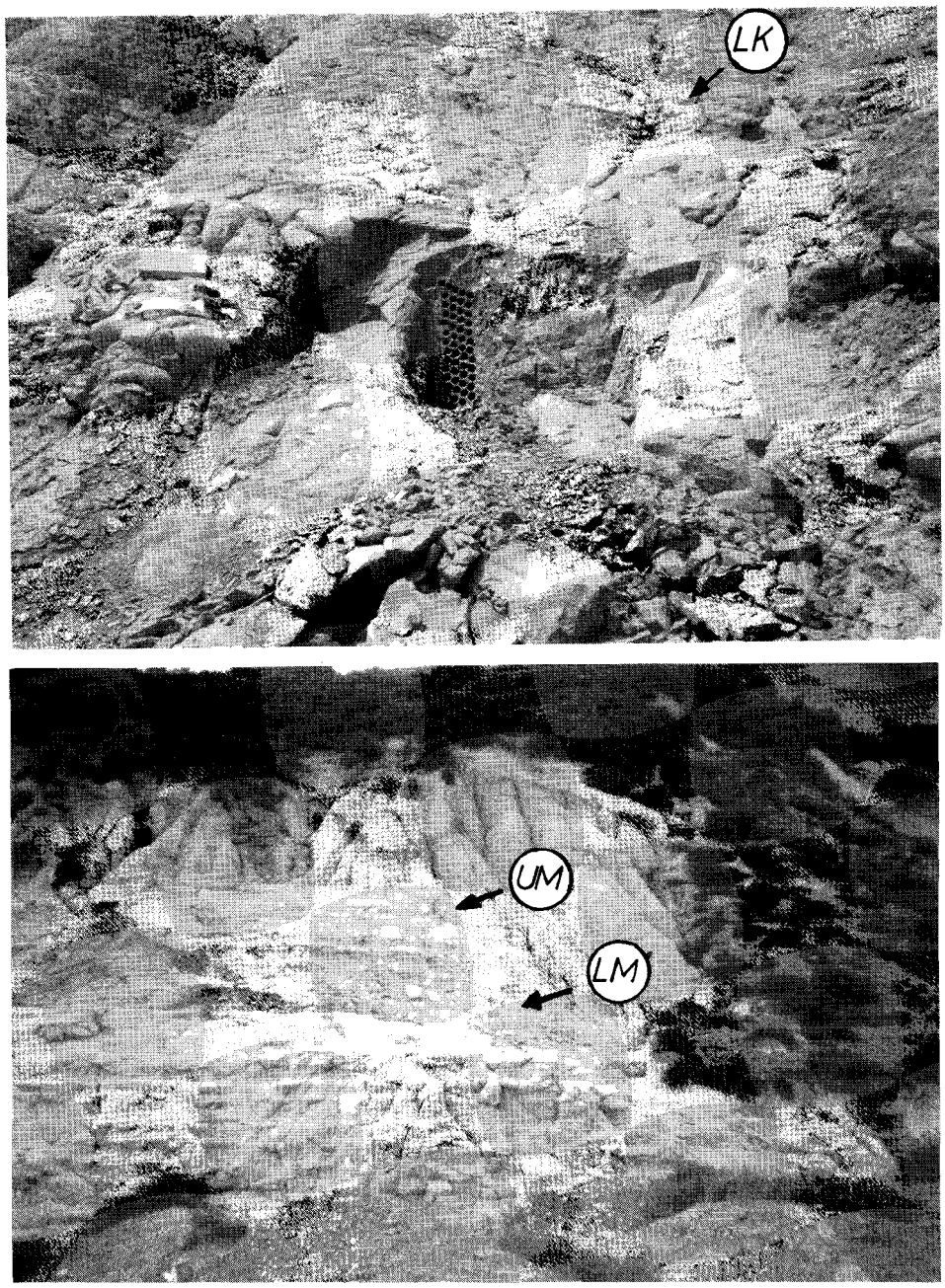

Fig. 3 Sampling sites of lower and upper Mammoth reversal records (lower picture) and lower Kaena reversal record (upper picture).

developed interactive and graphics-based computer program. Directions of the remanent magnetizations were calculated by means of least squares analysis (Kirschvink, 1980).

Susceptibility and anisotropy measurements have been determined using an AC bridge (KLY-1). Continuous measurements of magnetization during cooling and heating were performed with a fluxgate spinner magnetometer. The temperatures of the specimens are controlled either by a water-cooled furnace, or by a liquid nitrogen dewar.

4. Rock magnetism

The assessment of rockmagnetic parameters throughout the reversal records makes it possible to distinguish the paleointensity variations from variations in magnetic mineral contents. To accomplish this, the characteristics of the isothermal remanent magnetization (IRM) and the variation of the IRM, H_{CR} and initial susceptibility in the reversal records have been determined.

The rockmagnetic properties of the lower part of the Calabrian Trubi formation, have been the subject of an extensive study (chapter 4). The IRM and characteristic remanent magnetization (ChRM) of the Monte Singa Trubi sediment is carried by low-coercive magnetite and medium-coercive pyrrhotite. The demagnetization of pyrrhotite and magnetite takes place in respectively the temperature trajectories 210-360 °C and 480-620 °C. In the lower part of the Monte Singa section the contribution of pyrrhotite to the IRM is approximately 10% in the HCU's and 90% in the LCU's, the magnetite contribution to the ChRM is approximately 90% in the HCU's and 10% in the LCU's. The contribution of pyrrhotite to the remanence diminishes in the top of the Monte Singa section (chapter 3). The estimated grain size of magnetite is 0.1-0.2 micrometer in the HCU's and less than 0.1 micrometer in the LCU's. The average grain size of pyrrhotite is less than 2 micrometer in the HCU and LCU.

The reversal records of the pyrrhotite and magnetite components in the Calabrian Trubi formation indicate that magnetite and pyrrhotite acquired their remanent magnetization approximately at the same time. The pyrrhotite component, with respect to the magnetite component, provides slightly more transitional directions of the reversal. This indicates that the lock-in interval of pyrrhotite remanence is smaller. Close to lithological boundaries the magnetite component is more easily biased to present-day field directions than the pyrrhotite component.

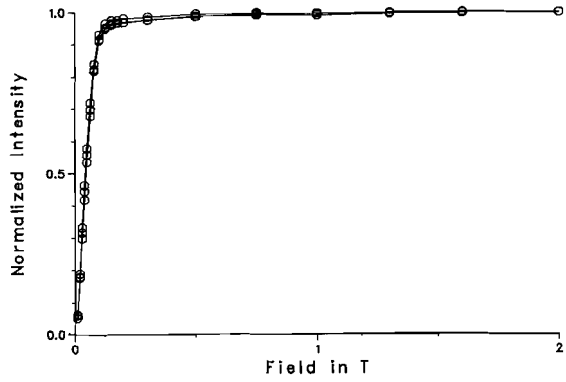

Fig. 4 Normalized IRM acquisition curves for 1 specimen from the lower Mammoth record (10.3 cm level) and 2 specimens from the upper Mammoth reversal record (8.7 and 29.0 cm level). The IRM_{2T} intensity for the lower and upper Mammoth specimens ranges from 1-4 A/m.

4.1 Characteristics of the IRM

The Mammoth and lower Kaena reversals were recorded in the white-beige-white coloured layers. The IRM acquisition curves of the specimens from these layers are saturated for more than 95% in a 0.25 T field (fig. 4). These characteristics correspond to the acquisition curves of the HCU's from the Calabrian Trubi (chapter 4) and point to a low content of (medium-coercive) pyrrhotite.

Stepwise thermal demagnetization of IRM_{2T} of specimens (fig. 5) from the same layers demonstrate the presence of a cation-deficient (CD) magnetite component, removed at approximately 600 °C (Heider and Dunlop, 1986; Linssen, 1988; chapter 4) and a pyrrhotite component removed in the range 300-350 °C. The temperature at which the pyrrhotite remanence is removed is slightly below the maximum blocking temperature of 360 °C observed in the Calabrian Trubi (Linssen, 1988; chapter 4).

Continuous low- and high-temperature treatment of the IRM_{2T} was performed in the temperature range -196 °C to 650 °C. The experimental procedure involved three steps (fig. 6). During the first step, the specimens acquired an IRM_{2T} at room temperature, after which the specimens were cooled to liquid nitrogen temperature (-196 °C) and warmed to room temperature. Subsequently the same specimens again acquired an IRM_{2T} and were

heated to 360 °C, in order to remove any pyrrhotite contribution (chapter 4). Finally, after cooling to room temperature, the specimens acquired an IRM_{2T} once more and were heated to 650 °C.

The cooling curves (from 20 to -196 °C) show an initial smooth remanence increase of approximately 5% between 20 and -150 °C, and a subsequent decrease of the same magnitude. On warming from liquid nitrogen temperature to room temperature the intensity of the remanent magnetization decreases to 90-95% of the initial IRM_{2T} at room temperature.

An increase of remanence on cooling is typical for small grained pyrrhotite (< 5 micrometer; Dekkers, 1988). The decrease of the IRM at approximately -156 °C is attributed to the Verwey transition of magnetite. The decrease of intensity at the Verwey transition is less for smaller grains (Hartstra, 1982). For very small grain sizes (<1 micrometer) the effects at the Verwey transition are not well known and must be estimated by extrapolation of the experimental data. If the initial remanence increase on cooling (due to pyrrhotite) is subtracted, one arrives at an extrapolated grain size for magnetite of 0.1-0.5 micrometer. This result agrees with the results of the Calabrian Trubi HCU sediment (chapter 4).

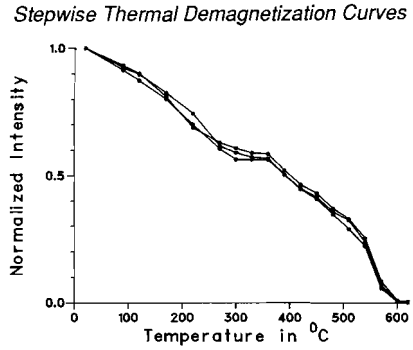

Fig. 5 Stepwise thermal demagnetization of IRM acquired in 2 T for specimens from the lower Mammoth record and upper Mammoth reversal record. The same samples were used for acquisition of IRM, see fig. 4. The remanent magnetizations of pyrrhotite and magnetite are removed near 320 and 580 °C respectively. The curves are normalized with respect to the IRM acquired at room temperature.

During the first heating treatment to 360 °C the pyrrhotite contents is altered to non-magnetic products (Linssen, 1988; chapter 4). Consequently, the newly acquired IRM_{2T} before the second heating cycle is carried by magnetite only. The alteration of pyrrhotite during the first heating cycle results in an increase of the magnetite remanence at 300-350 °C during the second heating cycle (chapter 4). The contribution of pyrrhotite to the IRM_{2T} is equal to the original IRM_{2T} minus the IRM_{2T} acquired before the second heating cycle, corrected for the increase of IRM observed in the second heating cycle. The contribution of magnetite to the IRM_{2T} is the remainder. The actual contributions of magnetite and pyrrhotite to the IRM_{2T} are respectively 90% and 10%, which is similar to the HCU's of the Monte Singa Trubi.

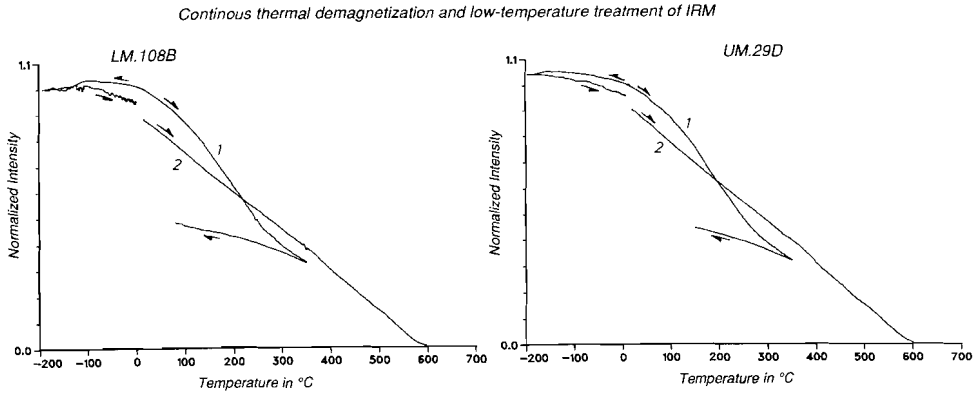

Fig. 6 IRM cooling and heating curves for two specimens from the lower Mammoth (LM.108B, 24.3 cm level) and upper Mammoth (UM.29D, 26.9 cm level) reversal records. The first heating curve to 360 °C is denoted '1', the second heating curve to 600 °C is denoted '2'. The sediments acquired an IRM in 2 T. The sense of heating and cooling is indicated with arrows. The intensity decrease due to the Verwey transition is indicated with a double arrow. All curves are normalized with respect to the IRM acquired before the first heating cycle. At 320 °C and 580 °C the remanent magnetizations of respectively pyrrhotite and magnetite are removed.

4.2 Susceptibilities and anisotropy of susceptibility

The most important constituents of the Calabrian Trubi are calcite, clay minerals (kaolinite+illite) and quartz; the average contribution of these minerals is respectively 55, 35 and 10% by weight (chapter 4). The total susceptibility of these minerals, dominated by the clay minerals, is at least 80.10^{-6} SI (see e.g. Collinson, 1983). This matrix susceptibility is about 50% of the average susceptibility of the sediment, being 160.10^{-6} SI (see e.g. table 2). As a consequence, the variations of the susceptibility of magnetic minerals are strongly buffered by the susceptibility of the non-magnetic minerals. The effect of the buffering mechanism is illustrated by the relation between the H_{CR} and IRM_{2T} variations on the one hand, and the susceptibility variations on the other (figs.11a-c). Although the H_{CR} and IRM_{2T} variations are also reflected in the susceptibility record, the amplitude of the susceptibility variations is far less.

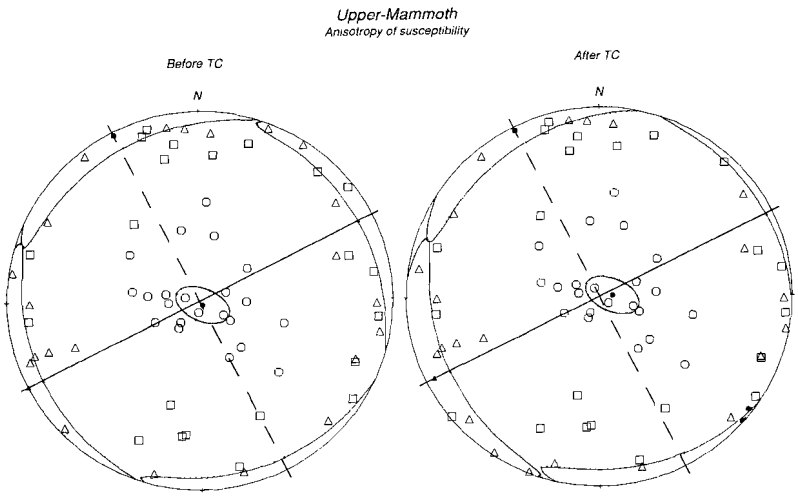

Fig. 7 Anisotropy components for specimens from the upper Mammoth record in an equal-area projection. Round, square and triangle symbols refer respectively to the K_{min}, K_{int} and K_{max} axes of the anisotropy ellipsoid. Corresponding closed symbols correspond to the average anisotropy axes. The anisotropy is dominated by flat-lying foliation, no lineation is present. The ellipses denote the angles of 95% confidence. The solid and dashed lines denote the average directions of respectively the K_{max} and K_{int}.

The buffering mechanism may also be demonstrated by the anisotropy of susceptibility. Clay minerals are expected to produce a strong foliation, whereas magnetite in marls are expected to produce a sub-horizontal lineation (Kodama and Sun, 1990). The results of the anisotropy measurements are shown in figure 7 and table 2. The low values of P (degree of anisotropy) and T (characterizing the shape of the susceptibility ellipsoid) demonstrate that the anisotropy is indeed determined by foliation ($F=K_{int}/K_{min}$), rather than by lineation ($L=K_{max}/K_{int}$). Due to the clay matrix contribution, the initial susceptibility is not further used for the characterization of remanent magnetic minerals in the sediment.

Table 2 Anisotropy of magnetic susceptibility

	N	X_i	L	F	P	T
upper Mammoth	22	160.5	1.0023	1.0112	1.0136	0.6516

Table 2. The magnetic susceptibility and the parameters of anisotropy for the sediment from the upper Mammoth record. Given are the number of specimens for which the anisotropy was determined (N), the average bulk susceptibility (X_i in 10^{-6} SI), the lineation (L), the foliation (F), the anisotropy degrees (P) and the T parameter (Jelinek, 1981; Hrouda, 1981). The calculation of the anisotropy parameters and the statistical analysis of the data is according to Jelinek (1977,1978,1981) and Hrouda (1981).

5. Demagnetization of NRM

For all records, a considerable number of specimens has been analysed, mostly by progressive stepwise thermal (TH) demagnetization and some by progressive stepwise alternating field (AF) demagnetization (figs.8,9a-c). The AF and TH demagnetization results show multiple components (figs. 8,9a-c). A viscous component induced during storage of the specimens in the laboratory and a more stable secondary magnetization with a present-day field direction are removed at 15 mT or 240 °C. The secondary component in the sediment from the Punta Piccola section is removed at a slightly higher temperature than the secondary component in the Calabrian sediment (210 °C).

Two components of the characteristic remanent magnetization (ChRM) with approximately the same direction are removed below 320 °C and 580 °C. The minerals carrying these components are pyrrhotite and magnetite (Linssen, 1988; chapter 4). Due to the small temperature trajectory in which the pyrrhotite component is isolated - 240-320 °C - the directions of the pyrrhotite component could not be established with sufficient accuracy. Only magnetite remanences were used for interpretation of the

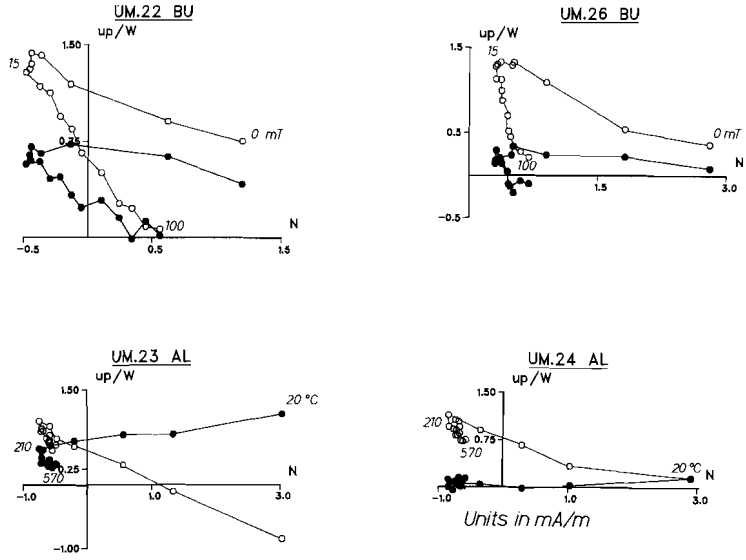

Fig. 8 Thermal and alternating field demagnetization diagrams (orthogonal projection, Zijderveld, 1967) of some specimens from the upper Mammoth reversal record. In the diagrams the open (closed) symbols denote projections of the NRM on the vertical (horizontal) plane. The first step corresponds to the initial remanence (20 °C), the first demagnetization step is at 90 °C, 30 °C increments are applied in the range 90-510 °C and 20 °C increments above 510 °C. The last demagnetization steps are at 550 °C. The AF demagnetization was performed with 2.5 mT increments in the range 0-20 mT, additional steps at 25 and 30 mT and 10 mT steps above 30 mT.

records.

The alternating field demagnetizations show that a single ChRM component is removed by fields between 15 and 100 mT. The coercive force spectra of magnetite and pyrrhotite have a large overlap, causing the seemingly unimodal decay during the alternating field demagnetization (Linssen, 1988). For specimens from the Mammoth reversal records, a high coercive remanent magnetization remains which cannot be isolated, mainly because AF demagnetization with fields exceeding 100 mT produce scattered results. This additional component has a north declination and a near zero inclination. The direction of this high coercive component does not correspond to any high temperature component. However, there is a close correspondence in direction and intensity between the component removed below 240 °C and the components removed below 15 mT plus the high-coercive component. Hence, the high coercive component must

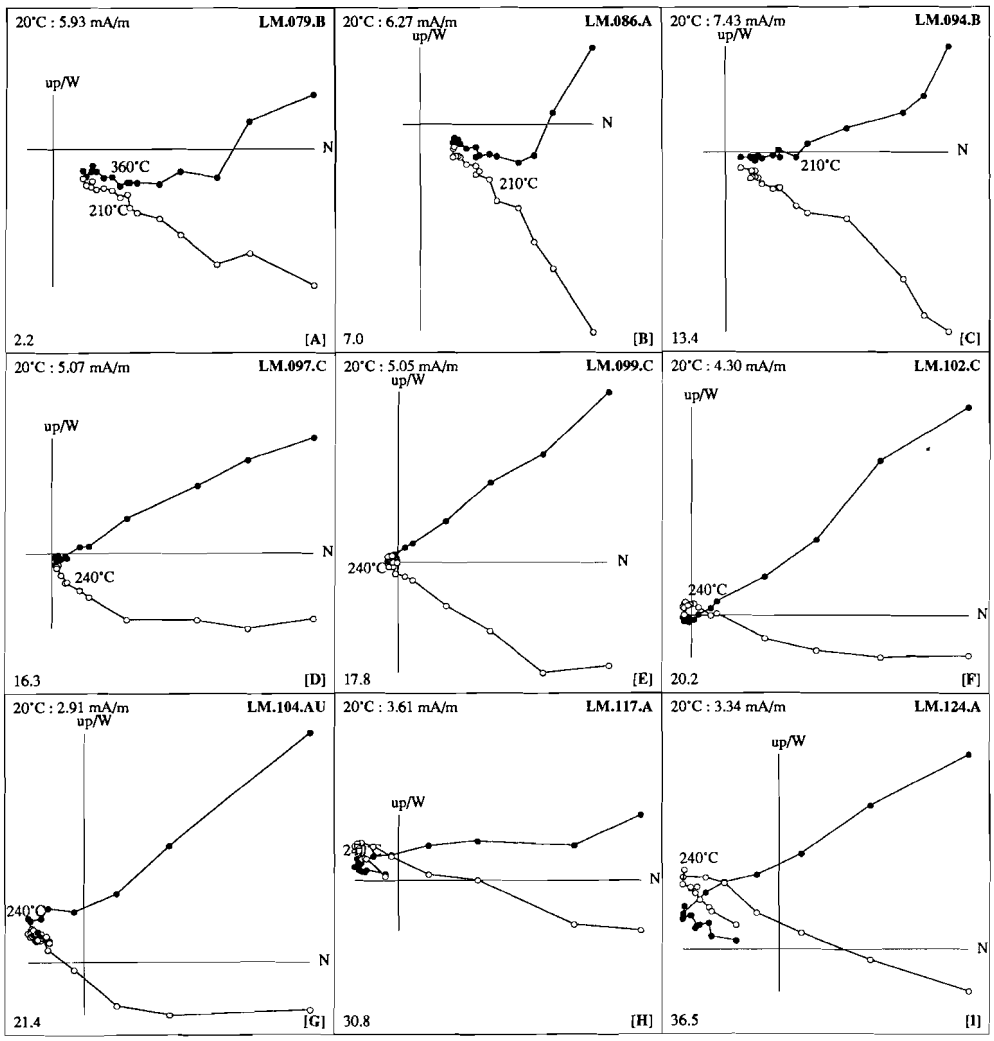

Fig. 9a Thermal demagnetization diagrams for specimens from the lower Mammoth reversal record. Open (closed) symbols denote projections on the vertical (horizontal) plane. The stratigraphic level of the specimens is indicated in the lower left corner of each diagram. The intensity at the first step is indicated in the upper left corner of each diagram. See also caption figure 8.

be a part of the low-temperature component. A common magnetic mineral with the observed high coercive force but with a low maximum blocking temperature is goethite (T_B < 120 °C; Heller, 1978). Most probably, this mineral is the carrier of the high-coercive

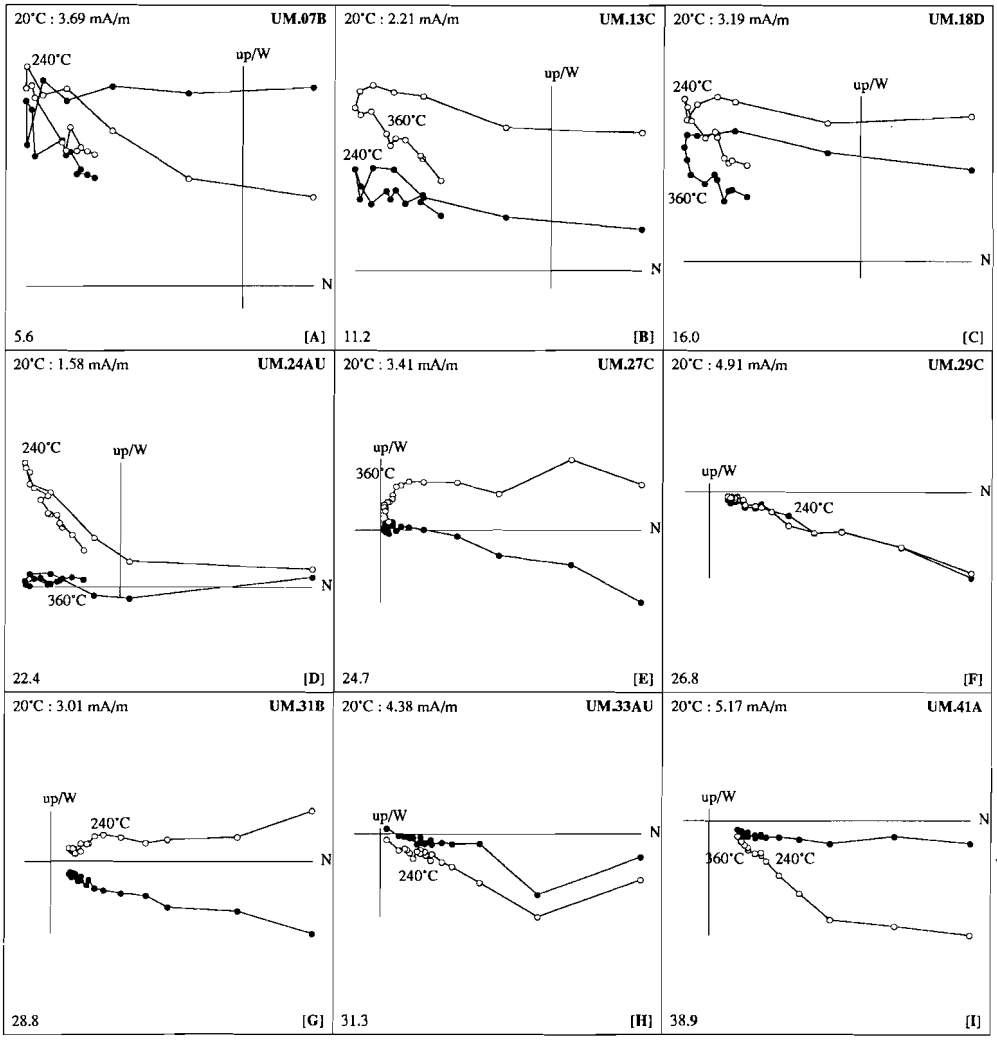

Fig. 9b Thermal demagnetization diagrams of specimens from the upper Mammoth reversal record. See also caption figs. 8,9a.

component.

Goethite acquires an important part of its IRM between 0.5 and 2 T (30-60% of J_{RS}, e.g. Heller, 1978; Dekkers, 1988). In the 0.5-2.0 T interval of the IRM acquisition curves almost no remanence increase is observed (fig. 4), demonstrating that the contribution of

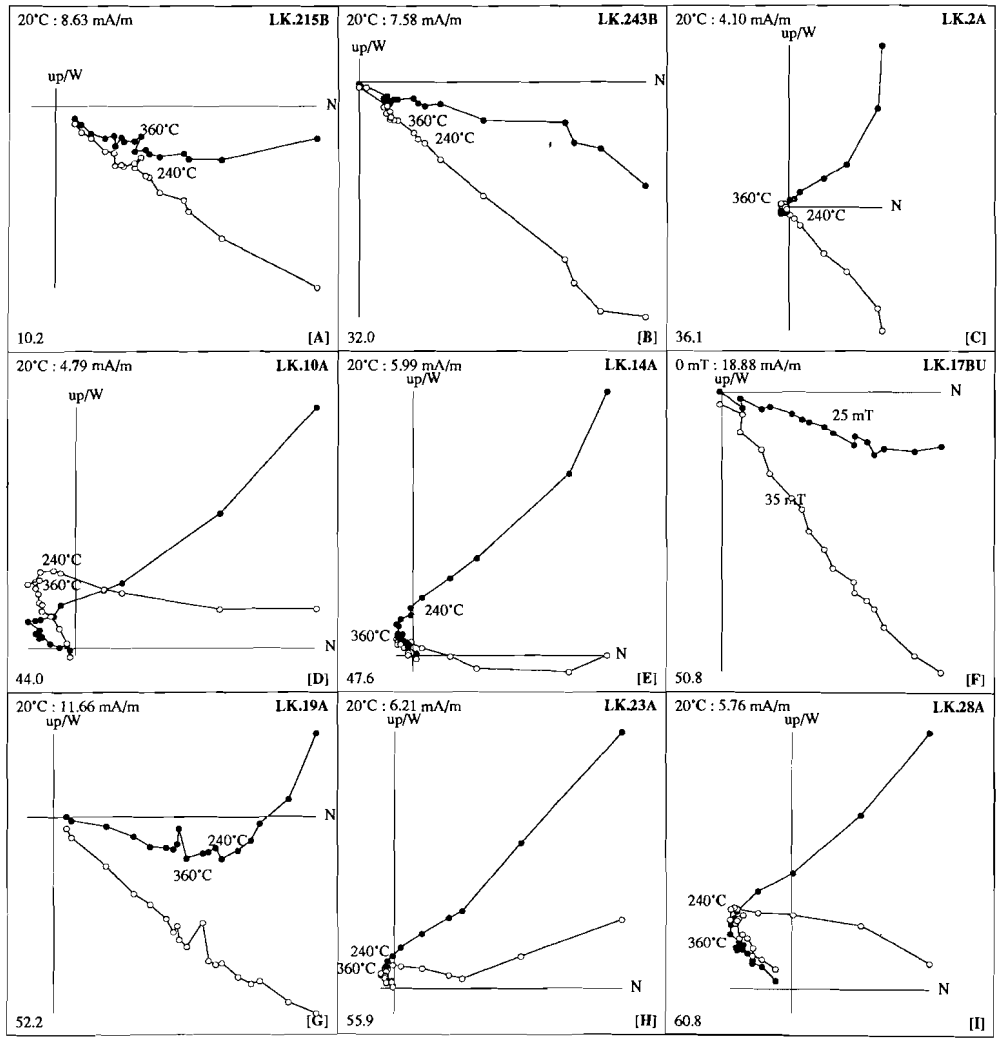

Fig. 9c Thermal demagnetization and one alternating field demagnetization diagram of specimens from the lower Kaena reversal record. See also caption figs. 8,9a.

goethite to the IRM is not significant. This is confirmed by the results of the stepwise thermal demagnetization of the IRM_{2T}, which shows no noticeable contribution of goethite (fig. 5). Apparently, goethite contributes to the ChRM, but not to the IRM.

It is important to establish whether goethite may have been produced from ChRM

carrying minerals. If so, this would affect the validity of the ChRM intensity data as an indicator of the variations of the paleomagnetic field intensity. A genetic relation between goethite and magnetite or goethite and pyrrhotite is easily determined since the remanent magnetization of goethite is approximately 1% of the remanent magnetization of magnetite and pyrrhotite. In other words, goethite entirely produced from pyrrhotite or magnetite causes a major decrease of NRM and IRM intensities. However, no relation is observed between the appearance of goethite magnetizations and any variation of pyrrhotite and magnetite magnetizations. On the contrary, the intensities of the ChRM and IRM of the Calabrian Trubi marls, the sediment from the lower Kaena record (showing no evidence for goethite magnetizations) and those of the Mammoth records are in the same order of magnitude. It may therefore be concluded that goethite is not produced from the ChRM or IRM carrying minerals. The less indurated Trubi sediment from the Calabrian section does not contain significant amounts of goethite (chapter 4), neither does the less indurated sediment from the lower Kaena reversal record. Based on these observations it is likely that goethite is produced from non-magnetic minerals during the induration process of the sediment.

6. The reversal records

Throughout the Punta Piccola section, the stable ChRM directions have significant deviations from the expected local geocentric axial dipole field declinations (0/180°) and inclinations (56/-56°) (table 3, figs.10a-c). The anomalous ChRM declinations are caused by the rotation of the Caltanisetta Basin of Sicily, which is 35° on average for the Punta Piccola section (Scheepers and Langereis, in prep.). Inclination errors are commonly observed in marine sediments and are ascribed to early compaction and dewatering of the sediment (Blow and Hamilton, 1978; Laj et al, 1982; Arason, 1986; Anson and Kodama, 1987; Celaya and Clement, 1988; Linssen, 1988, chapter 4).

The support for the primary origin of the ChRM component is based on the observations (a) that the ChRM component is removed near the Curie temperature of fine grained CD magnetite (578-600 °C), of (b) the recorded Pliocene clockwise rotation (35°)

Table 3 Directions of characteristic remanent magnetizations

		Normal polarity ChRM			Reversed polarity ChRM		
		Decl.	Incl.	a_{95}	Decl.	Incl.	a_{95}
lower Kaena	N-R	30.0	38.0	3.5	220.0	-39.0	2.2
upper Mammoth	R-N	21.0	29.3	5.4	209.3	-36.1	1.8
lower Mammoth	N-R	28.4	39.5	2.6	198.7	-35.1	3.1
Complete section		28.3	39.7	1.4	203.7	-36.9	1.8

Table 3. Average directions of characteristic remanent magnetizations above and below the Mammoth and lower Kaena reversal records and for the complete Punta Piccola section (Zachariasse et al., 1989; Scheepers and Langereis, in prep.). The a_{95} confidence angles were calculated with Fisher statistics.

of the sedimentary succession and (c) the inclination error of approximately 15 to 20°.

6.1 The lower Mammoth reversal record

The investigated sedimentary interval enclosing the lower Mammoth reversal record has a length of 40 cm. The interval is part of a white-beige-white unit (fig. 11a). The transition from beige to white marl is at the 29 cm level. The actual reversal occurs in the beige marl. The IRM_{2T} intensity and the H_{CR} slightly decrease towards the beige-white unit boundary. The decrease of the IRM_{2T} explains the lower post-reversal intensities of the ChRM. The non-transitional ChRM directions from the lower Mammoth record and those from the complete section are virtually identical (table 3). Hence, it may be concluded that the complete lower Mammoth reversal is recorded in the sampled sedimentary interval.

The declinations, inclinations and intensities of the ChRM are constant up to the 12 cm level. Above the 12 cm level the intensities decrease. The inclinations and declinations start changing at the 15 cm level. The inclinations increase to a maximum of approximately 70° at the 16 cm level. Between 16 and 18 cm the actual reversal takes place and at the 24 cm level the declination and inclination have returned to stable reversed polarity. The minimal ChRM intensities are present in the 16-21 cm interval and are approximately 15% of the non-transitional ChRM intensities (correction for the decrease of the IRM_{2T} applied). The lithological beige-white boundary at the 29 cm level produces a slight scatter of the ChRM.

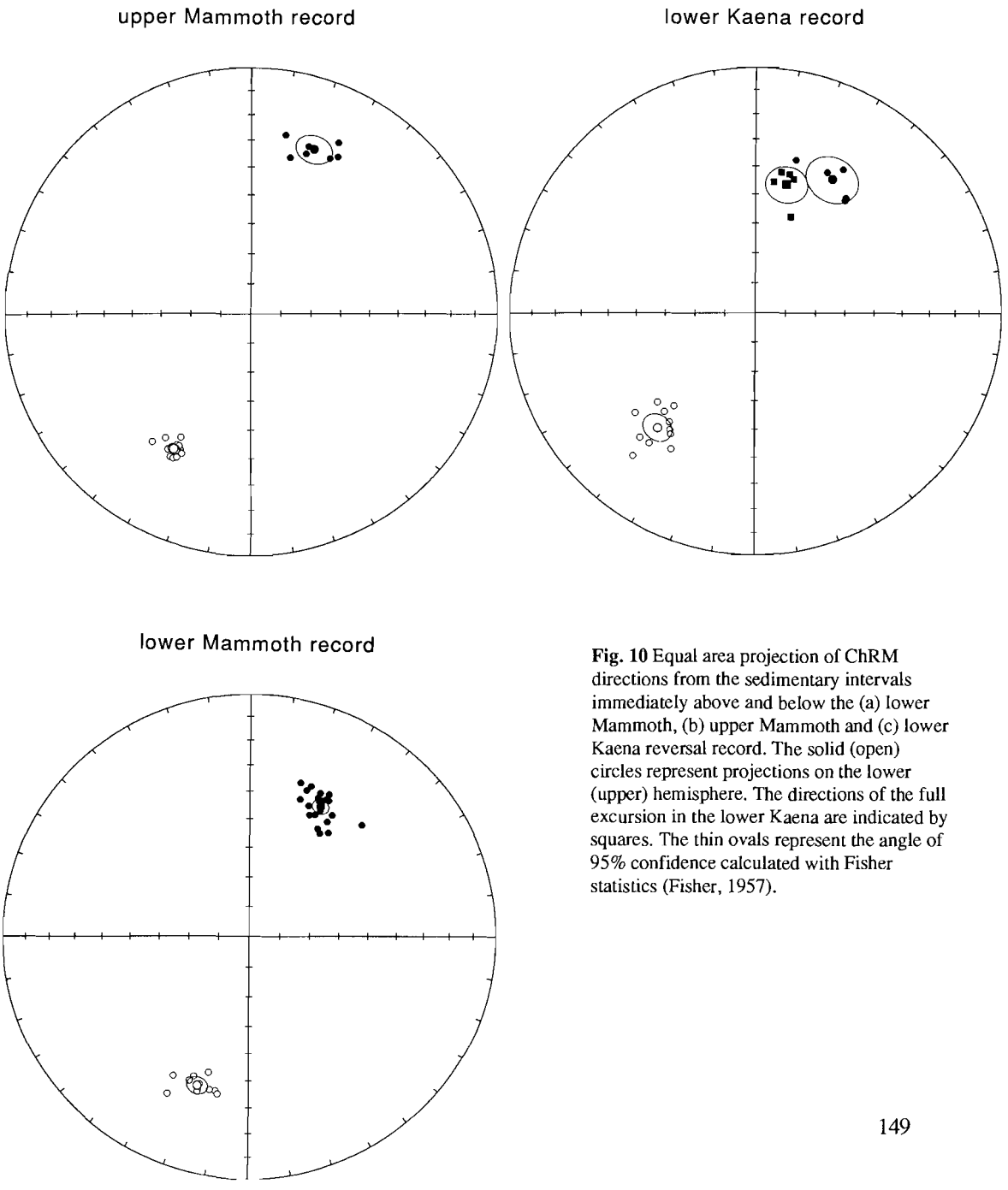

Fig. 10 Equal area projection of ChRM directions from the sedimentary intervals immediately above and below the (a) lower Mammoth, (b) upper Mammoth and (c) lower Kaena reversal record. The solid (open) circles represent projections on the lower (upper) hemisphere. The directions of the full excursion in the lower Kaena are indicated by squares. The thin ovals represent the angle of 95% confidence calculated with Fisher statistics (Fisher, 1957).

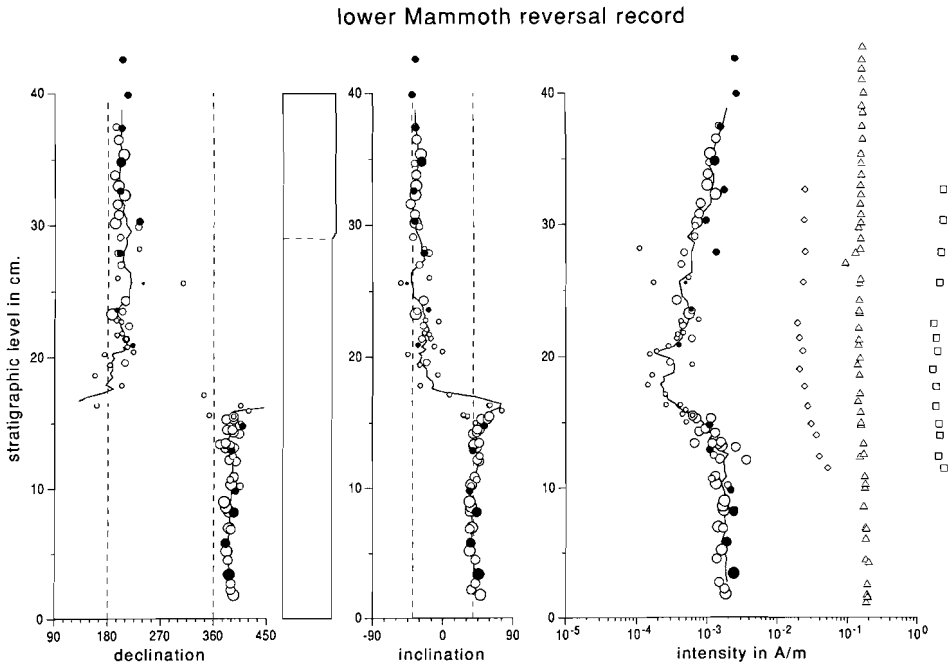

Fig. 11a. lower Mammoth ChRM reversal record. The ChRM is obtained with thermal demagnetization (open circles) and AF demagnetization (closed circles). The 5 different sizes of the circles correspond to the quality of the demagnetization results; large circles denote high quality components, smaller circles denote a poorer quality. The line in the record corresponds to a five-point running average. The column between the inclination and declination records denotes the lithology: the indurated parts are the white-beige-white units. The dashed line indicates the transition from the indurated white marl to the somewhat less indurated beige marl. The dashed lines in the declination and inclination records indicate the non-transitional polarity states. The non-transitional polarity state does not reflect the 35° rotation, but the inclination error has been accounted for (f=0.52). The squares denote IRM_{2T}, diamonds denote the corresponding H_{CR} and triangles denote initial susceptibilities (10^{-3} SI).

6.2 The upper Mammoth reversal

The investigated sedimentary interval enclosing the upper Mammoth reversal record has a length of 40 cm. The interval is part of a white-beige-white unit. The transition from beige to white marl is at the 38 cm level. The actual upper Mammoth polarity transition is recorded in the beige marl (fig. 11b).

From a rockmagnetic viewpoint, the upper Mammoth record is similar to the lower Mammoth reversal record: both the IRM_{2T} intensity and the H_{CR} slightly decrease towards the beige-white unit boundary. The non-transitional ChRM declinations deviate to W compared to the ChRM directions of the complete section (table 3). Furthermore, the

inclinations above the actual upper Mammoth reversal are notably lower than the average inclinations for the section. Probably, the investigated interval starts and ends with transitional directions.

Below the 17 cm level the directions are fairly constant, whereas the ChRM intensities - and to a minor extent the IRM_{2T} intensities - decrease. Probably the ChRM decrease below the 17 cm level has a rockmagnetic origin. Above the 17 cm level the decrease of ChRM intensity becomes more pronounced, the inclinations gradually steepen and the declinations show an eastward trend. Above the 20 cm level there is a clear and distinct steepening of the inclinations to values of -80°, whereas the declinations gradually change westward. Intensities are still decreasing in this interval. At the 25 cm level the inclinations are almost vertically upward directed and the declinations rapidly reverse to normal polarity. The inclinations reverse to normal polarity in the 25-27 cm interval. A

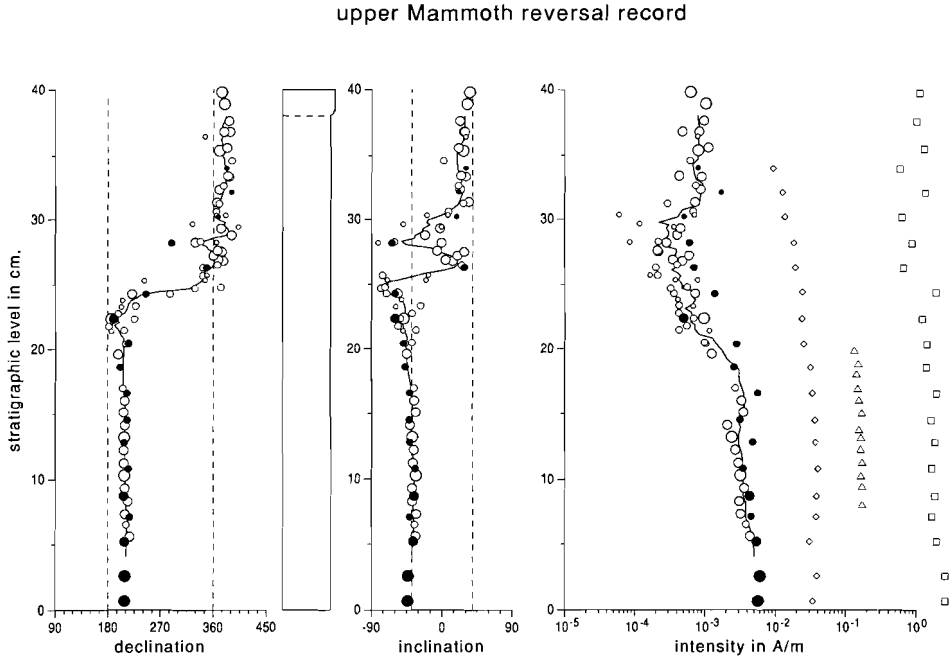

Fig. 11b upper Mammoth reversal record of ChRM. See also caption figure 12.

significant rebound to negative inclinations is observed in the 27-32 cm interval. Above the 32 cm level the inclinations and declinations gradually realign to stable axial dipole field directions.

The minimum ChRM intensities occur at the 27 cm level and are 5% of the intensity at the 17 cm level. The true intensity decrease during the reversal must be somewhat less regarding the overall IRM decrease. After correction for the IRM variations, a minimum ChRM intensity of approximately 10% of the pre-reversal intensity remains.

6.3 The lower Kaena reversal record

The length of the investigated sedimentary interval enclosing the lower Kaena reversal is 90 cm. The lowermost 25 cm of this interval is part of a grey unit, the uppermost 65 cm is part of a white-beige-white unit. The main part of the lower Kaena reversal is recorded in the white-beige marls (fig. 11c).

Apart from some slight variations near the grey-white unit boundary and the white-beige unit boundary the H_{CR} and IRM_{2T} are constant in the lower Kaena record. Hence, from a rockmagnetic viewpoint this record may be considered as homogeneous.

The stable normal and reversed ChRM directions demonstrate a clockwise rotation with respect to the average ChRM directions for the complete section (table 3). Other directional deviations which indicate that the reversal is not completed within the investigated interval are not observed.

In the sedimentary interval from 0-18 cm the declinations change from normal polarity (35°) to N. In the same interval the intensities increase to a maximum value. Between the 18 and 33 cm levels the declinations rotate clockwise and the intensities and the inclinations show minimum values. The coincidence of the minima and the lithological change of grey to white marl at the 24 cm level suggest the occurrence of an early remagnetization in this interval (compare upper Thvera reversal record in chapter 3). The ChRM reverses polarity in the interval 33-36 cm: the declination rotates via east and the intensity decreases to approximately 10% of the non-transitional value. Above the reversal, in the interval 36-47 cm, the intensities increase to pre-reversal values and the declinations slightly rotate clockwise. An irregular oscillation of the inclinations - between -10° and -55° - is observed in the 37-44 cm interval.

A full and rapid excursion to normal polarity is present in the interval 47-60 cm. In this interval, the intensities change to a minimum, a prominent maximum (twice that of the

pre-excursion intensity) and a subsequent minimum. The intensity minima correspond to the two polarity transitions of the excursion. The declination change at the onset of the excursion appears to be a logical continuation of the clockwise declination change starting at the 30 cm level. The R-N reversal of the full excursion is rapid, but also relatively smooth, whereas the subsequent N-R reversal proceeds almost instantaneous, just as the first N-R reversal. A very conspicuous characteristic is the rapid intensity increase during the full excursion. The maximum intensity is more than 20 times the ChRM intensity just below and above the excursion and more than 2 times the non-transitional ChRM intensities. Above the excursion the ChRM directions approach stable reversed polarity.

The intensity shows a wide minimum in the 60-90 cm interval. At the level of minimal ChRM intensities the declinations and inclinations show some anomalous values, probably related to remagnetizations.

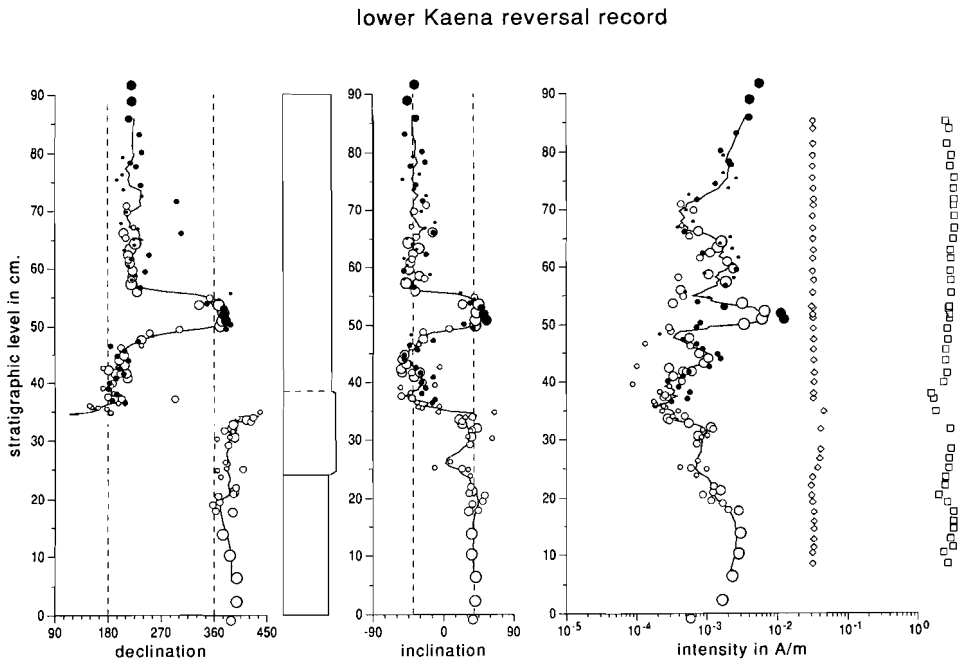

Fig. 11c lower Kaena reversal record of ChRM. The dashed line in the lithostratigraphic column indicates the boundary level between the white (lower) and beige (upper) layer, the solid line indicates the boundary between the grey (lower) and white (upper) layer. See also caption figure 11a. Note the "Punta Piccola" excursion in the 48-58 cm interval.

6.4 The Virtual Geomagnetic Poles

The transitional directions of the reversals have been characterized as virtual geomagnetic poles (VGP's) (figs.12a-c). The VGP's have been corrected for the rotation of the Caltanisetta Basin (35°). A generally accepted method for the correction of inclination errors is not available. Anson and Kodama (1987) performed redeposition experiments with kaolinite and fine-grained magnetite (<0.5 micrometer) in distilled water and sea water at various pressures (0-2.53 MPa). They showed that for fine-grained sediments the major part of the inclination shallowing occurs upon application of rather low-pressures, corresponding to the compaction stage of the sediment. The origin of the inclination shallowing is ascribed to an electrostatic interaction between the platy clay minerals and the magnetic minerals (Anson and Kodama, 1987).

The inclination error of the Punta Piccola sediment agrees well with the errors found by Anson and Kodama (1987). Most probably the inclination error of the Punta Piccola sediment is introduced by the same mechanism. Anson and Kodama showed that the relation

$$\tan I_o = f \,.\, \tan I_f \text{ (King, 1955)},$$

may be used for correction of the inclination error in fine-grained sediments (I_o is the observed inclination, f is the correction factor and I_f is the local geocentric axial dipole field inclination). The application of this relation yields f=0.52. The VGP's are given both before and after correction for the inclination error. If no correction is applied the VGP's are approximately 10-15° closer to the site resulting in an artificially enhanced number of transitional directions.

Since the Mammoth and lower Kaena reversal records proceed very rapidly, the number of transitional directions is low. As a result the VGP path corresponding to the actual reversal is not very accurately defined. For the lower Kaena reversal the N-E-S trend of the first reversal results in a VGP path which is constrained to a great-circle about 90° E of the site meridian. The S-W-N trend at the onset of the full excursion (second reversal) causes a VGP path that is constrained to a great circle about 90° W of the site meridian. The end of the full excursion (third reversal) is very rapid and results in a VGP jump from N to S with hardly any intermediate directions.

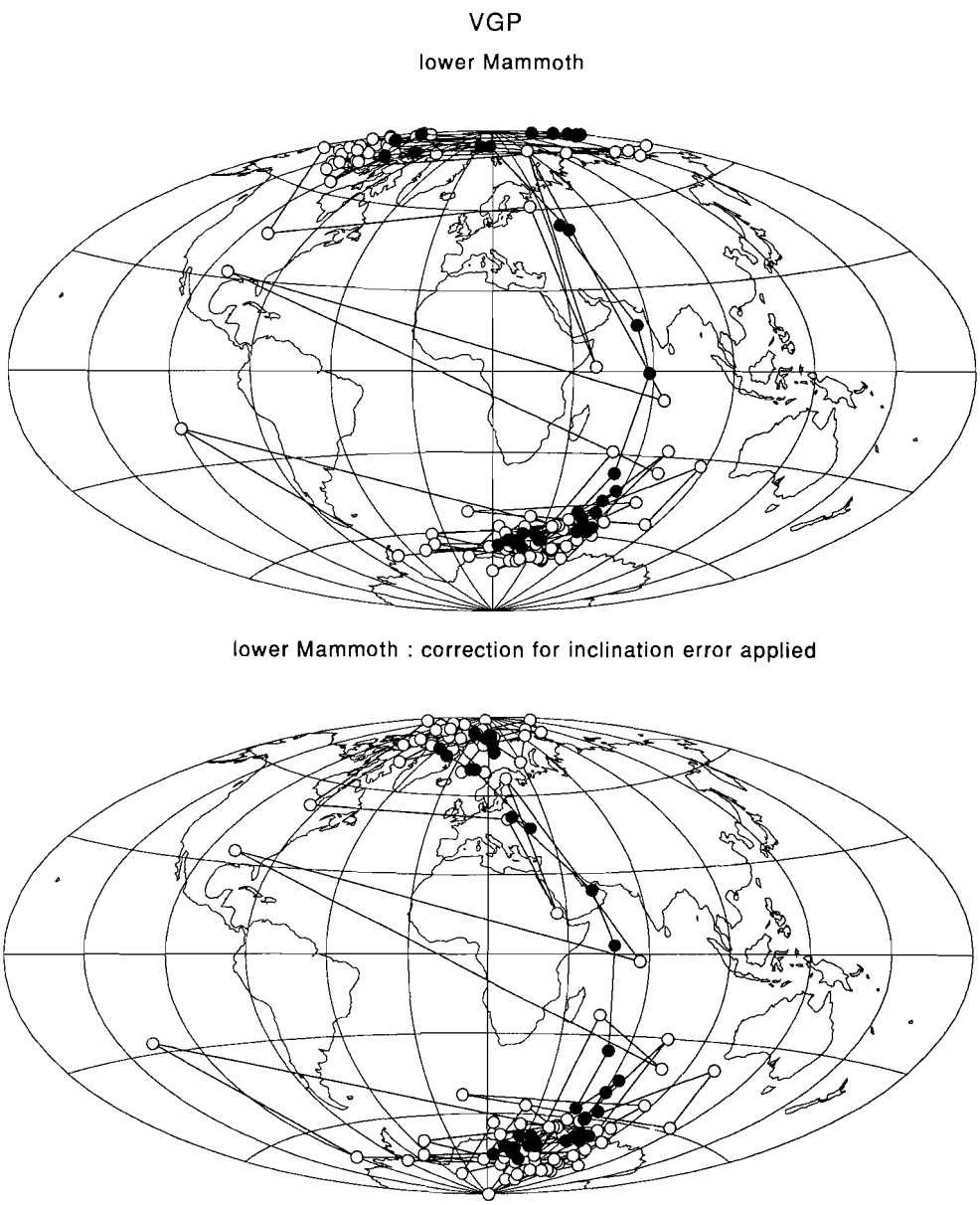

Fig. 12 Aitoff projection of the Earth centred around the site meridian (13.5°E) with the virtual geomagnetic poles (open circles) of the(a) lower Mammoth and (on the next pages) the (b) upper Mammoth and (c) lower Kaena reversal records. The closed circles correspond to a five-point running average for the intervals in which the actual polarity transitions occur. The VGP's are given both before and after correction for the inclination error (f=0.52).

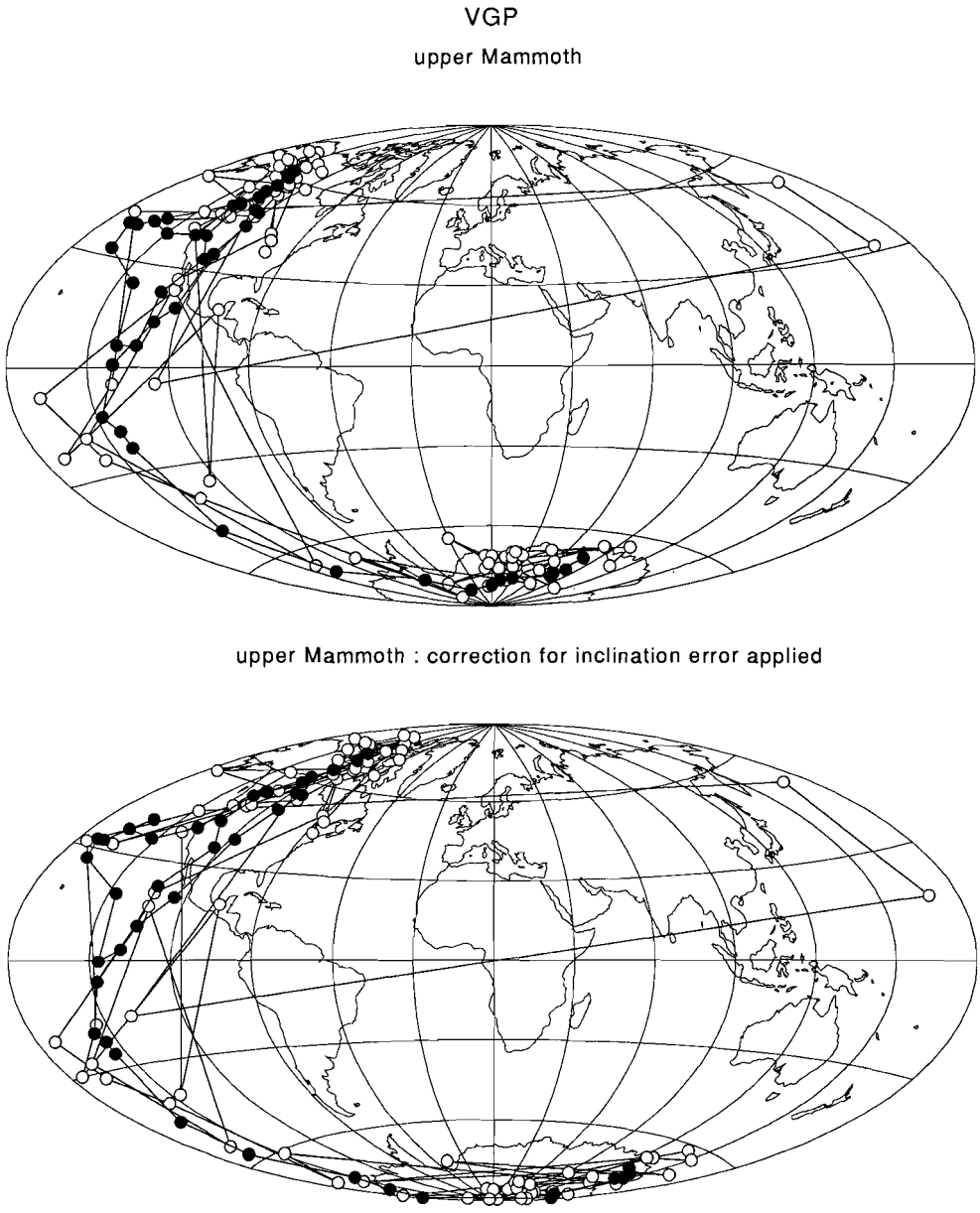

Fig. 12b See caption fig.12a.

VGP

lower Kaena

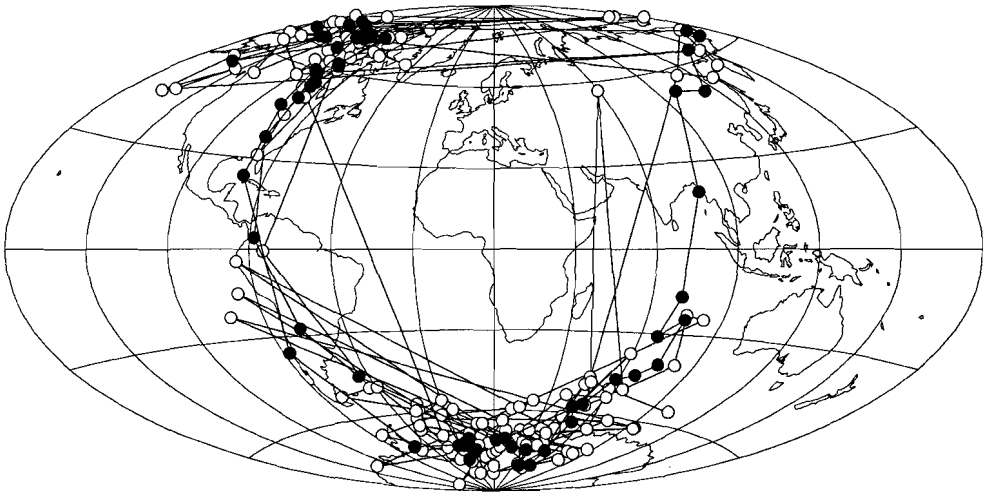

lower Kaena : correction for inclination error applied

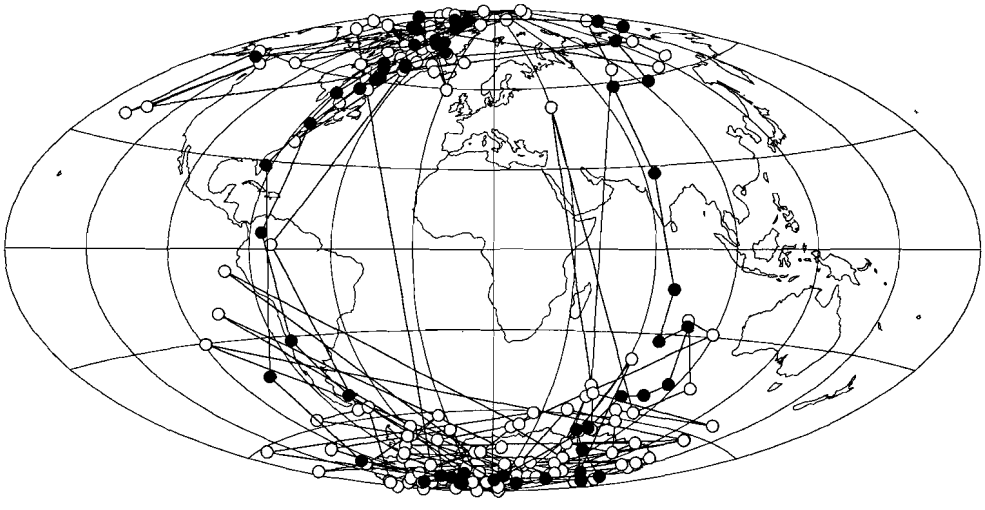

Fig. 12c See caption fig.12a.

In spite of the small amount of transitional directions, it is clear from the VGP plots that the upper Mammoth reversal record is far-sided. The upper Mammoth reversal record is the first dominantly far-sided northern-hemisphere record between the upper Thvera and the Matuyama Brunhes reversals. All Pliocene reversal records studied so far - from the upper Thvera to the lower Mammoth - share the fact that they are not far-sided (Linssen, 1988, chapter 3). Other far-sided reversal records from the same region have been reported to occur in Late Miocene deposits (e.g. Valet et al., 1988) at which time they were intermittent with near-sided reversal records.

7. Discussion

The process of remanence acquisition during deposition and compaction of the sediment acts as a filter on the recording process of ambient geomagnetic field changes. A sedimentary record of remanent magnetizations may seriously deviate from the true geomagnetic field changes which created the record (e.g. Hoffman and Slade, 1986; Rochette, 1990). However, the most rapid intensity changes in a reversal record indicate the upper limit of the smoothing process active during remanence acquisition (e.g. Constable, 1990).

In this respect, the rapid ChRM changes in the Punta Piccola records provide strong evidence that the smoothing process during acquisition of the remanence has been minor. The ChRM changes which are observed at the top of the excursion overlying the lower Kaena reversal record are the most rapid ones observed: within 2 cm (or 430 year) a 180° directional change and a ChRM intensity increase of a factor 20 occur. Apparently, the sediment was able to record directional changes taking place at a rate of 0.2°/yr and an intensity change of 5% of the initial intensity per year. It may be concluded that this sediment is an accurate recorder of rapid directional and intensity changes of the paleomagnetic field and the effects of smoothing on remanence acquisition are minor.

The assessment of the duration of a reversal depends on the (subjective) definition of its boundaries in the record. For the lower Mammoth reversal the duration can be determined rather straightforward since only one major change of directions and intensities is present (fig. 11a, table 4). In the upper Mammoth reversal record (fig. 11b) the actual

reversal and the excursion have been characterized as two parts of the same reversal since both the reversal and the excursion occur in the same intensity low. For the lower Kaena reversal record (fig. 11c) it is less easy to determine the duration of the reversal since a number of subsequent, perhaps isolated or perhaps related, events with stable field directions and intensities are present. For this reversal the durations of each of the events has been specified separately.

Table 4. Duration of reversal features

	Declination		Inclination		Intensity	
	cm	kyr	cm	kyr	cm	kyr
upper Piccola	2	0.4	3	0.7	3	0.7
lower Piccola	3	0.7	4	0.9	4	0.9
lower Kaena	3	0.7	12	2.6	13	2.9
upper Mammoth	10	2.1	18	3.8	23	4.9
lower Mammoth	4	0.8	9	1.8	23	5.6

Table 4. Duration of the reversal related characteristics of the Mammoth and lower Kaena records. The characteristics of the lower Kaena and the full excursion following the lower Kaena reversal (Piccola subchron) have been specified separately. The accumulation rate for the lower Mammoth record is estimated at 5.0 cm/kyr, for the upper Mammoth record at 4.7 cm/kyr and for the lower Kaena record at 4.6 cm/kyr (section 2).

For all records the duration of the directional reversal is between 0.7 and 3.8 kyr. Four out of the five polarity reversals show a full declination reversal within 1 kyr. In all cases the inclination change is slower than the declination change. Furthermore, for all polarity reversals the intensity minima enclose the directional variations. The observations also indicate that an intensity low is not necessarily followed by a polarity transition, as can be seen in the 60-80 cm interval in the lower Kaena record.

The common characteristics of the records indicate that, at least for the present reversals and those of the Calabrian Trubi (Linssen, 1988; chapter 3), a generalization of reversal features can be made. The observations indicate that a reversal is initiated by a mechanism which decreases the geomagnetic intensity first. The polarity transition then proceeds by a change of the inclination and is suddenly followed by a rapidly proceeding change of the declination. This indicates that the sources of the geomagnetic field reversals

are more or less zonally confined with respect to the site.

The Williams and Fuller (1981) model was extended to include paleosecular variations of the geomagnetic field during the reversal (Williams et al., 1988). However, the observed zonally confined rebound (aborted excursion) in the upper Mammoth reversal record cannot be explained in terms of secular variation, since paleosecular variation results in non-zonal components.

The lower Kaena and the upper Mammoth reversal records show examples of respectively a rapid full excursion and an aborted excursion. The existence of an excursion above the lower Kaena reversal record is supported by a study of a sequence of extrusive rocks in which probably a record of the lower Kaena reversal is present (Roperch and Duncan, 1990). The fact that from the three records which have been studied, two produce evidence for excursions is particular. Excursions have been reported previously (e.g. Hoffman, 1981), although they were never proved to be directly related to reversals. The Punta Piccola records indicate that a genetic relation between full excursions and reversals is likely since the observed excursions all occur in the vicinity of reversals. The existence of such a relation and the observation that reversals are preluded by decreased geomagnetic intensities indicates that the probability of reversal occurrences increases during times of decreased geomagnetic intensity. Furthermore, the source mechanism of the reversals must be able to release an enormous amount of energy in a very short (geological) time span since the intensity of the geomagnetic field can change by more than a factor 20 within 0.5 kyr, as can be observed in the Lower Kaena record.

The occurrence of an excursion near the boundaries of a polarity zone introduces the problem where to place the boundaries of polarity zones. With the progression of the resolution in magnetostratigraphic records one may even consider to denote the excursion a separate polarity interval, which in the present case results in two additional polarity intervals above the lower Kaena reversal boundary: one reversed (3 kyr) and one normal (1.5 kyr).

Acknowledgements

T.van Hoof assisted during collection of the samples. H.J.Meier is gratefully thanked for his assistance in the laboratory. Prof.Dr.J.D.A.Zijderveld and Dr.C.G.Langereis are thanked for their critical reading of the manuscript. The investigations were supported by the Netherlands Foundation for Earth Science Research (AWON) with financial aid from the Netherlands Organization for the Advancement of Pure Research (Z.W.O., now N.W.O.)

Chapter VI

Two Lower Pliocene sedimentary geomagnetic reversal records from Corfu

1. Introduction

Studies of the Pliocene magnetostratigraphy and sequences of reversal records in Mediterranean marine sedimentary sequences such as the Trubi formation (Calabria, Sicily) have greatly improved our knowledge of the long and short term variations of the geomagnetic field during this era (Zijderveld et al., 1986; Linssen, 1988; Zachariasse et al., 1989; chapter 3-5). The sediments, marly clays, were demonstrated to be of excellent quality for paleomagnetic research, although in some intervals in the sediment uncertainties exist with respect to the primary nature of the magnetizations. An important outcome of the studies of geomagnetic reversal records (Linssen, 1988) is that the observed maximum rate of geomagnetic field variation is high (0.2°/yr), and is approximately equal to the resolution given by the sample size and accumulation rate of those sediments (4-9 cm/kyr). Hence, actual geomagnetic changes may have been even more rapid.

The presently investigated Lower Pliocene reversal records were obtained from a sedimentary sequence on Corfu (Greece) which was deposited with an average accumulation rate of approximately 94 cm/kyr. Potentially, such rapidly accumulated sediments may provide a very high resolution record of the geomagnetic field variations. The detailed magnetostratigraphy of the sedimentary succession was successfully correlated to the polarity time scale. This makes it possible to compare the high sedimentation rate Corfu reversal records with the medium sedimentation rate reversal records investigated in Calabria. The Calabrian and Corfu sections are separated by only a moderate distance (700 km) and consequentially one expects the corresponding records to reflect the same regional characteristics of the geomagnetic field variations.

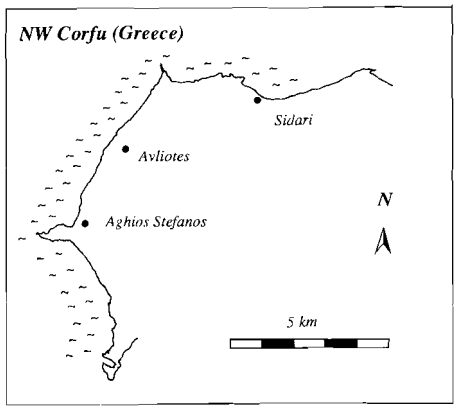

Fig. 1 Location of the investigated Lower Pliocene section in N.W.Corfu (Greece)

2. The Corfu coast section

The investigated succession of Lower Pliocene sediments is well exposed in a 10 km cliff section on the NW coast of the island of Corfu (19°6'E, 39°7'N; see figs. 1 and 2). The bedding plane of the sediment shows a small and uniform tilt (4° NEE). The length of the complete section is almost 10 km. The section starts at the Miocene/Pliocene boundary near the village of Aghios Stefanos and stretches to NE, stratigraphically upwards, to the village of Sidari. The stratigraphic thickness of the sedimentary succession is 500 m. At the base of the section, some 30-40 m of sediment directly overlying the Miocene/Pliocene boundary is not exposed.

The magnetostratigraphic investigations of the Corfu section revealed the presence of 5 polarity zones (fig. 3). A biostratigraphic investigation showed that all sediment samples contain *Globorotalia margaritae* and no *Globorotalia puncticulata* and situates the investigated part of the section in the *Margaritae* zone (Spaak, 1983). The combination of biostratigraphic and the magnetostratigraphic data (Cita, 1975,a,b; Zijderveld et al., 1986) demonstrate that the polarity zones in the Corfu section include the upper part of the Thvera, the complete Sidufjall and the lower part of the Nunivak subchrons from the Gilbert chron. In this paper, the detailed records of the two lowermost reversals from the Corfu section are presented, i.e. the upper Thvera (N-R) reversal record exposed near the

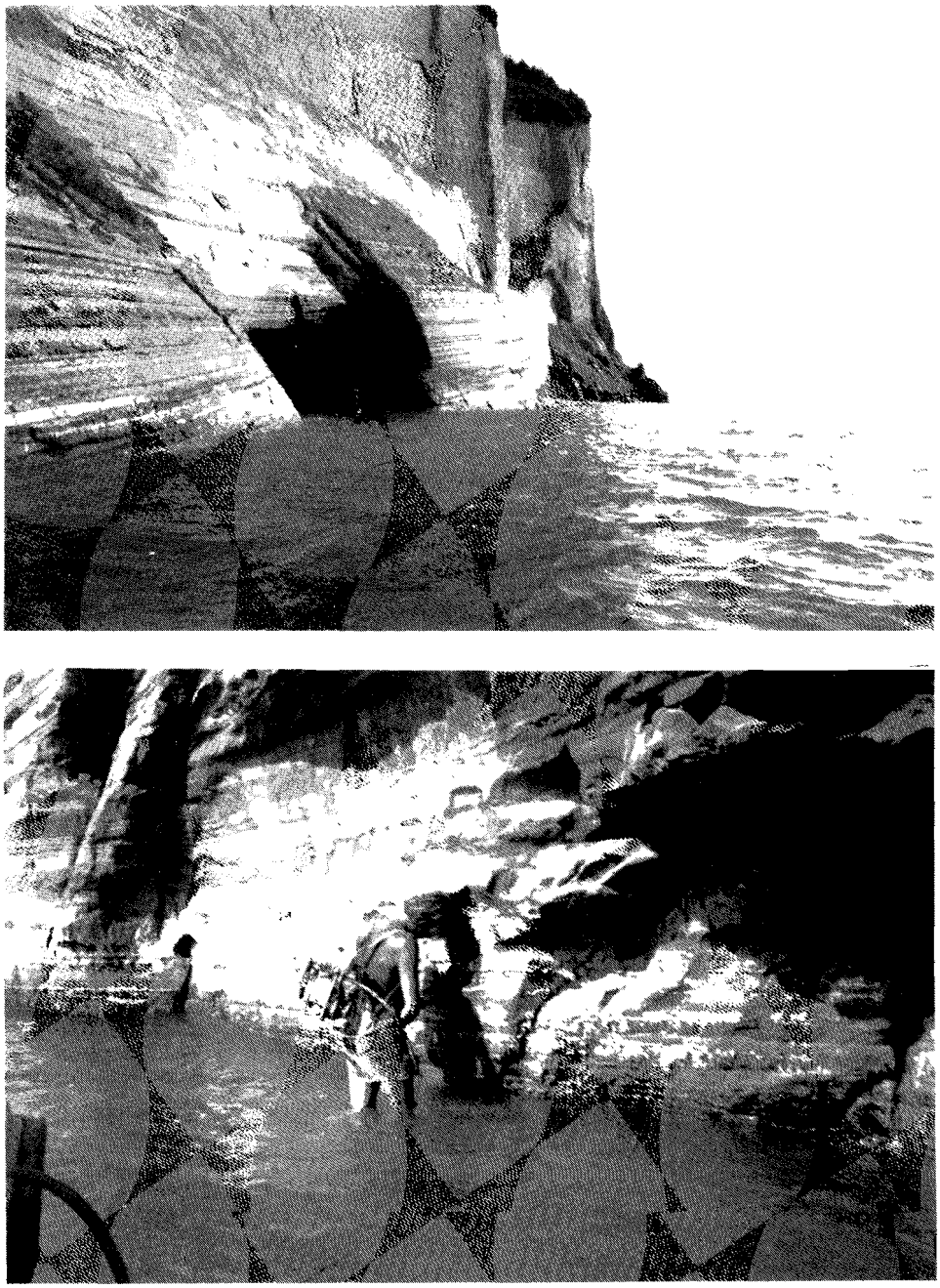

Fig. 2 Pictures of the Corfu section near Avliotes.

village of Aghios Stefanos and the lower Sidufjall (R-N) reversal record exposed near the village of Avliotes (fig. 1).

The lithology of the Corfu section shows an alternation of marine clays and sands (fig. 4, table 1). The sand layers are turbidites, many of which are fully developed. The thickness of both the sand and clay layers ranges from 0.5 to 120 cm. On average, 70% of the Corfu coast section consists of clay. Towards the top of the section an overall increase of the sand content is observed.

The average accumulation rate calculated for the complete sedimentary succession of clay and sand units is 94 cm/kyr. If we assume that the turbidites were deposited in little or no time, the average accumulation rate of the clays may be calculated and is in the range 56-69 cm/kyr (table 1).

Table 1. Accumulation rates for Pliocene Corfu section

Section (reversal)	Age (Ma)	Clay layers (%)	Acc. rate in cm/kyr	
			Sand + Clay	Clay
Aghios Stefanos (upper Thvera)	4.57	73	94	69
Avliotes (lower Sidufjall)	4.47	60	93	56

Table 1. Ages of the reversals (according to Berggren et al., 1985), average clay content of the reversal records and accumulation rates of the sediment. The accumulation rates are calculated both for sand plus clay units and for clay units only. In the case of the lower Sidufjall reversal record the accumulation rates near the reversals are the average accumulation rates of the under- and overlying polarity zones. In the case of the upper Thvera reversal record the accumulation rate of the overlying polarity zone has been used (upper Thvera), since the underlying polarity zone is not fully recorded.

3. Sampling procedures and laboratory treatment

The cliff section was sampled from sea by use of a small vessel; the cliffs could not be approached from land. The sampling equipment consisted of a petrol-engine driven drilling machine or an electric drill powered by a generator. The brass drills, one inch in diameter, are water cooled. The sampling interval ranges from 10 cm (near the centre of

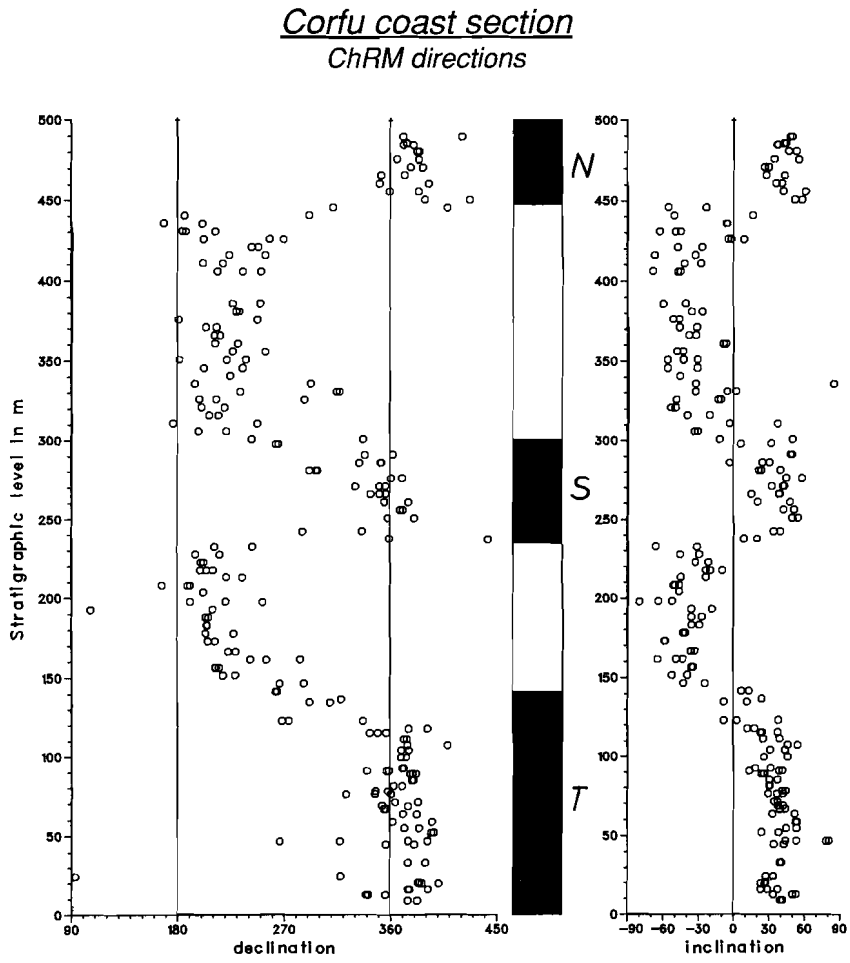

Fig. 3 Compilation of the magnetostratigraphic results of Corfu. From bottom to top: the normal polarity zones represent the (T)hvera, (S)idufjall and (N)univak subchrons.

the record), to 100 cm (at the edges of the record), providing a resolution of 100-1000 years. From each sampling level 3-5 cores were taken. The (vertical) exposure of the sedimentary sequence and the clear layering enabled an accurate determination of the stratigraphic position of the specimens.

The length of the upper Thvera record and the lower Sidufjall record (subtraction of the sand layer thickness has been applied) is respectively 30 and 15 m. Near the 6.5 m level in the lower Sidufjall record a normal fault is present with a vertical displacement of 3.5 m. Since the bedding tilt of the sediment is only 4° and the exposure of the record is along a cliff it was not possible to sample the complete record without traversing the fault.

Thermal demagnetizations were performed in tunnel furnaces with mu-metal shielding. The alternating field demagnetizations were applied to the specimens in stationary holders. The measurements of remanent magnetizations were performed with a 2-G Enterprises cryogenic magnetometer having a sensitivity of 10^{-11} Am^2 ; a small number of specimens were measured with a modified Jelinek spinner magnetometer having a sensitivity of 10^{-10} Am^2 . The reproducibility of both magnetometers is better than 1° for magnetizations exceeding 10^{-9} Am^2. Susceptibility and anisotropy measurements were performed with an AC bridge (KLY-1).

4. Demagnetization and rock magnetism

A change of the ChRM intensity may either be related to a change of the paleointensity, or to a change in the magneto-mineralogy. In order to determine the origin of ChRM intensity variations in the reversal record, some rockmagnetic parameters were measured.

The acquisition of the isothermal remanent magnetization (IRM) demonstrates that the Corfu specimens are almost saturated in a direct magnetic field of 0.3 T (fig. 5). The stepwise thermal demagnetization of the IRM (fig. 6) shows that the IRM is completely removed at 610-620 °C; slightly above the maximum blocking temperature of magnetite (T_B: 578 °C). Cation deficient (CD) magnetites (partly oxidized magnetites) have maximum blocking temperatures intermediate to those of magnetite and hematite (T_B: 680 °C) (e.g. Heider and Dunlop, 1986) and are common in marine sediments (e.g. chapter 4). The MDF and maximum blocking temperature suggest that CD magnetite is the carrier of the IRM.

The natural remanent magnetization of the Corfu specimens is comprised of a viscous and a characteristic remanent magnetization (fig. 7a). No secondary magnetization with the direction of the local present-day geomagnetic field has been observed. Viscous components are present in all specimens and are easily recognized because they show a direction directly related to the storage orientation of the specimens in the laboratory.

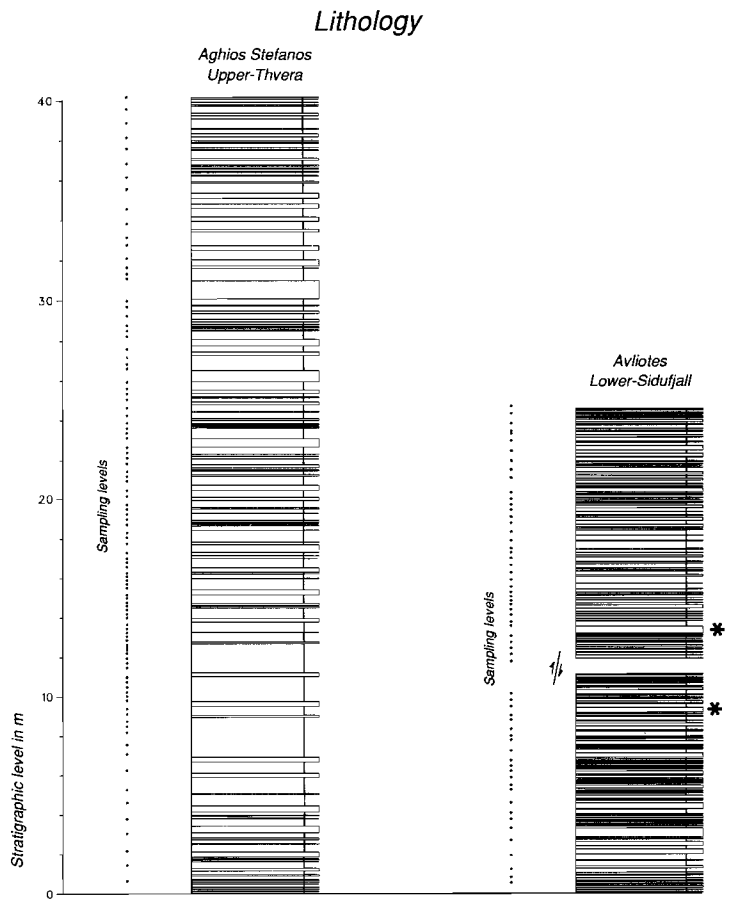

Fig. 4 Lithology of the Aghios Stefanos and Avliotes sections enclosing the upper Thvera and lower Sidufjall reversal records. The sandy layers are indurated relative to the clays. In the Avliotes section a normal fault is present; corresponding levels are labeled with an asterisk.

The intensities of the viscous and the characteristic remanent magnetizations (ChRM) are in the range 0.1-0.5 mA/m. The ChRM intensities are quite low compared to the marly clays from the Calabrian Trubi which have intensities of 2-10 mA/m (e.g. Linssen, 1988). The viscous component appears to be removed below 240 °C or 15 mT.

The ChRM is demagnetized at temperatures above 240 °C or with an alternating field

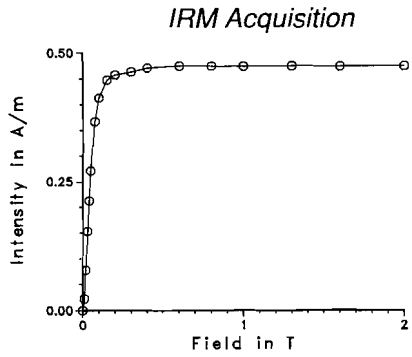

Fig. 5 IRM acquisition curve. The specimen from the upper Thvera record is saturated in low fields. The remanent coercive force of this specimen is 40.2 mT. These characteristics correspond to fine grained magnetite (e.g. Hartstra, 1982).

exceeding 15 mT. The maximum field required to completely demagnetize the NRM is approximately 100 mT. The majority of the thermal demagnetization results (~80%) become spurious above 350 °C. In spite of the presence of the viscous component and the spurious demagnetization results, the determination of the ChRM directions in the interval 240-350 °C is possible. The remainder of the specimens (~20%) produced spurious demagnetization results below 350 °C. These results were rejected (e.g. fig. 7a, specimen AS.004.3A).

The decay curves of the ChRM show a median destructive field (MDF) close to 30 mT which is characteristic for magnetite (fig. 7b). Although an accurate identification of magnetite by the assessment of the maximum blocking temperature (T_B) cannot be performed, the low MDF and the IRM demagnetization results suggest that magnetite is indeed the carrier of the ChRM.

In order to identify the spurious magnetization noticed during demagnetization of the NRM, the position of the specimens in the furnace was varied after each thermal demagnetization step. The results show a directional swing of the remanent magnetization after each heating step above 350 °C, corresponding to the variation of the sample position in the furnace. Hence, this spurious magnetization is a partial thermo-remanent magnetization (PTRM) and is acquired in the small magnetic field ambient in the furnace

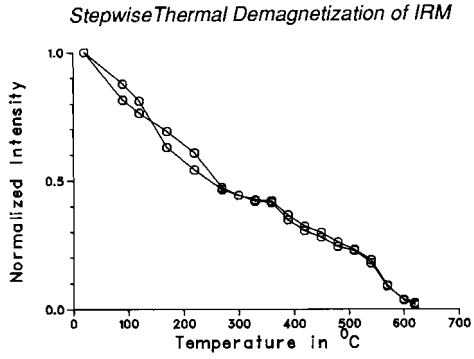

Fig. 6 Stepwise thermal demagnetization of IRM_{2T}. The maximum unblocking temperature is 610-620 °C (Heider and Dunlop, 1986), indicating that the IRM carrying mineral is cation-deficient magnetite.

(~10^{-8} T). Apparently, the carriers of the PTRM are produced during the heating procedure (see also Linssen, 1988). Thermal demagnetization of IRM does not give rise to spurious magnetizations. The ChRM intensities of the Corfu sediments are only 10-20% of the ChRM intensities of the Calabrian sediment, whereas the IRM intensities from Corfu are 50-100% of the IRM intensities from Calabria. If approximately the same amount of fine-grained magnetite is present in the Corfu sediment, as indicated by the IRM, but the ChRM intensity is much lower, it may be expected that the ChRM component of the Corfu sediment is more difficult to isolate from a viscous component.

The IRM (acquired in 2 T) in the upper Thvera and lower Sidufjall records are respectively in the ranges 0.2-0.6 A/m (fig. 10) and 0.4-0.8 A/m (fig. 11). The IRM minima are related to H_{CR} minima and ARM maxima, although the intensities of H_{CR} and ARM variations are less compared to the IRM variations (fig. 10). The inverse relation between variations in IRM and H_{CR} on the one hand and ARM on the other, exclude that the observed rock magnetic variations are caused by mere concentration changes. Rather, it is concluded that a grain size increase of magnetite causes the H_{CR} and IRM decrease (Hartstra, 1983).

The use of the susceptibility as an indicator of rock magnetic variations is very limited regarding the high clay mineral content of the samples and the moderate susceptibility values (table 2, fig. 10; chapter 4). The effect of the clay mineral

susceptibility is illustrated by the anisotropy which, because of the platy texture of the clay minerals, is biased towards a foliation more or less parallel to the bedding plane (table 2; fig. 8). Magnetic minerals are expected to produce a linear anisotropy. The susceptibility is not used as a rock magnetic parameter.

Table 2 Anisotropy of magnetic susceptibility

	N	X_i	L	F	P	P'	T
Aghios Stefanos	41	181.55	1.0028	1.0334	1.0363	1.0404	0.8415

Table 2. The magnetic susceptibility and the parameters of anisotropy for the sediment from the upper Thvera record. Listed are the number of specimens for which the anisotropy was determined (N), the average bulk susceptibility (X_i, the lineation (L), the foliation (F), the anisotropy degrees (P and P') and the T parameter (Jelinek, 1981; Hrouda, 1981). For at least one specimen from each stratigraphic level of the upper Thvera record the anisotropy of magnetic susceptibility has been determined. The low values of P and P' (related to the anisotropy degree) and T (characterizing the shape of the susceptibility ellipsoid) indicate only a modest anisotropy.

5. Non-transitional field

The average ChRM inclination values (40°) for the Corfu coast section are considerably lower than the geocentric axial dipole field inclination in Corfu (57°) (table 3). This inclination error is ascribed to electrostatic interactions between the platy clay-minerals and the ChRM carrying minerals during and shortly after deposition (e.g. Anson and Kodama, 1987). Hence, the presence of an inclination error indicates that the ChRM is a primary component. The inclination error has been corrected by

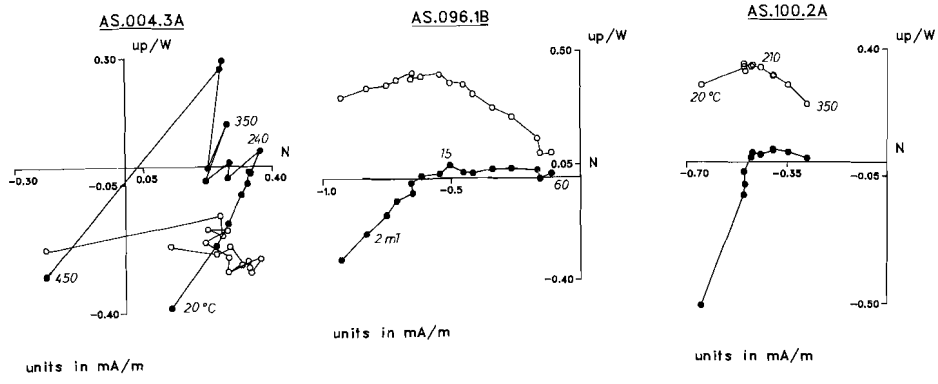

Fig. 7 a) Some representative thermal (AS.004.3A and AS.100.2A) and alternating field (AS.096.1B) demagnetization diagrams (Zijderveld, 1967).The closed (open) symbols denote the projections on the horizontal (vertical) plane.

tan I_o = f . tan I_f, in which I_o and I_f are respectively the observed inclination and the expected local axial geocentric dipole field inclination and f is the correction factor (King, 1955; Verosub, 1977; Blow and Hamilton, 1978; Anson and Kodama, 1987). For this sediment we arrive at f = 0.52 which is identical to the correction factor found for the Calabrian sediments.

The average ChRM declinations for the Corfu coast section (table 3) deviate from north/south directions. Apparently, the sedimentary succession rotated on average 16° clockwise after its deposition, which corresponds to earlier results (19.4°; Laj et al., 1982).

Table 3

	N	Decl.	Incl.	a_{95}
Corfu section				
Normal	69	8.5	40.0	4.4
Reversed	25	203.0	-41.0	9.2
Upper Thvera				
Normal	20	14.6	43.3	8.7
Reversed	28	191.9	-37.0	4.3

Table 3. Average ChRM declination and inclination values for the complete Corfu coast section and for the stable normal and reversed intervals preceding and following the upper Thvera reversal record. Statistics according to Fisher (1957).

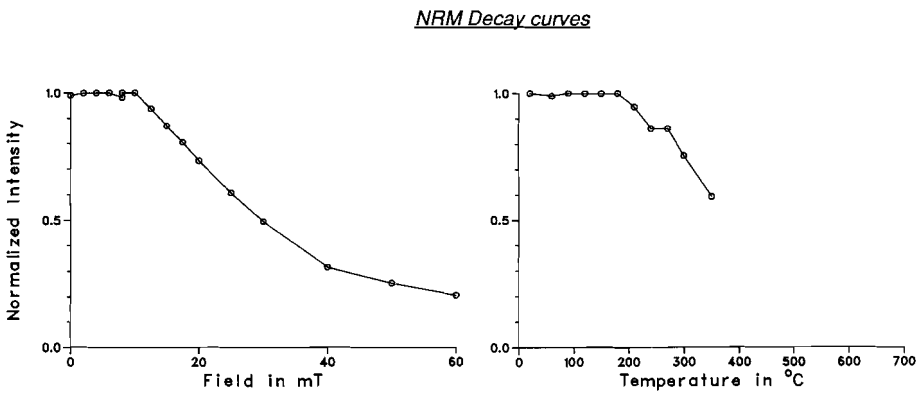

Fig. 7 b) normalized decay curves (AS.096.1B and AS.100.2A) of the ChRM.

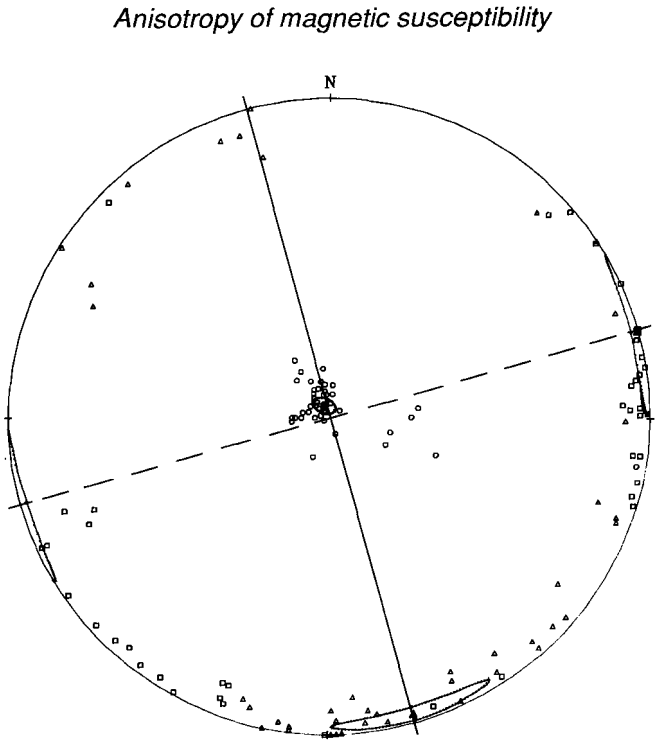

Fig. 8 Lambert equal area projections of the principal axes of magnetic susceptibility for specimens from the upper Thvera reversal record after correction for the bedding tilt. Triangles denote K_{max}, squares denote K_{int} and circles denote K_{min} of the individual specimens. Large (closed) symbols denote the principal axes of the mean susceptibility ellipsoid and ellipses denote the angles of confidence (according to Jelinek, 1978). The solid line represents the average K_{max} axis, the dashed line represents the average K_{int} axis. The anisotropy is characterized by foliation ($F=K_{int}/K_{min}$) rather than lineation ($L=K_{max}/K_{int}$). The K_{min} axis is almost perpendicular to the bedding plane. The results suggest that the anisotropy is dominated by the clay minerals.

6. Reversal records

6.1 The upper Thvera reversal record

The Aghios Stefanos section enclosing the upper Thvera N-R reversal record comprises 30 m of clay units. The intercalated sand layers have been discarded (see section 2). The record of directions and intensities of the ChRM shows an intensity low

between the 5 and the 25 m levels (fig. 10). The pre- and post reversal ChRM intensities are similar. The minimum intensity is near the 10 m level and is almost 5% of the maximum intensity. A correction of the ChRM intensity for the IRM_{2T} variation smoothes the ChRM variations somewhat, although a 20% minimum in the ChRM/IRM, with respect to the pre- and post-reversal values, remains present.

The directional changes of the ChRM are relatively smooth in the lower (0-9 m) and upper (15-30 m) intervals of the reversal records. In the interval in which the actual reversal occurs (9-15 m), a number of rapid changes take place, especially in the declination record. Most of the variations occurring in the declination record are not well defined due to scatter.

The reversal record starts with normal directed declinations and inclinations. In the 0-6.5 m interval the declination changes first in an anti-clockwise sense and subsequently in a clockwise sense (A in fig. 10). In the same interval the inclination smoothly shallows from 45 to 20° and steepens again to 70° (B). In the same interval the declination changes 90° (clockwise) and back (anti-clockwise) again. From the 6.5 m level to the 7.5 m level (C in fig. 10) the inclination decreases from values near 90° to 10° and towards the 9 m level (D) increases again with the same angle. In this interval the declination changes 100° clockwise. Between the 9 m level (D) and the 11.5 m level (G) the inclination first shallows (level 10.5 m, E) and subsequently steepens. In this interval the inclinations reach negative values ranging from -20 to -70°. The declinations change 180° clockwise, 180° anti-clockwise and 270°clockwise in this interval. Above the 11.5 m level the inclination and the declination, although some initial anomalous values are included, change smoothly to stable reversed polarity.

The two rapid eastward changes of the declination approximately at the 9 and 11.5 m levels correspond to low ChRM and IRM intensities. Furthermore, the complete record shows that the declinations in the low intensity intervals are deflected towards east. This deflection corresponds to the direction of the viscous component (eastward and shallow directed). Due to the sampling and storage orientations the viscous magnetizations have a dominant horizontal component: the cores were drilled horizontally and in a predominantly eastward direction. During the vertical storage of the cylindrical specimens in the laboratory (field inclination 67°) the specimens acquired a viscous component with a dominating SE horizontal direction (see fig. 5a). The ChRM directions from specimens with transitional directions but low ChRM intensities are therefore biased to SE. It may be

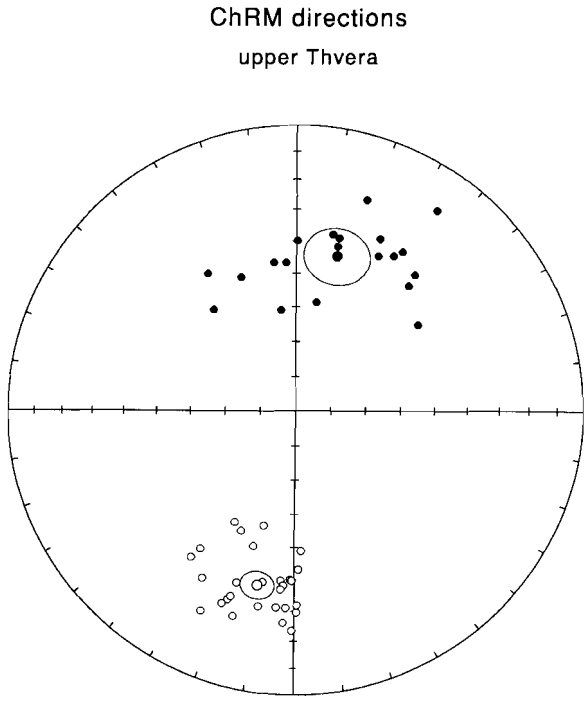

Fig. 9 Equal area projection of the pre- and post-reversal ChRM directions of the upper Thvera reversal record. Solid (open) symbols represent projections on the lower (upper) hemisphere. Circles of confidence on the 95% level (Fisher, 1957) are indicated. The ChRM directions reflect a 16° rotation of the sedimentary succession and an inclination error with respect to the local axial dipole field (57°).

concluded that the viscous component is not completely demagnetized at 240°C. Due to the storage orientation of the specimens, the effect of the viscous component on the inclination is somewhat less important, although a deflection to zero inclination values at low ChRM intensities is present.

It is concluded that the declination record is not very reliable in the low ChRM intensity intervals. Only at a limited number of levels near the centre of the reversal the intensity is high and reliable declination values are produced, for instance near the level marked F.

6.2 The lower Sidufjall reversal record

The lower Sidufjall R-N reversal record (fig. 11) contains clay layers up to a total thickness of 15 m. The record includes a normal fault at the 6.5 m level with a displacement of 3.5 m. The ChRM intensity record shows a wide and diffuse minimum, the centre of which cannot be accurately determined. The minimum intensities of the ChRM are 10-15% of the maximum intensities and no relation with the (small) IRM variations is observed.

The analysis of this record is complicated by the presence of the normal fault. Both the interval of the reversal record located below and the one located above the fault (respectively the interval 0-6.5 and 6.5-15 m) show non-consistent variations and many scattered values. The ChRM declinations and intensities seem to have been affected by the eastward directed and shallow viscous component.

The lower Sidufjall record shows a major inconsistency. Below the fault, in the 3 to 5 m interval, a declination change from reversed to normal polarity takes place, while also the inclination changes sign. Above the fault, the declination change seems to be present near the 8.5 m level. However, for the entire sedimentary interval above the fault the inclination shows only normal polarities. The record above the fault suggests an asynchronous reversal of declinations and inclinations which does not correspond with the synchronous reversal of declinations and inclinations below the fault. Moreover, the lower Sidufjall reversal record from Calabria does not show an asynchronous reversal of declinations and inclinations (Linssen, 1988). It is concluded that the interval above the fault is not reliable.The actual polarity change in the interval below the fault is best defined for the inclination record and seems to be completed in the interval 3-4 m.

7. Discussion

The upper Thvera reversal record from Calabria is characterized by a gradual steepening of the inclinations prior to a rapid inclination change. The declination change is gradual and anti-clockwise producing an almost perfectly constrained VGP trajectory along a great-circle 90°W of the site meridian. The record shows several directional oscillations before and after the actual reversal; the corresponding VGP's are located along the same great-circle 90°W of the site. The actual reversal of the geomagnetic field

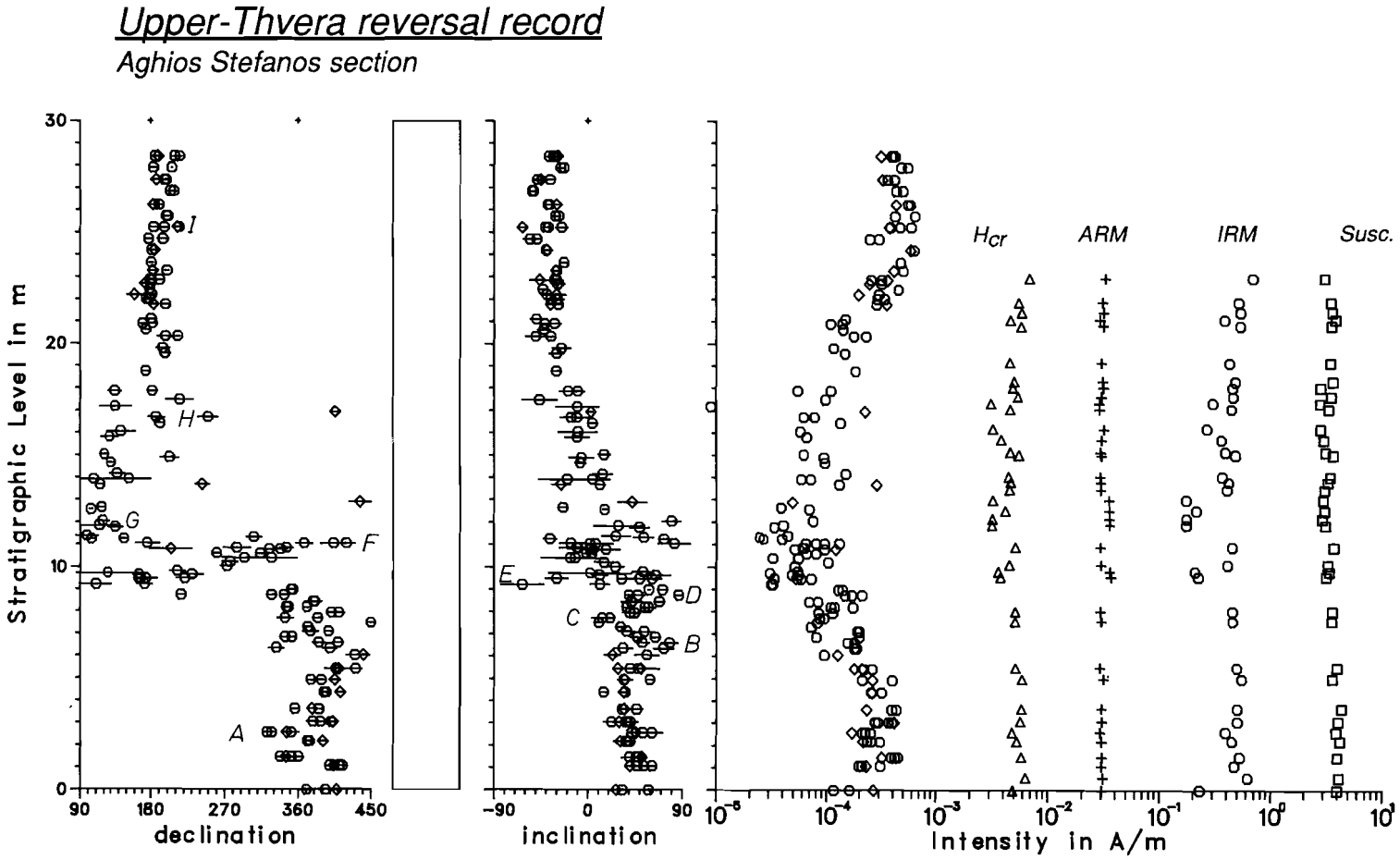
Upper-Thvera reversal record
Aghios Stefanos section
Stratigraphic Level in m
30
20
10
0
90
180
270
360
450
declination
-90
0
90
inclination
10⁻⁵
10⁻⁴
10⁻³
10⁻²
10⁻¹
10⁰
10¹
Intensity in A/m
Hcr
ARM
IRM
Susc.
A
B
C
D
E
F
G
H
I

direction takes place in a few kyr (1-3), whereas anomalous directions were recorded during 17 kyr. The duration of the intensity low is 26 kyr, which is long compared to the duration of the actual reversal.

Due to the bias by the viscous component, the Corfu record does not show the details found in the Calabrian upper Thvera reversal record. However, a few details could be accurately determined. In Corfu, the stratigraphic thickness of the interval in which an intensity low occurs is 19 m, corresponding to a time interval of 27.5 kyr (accumulation rate is 69 cm/kyr), and is similar to the duration of the intensity low of the Calabrian upper Thvera reversal record (26 kyr).

The Corfu inclination record shows some major pre-reversal oscillations (B,C,D; fig. 10) with a near constant period of 4 kyr, whereas in the corresponding part of the Calabrian record only anomalous inclination values are recorded with a duration of 10 kyr, preceded and followed by two rapid (~1 kyr) oscillations. Apparently, the Corfu and Calabrian records are different. This could imply that major differences between reversal records located at moderate distances may exist. However, the distance between the two records is only 700 km, which is small compared to the distance between the sites and the geomagnetic field source. Two alternative explanations provide a more plausible origin. The remagnetizations which possibly occurred in certain intervals of the Calabrian records may have caused the observed differences. Alternatively, it is possible that either the Calabrian or the Corfu sediments, in the interval where the pre-reversal oscillations occur, have accumulation rates which deviate from the average values. The reported average accumulation rates for the Corfu and Calabrian records are probably correct since the durations of the main intensity minima observed in the reversal records correspond.

The quality of the lower Sidufjall reversal record is largely affected by the presence of a normal fault and the viscous component. In spite of the low quality of most aspects of this reversal record, it was established that the inclination change occurs in a sedimentary interval of about 1 m, corresponding to a duration of 1.8 kyr (accumulation rate 56 cm/ kyr). The major inclination change in the Calabrian record is in the range 1.3-1.9 kyr which

Fig. 10 Record of the upper Thvera (N-R) reversal at the Aghios Stefanos section. Sand layers have been excluded from the stratigraphy. Circles (diamonds) denote the thermal (alternating field) demagnetization results. Error bars represent the maximum angular deviation (Kirschvink, 1980). ARM was acquired in a DC field of 0.036 mT and an AC field of 150 mT; IRM was acquired in a 2 T field. Susceptibilities are in 10^{-4} (SI). Index characters (A-I) refer to characteristic directions labeled in the VGP projections (fig. 12).

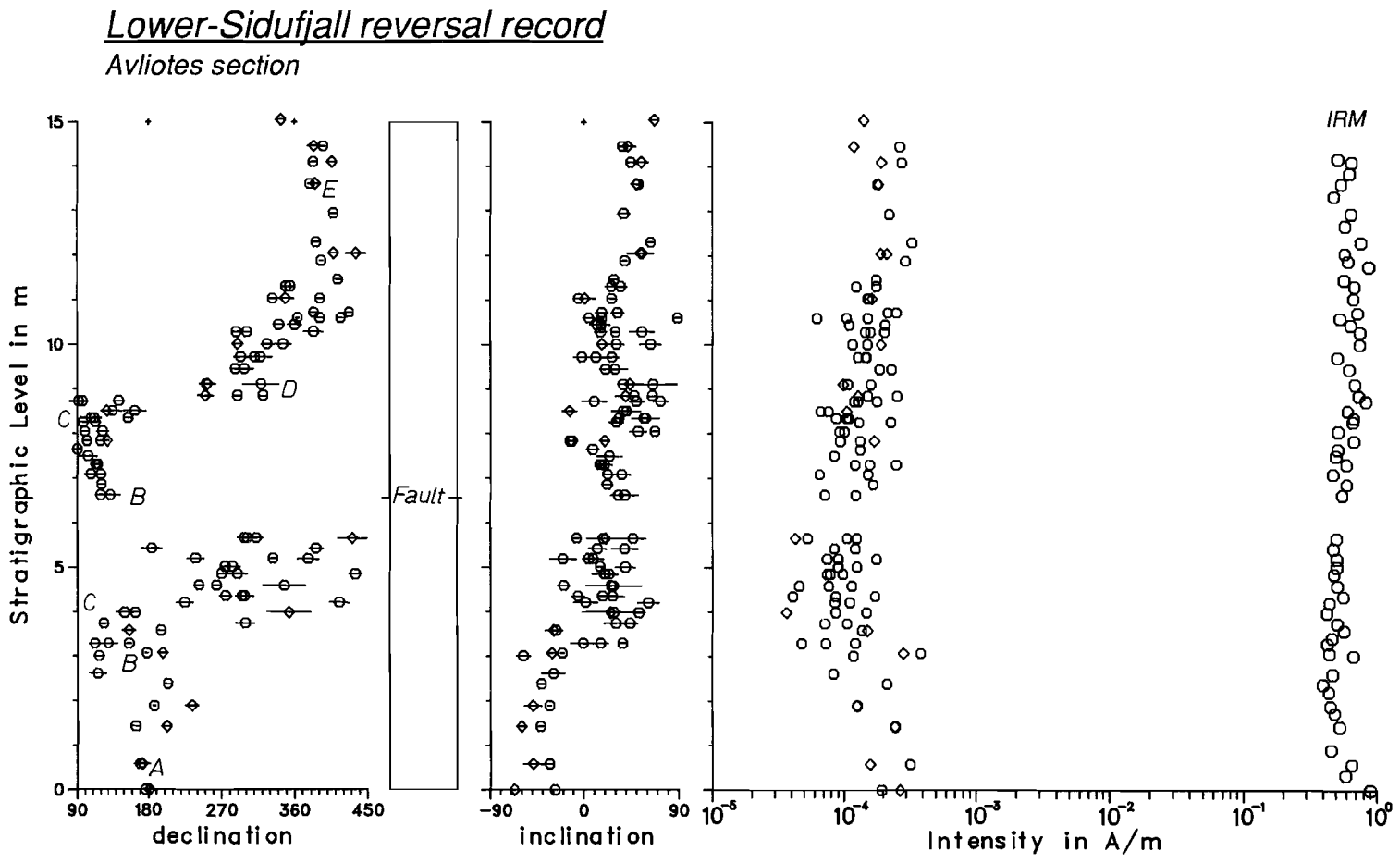
Lower-Sidufjall reversal record
Avliotes section
Stratigraphic Level in m
15
10
5
0
90
180
270
360
450
declination
E
D
C
B
C
B
A
Fault
-90
0
90
inclination
IRM
10^{-5}
10^{-4}
10^{-3}
10^{-2}
10^{-1}
10^{0}
Intensity in A/m

is in close correspondence.

8. Conclusions

The upper Thvera and the lower Sidufjall reversal records have been obtained from a rapidly accumulated marine sedimentary succession located in Corfu. The NRM of the clay sediment is comprised of a viscous component and a ChRM component which has a near-primary origin. The ChRM component is carried by magnetite. The ChRM records of both reversals are affected by the presence of the viscous component. Especially in the intervals with low intensities, the viscous component cannot be completely isolated from the ChRM component . Since the viscous component is shallow, the biasing effect of this component is predominantly present in the declination records and less in the inclination records.

The Calabrian upper Thvera reversal record (26 kyr; Linssen, 1988) and the corresponding Corfu record (27.5 kyr) show a close correspondence between the calculated duration of the intensity low. This seems to confirm the observed long period of low intensities in the upper Thvera reversal (Linssen, 1988). In spite of their proximity (700 km), the upper Thvera reversal record from Calabria (Linssen, 1988) and Corfu show some clear differences. The record from Corfu shows multiple oscillations with a period of 4 kyr, whereas the oscillations in the Calabrian record appear to have different periods (1 kyr and 10 kyr). Rather than indicating that large regional differences occur for the same reversal, this feature indicates that uncertainties exist in the influence of the viscous component on the ChRM and in the assessment of small scale accumulation rate variations in either the Corfu or the Calabrian upper Thvera sediment. Alternatively, the occurrences of small scale remagnetizations in the Calabrian records may account for the observed differences.

A more general conclusion is that the rapidly accumulated Corfu sediments have not revealed more detailed directional or intensity variations than the Calabrian records. Unfortunately, many other detailed characteristics in the Calabrian reversal records were not found in the Corfu records. In this respect it appears that the Calabrian Trubi sediment is a more accurate recorder of the field variations during geomagnetic reversals.

Fig. 11 Record of the lower Sidufjall (R-N) reversal at the Avliotes section. See also caption to fig. 10.

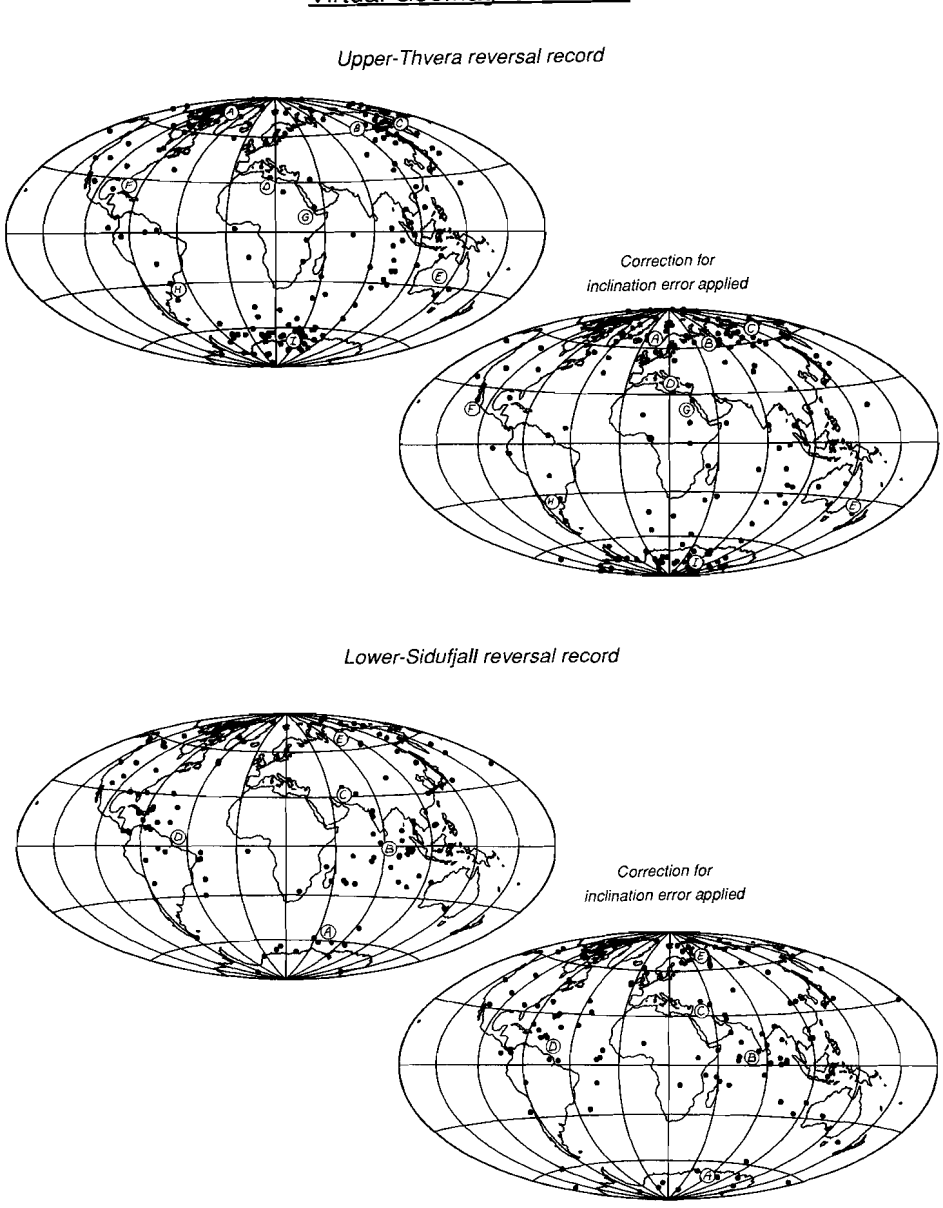

Fig. 12 Aitoff projection of the Earth centred around the site meridian with virtual geomagnetic pole positions of the upper Thvera and the lower Sidufjall ChRM directions both before and after the correction for the inclination error (f=0.52). The index characters refer to characteristic directions in figures 10 and 11.

Acknowledgments

H.J. Meier is thanked for his assistance in the laboratory. T.A.T. Mullender and H.K. Thio are thanked for their assistance during collection of the samples. Prof.Dr. J.D.A. Zijderveld and Dr. C.G. Langereis are thanked for critically reading the manuscript. The investigations were supported by the Netherlands Foundation for Earth Science Research (AWON) with financial aid from the Netherlands Organization for Scientific Research (Z.W.O., now N.W.O.).

Chapter VII

Conclusions

Eight lower Pliocene reversals recorded in Mediterranean marine sedimentary sequences with an established magnetostratigraphy have been investigated in detail. The records are situated in the Calabrian Monte Singa section (Trubi formation), the Sicilian Punta Piccola section (Trubi and Monte Narbone formations) and in the lower Pliocene of Corfu. All records are continuous, provide an accurate time control and have a reasonably high resolution.

The natural remanent magnetization (NRM) of the Trubi sediments from Calabria contains several components. The original remanent magnetization is carried by single domain pyrrhotite and (pseudo) single domain cation deficient magnetite. In addition, the NRM contains a secondary component with the direction of the present-day field and a viscous component acquired during storage in the laboratory. The remanences of pyrrhotite and magnetite could be isolated by means of thermal demagnetization. Alternating field demagnetization was not successful in separating the remanence of pyrrhotite and magnetite due to their overlapping coercive force spectra and the erratical response of pyrrhotite to alternating fields. The directions and intensities of the original remanent magnetizations were determined from specific segments in the blocking temperature spectrum, corresponding to the low-temperature (210-360 °C) pyrrhotite component, an indeterminate medium-temperature component and a high-temperature (480-620 °C) magnetite component. The more indurated sediments from the Punta Piccola section have a similar rockmagnetic content, although here thermal demagnetization was not successful in separating the pyrrhotite component from the secondary components. The original remanent magnetizations reflect the Pliocene rotations of Sicily and Calabria and furthermore demonstrate the presence of an inclination error introduced in the early stages of compaction of the sediment.

Conclusions

Remanent magnetic pyrrhotite is most abundant in the units with lowest carbonate content, whereas remanent magnetic magnetite is somewhat more abundant in the units with highest carbonate content. The pyrrhotite and magnetite of the Italian sections have been formed authigenically and must have acquired their remanence after deposition but before compaction. A delay between the pyrrhotite and magnetite components in the investigated samples is most probably limited to less than 1000 years, as may be seen in e.g. the lower Sidufjall reversal record. The pyrrhotite component shows somewhat more rapid variations in remanence than the magnetite component which suggests that the record of the pyrrhotite component is less smoothed during the remanence acquisition process. The original remanent magnetization of the Corfu sediments is carried by fine-grained magnetite. This remanent magnetization could not completely be isolated from the large viscous component and, in addition, shows spurious thermal demagnetization results above 400-450 °C. A small overlap of the secondary field component and the original remanence appears to be present in the Italian sediments as well. A large secondary component cannot be separated from the original remanence in the intervals in which the intensity of the original remanence is low. Low intensities typically occur in the centre of the polarity transitions. The effect is an apparent shift of the reversal to older or younger ages, depending on the sense of the polarity reversal (e.g. upper Nunivak). In general, results close to lithological boundaries were less reliable and of limited value for the interpretation of the reversal process. For instance, recent remagnetizations - with a present-day field direction - occur frequently at these levels (e.g. upper Sidufjall). Reversed remanent magnetizations occurring at lithological boundaries in an interval of normal polarity, such as in the upper Thvera record, indicate early remagnetizations or delayed magnetizations.

The continuity of the remanence acquisition process in time and the length of the lock-in interval largely determine whether the records accurately reflect the geomagnetic field variations. Apart from the early remagnetizations observed at lithological boundaries, the present results indicate a continuous remanence acquisition. However, recent investigations of other records in similar sediments suggest some evidence to the contrary (van Hoof and Langereis, submitted). Although the records are undoubtly of high quality, the question to which extent the present reversal records represent the actual geomagnetic variations could not be entirely and unequivocally solved. The interpretation of the records therefore partly relies on the assumption that the remanence acquisition process is continuous.

Conclusions

The lock-in interval acts as a filter on the rapid geomagnetic variations. The degree of smoothing may be estimated from the maximum rates of remanence variations. For instance, the lower Kaena reversal record shows a rapid R-N-R excursion, while the rock-magnetic parameters in the same interval show no variations of the magnetic properties. Independent observations confirm the existence of the excursion (Roperch & Duncan, 1990). It is unlikely that the observed variations are produced by early or late remagnetization processes. The observed rapid variations suggest that the geomagnetic field during the reversals changed by approximately 0.2°/yr and 5% of the initial intensity per year.

The subsequent reversals do not show a clear time-independent behaviour, as might be expected if a reversal would always proceed in an identical manner. However, several common characteristics have been observed in the reversal records. The least complicated lower Sidufjall and lower Nunivak reversal records are very similar to those of the youngest reversal (Matuyama-Brunhes, MB) from approximately the same latitude and suggest an axi-symmetrical (zonal) reversing field. A phenomenological model which described such zonal reversals was developed by Williams and Fuller (1978). However, subsequent modifications of this model were necessary when southern hemisphere records became available. In the present study a further generalization of these models is discussed in which it is assumed that the dipole energy during a reversal largely dissipates in non-magnetic energy or high-order field components. The transfer of only 2-4% of the original dipole field energy to low-order quadrupole or octupole components reproduces zonal reversal characteristics as found in both northern and southern hemisphere records.

The investigated records indicate that a reversal is initiated by a gradual decrease of the intensity and moderate directional variations which become increasingly intensified towards the centre of the reversal. Furthermore, an important result is that the interval of transitional directions and intensities in the Pliocene reversal records corresponds to a much shorter duration (0.2-4 kyr) than has been found in older and younger records (3-30 kyr). The intensity minimum coincides with the level at which the actual reversal occurs and is approximately 10% of the non-transitional field intensity. In the case of the upper Sidufjall reversal, the recorded field is anomalously steep during a 5-10 kyr period prior to the actual N-R reversal. The characteristics of the upper Sidufjall record agrees well with the stop-and-go movements observed in the well known Steens Mountain extrusive

reversal records.

The only reversal record with a very long total duration is the upper Thvera record: this reversal is completed in approximately 26 kyr. This long duration of the upper Thvera reversal is substantiated by independent records from Corfu and from Calabria. However, the directional variations observed in the records from Corfu and the Monte Singa do not agree in detail. A close correspondence might have been expected regarding the proximity of the sample locations. The observed differences are attributed to the difficulty in separating viscous components from the original remanence in the Corfu samples.

References

Anson, G.L., Kodama, K.P. (1987) Compaction-induced inclination shallowing of the post-depositional remanent magnetization in a synthetic sediment, Geophys.J.R.astr.Soc. 88:673-692 (1987)

Arason, P. Levi, S. (1986) Inclination shallowing recorded in some deep sea sediments, EOS 67:916.

Argyle, K.S., Dunlop, D.J. (1990) Low-temperature and high-temperature hysteresis of small multidomain magnetites (215-540 nm). J.Geophys.Res., 95:7069-7083.

Banerjee, S.K. (1971) New grain size limits for Paleomagnetic stability in Hematite, Nature Phys.Sci., 232:15-16.

Banerjee, S.K. King, J., Marvin, J. (1981) A rapid method for magnetic granulometry with applications to environmental studies, Geophys.Res.Lett., 8:333-336.

Bando, Y., Kiyama, M., Yamamoto, N., Shinjo, T., Takaki, H. (1965) The magnetic properties of alfa-Fe2O3 fine particles, J.Phys.Soc. Japan, 20:2086.

Bennett, C.E.G., Graham, J., Thornber, M.R. (1972) New observations on natural pyrrhotite Part 1:Mineragraphic techniques. Am.Min. 57:445-461.

Bennett, C.E.G., Graham, J. (1980) New observations on natural pyrrhotite. Part III. Thermomagnetic experiments., Am.Min., 65:800-807.

Berggren, W.A., Kent, D.V., Flynn, J.J., Van Couvering, J.A. (1985) Cenozoic geochronology, J.Geol.Soc.Am.Bull., 96:1407-1418.

Berner, R.A. (1984) Sedimentary pyrite formation: An update. Geochem.Cosmochem.Acta 48:605-615.

Blakemore, R. (1975) Magnetotactic bacteria. Science, 190:377-379.

Blow, R.A., Hamilton, N. (1978) Effect of compaction on the acquisition of detrtal remanent magnetizatiomn in fine-grained sediments. Geophys.J., 52:13-23.

Bloxham, J. (1986) The determination of fluid flow at the core surface from geomagnetic observations, Math. Geophys. Conf. Book 1-17

Bloxham, J. Gubbins, D. (1987) Thermal core-mantel interactions, Nature, 325:511-513.

Bogue, S.W. and Coe, R.S. (1982). Successive paleomagnetic reversal records from Kauai. Nature, 295:399-401.

Bogue, S.W. and Coe, R.S. (1984). Transitional paleointensities from Kauai, Hawaii, and geomagnetic reversal models. J.Geophys.Res., 89:10341-10354.

Bogue, S.W. and Hoffman, K.A. (1987). U.S. National report to International Union of Geodesy and Geophysics 1983-1986: Morphology of geomagnetic reversals. Rev.Geophys., 25:910-916.

Brolsma, M.J. (1978) Quantitative foraminiferal analysis and environmental interpretatio of the Pliocene and topmost Miocene on the south coast of Sicily. Utrecht Micropal.Bull., 18:1-159.

Brunhes, B. (1906) Récherces sur la direction d'aimantation des roches volcaniques. J.Phys., 5:705-724.

Bucur, I. (1978) Experimental study of the origin and properties of the defect moment in single domain hematite., Geophys.J.R.astr.Soc., 55:589-604.

Celaya, M.A., Clement, B.M. (1988) Inclination shallowing in deep sea sediment from the North Atlantic, Geophys.Res.Lett., 15:52-55.

Chang, S.R., Kirschvink, J.L. (1985). Possible biogenic magnetite fossils from the Miocene marine clay of Crete. In: J.L.Kirschvink, D.S.Jones and B.J.McFadden (eds.), Magnetite biomineralization and magnetoreception in organisms. Plenum Press, New York,pp.647-669.

Chikazumi, S. (1976) Current understanding of low-temperature phase transition of magnetite, particularly in relation to the behavior of magnetocrystalline anisotropy, AIP Conf. Proc. 21st Annual Conference on Magnetism and Magnetic Materials. 29:382-387.

Cita, M.B. (1973). The Miocen-Pliocene boundary: history and definition. In: T.Saiko and L.H.Burckle (eds.), Late Neogene Epoch boundaries. Micropal., Spec.Publ., 1:1-30.

Cita, M.B., Gartner, S. (1973) Studi sul Pliocene e sugli strati di passagio dal Miocene al Pliocene, IV.-The stratotype Zanclean foraminiferal and nannofossil biostratigraphy. Riv.Ital.Paleont.Stratigr., 79:503-558.

Clark, D.A. (1984) Hysteresis properties of sized dispersed monoclinic pyrrhotite grains. Geophys.Res.Lett. 11:173-176.

Clement, B.M., Kent, D.V. (1984). A detailed record of the lower Jaramillo polarity transition from a southern hemisphere deep-sea sediment core. J.Geophys.Res., 89:1049-1058.

Clement, B.M., Kent, D.V. (1985). A comparison of two sequential geomagnetic polarity transitions (upper-Olduvai and lower-Jaramillo) from the Southern Hemisphere. Phys.Earth Planet.Inter., 39:301-313.

Clement, B.M., Kent, D.V. (1986). Geomagnetic polarity transition records from five hydraulic piston core sites in the North Atlantic. In: Ruddiman, W.F., Kidd, R., Thomas, E. et al. (eds.), Init.Repts.DSDP, 94:831-852.

Clement, B.M., Kent, D.V. (1986/7) Short polarity intervals within the Matuyama: transitional field records from hydraulic cored sediments from the North Atlantic, Earth Planet.Sci.Lett., 81:253-264.

Clement, B.M. (1987) Paleomagnetic evidence of reversals resulting from helicity fluctuations in a turbulent core, J.Geophys.Res. 92:10629-10638.

Collinson, D.W. (1983) Methods in rock magnetism and paleomagnetism, Chapman and Hall, London, New York, 503 pp.

References

Constable, C.G., Parker, R.L. (1988) Statistics of the geomagnetic secular variation for the past 5m.y., J.Geophys.Res., 93:11569-11581.

Constable, C.G. (1990) A simple statistical model for geomagnetic reversals, J.Geophys.Res. 95:4587-4596.

Coupland, D.H., Voo, R.v.d. (1980) Long-term nondipole components in the geomagnetic field during the last 130 M.Y., J.Geophys.Res. 85:3529-3548.

Dankers, P.H.M. (1978) Magnetic properties of dispersed natural iron-oxides of known grain-size, Ph.D. thesis University of Utrecht, 142 pp.

Deer, W.A., Howie, R.A., Zussman J. (1977) An introduction to the rock-forming minerals, Longmans, London.

Dekkers, M.J. (1988) Magnetic properties of natural pyrrhotite part I: Behaviour of initial susceptibility and saturation magnetization related rockmagnetic parameters in a grain-size dependent framework. Phys.Earth Planet.Int. 52:376-393.

Dekkers, M.J. (1988) Some rockmagnetic parameters for natural geothite, pyrrhotite and fine grained hematite., (Ph.D. thesis University of Utrecht), Ultraiectina Geologica, 51:231 pp.

Dekkers, M.J., Linssen, J.H. (1988) Grain-size separation with the pipette centrifuge, ext.report, 20pp., University of Utrecht.

Dekkers, M.J., Linssen, J.H. (1991) Grain-size separation of haematite in the <5 micrometer range for rockmagnetic investigation., Geophys.J.Int., 104:423-427.

Dekkers, M.J. (1990) Magnetic monitoring of pyrrhotite alteration during thermal demagnetization. Geophys.Res.Lett., 17:779-782.

Dekkers, M.J., Linssen, J.H. (1989) Rock magnetic properties of fine-grained natural low-temperature hematite with referebce to remanence acquisition in red beds. Geophys.J.Int. 99:1-18.

Dodson, R., Dunn, J.R., Fuller, M., Williams, I., Ito, H., Schmidt, V.A., Wu, Y.M. (1978) Paleomagnetic record of a late Tertiary field reversal, Geophys.J.R.astr.Soc. 53:373-412.

Dunlop, D.J. (1971a) Magnetic properties of fine particle hematite, Ann.Geophys., 27:269-293.

Dunlop, D.J. (1971b) Hematite:Intrinsic and defect Ferromagnetism, Science 169:858-860.

Dunlop, D.J. (1972) Magnetic mineralogy of heated and unheated red sediments by coercivity spectrum analysis. Geophys.J.R.astr.Soc. 27:37-55.

Dunlop, D.J. (1981) The rock magnetism of fine particles, Phys.Earth Planet.Int., 26:1-26.

Dunlop, D.J. (1983) Viscous magnetization of 0.04-100 micrometer magnetite, Geophys.J.R.astr.Soc., 74:667-687.

Dunlop, D.J. (1986) Hysteresis properties of magnetite and their dependence on particle size: a test of pseudo-single-domain remanence models, J.Geophys.Res., 91:9569-9584.

Dunlop, D.J. (1987) Temperature dependence of hysteresis in 0.04-0.22 micrometer magnetite and implications for domain structure. Phys.Earth Planet.Int., 46:100-119.

Farina, M., Motta S.Esquivel, D., Lins de Barros, G.P. (1990) Magnetic iron-sulphur crystals from a magnetotactic microorganism. Nature, 343:256-343.

Fassbinder, J.W.E., Stanjek, H., Vali, H. (1990) Occurrence of magnetic bacteria in soil. Nature, 343:161-163.

McFadden, P.L., Merrill, R.T. (1986) Geodynamo energy source constraints from paleomagnetic data, Phys.Earth Planet.Int., 43:22-33.

Freeman, R. (1986). Magnetic mineralogy of pelegic limestones. Geophys.J.R.astr.Soc., 85:433-452.

Fuller, M., Williams, I., Hoffman, K.A. (1979) Paleomagnetic records of geomagnetic field reversals and the morphology of the transitional fields., Rev.Geophys., 17:179-203.

Fuller, M. (1987) A mechanism for reversals?, Nature 326:132-133.

Gardiner, R.B., Stacey, F.D. (1971) Electrical resistivity of the core., Phys.Earth Planet.Int. 4:406.

Graham, J., Bennett, C.E.G., van Riessen, A. (1987) Oxygen in pyrrhotite: 1. Thermomagnetic behavior and annealing of pyrrhotites containing small quantities of oxygen, Am.Min., 72:599-604.

Graham, J., McKenzie, C.D. (1987) Oxygen in pyrrhotite: 2. Determination of oxygen in natural pyrrhoites, Am.Min., 72:605-609.

Graham, J. (1987) Oxygen in pyrrhotite: 3. A mechanistic model, Am.Min., 72:610-611.

Grommé, C.S., Mankinen, E.A., Prévot, M., Coe, R.S. (1985) Steens Mountain geomagnetic polarity transition is a single phenomenon; Reply Valet, Laj and Tucholka, Nature, 318:487-488.

Gubbins, D., Roberts, N. (1983) Use of the frozen flux approximation in the interpretation of archeomagnetic and paleomagnetic data, Geophys.J.R.astr.Soc. 73:675-687.

Gubbins, D., Bloxham, J. (1987) Morphology of the geomagnetic field and implications for the geodynamo, Nature, 325:509-511.

Gubbins, D. (1987) Mechanism for geomagnetic polarity reversals, Nature 326:167-169.

Gubbins, D. (1988) Thermal core-mantle interactions and time-averaged paleomagnetic field., J.Geophys.Res., 93:3413-3420.

Haigh, G. (1957a) Observations on the magnetic transition in hematite at -15 °C, Phil.Mag., 2:877-890.

Haigh, G. (1957b) The effect of added Titanium and Aluminium on the magnetic behaviour of alfa Ferric oxide, Phil.Mag., 2:505-520.

Haggerty, S.E., Hargraves, R.B., Tompkins, L.A. (1990) Oxide mineralogy and magnetic properties of the Koidu kimberlite complex, Sierra Leone, west Africa, Geophys.J.Int 100:275-283.

Halgedahl, S.L., Fuller, M. (1981a) The dependence of magnetic domain structure upon magnetization state in polycrystalline pyrrhotite. Phys.Eath Planet.Int. 26:93-97.

Halgedahl, S.L., Fuller, M. (1981b) The dependence of magnetic domain structure upon magnetization state with emphasis upon nucleation as a mechanism for pseudo-single-domain behaviour, J.Geophys.Res.B 88:6505-6522.

Hall, A.J. (1986) Pyrite-pyrrhotine redox reactions in nature. Min.mag. 50:223-229.

Hamilton, E.C. (1959) Thickness and consolidation of deep-sea sediments. Bull.Geol.Soc.Am., 70:1399-1424.

Hartstra, R.L. (1982) Some rock magnetic parameters for natural Iron- Titanium oxides. Ph.D.Thesis, University of Utrecht, 145 pp.

Heider, F., Dunlop, D.J., Segiura, N. (1987) Magnetic properties of hydrothermally recrystallized magnetite crystals. Science 236:1287-1290.

Heller, F. (1978) Rockmagnetic studies of Upper-Jurassic limestones from Southern Germany. J.Geophys. 44:525-543.

Henshaw, P.C. Jr., Merill, R.T. (1980) Magnetic and chemical changes in marine sediments. Rev.Geophys.Space Phys., 18:483-504.

Herrero-Bervera, E. and Helsley, C.E. (1983). Paleomagnetism of a polarity transition in the lower(?) Triassic Chugwater Formation, Wyoming, J.Geophys.Res., 88:3506-3522.

Herrero-Bervera, E., Theyer, F. (1986). Non-axisymmetric behaviour of Olduvai and Jaramillo polarity transitions recorded in north-central Pacific deep-sea sediments. Nature, 322:159-162.

Herrero, E., Theyer, F., Helsley, C.E. (1987) Olduvai onset polarity transition:two detailed paleomagnetic records from North Central Pacific sediments, Phys. Earth Planet.Int., 49:325-342.

Hide, R. (1981) Self exciting dynamos and geomagnetic polarity changes, Nature 293:728-729.

Hilgen, F.J. (1987) Sedimentary rhythms and high-resolution chronostratigraphic correlations in the Mediterranean Pliocene. Newsl. Stratigr., 17:109-127.

Hilgen, F.J., Langereis, C.G. (1990) Periodicities of $CaCO_3$ cycles in the Pliocene of Sicily: discrepancies with the quasi-periods of the Earth's orbital cycles? Terra Nova, 1:409-415.

Hill, R. (1986) Chalk solution structures in cores from deep-sea drilling project Leg 94, in Init.Rpt. DSDP, 94:1129-1139.

Hillhouse, J. and Cox, A. (1976). Brunhes-Matuyama polarity transition. Earth and Planet.Sci.Lett., 29:51-64.

Hoffman, K.A. (1977). Polarity transition records and the geomagnetic dynamo. Science, 196:1329.

Hoffman, K.A. and Fuller, M. (1978). Transitional field configurations and geomagnetic reversal. Nature, 273: 715-718.

Hoffman, K.A.(1979). Behaviour of the geodynamo during reversal: A phenomenological model. Earth and Planet.Sci.Lettt.,44:7-17.

Hoffman, K.A. (1981a) Paleomagnetic excursions, aborted reversals and transitional fields, Nature, 294:67-69.

Hoffman, K.A. (1981b) Quantitative description of the geomagnetic field during the Matuyama-Brunhes polarity transition, Phys.Earth Planet.Int. 24:229-235.

Hoffman, K.A. (1983) Geomagnetic reversals and excursions: their paleomagnetic record and implications for the geodynamo, Rev.Geophys.Sp.Physics, 21:614-620.

Hoffman, K.A. (1984) A method for the display and analysis of transitional paleomagnetic data, J.Geophys.Res., 89:6285-6292.

Hoffman, K.A. and Slade, S.B. (1986). Polarity transition records and the acquisition of remanence: a cautionary note. Geophys.Res.Lett., 13:483-486.

Hoffman, K.A. (1986) Transitional field behaviour from Southern Hemisphere lavas: evidence for two stage reversals of the geodynamo, Nature 320:228-232.

Hoffman, K.A. (1988) Ancient geomagnetic reversals: Clues to the geodynamo, Sci.Am., 258(5):76-83.

Hoof, A.A.M.v., Langereis, C.G. (submitted) Delayed NRM acquisition of a magnetite component in two marine sedimentary reversal records.

Housen, B.A. and van der Pluijm B.A. (1990) Chlorite control of correlations between strain and anisotropy of magnetic susceptibility, Phys.Earth Planet.Int. 61:315-323.

Hrouda F. (1981) Magnetic anisotropy of rocks and its application in geology and geophysics. Geophysical Surveys, 5:37-82.

Jacobs, J.A. (1986) Magnetic reversals: From the core or the skies?, Nature,323:296-297.

Jelenska, M., Vincenz (1987) Origin of the magnetization of Permo-Carboniferous sediments of Spitsbergen, Svalbard Archipelago, Earth Planet.Sci.Lett., 85:173-182.

Jelinek, V. (1977) The statistical theory of measuring anisotropy of magnetic susceptibility of some igneous and metamorphic rocks. Geofyzika Brno.

Jelinek, V. (1978) Statistical processing of anisotropy of magnetic susceptibility on groups of specimens. Studia geophys. geod., 22:50-62.

Jelinek, V. (1981) Characterization of magnetic fabric of rocks. Tectonophysics, 79:562-567.

Kaiser, A.D., Verosub, K.L. (1985) Modelling polarity transitions with radial dipole sources: Geomagnetic field behavior at northern mid-latitudes, Geophys.Res.Lett., 12:777-780.

Karlin, R., Levi, S. (1985) Geochemical and sedimentological control of the magnetic properties of hemipelagic sediments. J.Geophys.Res. 90:10373-10392.

Karlin, R., Lyle, M., Heath, G.R. (1987) Authigenic magnetite formation in suboxic marine sediments, Nature, 326:490-493.

Kent, D.V., Lowrie, W. (1974) Origin of magnetic instability in sediment cores from the Central North Pacific., J.Geophys.Res., 79:2987.

King, J., Banerjee, S.K., Marvin, J., Ozdemir, O. (1982) A comparison of different magnetic methods for determining the relative grain size of magnetite in natural materials: some results from lake sediments, Earth Planet.Sci.Lett., 59:404-419.

King, J.W, Banerjee, S.K. and Marvin, J. (1983) A new rockmagnetic approach to selecting sediments for geomagnetic paleointensity studies: Application to paleointensity for the last 4000 years. J.Geophys.Res., 88:5911-5921

Kirschvink, J.L. (1980) The least squares line and plane and the analysis of paleomagnetic data. Geophys.J.R.Astron.Soc., 62:699-718.

Kissin, S.A., Scott, S.D. (1982) Phase relations involving pyrrhotite below 350 °C, Econ.Geol.77, 1739-1754.

Kligfield, R., Channel, J.E.T. (1981) Widespread remagnetization of Helvitic limestones. J.Geophys.Res.B 86:1888-1900.

Kodama, K.P., Sun, W.W. (1990) SEM and magnetic fabric study of a compacting sediment. Geophys.Res.Lett., 17:795-798.

Kono, M. (1987) Rikitake two-disk dynamo and paleomagnetism, Geophys.Res.Lett. 14:21-24.

Laj, C., Jamet, M., Sorel, D., Valente, J.P. (1982) First paleomagnetic results from Mio-Pliocene series of the Hellenic sedimentary arc., Tectonophysics, 86:45-67.

Laj, C. Guitton S., Kissel, C. (1987) Rapid changes and near-stationarity of the geomagnetic field during a polarity transition, Nature, 330:145-148.

Laj, C. Guitton, S., Kissel, C., Mazaud, A. (1988) Complex behavior of the geomagnetic field during three successive polarity reversals, 11-12 m.y.B.P. J.Geophys.Res., 93:11655-11666.

Langereis, C.G. (1984) Late Miocene magnetostratigraphy in the Mediterranean., Ultraiectina Geologica (Ph.D. thesis University of Utrecht), 34:195 pp.

Langereis, C.G., Zachariasse, W.J., Zijderveld, J.D.A. (1984) Late Miocene magnetobiostratigraphy of Crete. Mar.Micropal. 8:261-281.

Langereis, C.G., Linssen, J.H., Mullender, T.A.T., Zijderveld, J.D.A. (1989). Demagnetization. in: David E. James (editor), Encyclopedia of Geophysics. Van Nostrand Reinhold Company Inc., Stroudsburg, Pennsylvania.

Langereis, C.G., Hilgen, F.J. (in press) The Rosello composite: A Mediterranean and global reference section for the Early to early Late Pliocene.

Larson, E.E., Walker, T.R. (1985) Comment on 'Paleomagnetism of a polarity transition in the Lower (?) Triassic Chucwater Formation, Wyoming' by Emilio Herrero-Bervera and Charles E. Helsley, J.Geophys.Res., 90:2060-2062.

LeMouell, J.L. (1984) Outer-core geostrophic flow and secular variation of Earth's geomagnetic field, Nature 311:734-735.

Linssen, J.H. (1984). Rockmagnetic properties of Late Miocene marine clays from Crete. M.Sc.Thesis, University of Utrecht., 60pp.

Linssen, J.H. (1988) Preliminary results of a study of four succecessive sedimentary geomagnetic reversal records from the Mediterranean. (upper Thvera, lower and upper Sidufjall, lower Nunivak) Phys.Earth Planet. Inter., 52:207-231.

Linssen, J.H. (c) Evidence for single domain state transition for newly formed magnetite in sediments during thermal demagnetization ?

Linssen, J.H. (d, chapter 5) The Mammoth and lower Kaena geomagnetic sedimentary reversal records of the Punta Piccola section.

Linssen, J.H. (e, chapter 4) Rockmagnetism of the magnetite and pyrrhotite bearing sediments from the Trubi formation.

Linssen, J.H. (f) Antiparallel remanences observed in natural hematite during thermal demagnetization. Remanent coercivities of the defect and fundamental moment of hematite and the origin of its recovered magnetization.

Linssen, J.H. (g, chapter 3) A succession of five Early-Pliocene geomagnetic reversal records from the Mediterranean.

Linssen, J.H. (h, chapter 6) The high resolution Lower Pliocene sedimentary reversal records from Corfu (Greece).

Lovley, D.R., Stolz, F.J., Nord, G.L.Jr., Phillips, E.J.P. (1987) Anaerobic production of magnetite by a dissimilatory iron-reducing microorganism, 330:252-254.

Løvlie, R., Lowrie, W., Jacobs, M. (1971) Magnetic properties and mineralogy of four deep-sea cores, Earth Planet.Sci.Lett., 15:157-168.

Løvlie, R. (1974) Post-depositional remanent magnetization in re-deposited deep-sea sediments. Earth Planet.Sci.Lett., 29:219-226.

Løvlie, R. (1976) The intensity pattern of post-depositional remanence acquired in some marine sediments deposited during a reversal of the external magnetic field, Earth Planet.Sci.Lett., 30:209-214.

Lowrie, W., Heller, F., (1982) Magnetic properties of marine limestones, Rev.Geophys.Space Physics, 20:171-192.

References

Lu.G. Marshak, S., Kent, D.V. (1990) Characteristics of magnetic carriers responsible for Late Paleozoic remagnetization in carbonate strata of the mid-continent, U.S.A. Earth Planet.Sci.Lett., 99:351-361.

Lund, S.P., Karlin, R. (1990) Introduction to the special section on physical and biogeochemical processes responsible for the magnetization of sediments. J.Geophys.Res. 95:4353-4354.

Mankinen, E.A. and Dalrymple, G.B. (1979). Revised geomagnetic polarity time scale for the interval 0-5 myrs B.P. J.Geophys.Res., 84:615-626.

Mankinen, E.A., Prévot, M., Grommé, C.S. and Coe, S. (1985). The Steens Mountain (Oregon) geomagnetic polarity transition - 1. Directional history, duration of episodes, and rock magnetism, J.Geophys.Res., 90:10393-10416.

Mann, S., Sparks, N.H.C., Frankel, R.B., Bazylinski, D.A., Jannasch, H.W. (1990) Biomineralization of ferrimagnetic greigite (Fe3S4) and iron pyrite (FeS2) in a magnetotactic bacterium. 343:258-261.

Mazaud, A., Laj, C. (1989) Simulation of geomagnetic polarity reversals by a model of interacting dipole sources.,Earth Planet.Sci.Lett., 92:299-306.

Menocal, P.B. de, Ruddiman, F., Kent, D.V. (1990) Depth of post-depositional remanence acquisition in deep-sea sediments: a case study of the Brunhes-Matuyama reversal and oxygen isotopic Stage 19.1. Earth Planet.Sci.Lett, 99:1-13.

Merrill, R.T. (1970) Low-temperature treatments of magnetite and magnetite bearing rocks. J.Geophys.Res. 75:3343-3349

Merrill, R.T., McElhinny, M.W. (1977) Anomalies in the Time-averaged paleomagnetic field and their implications for the lower mantle, Rev.Geophys.Space Phys. 15:309-323.

Moskowitz, B.M., Frankel, R.B., Bazylinski, D.A., Jannasch, H.W., Lovley, D.R. (1989) A comparison of magnetite particles produced anaerobically by magnetotactic and dissimilatory iron-reducing bacteria. Geophys.Res.Lett, 16:665-668.

Neël, L. (1955) Some theoretical aspects of rock magnetism. Phil.Mag.Suppl.Adv.Phys., 4:113-190.

Officer, C.B. (1986) A conceptual model of core dynamics and the earth's magnetic field, J.Geophys., 59:89-97.

Olson, P. (1983). Geomagnetic polarity reversals in a turbulent core, Phys.Earth Planet.Int.,33:260-274.

Onufrienok, V.V., Zveginitsev, A.G. (1981) Magnetic ordering in hexagonal pyrrhotite at high temperature, Geom.Aeronomy, 21:666-668.

Parry, L.G. (1965) magnetic properties for dispersed magnetite powders. Philos.Mag., 11:303-312.

Prévot, M., Mankinen, E.A., Coe, R.S. and Grommé, C.S. (1985a). The Steens mountain (Oregon) geomagnetic polarity transition - 2. Field intensity variations and discussion of reversal models, J.Geophys.Res., 90:10417-10448.

References

Prévot, M., Mankinen, E.A., Grommé, C.S., Coe, R.S. (1985) How the geomagnetic field reverses polarity, Nature, 316:230-234.

O'Reilly, W. (1984) Rock and mineral magnetism, Blackie and Son Ltd. Glasgow, 220 pp.

Reynolds, R.L., Fishman, N.S., Wanty, R.B., Goldhaber, M.B. (1990) Iron sulphids minerals at Cement oil field, Oklahoma-Implications for the magnetic detection of oil fields. Geol.Soc.Am.Bull. (?).

Reynolds, R.L., Webring, M., Grausch, V.J.S., Tuttle, M. (1990) Magnetic forward models of Cement oil fieldm Oklahoma, based on rock magnetic, geochemical, and petrologica constraints. 55:344-353.

Rio, D.,Sprovieri, R., Raffi, I. (1984) Calcereous plankton biostratigraphy and biochronology of the Pliocene - Lower Pleistocene succession of the Capo Rossello area, Sicily. Mar.Micropal., 9:135-180.

Roberts, P.H. (1967) An introduction to magnetohydrodynamics. Longmans. London;Elsevier,New York.

Rochette, P. (1987) Metamorphic control of the magnetic mineralogy of black shales in the Swiss Alps: toward the use of 'magnetic isograde', Earth Planet.Sci.Lett., 84:446-456.

Rochette, P. (1990) Rationale of geomagnetic reversals versus remanence recording processes in rocks: a critical review. Earth Planet.Sci.Lett., 98:33-39.

Roperch, P., Chauvin, A. (1987) Transitional field behaviour: volcanic records from French Polynesia, Geophys.Res.Lett., 14:151-154

Roperch, P., Duncan, R.A. (1990) Records of geomagnetic reversals from volcanic islands of French Polynesia. 1. Paleomagnetic study of a polarity transition in a lava sequence from the island of Huahine. J.Geophys.Res., 95:2713-2726.

Salloway, J.C. (1983) The structure of the geomagnetic field during polarity transitions and excursions, Ph.D.Thesis, University of Edinburgh, 296pp.

Schneider, D.A., Kent, D.V. (1988) Inclination anomalies from Indian Ocean sediments and the possibility of a standing nondipole field., J.Geophys.Res., 93:11621-11630.

Schroeer, D., Nininger, R.C. (1967) Morin transition in alfa-Fe2O3 microcrystals, Phys.Rev.Lett., 19:632-634.

Schwarz, E.J., Harris, D.C. (1970) Phases in natural pyrrhotite and the effect of heating on their magnetic properties. J.Geomagn.Geoelec. 22:463-470.

Schwarz, E.J., Vaughan, D.J. (1972) Magnetic pphase relations of pyrrhotite J.Geomagn.Geoelec. 24:441-458.

Schwarz, E.J. (1975) Magnetic properties of pyrrhotite and their use in applied geology and geophysics., Geol.Surv.Can. Paper 74-59, 24pp.

Shive, P.N. (1985) Alignment of magnetic grains in fluids., Earth Planet.Sci.Lett., 72:117-124.

Smith, R.W. and Fuller, M. (1967) Alfa- hematite: stable remanence and memory., Science 156:1130-1133.

Soffel, H.C. (1977) Pseudo-single domain effects and single-domain multidomain transition in natural pyrrhotite deduced from domain structure observations., J.Geophys. 42:351-359.

Soffel, H.C. (1981) Domain structure of natural fine-grained pyrrhotite in a rock matrix (diabase)., Phys.Earth Plan.Int. 26:98-106.

Spaak, P. (1983) Accuracy in correlation and ecological aspects of the Mediterranean Pliocene. Utrecht Micropal.Bull., 28:1-160.

Sparks, N.H.C., Mann, S., Bazylinski, D.A., Lovley, D.R., Jannasch, H.W., Frankel, R.B. (1990) Structure and morphology of magnetite anaerobically-produced by a marine magnetotactic bacterium and a dissimilatory iron-reducing bacterium. Earth Planet.Sci.Lett., 98:14-22.

Stacey, F.D. and Banerjee S.K. (1974) The physical principles of rock magnetism, Elsevier Scien. Publ. Comp., Amsterdam-London-New York, 195 pp.

Suk, D., van der Voo, R., Peacor, D.R. (1990) Scanning and transmission electron microscope observations of magnetite and other iron phases in ordoviciuan carbonates from East Tennessee. J.Geophys.Res., 95:12327-12336.

Tarduno, J.A. (1990) Absolute inclination values from deep sea sediments: A reeximination of the Cretaceous pacific record. Geophys.Res.Lett. 17:101-104.

Tauxe, L., Badgley, C. (1984). Transition stratigraphy and the problem of remanence lock-in times in the Siwalik Red Beds. Geophys.Res.Lett., 11:611-613.

Taylor, G.R. (1982) A mechanism for framboid formationas illustrated by a volcanic exhalitive sediment, Mineral. Deposita 17:23-36.

Taylor, L.A. (1971) The Fe-O-S system. Oxidation of pyrrhotites and the formation of anomalous pyrrhotite, Carnegie Inst. Washington Yearb., 70:287-289.

Theyer, F., Herrero-Bervera, E., Hsu, V., Hammond, S.R. (1985). The zonal harmonic model of polarity transitions: A test using successive reversals. J.Geophys.Res. 90:1963-1982.

Tucker, P. (1980). A grain mobility model of post-depositional realignment. Geophys.J.R.Astron.Soc., 63:149-163.

Valet, J.P., Laj, C. (1984). Invariant and changing transitional field configuration in a sequence of geomagnetic reversals. Nature, 311:552-555.

Valet, J.P., Laj, C., Tucholka, P. (1985) Geomagnetic field: Volcanic record of reversal, Nature, 316:217-218

Valet, J.P. (1985). Inversions géomagnétiques du Miocène supérieur en Crète. Modalités du renversement et caractéristiques du champ de transition. Ph.D. Thesis, Paris.

Valet, J.P. Laj, Tucholka, P. (1986) High-resolution sedimentary record of a geomagnetic reversal, Nature, 322:27-32.

Valet, J.P., Laj, C., Langereis, C.G. (1988) Sequential geomagnetic reversals recorded in upper Tortonian marine clays in western Crete (Greece)., J.Geophys.Res., 93:1131-1151.

Valet, J.P., Tauxe, L., Clement, B. (1989) Equatorial and mid-latitude records of the last geomagnetic reversal from the Atlantic Ocean., Earth Planet.Sci.Lett., 94:371-384.

Valet, J.P., Tauxe, L., Clark, D.R. (1988) The Matuyama-Brunhes transition recorded from Lake Tecopa sediments (California), Earth Planet.Sci.Lett., 87:463-472.

Vali, H., Forster, O., Amarantidis, G., Petersen, N. (1987) Magnetotactic bacteria and their magnetofossils in sediments, Earth Planet.Sci.Lett., 86:389-400.

Velzen, A.J. van, Zijderveld, J.D.A. (1990) Rock magnetism of the Early Pliocene Trubi formation at Eraclea Minoa (Sicily), Geophys.Res.Lett., 17:791-794.

Visser, J.P. de, Ebbing, J.H.J., Gudjonsson, L., Hilgen, F.J., Jorissen, F.J., Verhallen, P.J.J.M., Zevenboom, D. (1989) The origin of rhythmic bedding in the pliocene Trubi formation of Sicily, Southern Italy. Paleogeography, paleoclimatology, paleoecology, 69:45-66.

Verosub, K.L., Cox, A., J.Geomagn.Geoelec. 23:235-242 (1971).

Verosub, K.L. (1977) Depositional and postdepositional process in the magnetization of sediments, Rev.Geoph.Space Phys., 15:129-143.

Walker, T. (1981) Nature and origin of hematite in the Moenkopi formation (Triasic), Colorado plateau: a contribution to the origin of magnetization in red beds. J.Geophys.Res., 86:317-333.

Weeks, R.J., Fuller, M., Williams, I. (1988) The effects of recording medium upon reversal records. Geophys.Res.Lett. 15:1255-1258.

Westrich, J.T. (1983) The consequences and controls of bacterial sulfate reduction in marine sediments. Ph.D. thesis, Yale University, 530 p.

Williams, I. and Fuller, M. (1981). Zonal harmonic models of reversal transition records. J.Geophys.Res., 86:11657-11665.

Williams, I. Weeks, R. and Fuller, M. (1988) A model for transition fields during geomagnetic reversals. Nature, 332:719-720.

Worm, H.U., Markert, H. (1987) Magnetic properties of fine particle titanomagnetites precipitated in a silicate matrix. Phys.Earth Planet.Int. 46:84-92.

Yoshida, J., Iida, S. (1977) X-ray diffraction study on the low-temperature phase of magnetite, J.Phys.Soc.Jap. 42,1:230-237.

Zachariasse, W.J., Zijderveld, J.D.A., Langereis, C.G., Hilgen, F.J., Verhallen, P.J.J.M. (1989) Early Late Pliocene biochronology and surface water temperature variations in the Mediterranean. Marine Micropaleontology, 14:339-355.

References

Zijderveld, J.D.A. (1967). A.C. demagnetization of rocks: analysis of results. In: D.W. Collinson et al. (eds) Methods in Palaeomagnetism, Elsevier, Amsterdam.

Zijderveld, J.D.A. (1975) Paleomagnetism of the Esterel rocks., Ph.D. thesis University of Utrecht.

Zijderveld, J.D.A., Zachariasse, W.J., Verhallen, P.J.J.M. and Hilgen, F.J. (1986). The age of the Miocene-Pliocene boundary. Newsl. Stratigr., 16:169-181.

Zijderveld, J.D.A., Hilgen, F.H., Langereis, C.G., Verhallen, P.J.J.M., Zachariasse, W.J., (submitted) Integrated magnetostratigraphy and biostratigraphy of the Upper Pliocene - Lower Pleistocene from the Monte Singa and Crotone areas in southern Calabria (Italy)

Appendix

Demagnetization results of the investigated Calabrian, Sicilian and Corfu reversal records. Refer to chapter 2-6 for the definition of the components.

The stratigraphic level is in cm's for the Calabrian and Sicilian records and in m's for the Corfu records. The declination ranges from 90°-450° or 0°-360° and has not been corrected for rotations. The inclination is not corrected for the inclination error. The intensity is in μA/m. The error value corresponds to the MAD (Kirschvink, 1980). The demagnetization quality factor ranges from 1-5 for the Calabrian and Sicilian records and from 1-3 for the Corfu records. Ahigher factor indicates a better quality.

	pp.
Calabria	
upper Thvera LT component	204
upper Thvera HT component	206
lower Sidufjall LT component	209
lower Sidufjall HT component	210
upper Sidufjall LT component	211
upper Sidufjall HT component	213
lower Nunivak LT component	216
lower Nunivak HT component	217
upper Nunivak (1986) LT component	218
upper Nunivak (1986) HT component	219
upper Nunivak (1987) LT component	220
upper Nunivak (1987) HT component	221
Sicily	
lower Mammoth HT component	223
upper Mammoth HT component	224
lower Kaena HT component	225
Corfu	
upper Thvera magnetite component	227
lower Sidufjall magnetite component	229

Calabria
upper Thvera reversal record
LT component

Sample	Level	Dec.	Inc.	Int.	Err.	Q
UT.01A	2.2	358.6	53.9	1084	23.4	2
UT.03A	3.5	373.4	47.2	798	16.1	3
UT.05A	5.2	357.4	38.4	1129	21.0	2
UT.07A	6.9	364.9	48.8	766	18.3	2
UT.09A	8.4	370.6	45.9	1280	12.1	2
UT.11A	10.0	374.9	33.8	1321	12.2	2
UT.13A	11.6	355.1	39.6	926	12.6	2
UT.15A	13.1	361.7	46.8	839	15.3	2
UT.17A	14.7	337.7	46.9	1177	25.7	3
UT.19A	16.3	359.4	52.6	980	19.6	1
UT.21A	18.6	385.5	54.8	987	13.0	4
UT.23A	19.5	366.3	39.5	614	18.4	2
UT.25A	21.1	373.7	43.7	822	28.9	2
UT.27A	22.7	376.3	39.4	1246	13.1	2
UT.29A	24.3	364.9	29.9	1238	16.6	2
UT.31A	25.9	402.3	54.7	889	21.5	2
UT.33A	27.5	384.4	41.7	1153	14.2	3
UT.35A	29.1	377.4	50.1	946	18.8	2
UT.37A	30.4	360.2	34.3	1291	12.9	2
UT.39A	32.0	361.3	45.2	977	13.7	3
UT.43A	35.0	376.5	44.9	934	23.4	2
UT.45A	36.7	360.0	55.2	881	13.6	4
UT.49A	40.0	352.8	41.4	1049	27.2	3
UT.51A	41.5	364.5	26.1	1441	17.7	3
UT.55A	44.8	368.3	28.0	796	9.8	3
PS1.01.5A	47.4	282.2	45.8	216	20.2	4
PS1.01.3A	47.6	245.0	-9.4	273	12.0	3
PS1.01.4B	47.7	232.1	5.4	169	25.7	4
PS1.01.2A	47.8	420.8	-6.2	3429	3.3	1
PS1.01.1A	47.8	429.1	1.7	3232	1.8	3
PS1.01.2B	48.1	416.3	-5.0	3782	1.7	1
UT.61A	50.5	359.8	51.3	198	26.7	4
UT.63A	52.8	363.3	54.2	346	19.4	4
PS1.02.3A	55.4	365.5	64.0	481	7.4	1
PS1.02.1A	55.5	337.2	52.4	389	12.1	2
PS1.02.3B	55.6	354.7	66.1	434	7.2	1
PS1.02.5A	55.6	376.0	55.7	478	14.9	4
PS1.02.5B	55.7	318.5	56.5	246	8.4	3
PS1.02.1B	55.8	340.1	56.5	394	9.0	1
PS1.02.3C	55.9	354.5	70.4	470	6.7	1
PS1.02.2C	55.9	320.5	53.8	503	7.3	1
PS1.02.4C	55.9	342.0	48.9	301	15.5	2
UT.67A	56.4	353.5	38.7	351	25.1	2
UT.69A	58.3	365.6	50.5	401	18.9	4
UT.73A	62.1	339.9	83.2	485	9.1	2
PS1.03.1A	62.3	370.2	61.3	485	7.8	1
PS1.03.5B	62.8	340.4	60.0	395	6.5	1
PS1.03.2B	62.9	348.6	47.6	293	10.5	1
PS1.03.4A	63.0	354.8	48.2	336	10.7	1
PS1.03.5C	63.1	351.2	56.1	525	8.4	1
PS1.03.2C	63.2	361.0	56.3	447	5.5	1
UT.75A	64.0	348.4	52.5	452	7.6	1
PS1.04.3A	70.0	349.7	49.8	246	7.9	1
PS1.04.1A	70.0	319.7	42.1	320	9.4	1
PS1.04.4A	70.0	310.3	33.7	239	11.6	2
PS1.04.1B	70.2	355.3	44.3	262	7.3	1
PS1.04.2B	70.2	355.3	60.8	300	8.7	1
PS1.04.1C	70.4	337.3	47.2	275	7.3	1
PS1.04.3C	70.4	343.0	48.1	330	10.2	1
PS1.05.3A	76.8	356.9	48.3	774	5.7	2
PS1.05.1A	76.8	344.8	43.8	252	9.2	2
PS1.05.4A	77.1	365.6	34.9	280	7.1	2
PS1.05.3C	77.4	339.0	43.6	258	6.8	2
PS1.05.2A	77.5	351.2	57.3	355	17.5	1
PS1.05.3D	77.7	341.4	38.3	347	6.2	1
PS1.05.2B	77.7	347.0	42.1	339	11.8	1
PS1.06.3A	81.9	331.0	16.2	275	10.5	2
PS1.06.4A	82.0	325.8	40.7	549	8.4	1
PS1.06.3B	82.2	298.4	20.1	314	18.3	2
PS1.06.2A	82.2	327.9	-25.2	581	15.5	3
PS1.06.4B	82.3	307.1	32.7	618	23.5	2
PS1.06.3C	82.5	321.7	14.3	278	15.7	1
PS1.06.4C	82.5	317.5	41.3	463	13.1	1
PS1.06.2B	82.5	307.6	-12.1	492	22.9	4
PS1.07.1A	84.5	373.4	26.1	269	9.0	1
PS1.07.3A	84.5	346.6	29.8	669	7.6	2
PS1.07.5B	84.6	300.0	28.2	495	15.9	2
PS1.07.2B	84.9	325.5	25.8	663	14.1	2
PS1.07.3B	84.9	309.8	17.3	600	11.6	2
PS1.08.4B	86.8	303.1	-3.5	528	15.5	1
PS1.08.5A	86.8	327.0	6.9	495	13.4	2
PS1.08.2B	86.8	315.0	3.8	398	26.9	3
PS1.08.3B	87.0	293.8	-8.2	423	20.5	3
PS1.09.4B	88.5	317.3	7.6	371	19.2	2
PS1.09.5A	88.6	332.0	31.3	328	14.8	4
PS1.09.2B	89.0	339.0	30.8	393	19.0	2
PS1.09.3B	89.0	286.5	17.4	303	11.9	3
PS1.10.4A	90.7	340.0	31.3	303	30.7	2
PS1.10.2B	90.9	266.4	9.9	204	13.6	3
PS1.10.4B	90.9	294.7	25.0	385	16.1	4

Reversal record data

Sample	Level	Dec.	Inc.	Int.	Err.	Q	Sample	Level	Dec.	Inc.	Int.	Err.	Q
PS1.10.3B	91.1	291.0	5.8	346	26.2	4	PS1.22.3A	113.2	209.3	-2.7	496	11.8	1
PS1.11.3A	92.4	282.4	20.5	579	8.0	4	PS1.23.3A	115.2	243.0	-10.2	1455	8.2	2
PS1.11.3B	92.8	260.4	7.6	260	11.0	1	PS1.23.2B	115.3	223.5	-0.7	340	15.2	2
PS1.11.2B	93.0	260.3	-4.9	99	36.3	3	PS1.23.3B	115.4	218.9	-21.2	560	10.4	1
PS1.11.5A	93.0	284.7	17.1	132	20.7	4	PS1.23.4B	115.4	243.5	-8.7	380	11.4	2
PS1.11.4B	93.2	267.8	-5.1	390	13.6	1	PS1.24.3B	116.9	223.7	-15.7	375	9.5	1
PS1.12.2B	94.6	279.0	16.9	371	4.3	2	PS1.24.2A	117.0	231.7	-25.6	451	19.2	2
PS1.12.3A	94.9	258.0	-21.3	384	10.5	1	PS1.24.4B	117.2	218.9	-12.6	470	7.5	1
PS1.12.4B	95.1	247.1	-4.2	254	23.2	3	PS1.25.4A	118.6	221.5	-12.6	397	12.7	1
PS1.12.3B	95.1	272.3	-7.0	226	21.4	4	PS1.25.7A	118.6	219.1	-25.1	649	13.8	2
PS1.13.6A	96.5	266.5	13.5	291	15.9	3	PS1.25.2B	118.8	217.0	-25.1	858	11.6	1
PS1.13.3A	96.7	221.0	-37.6	469	9.8	2	PS1.25.3B	118.8	214.0	-50.5	771	5.5	2
PS1.13.3B	96.9	219.0	-23.8	289	13.2	4	PS1.26.3A	120.3	209.7	-41.3	584	13.5	1
PS1.13.4B	97.0	156.0	-16.4	133	28.4	3	PS1.26.4A	120.4	224.8	-32.2	577	19.8	2
PS1.14.4B	98.9	236.1	-5.7	281	13.2	2	PS1.26.2A	120.9	210.0	-35.1	540	15.8	1
PS1.14.5A	99.0	244.0	11.4	455	12.9	2	PS1.27.4A	122.1	210.6	-22.0	512	24.0	2
PS1.14.3B	99.2	235.2	-14.4	338	26.4	2	PS1.27.3A	122.4	218.4	-32.0	470	15.0	1
PS1.14.2B	99.2	255.0	13.5	307	26.5	4	PS1.27.3B	122.8	225.0	-25.7	559	14.8	2
PS1.15.3B	100.9	271.1	-7.5	450	15.3	2	PS1.28.3A	124.3	209.8	-28.8	545	14.3	1
PS1.15.4B	101.0	269.4	13.8	413	14.9	4	PS1.28.4A	124.6	229.9	-36.9	671	10.5	2
PS1.15.2B	101.1	273.4	15.0	391	12.8	5	PS1.28.2A	124.7	209.1	-31.5	531	16.4	2
PS1.15.5A	101.3	324.2	40.3	190	12.7	3	PS1.29.5A	126.5	207.7	-19.7	720	6.9	2
PS1.16.5A	102.7	233.6	2.7	510	3.9	1	PS1.29.4A	126.9	212.6	-21.2	680	11.7	1
PS1.16.2B	102.8	282.1	14.9	216	13.3	6	PS1.29.2A	126.9	219.5	-47.5	628	11.7	2
PS1.16.4B	102.9	280.2	39.1	114	12.5	5	PS1.29.3A	126.9	231.5	-37.2	423	12.5	3
PS1.16.3B	103.3	269.3	19.9	204	7.0	5	PS1.30.4A	129.0	209.5	-19.2	619	19.8	2
PS1.17.4A	104.6	255.9	4.8	566	5.8	2	PS1.30.2A	129.1	189.2	-23.8	727	18.3	2
PS1.17.3A	104.8	257.8	-6.0	718	4.7	2	PS1.30.5A	129.5	219.1	-31.2	859	13.9	1
PS1.17.2B	105.0	216.4	-20.1	426	21.2	2	PS1.31.1A	131.3	186.5	-25.3	615	6.3	1
PS1.17.4B	105.0	275.9	-4.2	335	11.3	3	PS1.31.2B	131.4	209.7	-20.5	719	17.5	2
PS1.17.3B	105.1	252.4	-10.1	345	17.4	1	PS1.31.7A	131.4	212.0	-43.8	1110	17.0	2
PS1.18.3B	106.9	252.5	-10.4	929	20.2	3	PS1.32.3A	133.3	205.9	-36.8	1062	9.7	1
PS1.18.4A	106.9	255.7	-22.5	703	13.8	3	PS1.32.4A	133.3	202.4	-46.3	1288	19.6	1
PS1.18.2B	107.0	225.7	-4.2	598	24.9	2	PS1.32.2A	133.6	204.3	-34.1	1531	20.2	1
PS1.18.4B	107.2	240.1	-10.6	586	18.5	2	PS1.33.1A	135.2	206.8	-16.3	1123	6.1	1
PS1.19.3A	108.9	221.7	-20.9	789	7.2	3	PS1.33.2A	135.5	181.3	-35.4	687	22.4	1
PS1.19.3B	109.2	237.6	-8.0	493	14.6	2	PS1.33.4A	135.5	214.0	-35.8	1074	14.5	1
PS1.19.5A	109.3	237.2	-5.5	597	16.8	1	PS1.34.3A	136.9	216.2	-26.7	603	9.2	1
PS1.19.2B	109.3	230.3	-13.9	329	15.2	2	PS1.34.2A	137.2	205.1	-44.9	1342	9.4	4
PS1.19.4B	109.8	219.5	-7.6	412	27.0	4	PS1.34.4A	137.3	214.1	-33.4	1237	6.7	1
PS1.20.2B	110.7	225.4	-12.9	288	16.1	3	PS1.35.4A	139.1	208.8	-20.7	1223	29.1	4
PS1.20.3B	110.9	234.0	3.8	637	14.4	2	PS1.35.4B	139.3	220.3	-25.1	1240	8.4	1
PS1.20.4B	110.9	246.2	-16.8	558	6.2	2	PS1.35.1A	139.5	187.1	-44.6	1339	4.1	1
PS1.21.3A	112.8	241.1	-0.6	478	16.8	3	PS1.36.1A	141.1	208.9	-41.1	1616	3.9	1
PS1.21.2A	112.9	236.6	-0.7	595	8.8	1	PS1.36.3A	141.1	194.2	-34.4	857	9.9	1
PS1.21.2B	113.1	257.9	0.3	480	10.9	1	PS1.36.4A	141.4	211.8	-21.6	1212	5.6	1
PS1.22.5A	113.1	227.3	-4.9	424	8.9	3	PS1.37.1A	143.1	212.8	-26.6	482	11.3	1
PS1.22.2B	113.2	237.2	-13.8	341	11.8	1	PS1.38.2A	143.2	182.4	-49.3	668	5.4	2

Sample	Level	Dec.	Inc.	Int.	Err.	Q
PS1.38.4A	143.2	214.3	-36.9	425	17.3	2
PS1.37.3A	143.3	242.3	-48.4	697	13.4	1
PS1.38.7A	143.5	278.7	-5.2	450	8.7	3
PS1.38.6A	143.6	249.0	-6.0	522	5.6	1
PS1.37.3B	143.6	226.8	-12.2	656	13.7	2
PS1.39.1A	145.6	249.2	-26.5	345	10.6	1
PS1.39.5B	145.7	259.4	8.6	238	22.7	3
PS1.40.4A	146.8	276.3	14.3	291	6.4	4
PS1.40.3A	147.3	235.8	-11.4	358	8.2	2
PS1.40.1A	147.7	271.0	23.0	653	3.4	2
PS1.40.5B	147.7	259.8	10.1	248	8.6	3
PS1.41.3A	148.8	305.4	-55.2	1131	7.6	3
PS1.41.4A	148.8	238.1	-17.6	456	19.4	3
PS1.41.5B	149.4	244.9	-13.5	275	24.1	3
PS1.41.2B	149.4	251.7	-27.0	316	20.2	4
PS1.42.3A	152.8	234.3	-23.8	458	9.5	3
PS1.42.4A	153.1	236.1	-15.8	398	12.8	2
PS1.42.3B	153.2	247.9	-31.1	347	15.0	3
PS1.43.1A	156.8	215.7	-43.0	773	8.7	2
PS1.43.4A	157.0	201.7	-39.7	418	13.1	1
PS1.43.3A	157.0	210.3	-41.8	500	10.2	2
PS1.43.5A	157.2	205.2	-36.5	464	13.7	2
PS1.43.5C	157.9	220.3	-35.2	439	24.1	2
PS1.44.1A	162.8	216.1	-54.6	745	9.5	1
PS1.44.4A	163.0	237.4	-27.5	392	14.7	1
PS1.44.3A	163.1	211.6	-45.2	784	11.0	1
PS1.44.4C	164.0	235.5	-56.8	598	5.6	3
PS1.45.1A	170.0	181.4	-45.6	1146	10.0	1
PS1.46.1A	176.3	197.5	-39.8	1349	8.3	1
PS1.47.2A	182.0	207.2	-36.0	1991	7.7	3
PS1.48.2A	187.6	201.9	-31.8	2413	10.1	1
PS1.49.1A	194.2	202.5	-22.3	1028	12.3	2
PS1.50.1A	200.4	214.5	-4.6	2858	26.3	3

Calabria
upper Thvera reversal record
HT component

Sample	Level	Dec.	Inc.	Int.	Err.	Q
UT.01A	2.2	364.1	43.9	3700	2.3	2
UT.03A	3.5	361.6	43.6	2072	2.0	2
UT.05A	5.2	358.8	41.4	3186	2.2	3
UT.07A	6.9	358.0	42.2	2419	1.7	2
UT.09A	8.4	359.0	40.8	3245	2.6	2
UT.11A	10.0	370.9	39.7	3199	2.5	2
UT.13A	11.6	360.7	44.4	2937	2.6	2
UT.15A	13.1	361.9	41.2	2971	1.9	2
UT.17A	14.7	361.2	40.3	3493	2.9	2
UT.19A	16.3	365.0	44.7	2592	1.6	2
UT.21A	18.6	365.1	45.2	2445	1.8	2
UT.23A	19.5	360.3	38.0	2553	1.5	2
UT.25A	21.1	362.6	38.9	2658	3.0	2
UT.27A	22.7	363.4	43.4	3054	1.8	2
UT.29A	24.3	364.7	38.9	2968	2.5	2
UT.31A	25.9	366.1	41.8	3409	1.4	2
UT.33A	27.5	368.8	42.5	3287	1.8	2
UT.37A	30.4	365.1	39.4	3385	1.7	2
UT.39A	32.0	365.6	42.1	3127	1.5	2
UT.43A	35.0	368.9	45.2	3357	1.8	2
UT.45A	36.7	369.3	40.9	3027	1.9	2
UT.49A	40.0	363.4	38.3	3619	1.3	2
UT.51A	41.5	367.5	32.2	4102	1.3	2
UT.55A	44.8	362.1	32.5	2668	1.5	2
UT.57A	46.7	202.3	-32.8	1434	4.5	4
PS1.01.3A	47.6	200.1	-51.3	726	13.1	5
PS1.01.2A	47.8	385.0	4.1	1191	2.1	5
PS1.01.2B	48.1	391.0	-6.0	792	13.2	3
UT.61A	50.5	229.5	15.3	142	26.9	5
PS1.02.1A	55.5	370.7	47.2	207	16.3	5
PS1.02.5A	55.6	364.7	43.6	523	7.3	2
PS1.02.3B	55.6	355.0	51.0	416	11.0	3
PS1.02.5B	55.7	365.6	36.1	274	10.1	4
PS1.02.1B	55.8	384.1	12.2	298	20.7	4
PS1.02.4C	55.9	369.2	16.1	94	28.1	4
PS1.02.3C	55.9	395.9	-0.4	217	29.0	5
PS1.02.2C	55.9	348.1	18.8	302	0.5	5
UT.67A	56.4	360.9	54.2	533	7.8	3
UT.69A	58.3	328.1	26.3	116	20.7	5
UT.73A	62.1	324.7	72.6	223	9.4	4
PS1.03.1A	62.3	329.7	58.8	137	31.8	4
PS1.03.5B	62.8	348.8	62.6	224	8.5	5
PS1.03.2B	62.9	378.6	50.7	210	17.6	3

Reversal record data

Sample	Level	Dec.	Inc.	Int.	Err.	Q	Sample	Level	Dec.	Inc.	Int.	Err.	Q
PS1.03.4A	63.0	378.6	24.1	170	29.2	4	PS1.12.3A	94.9	182.4	-41.5	355	11.8	3
PS1.03.5C	63.1	374.4	60.8	377	13.1	3	PS1.12.3B	95.1	195.1	-28.5	349	8.0	3
PS1.03.2C	63.2	385.9	60.8	331	9.7	4	PS1.13.6A	96.5	201.1	-31.3	722	4.1	3
UT.75A	64.0	341.3	40.5	123	23.0	3	PS1.13.3A	96.7	198.1	-41.8	1028	4.4	2
PS1.04.3A	70.0	362.2	40.4	235	11.6	3	PS1.13.3B	96.9	201.4	-26.7	838	4.5	3
PS1.04.1A	70.0	342.5	54.2	469	4.4	3	PS1.13.4B	97.0	211.5	-27.6	534	9.5	4
PS1.04.4A	70.0	352.3	61.7	357	3.4	4	PS1.13.2B	97.2	220.2	-26.6	361	5.5	4
PS1.04.1B	70.2	388.3	52.3	180	17.4	3	PS1.14.4B	98.9	208.2	-31.8	437	12.0	4
PS1.04.2B	70.2	369.1	31.8	123	30.5	4	PS1.14.5A	99.0	215.1	-12.8	523	3.6	4
PS1.04.1C	70.4	377.3	49.0	465	3.2	3	PS1.14.2B	99.2	199.8	-32.1	327	16.8	3
PS1.04.3C	70.4	359.6	51.6	560	5.3	3	PS1.14.3B	99.2	206.4	-13.2	634	9.1	3
PS1.05.3A	76.8	363.5	37.8	664	2.2	4	PS1.15.3B	100.9	230.6	-4.7	374	3.7	3
PS1.05.1A	76.8	377.9	45.1	263	15.1	4	PS1.15.4B	101.0	214.6	-37.9	638	12.4	3
PS1.05.4A	77.1	369.6	38.4	946	2.5	3	PS1.15.2B	101.1	228.7	9.3	270	11.5	4
PS1.05.3C	77.4	357.1	41.0	633	5.1	3	PS1.15.5A	101.3	215.0	-24.5	495	5.3	4
PS1.05.2A	77.5	369.3	37.8	1053	3.6	3	PS1.16.5A	102.7	215.4	-17.6	839	5.7	3
PS1.05.3D	77.7	374.2	61.3	239	10.7	3	PS1.16.2B	102.8	248.7	-13.2	189	27.5	5
PS1.05.2B	77.7	363.8	42.1	1012	2.2	3	PS1.16.4B	102.9	199.7	-31.8	171	37.6	4
PS1.06.3A	81.9	362.7	25.6	1154	5.3	5	PS1.17.4A	104.6	221.3	-15.5	814	7.2	3
PS1.06.4A	82.0	379.2	37.6	286	19.8	3	PS1.17.3A	104.8	227.4	-25.2	754	3.8	3
PS1.06.3B	82.2	363.0	25.5	992	3.4	3	PS1.17.2B	105.0	199.5	-35.6	666	23.0	3
PS1.06.2A	82.2	375.7	-46.4	187	22.1	4	PS1.17.4B	105.0	231.5	-30.0	598	8.8	3
PS1.06.4B	82.3	347.1	27.8	1291	1.8	2	PS1.17.3B	105.1	225.1	-19.9	554	4.9	2
PS1.06.4C	82.5	349.8	25.5	1095	2.1	4	PS1.18.4A	106.9	199.5	-29.1	1883	3.6	2
PS1.06.3C	82.5	362.8	24.0	961	2.7	5	PS1.18.2B	107.0	194.5	-28.8	1737	2.8	2
PS1.07.3A	84.5	366.3	36.3	1103	5.3	4	PS1.18.4B	107.2	204.7	-31.9	1009	12.5	2
PS1.07.1A	84.5	362.2	26.4	1035	6.4	5	PS1.19.3A	108.9	198.3	-39.7	1536	4.8	3
PS1.07.5B	84.6	357.3	26.7	909	4.4	4	PS1.19.3B	109.2	201.6	-31.4	1261	3.4	3
PS1.07.2B	84.9	356.7	31.8	1127	4.3	3	PS1.19.2B	109.3	225.5	-21.7	503	12.4	2
PS1.07.3B	84.9	356.8	27.0	1295	1.0	3	PS1.19.5A	109.3	193.3	-32.4	1353	5.3	3
PS1.08.4B	86.8	359.0	15.3	810	5.2	3	PS1.19.4B	109.8	220.0	-32.3	544	20.1	3
PS1.08.5A	86.8	356.3	17.5	601	6.6	5	PS1.20.2B	110.7	199.5	-27.1	1308	2.7	3
PS1.08.3B	87.0	353.4	28.0	714	7.4	5	PS1.20.3B	110.9	196.5	-28.7	1551	3.2	3
PS1.09.4B	88.5	368.3	25.0	709	8.1	3	PS1.20.4B	110.9	237.9	-40.4	727	15.7	5
PS1.09.5A	88.6	367.4	26.3	673	2.8	4	PS1.21.3A	112.8	207.1	-26.5	1563	3.4	2
PS1.09.2B	89.0	376.1	23.5	641	4.6	3	PS1.21.2A	112.9	206.6	-26.4	1629	2.0	3
PS1.09.3B	89.0	364.1	19.5	588	4.5	4	PS1.22.5A	113.1	204.6	-33.0	1406	7.7	3
PS1.10.4A	90.7	360.5	21.4	650	2.2	4	PS1.21.2B	113.1	205.3	-25.9	1359	1.8	4
PS1.10.4B	90.9	352.7	19.5	471	6.1	4	PS1.22.3A	113.2	191.8	-29.8	2202	2.9	1
PS1.10.2B	90.9	351.7	13.8	494	5.8	5	PS1.22.2B	113.2	202.5	-21.6	1871	1.9	2
PS1.10.3B	91.1	359.6	30.3	469	9.9	4	PS1.23.3A	115.2	200.2	-30.3	2528	3.0	3
PS1.11.3A	92.4	225.2	-32.0	171	21.7	3	PS1.23.2B	115.3	199.8	-26.0	1735	7.1	2
PS1.11.3B	92.8	249.7	-32.6	146	36.8	3	PS1.23.3B	115.4	204.0	-27.0	2273	5.2	3
PS1.11.3B	92.8	235.4	-18.8	173	24.6	3	PS1.23.4B	115.4	199.4	-25.6	1697	5.1	3
PS1.11.5A	93.0	191.8	-27.0	232	19.2	3	PS1.24.3B	116.9	202.9	-23.5	1996	2.5	3
PS1.11.2B	93.0	222.7	-8.7	306	10.0	4	PS1.24.2A	117.0	203.0	-37.0	1822	5.3	3
PS1.11.4B	93.2	234.6	-10.0	410	10.9	4	PS1.24.4B	117.2	197.4	-27.8	1881	6.0	2
PS1.12.2B	94.6	237.6	-17.9	201	22.8	4	PS1.25.4A	118.6	197.4	-28.2	1644	1.9	2

Appendix

Sample	Level	Dec.	Inc.	Int.	Err.	Q
PS1.25.7A	118.6	189.0	-31.1	2607	4.0	2
PS1.25.3B	118.8	193.2	-37.2	2599	1.7	2
PS1.25.2B	118.8	194.4	-27.8	2343	2.9	2
PS1.26.3A	120.3	186.5	-38.0	2306	4.3	2
PS1.26.4A	120.4	194.6	-44.8	2369	4.1	2
PS1.26.2A	120.9	188.1	-38.0	2591	6.8	2
PS1.27.4A	122.1	181.4	-36.4	2306	5.4	2
PS1.27.3A	122.4	188.9	-34.7	2377	6.0	1
PS1.27.3B	122.8	190.1	-38.1	1986	5.2	2
PS1.28.3A	124.3	189.5	-31.4	2296	3.9	2
PS1.28.4A	124.6	201.4	-38.5	2266	2.5	1
PS1.28.2A	124.7	181.6	-35.8	2521	3.4	3
PS1.29.5A	126.5	184.0	-39.3	2681	2.8	2
PS1.29.3A	126.9	194.6	-37.7	3131	1.1	1
PS1.29.4A	126.9	194.0	-41.1	2621	3.0	1
PS1.29.2A	126.9	188.6	-36.3	2962	3.1	2
PS1.30.4A	129.0	195.5	-35.4	2656	5.1	2
PS1.30.2A	129.1	191.2	-34.7	3315	4.0	2
PS1.30.5A	129.5	189.8	-39.6	2495	3.0	1
PS1.31.3A	131.2	194.9	-40.7	4309	1.0	1
PS1.31.1A	131.3	177.5	-42.4	2565	6.5	2
PS1.31.2B	131.4	193.4	-34.7	2630	3.9	1
PS1.31.7A	131.4	194.4	-33.1	3194	1.5	1
PS1.32.3A	133.3	194.1	-34.1	3648	5.7	2
PS1.32.2A	133.6	193.8	-35.0	3363	6.7	2
PS1.33.1A	135.2	194.9	-29.6	3423	2.0	1
PS1.33.4A	135.5	192.7	-31.3	3919	1.5	2
PS1.33.2A	135.5	196.0	-29.9	3448	4.5	3
PS1.34.3A	136.9	198.6	-28.8	4072	3.8	2
PS1.34.2A	137.2	186.4	-31.0	4176	2.8	2
PS1.34.4A	137.3	195.7	-35.1	3465	3.7	2
PS1.35.3A	139.1	197.6	-34.2	4912	1.0	1
PS1.35.4A	139.1	195.3	-33.3	4095	2.5	2
PS1.35.4B	139.3	194.1	-29.9	3734	5.7	2
PS1.35.1A	139.5	185.0	-32.2	4364	2.4	1
PS1.36.1A	141.1	197.4	-28.9	4244	1.9	2
PS1.36.3A	141.1	196.4	-26.6	5257	2.2	2
PS1.36.4A	141.4	194.7	-28.7	4912	4.9	2
PS1.37.1A	143.1	206.0	-29.9	2630	3.3	2
PS1.38.2A	143.2	158.2	-48.0	1114	3.0	2
PS1.37.3A	143.3	223.4	-34.8	2200	5.2	5
PS1.37.3B	143.6	201.9	-28.0	1898	2.3	2
PS1.38.6A	143.6	253.4	0.1	333	16.8	4
PS1.39.4A	145.5	304.8	24.9	296	4.0	5
PS1.39.1A	145.6	345.2	44.3	550	11.7	5
PS1.39.2B	145.7	335.6	48.5	318	11.1	5
PS1.39.5B	145.7	169.2	9.8	314	23.0	5
PS1.40.4A	146.8	289.6	41.6	189	12.3	4
PS1.40.3A	147.3	195.2	2.7	264	0.0	5
PS1.40.1A	147.7	293.5	49.8	276	9.2	5
PS1.40.5B	147.7	183.5	41.9	318	20.6	5
PS1.41.4A	148.8	208.5	-22.5	514	10.9	2
PS1.41.3A	148.8	257.6	-63.7	435	14.6	4
PS1.41.1A	149.2	229.9	-10.5	549	15.8	4
PS1.41.5B	149.4	202.8	23.6	388	19.2	5
PS1.42.3A	152.8	231.9	-35.2	437	4.9	4
PS1.42.1A	153.0	240.9	-21.3	506	15.4	4
PS1.42.4A	153.1	212.4	-36.6	340	12.7	4
PS1.42.3B	153.2	219.8	-12.6	293	15.9	4
PS1.43.1A	156.8	203.2	-39.2	1089	5.3	3
PS1.43.4A	157.0	187.1	-37.9	581	6.6	2
PS1.43.3A	157.0	188.8	-46.3	685	5.2	3
PS1.43.5A	157.2	199.4	-40.0	744	2.9	2
PS1.43.5C	157.9	192.8	-38.2	600	7.2	2
PS1.44.1A	162.8	201.6	-40.9	1643	6.7	2
PS1.44.4A	163.0	195.9	-44.9	929	5.3	2
PS1.44.3A	163.1	197.3	-42.5	1841	1.4	2
PS1.44.4C	164.0	188.3	-40.7	1323	5.1	3
PS1.45.1A	170.0	190.7	-33.5	4136	2.2	2
PS1.46.1A	176.3	190.9	-31.6	5632	2.2	2
PS1.47.2A	182.0	192.4	-33.1	7448	1.9	2
PS1.47.3A	182.1	180.8	-38.9	7342	0.5	1
PS1.48.2A	187.6	190.0	-35.3	9233	1.8	3
PS1.49.1A	194.2	192.0	-33.9	4436	2.4	3
PS1.50.1A	200.4	185.2	-27.8	10590	3.7	2

Calabria
lower Sidufjall reversal record
LT component

Sample	Level	Dec.	Inc.	Int.	Err.	Q
Calabria /						
LS.48A	0.6	181.1	-13.6	287	10.4	5
LS.49A	2.6	177.3	-43.0	313	7.3	5
LS.50A	4.8	191.2	-32.2	418	7.8	4
LS.51A	5.7	182.0	-38.3	301	0.0	5
LS.52A	6.5	188.3	-39.6	406	3.1	4
LS.53.1A	7.4	191.6	-43.0	346	11.0	5
LS.54.1A	8.5	196.4	-46.6	648	7.7	4
LS.55.1A	9.3	206.6	-31.9	391	7.3	2
LS.56.1A	10.5	221.0	-37.0	330	16.9	4
LS.57.1A	11.5	199.4	-56.8	566	9.8	4
LS.13.2A	11.9	200.3	-37.0	327	21.4	3
LS.13.1A	12.2	208.9	-38.2	468	11.0	2
LS.13.1A	12.2	221.7	-37.2	191	15.6	3
LS.58.1A	12.3	206.8	-63.6	356	8.2	4
LS.14.1A	13.4	197.9	-39.2	624	14.5	4
LS.14.2A	13.4	175.0	-49.8	282	23.6	3
LS.59.1A	13.5	208.8	-47.8	491	11.1	2
LS.60.1A	14.1	206.8	-50.2	401	6.2	5
LS.15.1A	14.1	206.2	-33.3	622	8.5	2
LS.15.2A	14.7	204.3	-47.4	320	6.1	2
LS.61.1A	15.2	216.5	-37.0	609	16.9	4
LS.16.1A	15.2	198.6	-44.3	580	8.7	2
LS.16.1C	15.2	253.9	-34.2	641	14.9	4
LS.62.1A	16.1	200.8	-54.2	541	12.2	4
LS.17.1A	17.0	194.6	-33.7	445	7.5	4
LS.63.1A	17.2	187.4	-50.9	493	20.1	5
LS.17.2A	17.2	207.0	-42.0	538	24.3	3
LS.18.1A	17.9	199.3	-27.1	492	13.6	3
LS.18.2A	18.0	216.9	-20.5	474	14.9	2
LS.64.1A	18.1	143.2	-42.2	316	29.7	4
LS.65.1A	19.0	189.3	-46.8	501	4.9	2
LS.19.1A	19.5	204.6	-25.5	398	17.9	5
LS.19.2A	19.5	204.3	-18.9	261	11.0	4
LS.20.2A	20.4	200.4	-29.3	274	10.2	4
LS.20.1A	20.7	214.5	-56.5	170	13.6	4
LS.21.1A	21.4	366.7	52.3	419	5.1	4
LS.706.2	21.9	347.9	64.0	767	4.4	4
LS.21.2A	21.9	358.9	33.7	431	11.9	3
LS.22.2A	23.0	338.0	42.5	171	27.2	2
LS.22.1A	23.2	320.3	49.8	217	20.0	3
LS.23.1A	24.4	350.5	55.4	661	10.6	3
LS.23.2A	24.8	330.7	50.2	520	6.8	3

Sample	Level	Dec.	Inc.	Int.	Err.	Q
LS.27.1A	25.4	389.9	31.3	172	22.3	4
LS.24.1A	26.3	303.1	17.6	357	18.4	5
LS.24.2A	27.4	303.6	66.1	284	13.7	3
LS.28.1A	27.4	310.1	48.9	294	7.6	4
LS.25.2A	28.1	370.4	55.7	348	22.7	3
LS.30.1A	30.6	378.2	42.4	331	14.1	2
LS.31.1A	31.7	387.3	61.0	491	14.6	4

Calabria
lower Sidufjall reversal record
HT component

Sample	Level	Dec.	Inc.	Int.	Err.	Q
LS.47A	-1.2	185.2	-29.9	4246	2.5	4
LS.48A	0.6	185.2	-34.9	1169	2.3	2
LS.49A	2.6	192.3	-32.1	572	4.8	3
LS.50A	4.8	197.4	-33.9	641	2.4	2
LS.51A	5.7	197.8	-44.6	640	4.9	2
LS.52A	6.5	202.7	-38.2	587	5.8	3
LS.706.17	6.9	213.1	-52.2	412	2.8	4
LS.53.1A	7.4	191.4	-37.7	672	6.0	3
LS.706.16	7.9	207.7	-39.2	838	6.8	4
LS.54.1A	8.5	199.3	-37.4	612	5.7	3
LS.706.15	8.9	213.3	-37.2	853	6.7	4
LS.55.1A	9.3	203.1	-38.1	746	7.4	2
LS.706.14	9.9	212.0	-43.4	1043	3.2	2
LS.56.1A	10.5	207.3	-37.4	625	4.2	4
LS.706.13	10.9	211.9	-36.8	1006	2.6	2
LS.57.1A	11.5	200.7	-43.9	758	4.5	3
LS.706.12	11.9	206.7	-40.0	1134	3.7	3
LS.13.2A	11.9	201.1	-42.4	730	0.8	2
LS.13.1A	12.2	206.6	-38.4	740	4.8	3
LS.58.1A	12.3	193.0	-62.2	1618	5.2	3
LS.706.11	12.9	208.4	-41.0	964	4.8	2
LS.14.1A	13.4	228.3	-12.3	339	33.1	4
LS.14.2A	13.4	194.7	-56.4	667	2.5	3
LS.59.1A	13.5	195.0	-46.1	854	7.7	3
LS.706.10	13.9	211.3	-41.6	1379	4.2	2
LS.60.1A	14.1	194.5	-44.9	775	3.6	3
LS.15.1A	14.1	206.4	-40.8	691	5.4	2
LS.15.2A	14.7	205.9	-42.4	716	2.7	2
LS.706.9	14.9	210.6	-42.9	1320	5.2	3
LS.61.1A	15.2	201.7	-35.4	906	8.6	4
LS.16.1A	15.2	206.3	-46.0	973	3.3	3
LS.16.1C	15.2	200.5	-42.6	1217	2.4	2
LS.706.8	15.9	213.0	-45.0	1626	2.7	2
LS.62.1A	16.1	201.0	-41.1	1034	6.7	3
LS.706.7	16.9	205.8	-42.9	1011	4.4	3
LS.17.1A	17.0	208.1	-41.0	813	4.0	2
LS.63.1A	17.2	189.2	-47.2	673	8.5	3
LS.17.2A	17.2	198.3	-39.1	1140	4.6	3
LS.706.6	17.9	179.3	-22.9	342	3.4	4
LS.18.1A	17.9	202.8	-38.0	845	1.4	2
LS.18.2A	18.0	205.9	-39.7	688	2.8	3
LS.64.1A	18.1	178.6	-31.8	222	13.9	4
LS.706.5	18.9	184.8	-10.5	285	13.9	4
LS.65.1A	19.0	168.8	-30.6	392	14.6	5
LS.19.1A	19.5	198.0	-33.9	329	7.5	3
LS.19.2A	19.5	210.0	-28.7	247	15.2	2
LS.66.1A	19.8	340.1	42.1	179	0.0	5
LS.706.4	19.9	90.4	65.0	141	9.8	5
LS.20.2A	20.4	227.5	7.9	116	21.8	4
LS.706.3	20.9	410.5	63.2	286	10.9	4
LS.21.1A	21.4	368.9	38.6	287	6.8	4
LS.706.2	21.9	379.4	56.0	644	7.0	4
LS.21.2A	21.9	359.6	40.0	676	3.7	2
LS.706.1	22.9	385.2	48.1	1035	6.9	4
LS.22.2A	23.0	361.7	39.7	725	3.8	2
LS.22.1A	23.2	350.9	44.0	402	3.7	2
LS.23.1A	24.4	349.1	44.3	495	7.4	3
LS.23.2A	24.8	358.3	36.6	668	5.6	2
LS.27.1A	25.4	354.9	42.9	639	4.0	4
LS.24.1A	26.3	346.2	40.1	809	4.1	3
LS.24.2A	27.4	347.7	35.5	669	6.4	2
LS.28.1A	27.4	354.4	40.7	731	4.8	2
LS.25.1A	28.0	353.3	42.5	813	2.5	2
LS.25.2A	28.1	361.0	38.1	1019	2.6	2
LS.29.1A	28.9	345.7	39.9	721	4.7	3
LS.30.1A	30.6	362.2	37.8	804	5.2	2
LS.31.1A	31.7	366.7	45.0	1024	4.2	2

Calabria
upper Sidufjall reversal record
LT component

Sample	Level	Dec.	Inc.	Int.	Err.	Q
PS2.001A	4.7	379.1	-11.6	3073	4.2	1
PS2.002A	7.2	360.9	10.5	2368	5.8	1
PS2.003A	9.5	358.5	21.4	2332	6.9	1
PS2.004A	12.2	353.6	27.1	1064	17.3	1
PS2.005A	14.5	365.4	18.5	2208	6.5	1
PS2.006A	17.2	374.9	22.5	2834	2.5	1
PS2.007A	19.5	373.3	-6.2	1636	7.7	1
PS2.008A	22.2	398.0	-18.3	1641	4.7	2
PS2.009A	24.5	370.3	10.6	6281	6.4	1
PS2.010A	27.2	361.7	10.3	2170	7.3	1
PS2.010A	27.2	361.7	10.3	2170	7.3	1
PS2.011B	29.7	397.4	-8.3	3243	10.1	1
PS2.013B	34.7	356.6	-24.6	1967	5.1	1
PS2.014B	37.4	353.3	-0.4	2145	6.1	1
PS2.015B	39.7	389.7	-11.4	6466	2.6	1
PS2.016B	42.2	97.3	69.0	605	8.8	4
PS2.017B	44.5	200.9	71.5	525	18.7	3
PS2.018C	47.6	235.7	75.6	425	10.2	3
PS2.019B	49.5	288.2	54.7	300	19.9	4
PS2.020B	52.2	108.2	77.7	281	11.8	2
PS2.021B	54.7	362.4	72.8	513	6.5	2
PS2.022B	57.2	170.1	55.0	319	27.3	2
PS2.023B	59.5	171.4	22.7	164	40.7	4
PS2.024B	62.2	328.6	83.7	171	35.9	5
PS2.024D	62.6	357.1	68.9	188	11.8	4
PS2.025B	64.7	353.4	65.4	203	19.4	4
PS2.025C	64.9	408.8	55.4	315	6.9	1
PS2.026B	67.4	352.7	64.2	326	17.7	1
PS2.026B	67.4	352.7	64.2	326	17.7	2
PS2.026C	67.6	351.2	50.5	343	11.3	1
PS2.027B	69.9	333.0	64.5	215	11.1	2
PS2.029B	72.6	387.8	78.0	192	25.7	2
PS2.028B	72.6	319.9	65.7	248	14.6	3
PS2.030B	74.7	329.2	70.4	354	7.3	3
PS2.030C	74.9	360.3	66.3	420	7.9	1
PS2.031B	77.4	281.2	62.6	160	8.9	3
PS2.031B	77.4	442.8	58.4	120	12.2	3
PS2.031C	77.6	333.9	63.3	153	2.4	2
PS2.032A	79.5	362.8	51.8	225	14.9	4
PS2.032C	79.9	313.4	64.0	230	10.9	3
PS2.033C	82.6	359.9	44.2	210	15.5	4
PS2.034A	84.5	360.9	53.5	244	30.0	2
PS2.034C	84.9	318.0	65.1	256	9.3	2
PS2.035A	85.9	379.0	60.1	207	20.1	2
PS2.038A	89.5	177.9	-13.4	174	24.0	4
PS2.039A	89.7	172.5	-24.4	198	5.3	1
PS2.038C	89.9	190.1	-0.9	299	7.8	2
PS2.039B	89.9	173.9	-13.1	279	13.4	2
PS2.040A	92.2	198.9	-41.7	342	13.3	2
PS2.041A	93.2	215.2	-29.4	395	10.9	2
PS2.042A	94.5	200.1	-39.8	586	10.3	3
PS2.042C	94.9	210.0	-32.1	1022	5.6	2
PS2.043B	96.1	202.4	-30.3	1100	4.6	1
PS2.045A	97.0	193.6	-40.4	1350	2.7	2
PS2.045B	97.2	207.5	-43.0	1030	2.1	1

PS2.044A	97.2	198.7	-24.9	1023	3.2	1
PS2.046A	98.2	189.9	-26.2	698	5.8	1
PS2.046C	98.6	181.4	-20.4	439	5.9	1
PS2.047A	99.5	179.2	-10.2	486	9.4	1
PS2.048A	100.9	159.2	-37.2	650	7.1	1
PS2.049A	102.0	178.3	-28.4	177	18.3	3
PS2.050A	103.2	206.3	-36.9	196	17.9	4
PS2.050C	103.6	207.3	-26.2	367	6.1	1
PS2.051C	104.9	257.9	53.7	225	13.5	2
PS2.054A	106.9	118.7	6.4	144	21.9	2
PS2.055B	107.4	216.6	58.4	78	7.3	2
PS2.056A	107.7	191.5	-49.5	183	23.6	5
PS2.057A	108.2	132.1	-45.5	293	16.9	2
PS2.058A	108.7	235.9	-77.1	263	18.2	2
PS2.059A	109.2	173.8	-31.3	272	2.4	3
PS2.060A	109.5	256.4	-69.4	281	19.1	3
PS2.060C	109.9	218.6	-19.6	235	19.1	3
PS2.061A	110.2	215.8	-28.2	552	7.5	1
PS2.062A	110.7	202.6	-39.8	509	9.0	2
PS2.063A	111.0	212.1	-42.4	2214	4.1	1
PS2.064A	111.7	184.8	-32.1	539	11.8	2
PS2.065A	112.2	199.2	-41.4	472	10.1	2
PS2.066A	112.7	217.4	-36.1	200	31.4	3
PS2.067A	113.2	212.5	-23.7	448	12.2	1
PS2.068A	113.7	205.7	-43.5	657	6.7	2
PS2.069A	114.2	202.9	-40.2	2315	1.7	1
PS2.070A	114.7	202.0	-36.8	1204	4.8	1
PS2.071B	115.4	179.9	-39.5	1536	4.2	1
PS2.072A	115.7	191.4	-63.5	244	19.7	4
PS2.073A	116.2	188.2	-39.5	1974	2.6	1
PS2.074A	116.7	191.5	-41.2	1705	4.2	1
PS2.076A	117.7	203.1	-37.5	2090	2.6	1
PS2.077A	118.2	187.0	-34.3	1405	3.6	1
PS2.078A	118.5	201.7	-39.8	797	6.6	1
PS2.078C	118.9	181.8	-8.5	497	12.5	2
PS2.079A	119.0	186.1	-26.3	375	12.5	1
PS2.080B	119.9	204.4	-31.0	445	15.5	3
PS2.081B	120.4	231.5	-38.6	296	30.1	3
PS2.082A	120.5	211.6	-39.3	420	6.6	1
PS2.082C	120.9	221.0	-26.9	370	11.2	2
PS2.083A	121.2	180.4	-27.2	272	25.6	2
PS2.084B	121.9	182.6	-49.2	354	10.1	1
PS2.085B	122.4	194.7	-26.1	385	5.6	1
PS2.086A	122.7	201.2	-33.0	415	6.5	2
PS2.087A	123.2	189.7	-26.6	1342	8.8	1
PS2.088A	123.7	187.0	-30.1	560	7.9	2
PS2.089A	124.2	182.1	-31.7	847	5.3	1
PS2.090A	124.7	175.3	-36.8	340	19.4	3
PS2.092A	125.7	194.4	-41.9	2364	4.2	1
PS2.094A	126.7	197.9	-37.8	1988	3.4	1
PS2.096A	127.5	194.2	-44.1	2618	2.0	1
PS2.100A	129.5	179.9	-38.3	1234	13.8	3
PS2.101B	130.4	172.4	-42.2	1483	8.4	1
PS2.102A	130.7	178.1	-32.7	2424	3.2	2
PS2.103A	131.2	443.3	-49.0	2476	5.4	1
PS2.104A	131.7	187.9	-49.6	3106	4.6	2
PS2.105A	132.0	182.9	-45.0	2491	6.5	1
PS2.106A	132.7	182.0	-47.7	4663	3.0	3
PS2.107.2A	133.0	179.4	-47.5	1929	1.8	1
PS2.108A	133.7	175.4	-45.3	7640	1.9	1
PS2.109.2A	134.0	174.1	-44.9	2307	4.6	2
PS2.110.1A	134.7	192.2	-45.5	8948	8.4	2
PS2.111A	135.2	186.7	-19.1	899	4.0	1
PS2.112A	135.5	188.5	-43.6	2721	3.9	2
PS2.114A	136.5	193.1	-40.0	1342	10.0	2
PS2.115A	137.0	195.9	-38.3	1232	4.0	1
PS2.116A	137.5	206.5	-39.0	2791	13.2	2
PS2.117A	138.0	192.7	-40.0	5741	1.7	1
PS2.118A	138.5	202.9	-53.6	7751	1.8	3
PS2.119A	139.2	194.3	-40.9	6607	1.9	1
PS2.120A	139.7	192.0	-38.6	2515	12.9	3
PS2.121A	140.2	198.5	-35.9	2085	3.5	1
PS2.122A	140.7	191.0	-37.0	3395	15.5	3
PS2.123A	141.2	204.4	-41.8	6425	1.3	1
PS2.124A	141.9	198.2	-50.2	2546	5.4	3
PS2.125A	142.0	189.1	-37.2	1813	4.7	1
PS2.126A	142.7	200.3	-44.6	2384	16.3	3
PS2.127A	143.2	190.7	-33.2	2247	5.2	1
PS2.128A	143.7	190.8	-46.5	3265	9.9	3
PS2.129A	144.2	180.6	-31.3	1123	5.0	1
PS2.130A	144.7	206.8	-38.4	1497	12.4	4
PS2.131A	145.2	193.9	-42.8	2318	1.4	1
PS2.132A	145.7	182.3	-41.0	1996	19.5	3
PS2.133A	146.2	200.5	-32.5	1125	5.0	1
PS2.134A	146.7	174.9	-32.7	1655	6.3	3
PS2.136A	147.5	161.6	-32.9	1192	10.7	4
PS2.137A	148.2	191.9	-29.4	1154	3.2	1
PS2.138A	148.7	168.6	-34.9	1656	16.4	3
PS2.139A	149.0	187.0	-20.9	926	4.2	1
PS2.140A	149.5	163.9	-43.5	1097	21.9	4
PS2.141A	150.2	188.8	-31.2	1100	4.4	1
PS2.142A	150.7	192.9	-23.2	1654	7.9	3
PS2.143A	151.0	188.5	-26.4	906	7.7	1
PS2.144A	151.9	166.3	-32.0	1205	9.9	3
PS2.145A	152.4	185.7	-26.3	781	10.8	1
PS2.146A	152.9	147.1	-52.6	1291	9.8	4
PS2.147A	153.4	198.2	-34.2	849	13.8	1
PS2.148A	153.9	201.0	-15.8	729	12.3	3
PS2.149A	154.4	186.9	-30.3	810	6.8	1
PS2.150A	154.9	179.6	-43.9	1064	6.9	2
PS2.151A	155.4	189.9	-39.1	912	6.8	1
PS2.152A	155.9	207.1	-54.1	906	0.0	5

Sample	Level	Dec.	Inc.	Int.	Err.	Q
PS2.153A	156.4	424.4	-37.7	818	10.5	3
PS2.155A	157.4	182.8	-35.4	828	11.2	1
PS2.156A	157.9	148.4	-17.7	1687	5.1	4
PS2.157A	158.4	182.1	-32.6	944	11.1	1
PS2.158A	158.9	163.8	-55.2	1197	14.0	3
PS2.159A	159.4	185.0	-36.2	1114	11.6	1
PS2.160A	159.9	186.6	-41.1	1494	0.0	5
PS2.161A	160.4	177.7	-43.4	1471	9.3	1
PS2.162A	160.9	222.1	-17.1	2422	6.0	3
PS2.163A	161.4	192.5	-37.8	923	10.6	2
PS2.164A	161.9	198.7	-57.8	976	13.7	2
PS2.165A	162.4	191.2	-48.6	854	8.7	1
PS2.166A	162.9	175.0	-55.6	1517	18.8	3
PS2.167A	163.4	205.4	-33.8	765	9.6	1
PS2.168C	163.9	208.5	-28.8	920	11.9	3
PS2.169A	164.4	200.4	-43.4	1090	2.8	1
PS2.170A	164.9	193.8	-50.2	2229	8.8	2
PS2.171A	166.2	213.0	-40.5	1453	4.2	1
PS2.172A	167.4	204.9	-46.1	1961	3.4	2
PS2.173A	168.7	204.4	-46.0	1025	8.4	2
PS2.175A	171.2	209.4	-37.7	474	12.4	2
PS2.176A	172.4	172.1	-38.5	771	4.9	2
PS2.177A	173.7	210.3	-35.6	395	14.9	2
PS2.178A	174.9	164.5	-58.7	560	15.8	5
PS2.179A	176.2	212.7	-32.9	468	9.6	1
PS2.181A	178.7	200.8	-39.6	441	10.6	1
PS2.183A	181.2	206.5	-35.3	474	6.6	2
PS2.185A	183.7	196.3	-42.7	425	10.4	1
PS2.189A	188.7	203.0	-41.6	608	11.0	2
PS2.191A	192.4	201.1	-38.3	533	7.2	1
PS2.193A	197.4	195.6	-25.3	575	9.2	1
PS2.193A	197.4	204.1	-47.9	633	3.9	2
PS2.195A	202.4	204.9	-45.9	811	6.4	1

Calabria
upper Sidufjall reversal record
HT component

Sample	Level	Dec.	Inc.	Int.	Err.	Q
PS2.001A	4.7	373.2	19.8	1032	3.8	2
PS2.002A	7.2	371.0	15.4	944	10.4	3
PS2.003A	9.5	363.1	30.4	920	7.0	2
PS2.004A	12.2	369.7	36.3	1678	7.0	3
PS2.005A	14.5	372.0	25.3	1176	5.4	2
PS2.006A	17.2	378.2	27.5	1330	2.2	1
PS2.007A	19.5	363.8	-1.9	599	9.6	2
PS2.008A	22.2	384.1	4.2	976	2.8	1
PS2.009A	24.5	374.8	3.7	3006	5.1	1
PS2.010A	27.2	370.4	20.2	1684	5.2	2
PS2.011B	29.7	399.7	-0.6	2263	3.4	1
PS2.013B	34.7	371.5	-26.5	1261	8.8	2
PS2.014B	37.4	359.7	-5.7	1208	14.0	1
PS2.015B	39.7	394.9	-8.0	2200	6.0	1
PS2.016B	42.2	381.5	55.1	526	16.8	3
PS2.017B	44.5	210.0	-7.5	252	10.5	4
PS2.018C	47.6	213.0	72.2	272	15.4	4
PS2.019B	49.5	181.2	44.8	312	23.3	4
PS2.020B	52.2	158.0	60.9	320	14.3	3
PS2.021B	54.7	391.3	61.8	673	5.9	2
PS2.022B	57.2	406.1	59.5	455	18.8	4
PS2.023B	59.5	394.1	48.2	326	20.7	5
PS2.024B	62.2	387.4	30.3	535	4.4	4
PS2.024D	62.6	386.6	40.4	645	9.9	4
PS2.025B	64.7	387.8	34.5	618	7.9	3
PS2.025C	64.9	398.1	69.8	306	17.0	3
PS2.026B	67.4	379.6	37.6	638	7.2	2
PS2.026C	67.6	380.5	58.0	185	9.2	3
PS2.026C	67.6	373.5	17.4	367	11.3	3
PS2.027B	69.9	398.2	33.6	294	5.5	3
PS2.029B	72.6	383.9	42.1	191	5.1	2
PS2.028B	72.6	380.3	32.6	432	3.4	3
PS2.030B	74.7	377.4	34.5	258	22.7	4
PS2.030C	74.9	367.9	32.4	426	7.8	3
PS2.031B	77.4	359.5	35.2	137	14.6	4
PS2.031C	77.6	361.8	53.2	120	26.9	5
PS2.032C	79.9	380.0	29.8	225	13.9	3
PS2.033C	82.6	279.1	65.7	351	21.0	5
PS2.034A	84.5	193.6	-36.2	391	15.9	3
PS2.034C	84.9	189.4	50.7	113	19.1	3
PS2.035A	85.9	196.2	-39.3	450	16.4	3
PS2.039A	89.7	170.5	-8.0	312	12.4	5
PS2.038C	89.9	185.9	-19.8	279	11.6	4

Sample	Level	Dec.	Inc.	Int.	Err.	Q
PS2.039B	89.9	172.6	-18.3	419	4.4	4
PS2.040A	92.2	202.6	-40.6	445	14.1	2
PS2.041A	93.2	190.3	-5.1	443	8.6	4
PS2.042A	94.5	208.6	-32.7	479	13.5	2
PS2.042C	94.9	207.8	-40.0	375	15.5	3
PS2.043B	96.1	185.0	-23.7	609	7.7	4
PS2.045A	97.0	211.8	-22.3	353	17.0	3
PS2.045B	97.2	198.8	-35.9	447	19.4	4
PS2.046A	98.2	190.0	-28.0	603	6.3	2
PS2.046C	98.6	170.2	-25.8	441	5.9	3
PS2.047A	99.5	167.0	-16.2	384	5.4	3
PS2.048A	100.9	178.7	-37.4	459	7.9	3
PS2.050C	103.6	165.6	-18.3	287	8.9	3
PS2.051C	104.9	354.2	31.3	282	4.9	3
PS2.052A	105.4	349.1	-5.2	740	5.7	2
PS2.053A	106.0	366.1	25.1	753	2.4	3
PS2.054A	106.9	349.9	-5.2	806	5.2	2
PS2.055B	107.4	357.0	23.1	669	4.6	3
PS2.056A	107.7	351.1	-4.8	482	8.8	3
PS2.057A	108.2	360.0	-14.1	437	10.7	5
PS2.058A	108.7	361.6	15.9	685	13.1	2
PS2.059A	109.2	364.6	-12.4	231	16.5	5
PS2.060A	109.5	362.0	11.6	688	12.3	3
PS2.060C	109.9	358.9	19.2	588	4.0	4
PS2.061A	110.2	358.3	17.9	349	8.2	4
PS2.062A	110.7	347.9	-14.6	282	10.5	3
PS2.063A	111.0	231.4	-52.4	199	22.6	4
PS2.064A	111.7	351.5	-77.4	281	15.8	4
PS2.065A	112.2	185.6	-51.5	169	8.1	3
PS2.066A	112.7	297.7	-72.3	407	13.5	4
PS2.067A	113.2	189.0	-41.8	589	2.7	3
PS2.068A	113.7	201.7	-37.5	594	7.7	2
PS2.069A	114.2	185.2	-46.3	622	4.4	3
PS2.070A	114.7	342.4	-44.7	338	21.9	4
PS2.071B	115.4	156.1	-21.1	164	37.2	4
PS2.072A	115.7	361.8	-16.4	268	17.1	4
PS2.073A	116.2	188.8	-40.2	809	4.0	2
PS2.074A	116.7	179.3	-54.2	518	7.3	2
PS2.076A	117.7	192.6	-44.3	854	9.8	2
PS2.077A	118.2	170.1	-43.6	625	7.4	2
PS2.078A	118.5	193.8	-44.7	900	8.3	3
PS2.078C	118.9	186.5	-38.6	886	2.7	3
PS2.079A	119.0	183.9	-44.9	715	3.8	3
PS2.080B	119.9	190.8	-36.9	953	6.5	2
PS2.081B	120.4	187.8	-45.5	796	10.5	1
PS2.082A	120.5	206.2	-45.2	876	14.0	3
PS2.082C	120.9	181.8	-39.2	938	5.5	3
PS2.083A	121.2	181.9	-39.2	502	6.3	4
PS2.085B	122.4	181.1	-52.8	625	7.4	1
PS2.086A	122.7	203.2	-45.4	907	6.1	2
PS2.087A	123.2	179.8	-39.1	1206	6.3	3
PS2.088A	123.7	190.2	-44.9	1070	5.5	2
PS2.089A	124.2	179.1	-43.3	1068	6.5	3
PS2.090A	124.7	191.6	-46.2	1076	5.0	2
PS2.092A	125.7	187.1	-39.9	1546	5.5	1
PS2.094A	126.7	192.9	-35.6	1750	1.7	1
PS2.096A	127.5	193.4	-36.6	1662	2.0	1
PS2.101B	130.4	185.9	-34.8	1938	1.5	4
PS2.102A	130.7	183.8	-34.3	2104	3.4	4
PS2.103A	131.2	439.8	-38.5	2012	0.8	4
PS2.104A	131.7	186.6	-36.8	2078	1.6	3
PS2.105A	132.0	185.4	-33.2	2017	0.5	4
PS2.107.2A	133.0	178.4	-34.2	2147	0.7	4
PS2.108A	133.7	178.8	-35.6	2047	1.2	3
PS2.109.2A	134.0	181.5	-33.6	2275	1.0	3
PS2.110.1A	134.7	188.7	-28.9	2127	0.8	4
PS2.111A	135.2	187.3	-27.0	2137	1.3	4
PS2.114A	136.5	194.2	-34.9	2102	6.9	4
PS2.115A	137.0	188.1	-27.7	2148	1.2	4
PS2.116A	137.5	190.2	-31.5	2309	1.5	4
PS2.117A	138.0	188.1	-27.4	2690	1.5	4
PS2.119A	139.2	193.3	-24.8	2831	1.5	4
PS2.120A	139.7	189.7	-32.0	2234	2.0	4
PS2.121A	140.2	191.7	-19.4	1751	3.4	4
PS2.122A	140.7	184.7	-21.6	1547	4.2	4
PS2.123A	141.2	198.3	-22.4	2115	0.6	4
PS2.124A	141.9	190.4	-28.6	1916	5.3	4
PS2.125A	142.0	186.2	-22.3	1978	0.4	4
PS2.126A	142.7	179.4	-29.7	1317	2.4	3
PS2.127A	143.2	185.7	-20.3	1681	2.2	4
PS2.128A	143.7	186.3	-28.5	1846	0.6	4
PS2.129A	144.2	183.1	-23.5	1903	1.5	4
PS2.130A	144.7	184.0	-26.2	2022	5.2	4
PS2.131A	145.2	189.0	-30.7	2300	1.5	4
PS2.132A	145.7	182.8	-37.2	2336	1.9	4
PS2.133A	146.2	189.5	-30.6	2515	0.6	4
PS2.134A	146.7	182.0	-31.2	2330	0.7	3
PS2.136A	147.5	185.5	-33.9	3511	4.8	4
PS2.137A	148.2	187.5	-32.3	3199	0.4	3
PS2.138A	148.7	181.2	-35.0	2726	1.4	4
PS2.139A	149.0	190.8	-32.9	3030	0.5	3
PS2.140A	149.5	185.8	-32.8	3063	3.1	4
PS2.141A	150.2	189.1	-31.3	3828	0.6	2
PS2.142A	150.7	185.7	-34.6	4337	4.7	5
PS2.143A	151.0	191.4	-33.4	3523	0.5	2
PS2.144A	151.9	192.3	-34.3	2800	2.2	3
PS2.145A	152.4	189.8	-32.5	3257	0.6	3
PS2.146A	152.9	187.1	-35.5	2828	6.3	4

Reversal record data

Sample	Level	Dec.	Inc.	Int.	Err.	Q
PS2.147A	153.4	191.8	-34.5	3079	1.9	4
PS2.148A	153.9	189.8	-36.9	2856	4.4	4
PS2.149A	154.4	190.4	-34.6	2752	3.4	4
PS2.150A	154.9	184.1	-38.8	2476	1.9	4
PS2.151A	155.4	191.2	-33.4	2987	0.7	3
PS2.152A	155.9	183.5	-33.6	2632	4.2	3
PS2.153A	156.4	442.5	-43.9	2950	1.0	3
PS2.155A	157.4	183.5	-34.7	2934	0.8	3
PS2.156A	157.9	181.3	-34.9	2874	3.5	4
PS2.157A	158.4	185.4	-33.3	3537	0.4	3
PS2.158A	158.9	179.8	-39.7	3559	0.7	3
PS2.159A	159.4	186.0	-35.3	4452	1.4	3
PS2.160A	159.9	183.8	-38.4	4613	4.5	4
PS2.161A	160.4	185.7	-32.4	5785	0.6	3
PS2.162A	160.9	186.5	-32.7	4775	1.5	4
PS2.163A	161.4	191.0	-34.8	4655	0.6	3
PS2.164A	161.9	195.5	-39.8	3374	3.0	4
PS2.165A	162.4	205.7	-38.8	2995	2.2	3
PS2.166A	162.9	204.4	-38.7	2549	2.4	3
PS2.167A	163.4	212.2	-36.9	2196	0.7	3
PS2.168C	163.9	209.3	-38.6	2149	2.4	4
PS2.169A	164.4	213.8	-38.1	1932	1.2	3
PS2.170A	164.9	219.8	-39.2	1554	0.8	3
PS2.171A	166.2	226.9	-35.3	2336	6.6	4
PS2.176A	172.4	196.5	-44.0	1306	1.2	4
PS2.177A	173.7	204.7	-36.2	1304	1.6	3
PS2.178A	174.9	193.7	-39.6	1404	2.8	4
PS2.179A	176.2	199.8	-39.4	1633	0.4	3
PS2.181A	178.7	201.2	-40.6	1497	0.5	3
PS2.183A	181.2	200.9	-39.8	1429	0.6	3
PS2.185A	183.7	210.5	-38.7	1250	1.5	3
PS2.189A	188.7	198.3	-42.5	1836	0.8	3
PS2.191A	192.4	195.9	-40.1	1673	0.8	3
PS2.193A	197.4	199.0	-37.0	1455	1.2	3
PS2.195A	202.4	194.5	-39.7	2853	0.8	3
PS2.197A	207.4	198.8	-39.9	2664	0.6	4
PS2.029B	72.6	150.6	39.7	80	6.3	5
PS2.034C	84.9	389.2	61.2	120	20.7	5
PS2.035A	85.9	423.9	42.9	117	11.2	5
PS2.040A	92.2	430.3	49.7	102	5.6	5
PS2.042A	94.5	395.6	61.3	130	26.3	5
PS2.045A	97.0	385.0	34.6	82	14.6	5
PS2.046A	98.2	408.5	60.5	90	9.8	5
PS2.048A	100.9	423.6	56.9	90	14.6	5
PS2.050A	103.2	400.7	20.9	158	19.3	5
PS2.056A	107.7	390.7	41.8	165	7.2	4
PS2.058A	108.7	442.0	63.7	92	7.0	5
PS2.060A	109.5	422.8	63.7	134	14.4	5
PS2.062A	110.7	394.8	24.0	101	7.6	5

Sample	Level	Dec.	Inc.	Int.	Err.	Q
PS2.064A	111.7	415.0	68.2	97	27.0	5
PS2.066A	112.7	403.5	59.0	99	20.5	5
PS2.068A	113.7	409.3	28.2	112	19.2	5
PS2.070A	114.7	423.0	56.7	128	2.9	5
PS2.078A	118.5	403.1	55.0	35	18.4	5
PS2.082A	120.5	439.0	39.9	84	3.7	5

Calabria
lower Nunivak reversal record
LT component

Sample	Level	Dec.	Inc.	Int.	Err.	Q
PS5.01.4A	-1.3	189.0	-11.0	125	23.1	3
PS5.02.4A	2.3	148.9	-33.5	63	20.7	5
PS5.03.2A	5.9	199.5	-21.7	117	18.2	2
PS5.03.4A	6.0	178.0	-33.2	115	16.7	4
PS5.05.2A	12.9	200.7	-28.0	138	4.8	2
PS5.06.3A	16.7	202.8	-22.1	147	7.7	3
PS5.07.2A	20.0	179.2	-22.7	79	20.6	3
PS5.07.3A	20.2	245.5	-39.2	84	25.3	5
PS5.08.3A	22.2	267.3	10.7	36	37.2	5
PS5.09.3A	24.5	204.5	-43.9	242	22.0	3
PS5.09.2A	24.6	183.6	-19.2	154	4.6	3
PS5.10.3A	27.9	213.9	-43.8	329	4.8	1
PS5.11.2A	29.7	184.2	-22.2	213	7.2	1
PS5.11.3A	29.7	179.3	-46.2	393	0.8	1
PS5.12.3A	32.5	115.3	-33.5	248	7.0	4
PS5.13.2A	35.1	203.3	-27.7	151	7.7	2
PS5.13.3A	35.3	178.6	-49.1	222	7.7	2
PS5.14.1A	37.5	163.1	-61.4	92	20.4	3
PS5.15.1A	39.6	213.0	-48.4	97	0.0	4
PS5.15.3A	39.7	160.8	-50.5	308	14.4	1
PS5.15.2A	39.7	190.1	-29.0	303	0.5	2
PS5.15.3A	39.7	178.5	-59.2	272	18.8	2
PS5.16.1A	42.4	251.7	-44.3	504	10.7	4
PS5.16.2A	42.5	207.6	-30.8	396	13.1	2
PS5.16.1B	42.7	207.1	-43.0	433	18.5	2
PS5.16.1B	42.7	223.8	-59.8	231	24.9	3
PS5.17.3A	44.1	110.7	-66.6	226	23.8	3
PS5.17.3A	44.1	225.6	-32.5	245	32.2	4
PS5.17.2A	44.3	200.5	-18.0	270	11.2	2
PS5.17.1A	44.4	254.9	-74.8	351	16.8	4
PS5.18.3A	47.0	242.3	-48.2	104	10.6	4
PS5.18.3A	47.0	236.6	-51.2	116	21.0	4
PS5.18.2A	47.1	169.3	-15.4	139	12.7	4
PS5.18.1A	47.3	303.9	-71.6	422	9.5	4
PS5.19.2A	49.6	192.5	-25.5	107	12.5	2
PS5.19.3A	49.6	189.9	-45.9	80	25.7	3
PS5.19.3A	49.6	185.4	-15.0	71	33.8	5
PS5.19.1A	49.8	238.1	-62.3	238	8.7	4
PS5.20.2A	52.1	193.2	-18.6	121	10.2	3
PS5.20.4B	52.2	397.7	-12.0	135	8.8	4
PS5.20.4B	52.2	235.3	-50.4	102	36.5	5
PS5.21.3A	54.9	395.4	12.1	199	12.0	3
PS5.21.3A	54.9	434.7	-36.6	39	15.3	4
PS5.21.2A	55.1	185.2	11.7	93	13.2	4
PS5.22.3A	57.6	422.9	5.2	137	8.2	4
PS5.22.3A	57.6	390.4	31.7	96	24.6	4
PS5.22.1A	57.7	381.6	37.3	160	19.9	4
PS5.22.2A	57.9	373.4	77.6	79	18.3	3
PS5.23.4A	60.7	364.5	42.9	133	13.0	2
PS5.23.2A	60.7	399.7	61.1	274	9.3	3
PS5.23.4A	60.7	370.6	55.0	313	10.7	3
PS5.23.1A	60.8	397.4	30.1	249	17.6	3
PS5.24.2A	63.9	359.6	49.7	213	11.8	2
PS5.24.1A	64.0	368.3	46.5	302	10.3	1
PS5.24.1B	64.1	374.9	36.9	190	13.1	2
PS5.24.1B	64.1	372.2	59.0	128	27.0	3
PS5.25.1A	66.7	389.0	66.8	183	10.4	2
PS5.25.2A	67.0	398.2	57.8	260	10.6	2
PS5.25.2A	67.0	390.0	61.2	194	15.7	4
PS5.25.4B	67.1	354.1	51.5	377	18.5	2
PS5.26.2A	69.7	414.2	56.2	185	7.7	2
PS5.26.3A	69.9	348.6	59.3	37	20.1	4
PS5.26.4A	70.0	394.5	54.6	350	13.1	2
PS5.26.4A	70.0	381.1	38.2	149	31.9	2
PS5.27.4A	72.8	380.9	28.2	265	8.4	2
PS5.27.4A	72.8	374.0	30.1	240	15.6	2
PS5.27.2A	73.2	384.6	43.1	454	8.5	2
PS5.28.3B	76.3	358.0	52.1	274	10.2	1
PS5.28.2A	76.3	372.5	44.0	353	10.3	2
PS5.28.3B	76.3	388.5	51.1	236	15.6	4
PS5.29.2A	79.1	367.7	6.8	145	20.8	2
PS5.30.2A	82.2	385.4	55.1	300	6.8	1
PS5.31.2A	84.5	359.8	58.0	368	15.8	3
PS5.31.3A	84.5	365.4	23.7	690	7.2	3
PS5.32.2A	87.2	378.5	58.5	256	7.7	2
PS5.32.3A	87.2	386.0	34.9	778	5.7	2
PS5.33.2A	89.6	374.6	52.9	268	9.8	3
PS5.33.3A	89.8	406.3	5.5	769	7.2	2
PS5.34.2A	92.0	375.6	51.9	299	7.5	2
PS5.36.2A	96.5	364.7	45.2	316	8.8	2
PS5.36.3A	96.7	412.5	13.1	392	11.2	4
PS5.37.3A	98.6	302.9	-78.6	31	24.2	5
PS5.38.2A	101.1	344.8	31.9	66	23.0	1
PS5.38.3A	101.1	416.7	73.8	62	19.9	5
PS5.39.3A	103.6	396.7	49.3	106	16.6	3
PS5.40.2A	106.0	345.4	74.2	129	8.4	2
PS5.40.3A	106.0	390.4	49.3	229	20.3	4
PS5.42.2A	110.6	365.4	46.8	133	14.7	2
PS5.44.2A	116.0	140.4	10.0	41	24.0	2
PS5.46.3A	120.4	323.5	22.6	71	15.0	4
PS5.46.2A	120.9	384.7	61.1	131	18.9	3

Reversal record data

Sample	Level	Dec.	Inc.	Int.	Err.	Q
PS5.47.3A	123.4	350.5	58.1	338	11.0	3
PS5.48.2A	125.9	348.2	38.7	442	8.6	1
PS5.48.3A	126.2	398.1	51.7	386	0.0	4
PS5.49.3A	128.0	315.4	50.7	321	3.5	5
PS5.50.2A	130.9	364.4	34.5	180	22.2	1
PS5.51.3A	133.4	358.8	55.8	265	24.5	4
PS5.52.2A	136.3	354.2	48.8	214	20.4	2
PS5.53.4A	141.2	381.0	66.6	634	20.0	4
PS5.54.3A	146.2	390.7	46.6	1608	11.8	4

Calabria
lower Nunivak reversal record
HT component

Sample	Level	Dec.	Inc.	Int.	Err.	Q
PS5.01.4A	-1.3	187.7	-22.8	631	4.1	3
PS5.03.2A	5.9	199.5	-30.8	345	5.2	3
PS5.05.2A	12.9	201.4	-32.9	1022	3.4	3
PS5.06.3A	16.7	192.6	-35.9	642	1.1	4
PS5.07.2A	20.0	195.0	-26.1	322	1.0	2
PS5.07.3A	20.2	190.3	-33.0	575	2.4	4
PS5.08.3A	22.2	194.9	-28.8	516	4.9	5
PS5.09.3A	24.5	188.5	-33.9	620	6.6	5
PS5.09.2A	24.6	196.0	-35.1	425	6.6	3
PS5.10.3A	27.9	192.2	-37.4	731	3.3	3
PS5.11.2A	29.7	198.8	-42.1	507	4.5	3
PS5.11.3A	29.7	193.0	-31.4	884	2.5	4
PS5.12.3A	32.5	180.5	-35.0	792	3.3	3
PS5.13.2A	35.1	194.7	-33.8	354	5.9	4
PS5.13.3A	35.3	193.0	-35.2	499	2.4	4
PS5.14.1A	37.5	195.4	-38.7	354	2.6	5
PS5.15.1A	39.6	189.9	-40.6	1809	1.8	3
PS5.15.2A	39.7	197.5	-37.4	1472	1.4	2
PS5.15.3A	39.7	198.4	-33.3	1063	2.9	3
PS5.15.3A	39.7	199.2	-40.8	1173	3.5	4
PS5.16.1A	42.4	195.9	-36.9	1162	2.2	4
PS5.16.1B	42.7	196.5	-40.8	1440	2.0	4
PS5.17.3A	44.1	204.3	-28.1	906	1.6	4
PS5.17.3A	44.1	207.4	-17.3	750	3.2	4
PS5.17.2A	44.3	198.7	-36.0	743	2.7	3
PS5.17.1A	44.4	202.4	-31.9	831	4.4	4
PS5.18.3A	47.0	196.2	-36.2	665	6.6	4
PS5.18.3A	47.0	189.4	-27.3	679	2.5	4
PS5.18.1A	47.3	195.4	-38.1	763	2.7	4
PS5.19.3A	49.6	178.9	-22.2	620	5.6	4
PS5.19.3A	49.6	190.3	-8.4	600	2.3	4
PS5.19.1A	49.8	181.5	-12.7	644	3.5	5
PS5.20.2A	52.1	188.2	-18.6	576	0.6	4
PS5.20.4B	52.2	198.2	-11.0	454	3.2	4
PS5.20.4B	52.2	200.0	-0.7	355	6.0	4
PS5.20.1A	52.5	180.7	-18.6	602	1.0	3
PS5.21.1A	54.6	193.0	-10.6	485	0.6	4
PS5.21.3A	54.9	211.5	-11.1	219	14.5	4
PS5.21.3A	54.9	215.2	11.3	194	18.5	5
PS5.21.2A	55.1	186.6	5.8	547	3.5	5
PS5.22.3A	57.6	208.0	40.4	346	6.6	3
PS5.22.3A	57.6	205.2	-3.2	257	9.0	4
PS5.22.1A	57.7	196.2	22.0	266	12.3	5

Sample	Level	Dec.	Inc.	Int.	Err.	Q
PS5.23.4A	60.7	191.6	1.8	284	10.8	3
PS5.23.4A	60.7	149.1	73.8	268	8.6	3
PS5.23.2A	60.7	160.4	68.8	348	16.8	5
PS5.23.1A	60.8	169.6	32.3	217	18.7	5
PS5.24.2A	63.9	188.3	78.9	341	7.6	3
PS5.24.1A	64.0	363.8	65.9	352	9.2	3
PS5.24.1B	64.1	290.2	69.4	353	5.3	3
PS5.24.1B	64.1	232.2	79.4	162	3.8	4
PS5.25.1A	66.7	204.5	78.2	246	4.4	5
PS5.25.2A	67.0	384.6	63.4	431	2.1	2
PS5.25.2A	67.0	347.2	61.8	348	4.3	3
PS5.25.4B	67.1	371.3	48.8	335	5.3	3
PS5.26.2A	69.7	384.3	53.7	357	3.9	3
PS5.26.4A	70.0	370.4	64.1	667	4.0	2
PS5.26.4A	70.0	359.3	59.1	507	9.2	3
PS5.27.4A	72.8	369.3	59.4	493	8.4	2
PS5.27.4A	72.8	350.8	40.4	302	8.0	3
PS5.27.2A	73.2	372.0	53.5	612	2.6	2
PS5.28.3B	76.3	358.0	57.0	678	0.9	2
PS5.28.2A	76.3	380.8	45.0	886	1.9	3
PS5.28.3B	76.3	349.7	25.4	380	8.0	4
PS5.29.2A	79.1	377.6	47.0	1046	2.4	3
PS5.30.2A	82.2	370.9	64.9	639	3.8	2
PS5.31.2A	84.5	359.5	56.8	749	2.2	2
PS5.31.3A	84.5	395.2	32.4	569	27.7	5
PS5.32.2A	87.2	370.6	78.9	640	10.6	4
PS5.33.2A	89.6	313.2	75.7	501	5.1	3
PS5.34.2A	92.0	367.9	63.4	530	1.4	2
PS5.36.2A	96.5	380.7	58.5	644	4.3	3
PS5.38.2A	101.1	388.8	78.0	171	5.2	3
PS5.39.3A	103.6	386.5	42.3	420	7.8	5
PS5.40.2A	106.0	370.8	54.2	375	4.8	3
PS5.40.3A	106.0	388.2	46.1	651	8.6	4
PS5.41.4A	108.0	406.5	40.1	380	7.1	5
PS5.42.2A	110.6	381.5	52.2	395	0.6	3
PS5.46.2A	120.9	363.8	41.8	386	4.8	3
PS5.47.3A	123.4	365.0	40.1	808	3.4	5
PS5.48.2A	125.9	369.9	41.9	1783	0.4	1
PS5.48.3A	126.2	361.3	33.3	1328	5.0	4
PS5.49.3A	128.0	367.7	29.5	869	5.9	5
PS5.50.3A	130.7	359.4	36.7	888	17.1	5
PS5.50.2A	130.9	370.5	42.9	1385	1.3	1
PS5.51.3A	133.4	364.4	33.4	1005	4.3	4
PS5.52.2A	136.3	370.2	42.4	1080	1.6	2
PS5.53.4A	141.2	360.6	20.6	2019	5.9	4
PS5.54.3A	146.2	367.9	32.7	3318	1.8	4
PS5.55.3A	151.7	353.7	29.2	1717	3.2	4

Calabria
upper Nunivak (1986) reversal record
LT component

Sample	Level	Dec.	Inc.	Int.	Err.	Q
PS6.01.4A	3.4	359.0	53.5	707	10.8	4
PS6.04.1A	12.2	383.0	48.1	667	20.6	3
PS6.04.6A	13.5	369.5	62.6	741	5.7	4
PS6.05.1A	14.8	373.5	67.8	311	4.5	4
PS6.06.2C	15.6	370.9	58.9	818	13.1	2
PS6.06.1A	16.0	336.8	49.1	410	16.9	4
PS6.07.1A	17.5	384.0	65.6	400	5.0	4
PS6.08.2C	17.9	369.5	57.9	561	7.4	2
PS6.08.1A	18.6	351.2	35.2	485	7.0	4
PS6.09.1A	20.3	372.2	48.3	342	4.0	4
PS6.10.1B	21.2	366.2	45.3	249	23.9	2
PS6.10.1A	21.4	395.0	62.5	338	2.2	4
PS6.11.1B	23.1	355.1	40.5	208	11.4	2
PS6.11.1A	23.3	363.6	51.7	205	2.7	4
PS6.12.3C	24.2	345.2	58.1	382	7.2	2
PS6.12.1A	24.4	371.6	54.8	91	1.9	4
PS6.13.1C	25.7	355.9	56.3	207	11.3	2
PS6.13.1A	26.1	375.6	66.5	77	6.0	3
PS6.14.1C	27.2	343.5	56.5	43	14.1	2
PS6.14.1A	27.6	367.7	60.7	157	1.8	3
PS6.15.1B	28.4	360.7	57.3	44	0.0	5
PS6.16.1A	29.7	359.3	64.2	114	5.0	3
PS6.17.1A	31.4	371.2	66.3	168	8.3	3
PS6.18.1A	32.2	290.1	40.3	192	13.7	3
PS6.18.2B	32.2	362.8	65.2	311	12.2	3
PS6.19.1A	33.1	346.3	60.3	266	11.9	4
PS6.20.2A	34.7	320.1	59.9	128	31.0	2
PS6.20.1A	34.7	333.2	58.3	153	8.4	4
PS6.22.1A	38.0	303.1	43.8	222	17.5	4
PS6.24.1A	41.6	205.5	-43.6	290	20.7	4
PS6.25.1A	44.0	212.8	-52.6	55	12.9	3
PS6.34.1A	62.7	204.7	-21.8	54	11.9	4
PS6.35.1A	65.3	148.5	-35.7	25	27.7	3
PS6.38.1C	71.5	222.2	-42.2	84	9.1	5

Calabria
upper Nunivak (1986) reversal record
HT component

Sample	Level	Dec.	Inc.	Int.	Err.	Q
PS6.01.1CL	2.4	377.8	70.8	631	7.5	5
PS6.01.3AL	2.8	378.4	60.7	851	10.5	4
PS6.01.4B	3.2	373.2	50.3	1234	4.6	2
PS6.01.1CU	3.5	355.3	58.2	851	2.2	4
PS6.01.3AU	3.8	351.6	52.8	838	4.0	3
PS6.02.2AL	6.2	365.1	58.5	1296	1.2	1
PS6.02.3AL	6.3	366.9	48.3	2216	3.3	3
PS6.02.2AU	7.3	361.9	59.8	1468	1.5	3
PS6.02.3AU	7.4	358.5	56.8	2162	1.8	3
PS6.03.3AL	9.0	362.3	44.7	824	4.1	3
PS6.03.2AL	9.1	353.4	55.9	1298	2.6	2
PS6.03.2AU	10.1	354.5	45.3	1082	1.7	4
PS6.03.3AU	10.1	349.9	49.3	1309	4.7	5
PS6.04.1A	12.2	368.6	56.2	1358	1.9	1
PS6.04.2AL	12.2	350.2	54.3	1317	1.1	2
PS6.04.3AL	12.2	343.8	50.4	1663	4.8	3
PS6.04.4AL	12.3	365.6	43.6	1243	2.0	3
PS6.04.2AU	13.2	355.0	54.8	1224	1.8	4
PS6.04.3AU	13.2	347.9	46.6	1658	3.1	4
PS6.04.4AU	13.3	362.1	58.4	1615	5.2	4
PS6.05.4AL	14.3	368.7	58.4	1610	6.3	3
PS6.05.2AL	14.4	353.5	63.3	1846	1.7	2
PS6.05.3AL	14.4	348.8	56.5	1444	1.8	3
PS6.05.4AU	15.3	359.2	61.0	1487	1.1	3
PS6.05.2AU	15.4	349.9	56.5	425	4.0	3
PS6.06.4AL	15.4	361.0	53.0	1474	4.9	3
PS6.05.3AU	15.4	350.9	62.2	2083	3.0	5
PS6.06.3AL	15.5	358.9	61.3	1869	2.4	3
PS6.06.2C	15.6	364.6	60.9	1329	2.6	2
PS6.06.2AL	16.0	360.0	64.7	998	4.0	3
PS6.07.2BL	16.4	360.5	53.5	1298	9.6	3
PS6.06.4AU	16.4	343.3	61.3	1258	2.9	4
PS6.06.3AU	16.5	356.4	56.3	1976	1.0	2
PS6.07.2AL	16.6	352.9	54.3	728	4.4	4
PS6.07.3AL	16.8	352.8	57.1	1899	2.3	3
PS6.06.2AU	17.0	363.3	70.0	1612	1.9	4
PS6.07.2BU	17.5	367.3	52.7	785	4.9	3
PS6.07.2AU	17.6	356.9	53.4	874	2.7	3
PS6.08.2C	17.9	378.5	56.1	617	4.1	1
PS6.07.3AU	17.9	365.0	54.8	1781	1.0	2
PS6.08.3CL	17.9	377.1	49.2	842	8.3	2
PS6.08.3AL	18.2	367.1	59.9	1055	2.3	3
PS6.08.2AL	18.3	361.8	65.3	682	5.6	4
PS6.08.3CU	19.0	380.9	52.6	747	3.7	3
PS6.08.3AU	19.3	372.2	59.4	1173	2.0	3
PS6.08.2AU	19.4	372.7	59.6	447	2.4	4
PS6.09.2CL	19.5	371.8	39.8	620	4.1	3
PS6.09.3AL	19.8	373.8	56.2	911	4.5	3
PS6.09.2AL	20.0	348.7	49.2	300	3.9	3
PS6.09.2CU	20.5	359.8	57.9	634	5.4	3
PS6.09.3AU	20.9	370.3	51.3	1082	2.3	2
PS6.10.3AL	20.9	356.8	51.8	974	2.3	3
PS6.09.2AU	21.1	336.0	59.1	312	3.2	4
PS6.10.1B	21.2	373.7	54.2	336	4.1	2
PS6.10.3AU	21.9	340.4	53.4	919	1.7	3
PS6.11.2AL	22.5	318.4	53.3	142	7.3	4
PS6.11.3AL	22.5	336.0	54.7	400	1.7	4
PS6.12.3AL	24.0	332.3	63.9	112	12.1	4
PS6.12.3C	24.2	334.3	60.9	177	9.0	4
PS6.13.3AL	25.6	310.0	55.5	159	4.1	5
PS6.13.1C	25.7	319.1	78.0	103	5.6	3
PS6.14.3AL	26.9	224.3	-42.1	170	4.0	4
PS6.15.3DL	27.8	240.2	-30.7	372	14.1	4
PS6.14.2AU	28.2	261.8	22.0	113	1.1	2
PS6.15.3DU	28.8	221.0	-42.1	424	8.3	4
PS6.16.2DL	28.9	211.9	-41.3	526	11.0	4
PS6.16.3AL	29.3	244.4	-16.6	380	8.3	4
PS6.16.2AL	29.7	254.2	26.2	269	6.1	5
PS6.16.2DU	29.9	232.1	-48.5	446	3.2	3
PS6.17.2DL	30.0	233.2	-40.7	426	9.4	3
PS6.17.3CL	30.2	243.8	-29.7	510	3.1	3
PS6.16.3AU	30.4	236.3	-30.4	454	1.3	5
PS6.16.2AU	30.7	243.1	-47.3	345	9.0	5
PS6.17.2AL	30.9	238.8	-28.6	484	1.6	3
PS6.17.2DU	31.0	208.4	-55.0	835	5.5	3
PS6.18.2DL	31.0	217.6	-50.5	803	6.8	4
PS6.18.3BL	31.2	218.4	-43.2	681	5.1	4
PS6.17.3CU	31.3	228.6	-37.2	689	2.0	5
PS6.18.2AL	31.9	214.9	-45.2	280	12.9	5
PS6.18.2DU	32.0	203.8	-53.4	881	14.0	4
PS6.18.2B	32.2	217.8	-47.8	628	2.6	1
PS6.18.1A	32.2	210.6	-49.5	494	4.9	5
PS6.18.3BU	32.3	213.4	-37.4	813	2.9	3
PS6.18.2AU	32.9	206.7	-50.8	250	5.0	4
PS6.19.3AL	33.1	224.3	-6.5	209	4.8	4
PS6.19.3AU	34.1	226.0	-34.9	353	4.3	5
PS6.20.2A	34.7	231.2	-35.0	284	5.1	4
PS6.20.3AU	35.2	231.2	13.4	61	5.8	5
PS6.21.3AL	35.4	225.7	-34.9	696	2.8	5
PS6.21.3AU	36.4	223.6	-34.0	619	2.6	5
PS6.23.1A	40.9	178.5	-49.8	754	4.0	3

Sample	Level	Dec.	Inc.	Int.	Err.	Q
PS6.24.1A	41.6	205.2	-45.9	976	4.5	4
PS6.25.1A	44.0	191.6	-52.1	324	5.4	4
PS6.27.1B	48.2	198.2	-65.0	58	5.0	4

Calabria
upper Nunivak (1987) reversal record
LT component

Sample	Level	Dec.	Inc.	Int.	Err.	Q
UN.101.A	17.5	375.4	65.2	456	12.5	2
UN.103.A	18.7	373.3	62.8	587	10.9	2
UN.106.A	19.9	389.2	60.7	278	6.8	3
UN.109.C	21.1	357.9	58.1	223	7.7	2
UN.112.A	22.7	347.8	54.9	268	6.0	2
UN.113.C	23.0	337.6	57.6	183	9.3	2
UN.114.A	23.4	379.2	55.4	200	7.2	2
UN.114.D	23.4	355.8	54.2	169	7.0	2
UN.117.A	24.6	361.5	43.7	255	8.7	3
UN.117.C	24.7	347.3	42.3	145	9.7	2
UN.118.C	25.2	346.2	58.6	200	6.2	2
UN.119.A	26.0	342.1	41.9	127	7.7	2
UN.120.C	26.2	355.4	24.3	93	19.3	4
UN.121.C	26.7	346.3	54.8	158	8.1	2
UN.121.A	27.0	344.0	54.8	121	8.6	2
UN.122.C	27.1	396.8	56.5	104	17.6	5
UN.123.A	27.4	345.7	39.2	163	5.2	2
UN.124.BL	27.4	327.1	43.3	88	23.7	3
UN.123.C	27.5	350.9	43.2	129	7.4	2
UN.125.BL	27.9	358.6	57.9	136	18.7	4
UN.126.BL	28.3	369.9	59.3	138	10.3	3
UN.125.A	28.4	346.7	46.3	153	8.7	2
UN.124.BU	28.4	348.4	12.3	110	20.4	3
UN.126.B	28.8	351.7	37.4	110	12.8	2
UN.127.BL	28.8	333.9	54.2	174	8.5	3
UN.125.BU	28.9	379.3	29.6	63	9.9	4
UN.128.BL	29.2	324.8	65.9	114	20.9	3
UN.127.C	29.3	379.8	-31.6	265	8.8	2
UN.126.BU	29.3	355.0	21.6	96	6.6	4
UN.127.A	29.4	345.7	26.2	149	7.1	2
UN.129.BL	29.6	340.5	42.5	246	4.7	3
UN.128.C	29.8	359.7	34.9	92	13.0	4
UN.127.BU	29.9	343.1	38.5	134	3.2	3
UN.129.A	30.0	349.2	60.3	198	9.8	3
UN.130.BL	30.1	319.2	51.7	161	13.7	3
UN.129.C	30.2	352.6	59.3	147	3.4	3
UN.128.BU	30.3	325.2	45.2	124	6.9	4
UN.129.BU	30.6	340.4	35.2	163	9.1	2
UN.130.C	30.6	330.4	56.5	194	11.9	2
UN.131.BL	30.7	316.6	36.9	208	16.1	3
UN.131.C	31.1	339.0	46.9	144	12.9	2
UN.130.BU	31.1	326.5	55.2	245	9.9	3
UN.131.A	31.2	339.2	37.3	85	29.7	2

Sample	Level	Dec.	Inc.	Int.	Err.	Q
UN.132.BL	31.2	321.9	35.0	136	12.0	3
UN.133.BL	31.6	332.9	51.5	109	13.6	3
UN.131.BU	31.7	338.5	51.1	174	5.3	4
UN.133.C	32.0	370.0	49.0	71	6.2	2
UN.134.BL	32.0	339.5	37.9	101	23.9	3
UN.133.A	32.1	307.8	44.7	68	15.8	5
UN.132.BU	32.2	346.0	22.3	203	14.1	3
UN.135.BL	32.5	357.9	34.8	152	12.2	3
UN.134.C	32.5	358.2	51.7	185	9.0	4
UN.133.BU	32.6	429.7	32.6	104	18.6	5
UN.136.BL	32.8	328.8	51.5	144	20.5	4
UN.135.C	32.9	371.6	59.8	136	4.9	3
UN.134.BU	33.0	360.0	-9.1	172	11.5	4
UN.136.C	33.4	330.9	36.0	66	9.3	3
UN.135.BU	33.5	259.6	58.6	75	15.3	5
UN.138.BL	33.8	326.6	46.6	159	24.0	4
UN.136.BU	33.9	344.4	7.3	170	15.9	3
UN.137.C	33.9	339.5	48.9	231	8.7	3
UN.138.A	34.3	319.8	42.7	67	17.2	3
UN.139.BL	34.3	341.0	53.6	161	19.8	4
UN.137.AU	34.6	299.5	48.7	123	7.8	3
UN.140.BL	34.7	370.3	56.5	91	13.5	4
UN.139.A	34.8	350.3	52.1	144	12.4	5
UN.141.BL	35.2	391.4	50.6	261	13.3	5
UN.140.BU	35.7	346.4	52.8	119	9.8	3
UN.141.BU	36.2	444.8	79.9	95	19.5	5

Calabria
upper Nunivak (1987) reversal record
HT component

Sample	Level	Dec.	Inc.	Int.	Err.	Q
UN.087.BL	10.0	368.7	62.4	963	3.0	3
UN.088.BL	10.5	363.2	54.0	1050	1.9	3
UN.089.BL	11.0	365.6	50.8	954	1.0	3
UN.087.BU	11.0	363.2	61.6	1130	4.6	4
UN.090.BL	11.5	366.5	57.9	964	3.5	2
UN.089.BU	12.0	366.1	59.6	1306	3.9	3
UN.091.BL	12.0	353.6	56.6	917	4.0	3
UN.092.BL	12.5	349.2	55.3	881	0.1	4
UN.091.BU	13.0	358.6	51.6	1056	2.6	3
UN.093.BL	13.0	327.8	72.1	571	1.7	4
UN.094.BL	13.5	333.0	59.1	308	3.2	4
UN.093.BU	14.0	371.6	59.0	397	5.8	4
UN.095.BL	14.0	345.9	67.5	850	3.0	4
UN.096.BL	14.5	357.0	57.8	1103	2.2	2
UN.097.BL	15.0	351.6	55.1	859	3.2	4
UN.098.BL	15.5	331.0	66.0	707	4.3	5
UN.097.BU	16.0	349.1	56.2	1019	0.7	2
UN.099.BL	16.0	352.2	57.9	1302	2.1	2
UN.100.BL	16.5	330.8	65.9	369	3.3	4
UN.101.BL	17.0	313.3	71.5	398	1.1	5
UN.101.A	17.5	370.1	59.7	374	3.1	1
UN.102.BL	17.5	256.1	65.7	265	8.3	5
UN.101.BU	18.0	316.8	65.9	313	5.2	4
UN.103.BL	18.2	327.2	65.5	486	6.0	4
UN.104.BL	18.6	329.6	55.5	690	1.8	2
UN.103.A	18.7	354.8	66.2	511	2.9	1
UN.105.BL	19.1	303.3	59.9	435	5.1	4
UN.103.BU	19.2	317.7	43.6	783	4.0	3
UN.106.BL	19.5	316.7	66.5	385	7.9	4
UN.106.A	19.9	358.4	55.8	396	3.8	1
UN.105.BU	20.1	316.4	62.0	266	3.1	4
UN.109.BL	20.6	290.9	67.8	225	8.9	5
UN.110.BL	21.0	284.9	66.7	370	4.3	4
UN.109.C	21.1	269.9	63.0	91	6.8	2
UN.111.BL	21.5	277.9	49.7	296	3.1	5
UN.109.BU	21.6	254.9	32.1	142	11.7	5
UN.111.BU	22.0	254.2	22.0	263	2.8	3
UN.112.BL	22.2	292.9	59.9	385	3.1	4
UN.113.BL	22.5	271.9	54.9	252	3.8	3
UN.113.C	23.0	331.2	46.1	200	6.7	2
UN.114.A	23.4	329.0	49.9	266	5.7	2
UN.114.D	23.4	320.2	34.9	110	8.1	2
UN.116.BL	24.0	280.7	34.1	168	4.2	3

Appendix

Sample	Level	Dec.	Inc.	Int.	Err.	Q
UN.115.AU	24.5	288.5	-2.4	148	9.7	5
UN.117.A	24.6	299.9	-11.7	180	10.7	3
UN.117.C	24.7	335.0	65.8	177	9.7	2
UN.118.BL	24.8	258.1	44.7	255	9.7	4
UN.117.BU	25.1	260.2	39.9	373	7.4	3
UN.118.C	25.2	319.0	56.1	131	17.6	4
UN.119.BL	25.5	251.7	32.7	288	8.0	3
UN.119.A	26.0	294.6	18.1	116	11.7	2
UN.120.C	26.2	316.2	6.6	96	20.7	4
UN.119.BU	26.5	272.5	32.4	317	9.9	3
UN.121.BL	26.5	289.6	36.9	208	5.1	3
UN.121.C	26.7	309.6	55.2	84	8.0	2
UN.123.BL	26.9	257.3	59.3	145	2.9	5
UN.121.A	27.0	314.1	47.8	113	7.3	5
UN.122.C	27.1	323.0	26.1	109	24.4	5
UN.123.A	27.4	281.8	-28.4	120	9.5	2
UN.121.BU	27.5	278.5	30.8	174	6.1	3
UN.123.C	27.5	358.3	48.7	74	13.5	4
UN.125.BL	27.9	312.6	51.5	104	12.3	5
UN.126.BL	28.3	286.0	16.8	162	14.8	5
UN.125.A	28.4	254.1	-24.1	153	5.0	2
UN.124.BU	28.4	301.6	10.9	105	8.2	5
UN.126.B	28.8	299.6	20.1	104	11.5	4
UN.125.BU	28.9	255.7	51.5	208	7.9	5
UN.128.BL	29.2	241.2	-37.3	430	2.9	4
UN.127.C	29.3	394.3	-16.0	84	11.5	5
UN.127.A	29.4	256.9	-42.2	216	2.4	3
UN.129.BL	29.6	236.3	-42.8	471	9.0	4
UN.128.C	29.8	217.1	-38.2	359	3.9	4
UN.127.BU	29.9	234.7	-6.8	301	2.5	4
UN.129.A	30.0	230.4	-38.5	347	3.0	5
UN.130.BL	30.1	229.7	-43.7	658	2.4	4
UN.129.C	30.2	239.6	-38.4	317	10.5	5
UN.128.BU	30.3	235.4	-46.9	554	2.8	4
UN.129.BU	30.6	240.0	-31.8	502	2.8	3
UN.130.C	30.6	230.4	-39.2	222	8.0	5
UN.131.BL	30.7	233.6	-35.7	556	3.3	4
UN.131.C	31.1	207.8	-38.9	426	3.9	2
UN.130.BU	31.1	230.1	-42.1	594	3.0	4
UN.131.A	31.2	224.4	-37.3	283	5.1	5
UN.132.BL	31.2	240.4	-39.3	564	2.5	5
UN.133.BL	31.6	255.5	28.2	180	7.8	5
UN.131.BU	31.7	223.5	-36.1	543	2.5	4
UN.134.BL	32.0	221.2	-38.6	476	1.2	4
UN.133.B	32.1	205.0	-34.5	253	5.8	3
UN.133.A	32.1	223.0	-31.7	318	3.8	5
UN.132.BU	32.2	237.6	-40.0	586	3.8	4
UN.134.C	32.5	202.2	-39.5	163	2.7	4
UN.135.BL	32.5	223.1	-48.5	641	2.5	4
UN.136.BL	32.8	229.3	-20.9	322	3.7	5
UN.135.C	32.9	250.7	-46.6	27	13.2	5
UN.134.BU	33.0	235.8	-25.5	595	6.4	5
UN.136.C	33.4	221.1	-39.5	206	7.6	5
UN.135.BU	33.5	225.2	-35.2	660	2.5	5
UN.138.BL	33.8	222.1	-46.7	864	1.0	2
UN.136.BU	33.9	228.4	-35.1	734	3.4	3
UN.137.C	33.9	246.6	-36.1	151	11.4	3
UN.138.A	34.3	219.1	-36.0	192	4.7	3
UN.139.BL	34.3	224.7	-6.9	193	10.8	5
UN.137.AU	34.6	223.3	-30.9	397	3.6	5
UN.140.BL	34.7	228.3	-37.1	613	5.2	5
UN.138.BU	34.8	234.9	-42.6	698	2.0	5
UN.140.A	35.2	204.3	-32.6	416	5.0	3
UN.139.BU	35.3	222.4	14.8	142	4.7	4
UN.141.A	35.7	222.6	-47.6	541	1.8	3
UN.140.BU	35.7	225.7	-33.9	434	4.5	5
UN.141.BU	36.2	248.7	-23.1	295	3.3	5

Sicily
lower Mammoth reversal record
HT component

Sample	Level	Dec.	Inc.	Int.	Err.	Q
LM.080.A	1.8	34.0	48.0	1852	3.0	1
LM.079.B	2.2	29.0	36.0	1781	5.0	2
LM.081.B	2.7	29.0	41.0	1492	2.0	2
LM.080.BU	3.4	26.1	45.2	2400	8.0	1
LM.082.B	3.6	28.0	37.0	2217	21.0	5
LM.083.A	4.5	24.0	41.0	1382	5.0	2
LM.084.B	5.2	22.0	34.0	1632	5.0	1
LM.083.BU	5.8	19.5	35.2	1900	7.0	2
LM.085.B	6.9	29.0	34.0	1701	4.0	2
LM.086.A	7.0	26.0	37.0	1455	4.0	1
LM.086.BU	8.2	34.0	42.7	2400	3.0	2
LM.088.AU	8.3	25.9	35.0	1739	4.0	1
LM.088.B	8.6	21.2	35.7	1698	5.7	1
LM.089.AU	9.0	17.7	34.0	1772	4.0	1
LM.089.BU	9.8	36.8	33.5	2200	20.6	3
LM.090.AU	10.2	45.0	36.0	2004	16.0	3
LM.090.B	10.3	29.8	35.5	1348	3.1	1
LM.091.AU	10.7	28.0	43.4	1178	4.0	3
LM.091.B	10.9	34.0	39.5	1327	5.2	2
LM.093.BL	12.1	37.0	46.0	3647	3.0	2
LM.092.AU	12.2	25.5	44.0	1519	4.0	2
LM.093.AU	12.5	32.0	47.0	1253	4.0	3
LM.092.BU	12.9	30.4	37.9	1100	5.0	3
LM.093.BU	13.1	34.0	43.0	2544	5.0	2
LM.093.C	13.2	19.8	39.9	1606	3.9	1
LM.095.AL	13.3	27.0	37.5	1466	3.7	2
LM.094.AU	13.4	19.0	41.0	661	4.0	2
LM.094.B	13.4	10.0	39.4	1188	4.7	2
LM.094.CL	13.5	20.0	46.0	1578	5.0	2
LM.095.CL	14.2	43.0	38.0	1308	4.0	2
LM.095.AU	14.3	33.3	43.0	773	5.0	2
LM.094.CU	14.5	22.0	47.0	1000	6.0	2
LM.096.BL	14.5	31.0	44.0	951	6.0	2
LM.095.BU	14.8	48.8	52.7	1100	7.5	3
LM.096.AU	15.0	45.0	41.0	505	8.0	4
LM.095.CU	15.3	33.0	49.0	1148	7.0	2
LM.097.BL	15.3	21.0	57.0	710	8.0	2
LM.096.BU	15.5	33.0	59.0	627	6.0	2
LM.096.C	15.5	33.3	31.0	619	5.5	4
LM.098.AL	15.6	352.3	26.1	446	8.3	4
LM.097.AU	15.9	59.0	75.0	496	15.0	4
LM.097.BU	16.3	161.0	59.0	416	6.0	4
LM.097.C	16.3	45.1	60.4	260	10.1	4
LM.099.BL	16.7	149.0	25.0	293	14.0	5
LM.098.C	17.1	342.6	7.5	254	15.7	4
LM.099.AU	17.2	164.0	-17.0	169	7.0	5
LM.099.BU	17.7	173.0	18.0	357	14.0	5
LM.099.C	17.8	204.4	-29.4	143	14.7	4
LM.100.BL	18.1	189.0	-20.0	268	8.0	5
LM.101.AL	18.6	158.1	-7.1	166	15.3	4
LM.100.AU	18.7	186.0	-28.0	302	8.0	5
LM.100.BU	19.1	205.0	-13.0	324	9.0	5
LM.102.BL	19.4	183.0	-30.0	618	3.0	4
LM.101.AU	19.6	209.0	-21.3	300	23.0	3
LM.102.AU	20.1	153.0	-32.0	190	4.0	5
LM.102.C	20.2	174.0	-45.0	154	5.0	4
LM.103.AU	20.4	222.7	-1.0	192	15.0	4
LM.102.BU	20.4	173.0	-28.0	234	10.0	5
LM.103.CL	20.4	210.0	-34.0	147	9.0	5
LM.104.BL	20.8	213.0	-11.0	283	10.0	4
LM.103.BU	20.9	221.8	-32.2	400	10.0	4
LM.104.AU	21.4	210.5	-27.4	616	4.0	3
LM.103.CU	21.4	211.0	-16.0	372	6.0	4
LM.105.BL	21.7	195.0	-18.0	386	6.0	4
LM.104.BU	21.8	204.0	-24.0	461	10.0	4
LM.105.AU	22.4	216.0	-25.0	456	3.0	3
LM.105.BU	22.7	203.0	-6.0	430	6.0	4
LM.106.CL	22.8	194.0	-23.0	779	4.0	4
LM.106.AU	23.3	186.6	-34.5	562	5.0	1
LM.107.AU	23.5	205.0	-33.0	619	5.0	3
LM.106.BU	23.6	195.4	-18.8	600	5.0	4
LM.106.CU	23.9	192.0	-17.0	569	5.0	5
LM.108.AU	24.3	210.0	-25.0	373	4.0	2
LM.109.BU	25.6	240.3	-45.9	500	5.0	5
LM.109.C	25.6	307.8	-53.5	174	13.7	4
LM.110.AU	26.0	196.0	-18.0	551	8.0	4
LM.111.AU	27.0	202.0	-30.0	435	6.0	3
LM.112.BU	27.9	201.3	-23.5	1400	2.3	3
LM.112.C	27.9	196.8	-17.6	481	4.2	3
LM.113.B	28.2	233.4	-23.8	110	22.4	4
LM.114.AU	29.1	201.0	-38.0	682	12.0	3
LM.115.AU	29.9	232.0	-30.0	697	4.0	3
LM.116.A	30.2	192.1	-34.9	742	1.6	1
LM.115.BU	30.3	233.9	-36.1	1000	10.0	3
LM.117.A	30.8	197.8	-35.8	789	3.9	2
LM.118.A	31.6	196.4	-40.8	820	4.5	2
LM.119.A	32.3	208.1	-35.4	1346	2.7	1
LM.118.BU	32.6	200.7	-36.8	1800	3.2	3
LM.120.A	33.0	197.5	-34.4	1016	2.4	1
LM.121.A	33.8	190.9	-34.2	1040	3.1	2
LM.122.A	34.7	202.4	-35.9	1088	2.9	3

Sample	Level	Dec.	Inc.	Int.	Err.	Q
LM.121.BU	34.8	201.9	-27.4	1300	10.0	2
LM.123.A	35.4	207.0	-27.7	1121	2.9	1
LM.124.A	36.5	197.8	-32.8	1360	3.8	2
LM.124.BU	37.4	204.4	-33.5	1600	1.1	3
LM.125.A	37.5	193.5	-34.7	1511	4.2	3
LM.127.BU	39.9	215.1	-38.6	2700	3.1	3
LM.130.BU	42.6	206.8	-33.5	2600	6.5	3

Sicily
upper Mammoth reversal record
HT component

Sample	Level	Dec.	Inc.	Int.	Err.	Q
UM.02.BU	0.7	207.8	-43.9	5700	3.2	1
UM.04.BU	2.6	207.9	-44.0	6000	6.2	1
UM.06.BU	5.2	208.3	-36.6	5400	9.9	2
UM.07.B	5.6	217.0	-34.0	4384	2.0	2
UM.08.C	6.5	211.0	-35.0	3845	3.0	3
UM.08.BU	7.1	217.0	-41.0	4600	8.4	3
UM.09.C	7.3	209.0	-33.0	3198	4.0	2
UM.10.C	8.3	214.0	-38.0	3027	3.0	2
UM.10.BU	8.7	207.1	-35.8	4300	7.8	2
UM.11.C	9.3	209.0	-38.0	3607	3.0	2
UM.12.C	10.3	208.0	-33.0	3196	2.0	1
UM.12.BU	10.8	215.0	-34.1	3500	3.4	3
UM.13.C	11.2	207.0	-37.0	2973	2.0	2
UM.14.C	12.2	207.0	-36.0	2708	2.0	2
UM.14.BU	12.8	208.3	-40.8	4800	5.4	3
UM.15.C	13.2	208.0	-38.0	2429	4.0	1
UM.16.C	14.1	209.0	-41.0	2106	2.0	2
UM.16.BU	14.5	213.2	-42.1	3200	5.4	3
UM.17.C	15.1	207.0	-34.0	3544	2.0	2
UM.18.D	16.0	209.0	-36.0	3307	2.0	2
UM.18.BU	16.6	212.5	-41.4	5700	3.1	3
UM.19.C	17.0	206.0	-36.0	2710	4.0	3
UM.20.BU	18.6	201.9	-47.1	2600	5.7	3
UM.21.AU	19.6	197.8	-44.9	1257	4.0	2
UM.22.BU	20.4	215.8	-49.2	2800	7.4	3
UM.23.AL	20.4	211.0	-47.0	1034	3.0	3
UM.22.AU	20.5	216.0	-38.0	992	4.0	3
UM.24.AL	21.4	186.0	-50.0	1154	3.0	4
UM.23.AU	21.5	208.0	-33.0	433	5.0	3
UM.24.C	21.8	181.5	-55.7	557	5.8	3
UM.24.BU	22.4	190.4	-59.6	500	10.0	2
UM.24.AU	22.4	185.6	-48.5	971	3.0	1
UM.25.AL	22.4	226.0	-53.0	694	4.0	3
UM.25.B	22.8	198.2	-37.8	429	2.0	3
UM.26.AL	23.3	203.0	-59.0	679	4.0	4
UM.25.AU	23.4	228.0	-27.0	433	5.0	3
UM.26.C	23.8	204.5	-52.2	410	4.3	4
UM.26.BU	24.3	245.3	-60.0	1400	5.7	3
UM.26.AU	24.3	221.0	-57.0	725	3.0	2
UM.27.AL	24.3	286.0	-71.0	364	7.0	3
UM.27.C	24.7	329.3	-78.4	325	8.2	3
UM.27.B	24.8	12.6	-72.8	565	5.5	3
UM.27.AU	25.3	346.0	-21.0	376	8.0	4

Sample	Level	Dec.	Inc.	Int.	Err.	Q
UM.28.AL	25.3	242.0	-70.0	787	4.0	4
UM.28.C	25.7	342.1	-75.6	212	5.1	3
UM.28.D	25.7	348.5	-17.9	164	10.1	4
UM.28.BU	26.3	348.8	28.8	700	18.3	3
UM.28.AU	26.3	342.0	28.0	200	3.0	3
UM.29.AL	26.5	7.0	25.0	401	3.0	3
UM.29.C	26.8	16.5	13.4	478	4.7	2
UM.29.B	26.9	8.4	3.9	345	5.4	2
UM.30.AL	27.2	0.0	19.0	592	5.0	2
UM.29.AU	27.5	14.0	28.0	216	4.0	2
UM.30.C	27.6	7.3	-7.1	210	5.2	2
UM.30.BU	28.2	289.1	-64.2	600	10.0	3
UM.30.AU	28.2	329.0	-1.0	281	4.0	2
UM.30.AU	28.2	5.0	-82.0	84	24.0	4
UM.31.AL	28.3	338.0	-61.0	218	10.0	3
UM.31.B	28.8	30.7	-22.3	398	6.1	2
UM.32.AL	29.3	13.0	-3.0	445	3.0	2
UM.31.AU	29.4	42.0	-1.0	355	7.0	4
UM.31.AU	29.4	48.0	-36.0	92	25.0	5
UM.32.C	29.6	323.5	-49.6	116	10.4	4
UM.32.BU	30.2	8.1	17.6	500	10.0	4
UM.32.AU	30.3	21.0	-20.0	59	10.0	4
UM.33.AL	30.3	5.0	7.0	694	7.0	4
UM.33.B	30.6	4.5	8.1	677	3.5	3
UM.34.AL	31.2	10.0	27.0	293	6.0	3
UM.33.AU	31.3	6.0	34.0	717	4.0	2
UM.34.BU	32.1	31.1	21.1	1700	10.0	4
UM.34.AU	32.3	10.0	23.0	864	6.0	2
UM.35.B	32.6	18.0	21.0	741	6.0	3
UM.43.A	33.3	27.0	30.0	898	4.0	2
UM.36.C	33.4	25.0	24.0	426	7.0	2
UM.36.BU	34.0	23.2	30.2	800	10.0	4
UM.44.A	34.0	8.0	13.0	700	3.0	5
UM.37.A	34.6	32.0	2.0	623	5.0	3
UM.45.A	35.4	11.0	27.0	807	2.0	1
UM.38.A	35.6	24.0	21.0	1122	3.0	2
UM.46.A	36.4	346.0	30.0	788	4.0	4
UM.39.A	36.8	29.0	28.0	833	5.0	2
UM.47.A	36.8	19.0	29.0	481	4.0	2
UM.40.A	37.6	27.0	23.0	969	3.0	2
UM.41.A	38.9	19.0	32.0	1036	3.0	1
UM.42.A	39.8	14.0	35.0	625	3.0	1

Sicily
lower Kaena reversal record
HT component

Sample	Level	Dec.	Inc.	Int.	Err.	Q
LK.201.B	-0.9	28.3	37.3	587	6.4	2
LK.205.B	2.3	38.2	40.3	1651	4.0	1
LK.210.B	6.4	38.5	41.2	2263	4.6	1
LK.215.B	10.2	27.0	36.0	2799	5.5	1
LK.220.B	13.8	14.8	35.9	2928	5.0	1
LK.225.B	17.7	31.5	32.2	2760	4.4	2
LK.226.AL	17.9	2.9	44.8	1972	5.0	3
LK.226.AU	19.0	357.9	36.9	1646	5.9	3
LK.228.AL	19.5	9.7	50.2	1128	3.9	3
LK.228.AU	20.5	7.6	53.0	868	4.9	3
LK.230.BL	20.9	32.9	32.9	1200	4.0	3
LK.230.A	21.2	34.6	37.1	1531	3.8	2
LK.230.BU	21.9	37.5	35.1	1239	4.7	3
LK.234.AL	23.7	11.2	34.3	696	3.3	4
LK.234.AU	24.8	5.4	31.4	967	4.0	4
LK.235.A	25.0	49.8	23.6	584	7.6	3
LK.236.AL	25.1	21.6	-11.9	407	28.9	4
LK.236.AU	26.2	19.2	8.2	732	3.7	4
LK.238.AL	26.3	24.6	-15.5	868	15.7	5
LK.238.AU	27.3	27.2	8.1	949	1.8	5
LK.240.AL	29.2	24.7	33.8	714	10.1	3
LK.240.AU	30.2	4.6	62.0	824	3.6	4
LK.242.AL	30.5	26.4	31.0	1000	8.0	4
LK.241.A	30.5	35.0	35.3	740	7.4	2
LK.242.AU	31.5	31.3	34.3	857	3.5	4
LK.244.AL	31.7	18.0	36.6	1220	6.3	3
LK.243.B	32.0	30.6	42.6	1119	3.7	2
LK.244.AU	32.7	13.5	15.0	332	4.7	5
LK.244.B	32.7	32.3	23.6	548	7.4	2
LK.245.A	33.2	63.0	23.7	290	9.0	3
LK.245.B	33.5	55.3	19.7	273	12.6	2
LK.246.BL	33.8	39.6	27.6	321	15.1	4
LK.246.A	33.9	67.3	37.1	482	7.1	3
LK.248.AL	34.8	185.3	-7.0	227	7.4	4
LK.246.BU	34.8	78.4	64.7	384	6.7	4
LK.001.A	35.5	178.0	-28.0	252	8.0	4
LK.248.B	35.7	163.1	-32.4	238	12.9	4
LK.248.AU	35.8	152.1	-5.8	181	7.3	4
LK.002.A	36.1	149.1	-17.4	181	15.2	4
LK.001.BU	36.5	209.6	-14.5	309	0.3	4
LK.249.A	36.5	197.7	-33.9	172	18.1	4
LK.002.BU	37.0	187.4	-11.0	522	2.4	4
LK.003.A	37.3	203.9	-40.2	238	4.0	3

Appendix

Sample	Level	Dec.	Inc.	Int.	Err.	Q
LK.250.B	37.3	293.8	-40.6	273	19.5	3
LK.251.A	37.7	180.7	-53.9	253	19.2	3
LK.003.BU	38.1	195.3	-27.7	570	6.1	4
LK.004.A	38.2	190.0	-42.2	210	3.7	4
LK.004.BU	39.0	181.3	-22.7	392	2.8	4
LK.005.A	39.1	172.1	-55.2	290	7.6	4
LK.253.C	39.5	185.4	-11.0	86	32.5	4
LK.006.A	40.0	188.7	-26.2	442	7.8	3
LK.005.BU	40.0	182.7	-27.7	273	11.2	4
LK.006.BU	40.9	193.2	-13.3	453	4.6	4
LK.255.A	40.9	213.8	-37.8	330	8.9	2
LK.007.BU	41.6	207.2	-29.4	554	8.6	4
LK.007.D	41.7	201.2	-40.6	499	4.2	3
LK.008.A	41.7	192.6	-53.1	454	6.6	2
LK.256.A	41.7	211.5	-30.0	609	9.6	2
LK.257.A	42.3	181.2	-54.0	288	9.0	2
LK.008.BU	42.5	200.1	-35.1	1075	8.4	4
LK.257.B	42.6	172.0	-5.1	100	31.4	4
LK.009.A	43.1	208.4	-47.3	899	5.4	2
LK.009.BU	43.9	215.2	-49.5	1558	4.8	4
LK.010.A	44.0	199.2	-52.1	1035	3.9	2
LK.010.BU	44.7	196.3	-49.9	1408	5.9	4
LK.011.A	44.8	207.5	-49.7	779	5.6	2
LK.011.BU	45.6	208.5	-33.1	867	2.7	4
LK.012.C	46.2	202.9	-40.5	578	7.9	3
LK.012.BU	46.5	184.6	-43.0	713	10.3	4
LK.013.A	46.6	237.2	-31.6	132	22.6	4
LK.013.BU	47.3	231.2	-13.0	457	1.3	4
LK.014.A	47.6	237.2	-25.7	560	7.5	2
LK.014.BU	48.3	256.4	-40.9	213	42.2	5
LK.015.A	48.8	251.2	-25.7	308	18.4	3
LK.016.A	49.4	301.4	7.5	290	14.7	3
LK.015.BU	49.4	20.1	38.0	708	1.0	4
LK.017.A	50.0	10.5	41.3	3368	1.7	1
LK.016.BU	50.2	27.9	26.0	810	6.6	4
LK.017.BU	50.8	20.4	55.8	12434	2.6	2
LK.018.A	50.9	14.0	41.5	6016	2.9	1
LK.018.BU	51.8	16.6	51.9	11226	3.0	2
LK.019.A	52.2	16.0	42.8	6575	1.7	1
LK.019.BU	53.0	16.8	49.1	1761	4.3	3
LK.020.C	53.6	8.1	45.3	3150	2.5	1
LK.021.A	53.6	334.8	24.4	330	14.0	2
LK.020.BU	53.8	347.7	34.2	736	17.7	4
LK.021.BU	54.5	8.6	39.7	1075	1.5	5
LK.022.A	54.8	352.9	39.9	463	6.6	3
LK.022.BU	55.6	28.1	21.7	491	9.0	5
LK.023.A	55.9	229.6	-36.2	424	6.0	2
LK.023.BU	56.6	235.4	-37.9	1828	5.2	4
LK.024.A	57.3	220.4	-47.8	1866	4.4	1
LK.024.BU	58.0	220.5	-50.3	2400	4.8	5
LK.025.A	58.1	220.1	-23.9	395	10.5	3
LK.026.A	58.6	222.3	-31.0	1065	4.9	2
LK.025.BU	58.8	227.5	-17.3	927	0.9	5
LK.026.BU	59.4	243.2	-50.6	2631	3.5	4
LK.027.A	59.6	222.0	-44.0	2356	4.0	2
LK.027.BU	60.4	215.2	-46.5	2298	2.1	5
LK.028.A	60.8	217.6	-42.3	1949	3.8	2
LK.029.A	61.5	215.6	-40.1	810	4.7	3
LK.028.BU	61.6	218.9	-50.3	2785	4.5	5
LK.029.BU	62.3	249.5	-22.2	869	9.3	4
LK.030.A	62.4	214.4	-39.0	1110	4.5	2
LK.030.BU	63.2	208.6	-34.5	2302	1.9	5
LK.031.A	63.4	218.7	-31.5	1426	3.7	1
LK.031.BU	64.1	225.4	-39.7	1534	1.7	5
LK.032.A	64.4	226.9	-44.7	1620	3.1	1
LK.032.BU	65.2	224.4	-46.3	2134	5.0	5
LK.033.A	65.4	211.2	-34.4	570	11.9	3
LK.033.BU	66.1	304.7	-12.5	479	7.1	4
LK.034.A	66.2	207.2	-13.7	761	5.9	2
LK.034.BU	66.9	230.7	-23.4	384	10.0	5
LK.035.A	67.1	223.8	-40.7	439	7.6	4
LK.035.BU	67.9	202.9	-10.5	638	5.0	5
LK.036.A	68.1	232.6	-65.1	188	21.5	5
LK.037.D	69.8	213.4	-37.1	657	4.4	3
LK.037.BU	69.8	211.5	-28.4	509	1.7	5
LK.038.A	69.9	220.2	-59.1	247	19.5	5
LK.039.A	70.9	212.4	-21.8	431	6.2	3
LK.039.BU	71.6	297.0	-26.5	727	8.1	4
LK.040.BU	72.5	238.0	-22.0	558	7.3	5
LK.041.BU	73.7	206.8	-36.9	2017	6.4	5
LK.042.BU	74.4	236.1	-35.6	1322	7.4	4
LK.043.BU	75.4	195.7	-52.1	2608	4.4	5
LK.044.BU	76.3	204.8	-30.4	1708	4.3	5
LK.045.BU	77.7	228.1	-42.4	2247	5.3	4
LK.046.BU	78.3	218.5	-23.6	2097	5.7	4
LK.047.BU	79.3	205.9	-38.8	1730	8.3	5
LK.048.BU	80.1	237.9	-26.9	1565	6.0	4
LK.051.BU	83.1	233.7	-49.3	2602	5.2	4
LK.054.BU	85.9	216.7	-35.2	3970	3.8	3
LK.057.BU	88.9	221.4	-45.7	3998	2.4	2
LK.060.BU	91.7	219.7	-37.0	5528	2.5	2

Corfu
upper Thvera reversal record
magnetite component

Sample	Level	Dec.	Inc.	Int.	Err.	Q
AS.001.1C	-0.01	47.7	27.5	269	5.0	2
AS.001.1B	-0.01	33.6	33.6	162	7.5	2
AS.001.4A	-0.01	10.4	58.1	116	9.6	2
AS.003.1C	1.07	44.0	40.6	231	3.7	2
AS.003.1B	1.07	54.7	46.9	199	3.5	2
AS.003.3A	1.07	50.8	53.3	309	10.2	3
AS.003.4A	1.07	38.5	61.1	211	2.6	3
AS.004.1C	1.47	344.8	51.7	322	4.0	2
AS.004.1B	1.47	337.7	48.2	391	4.2	1
AS.004.3A	1.47	0.3	40.0	449	6.9	1
AS.004.4A	1.47	351.5	46.4	421	4.0	1
AS.005.1C	2.17	31.1	31.6	218	6.3	2
AS.005.4A	2.17	14.0	40.3	306	4.9	1
AS.005.1B	2.17	13.8	37.7	236	4.0	2
AS.005.3A	2.17	11.5	36.9	257	4.9	2
AS.006.2A	2.56	345.7	45.9	172	3.0	2
AS.006.4A	2.56	321.1	52.4	213	5.2	1
AS.006.1B	2.56	327.3	42.4	253	2.8	2
AS.006.3A	2.56	351.6	60.8	228	9.9	2
AS.007.2B	3.05	43.3	30.4	415	6.0	2
AS.007.1C	3.05	41.7	40.9	297	6.8	1
AS.007.2A	3.05	18.5	23.3	279	7.7	2
AS.007.3A	3.05	41.1	37.0	369	6.6	2
AS.007.4A	3.05	27.7	38.4	396	3.9	2
AS.008.2A	3.61	17.5	35.3	234	5.1	2
AS.008.3A	3.61	25.9	33.4	435	4.1	2
AS.008.4A	3.61	356.1	46.7	395	5.3	2
AS.009.1C	4.38	52.3	34.9	261	4.6	2
AS.009.3A	4.38	34.9	15.7	258	4.0	1
AS.009.4A	4.38	32.1	36.2	320	4.0	1
AS.010.1C	4.93	45.4	36.1	265	6.8	2
AS.010.3A	4.93	28.8	59.1	214	2.7	2
AS.010.4A	4.93	15.8	35.1	399	4.1	2
AS.011.1C	5.43	46.6	29.5	214	2.7	2
AS.011.1A	5.43	50.2	50.9	181	17.0	3
AS.011.4A	5.43	46.9	48.5	263	4.9	2
AS.011.3A	5.43	71.0	41.1	222	7.4	3
AS.012.1C	6.04	80.7	24.2	128	7.6	3
AS.012.3A	6.04	70.2	56.3	96	11.2	3
AS.013.3A	6.35	39.3	34.3	180	8.6	2
AS.013.4A	6.35	333.2	72.1	189	9.6	2
AS.014.3A	6.60	49.3	51.8	157	6.4	2
AS.014.4A	6.60	25.6	77.7	181	7.6	2
AS.015.1B	6.85	343.8	47.6	200	6.4	1
AS.015.4A	6.85	352.5	64.1	81	4.5	2
AS.016.3A	7.10	37.9	37.7	200	4.1	2
AS.016.4A	7.10	15.2	53.7	191	9.7	2
AS.017.4A	7.29	12.4	32.1	73	4.9	2
AS.018.3A	7.50	89.9	10.7	83	4.6	2
AS.019.3A	7.70	24.2	21.7	95	4.2	2
AS.019.4A	7.70	344.0	14.2	87	10.4	3
AS.020.4A	7.95	41.2	44.8	114	5.1	2
AS.020.3A	7.95	50.5	40.7	85	6.8	3
AS.021.3A	8.20	345.6	57.9	110	6.7	1
AS.021.1B	8.20	348.1	37.8	119	3.9	2
AS.021.4A	8.20	11.1	54.6	175	3.1	2
AS.022.3A	8.44	19.3	41.9	70	9.8	2
AS.022.4A	8.44	20.6	68.1	84	4.8	2
AS.023.3A	8.74	327.0	39.6	171	3.2	1
AS.023.2A	8.74	342.9	47.9	212	5.7	2
AS.023.4A	8.74	216.5	86.4	148	3.4	2
AS.024.3A	8.97	353.4	58.1	129	0.9	1
AS.024.4A	8.97	351.4	70.9	141	4.8	2
AS.025.3A	9.21	109.7	-62.7	33	20.4	2
AS.025.4A	9.21	172.5	11.9	32	9.1	3
AS.026.3A	9.47	221.2	-30.0	73	10.6	1
AS.027.4A	9.47	167.5	61.3	59	8.8	2
AS.026.1B	9.47	174.0	49.6	54	13.4	3
AS.026.4A	9.47	165.1	32.8	34	3.8	3
AS.028.4A	9.63	230.0	64.4	56	13.7	2
AS.028.3A	9.63	165.4	11.6	49	7.4	3
AS.029.3A	9.71	125.1	2.4	31	39.7	3
AS.030.4A	9.79	212.0	52.5	55	9.7	2
AS.032.4A	10.00	272.7	27.0	52	7.6	3
AS.033.4A	10.20	276.7	15.9	104	9.4	2
AS.034.3A	10.39	294.2	-17.2	33	26.9	2
AS.034.4A	10.39	327.0	-12.4	56	31.4	3
AS.035.3A	10.59	313.5	3.7	66	4.1	3
AS.035.4A	10.59	260.0	-1.8	81	3.8	3
AS.036.1A	10.79	204.4	5.9	122	25.6	3
AS.036.3A	10.79	338.3	1.9	52	7.7	2
AS.036.4A	10.79	324.4	17.6	97	5.3	2
AS.037.3A	10.84	345.6	-9.7	63	8.0	3
AS.037.4A	10.84	284.7	-10.7	61	16.6	3
AS.038.3A	11.04	59.5	-16.6	81	10.2	1
AS.038.1B	11.04	7.8	2.1	65	10.2	2
AS.038.2A	11.04	43.8	7.5	132	16.3	2
AS.038.4A	11.04	175.6	81.9	97	15.1	3
AS.039.3A	11.24	103.8	-36.2	27	5.9	2
AS.039.4A	11.24	146.0	72.3	40	5.1	3
AS.040.4A	11.32	305.4	53.3	25	9.3	3

Appendix

Sample	Level	Dec.	Inc.	Int.	Err.	Q
AS.041.4A	11.39	98.4	27.3	45	13.3	3
AS.043.1B	11.77	135.1	49.4	34	9.0	3
AS.044.4A	11.85	113.9	29.6	41	23.5	3
AS.045.4A	12.04	118.2	79.4	76	8.9	3
AS.048.4A	12.56	103.4	16.5	70	1.8	3
AS.049.4A	12.65	116.9	-24.0	39	4.8	3
AS.050.1A	12.89	76.5	42.8	49	13.5	2
AS.054.1A	13.68	242.5	-26.1	289	8.7	3
AS.054.4A	13.68	114.5	11.8	131	4.9	1
AS.054.4A	13.68	114.5	11.8	131	4.9	2
AS.055.1B	13.92	107.1	4.5	72	16.9	2
AS.055.4A	13.92	152.4	-19.9	59	27.1	2
AS.056.4A	14.16	137.7	14.6	150	9.4	2
AS.058.4A	14.65	129.4	-7.6	97	5.2	2
AS.059.4A	14.89	202.4	-6.5	95	12.0	2
AS.060.4A	15.03	120.5	15.8	62	5.9	2
AS.063.4A	15.80	127.8	-11.0	66	11.7	2
AS.064.4A	16.05	142.4	-10.0	58	18.4	2
AS.066.4A	16.43	190.7	4.1	134	4.7	2
AS.067.4A	16.69	186.1	-16.7	62	10.0	2
AS.067.1B	16.69	249.2	-11.3	78	12.2	3
AS.068.1A	16.93	45.6	2.7	225	1.9	1
AS.069.4A	17.18	135.1	-10.5	9	20.6	2
AS.071.4A	17.48	214.8	-46.5	98	16.7	1
AS.073.1B	17.87	181.6	-10.1	55	6.0	2
AS.073.4A	17.87	134.9	-19.2	110	8.5	2
AS.076.4A	18.76	173.6	-30.3	184	3.6	1
AS.080.4A	19.56	196.7	-30.2	148	6.4	1
AS.081.4A	19.79	194.1	-25.5	117	8.2	2
AS.083.2A	20.33	197.5	-49.5	232	10.1	2
AS.083.4A	20.33	212.3	-35.2	179	2.2	2
AS.084.4A	20.64	173.9	-41.7	143	5.8	2
AS.085.1B	20.91	181.7	-31.8	110	6.0	2
AS.085.4A	20.91	169.9	-40.8	141	2.7	2
AS.086.4A	21.11	180.3	-49.0	150	6.2	2
AS.088.1A	21.76	183.3	-35.9	356	2.8	2
AS.088.4A	21.76	197.3	-28.5	287	3.8	1
AS.089.1B	22.01	174.5	-29.6	291	6.0	2
AS.089.4A	22.01	177.9	-35.6	339	3.8	2
AS.090.1B	22.20	159.5	-30.3	197	9.0	2
AS.090.4A	22.20	180.9	-39.7	300	4.8	1
AS.091.4A	22.44	178.5	-43.2	455	4.4	2
AS.092.2	22.69	172.8	-27.6	247	4.9	2
AS.092.4A	22.69	179.4	-29.5	318	4.5	2
AS.093.2A	22.86	181.1	-46.3	358	9.4	2
AS.093.1B	22.86	179.2	-32.0	319	2.3	1
AS.093.4A	22.86	190.3	-30.5	256	5.7	2
AS.094.1B	23.26	182.4	-31.0	410	3.2	1
AS.094.4A	23.26	199.2	-30.2	498	2.2	2
AS.095.4A	23.63	180.6	-23.5	472	2.4	2
AS.096.1B	24.19	184.5	-39.5	585	2.1	1
AS.096.4A	24.19	181.4	-40.0	629	2.5	2
AS.097.1B	24.69	177.3	-48.9	301	3.6	1
AS.097.4A	24.69	194.7	-55.4	250	6.5	2
AS.098.1B	25.21	212.1	-62.8	375	3.6	2
AS.098.2A	25.21	183.6	-38.1	591	3.1	1
AS.098.1C	25.21	213.9	-40.7	381	4.2	2
AS.098.4A	25.21	196.4	-25.5	468	5.4	2
AS.099.1B	25.71	200.3	-28.3	641	1.4	1
AS.099.4A	25.71	198.7	-31.4	422	2.6	2
AS.100.1B	26.22	182.8	-30.0	431	4.7	2
AS.100.2A	26.22	184.3	-36.8	584	1.5	1
AS.100.4A	26.22	190.4	-38.4	553	3.2	2
AS.101.1B	26.85	203.6	-51.7	500	4.3	2
AS.101.4A	26.85	207.8	-53.3	431	2.5	2
AS.102.1B	27.36	186.7	-45.1	325	7.2	2
AS.102.1C	27.36	198.3	-36.2	418	4.0	2
AS.102.4A	27.36	196.5	-48.5	363	4.1	2
AS.103.1B	27.90	182.9	-26.1	553	3.5	1
AS.103.4A	27.90	204.8	-23.2	480	0.5	2
AS.104.1B	28.41	188.9	-29.0	314	4.4	2
AS.104.1C	28.41	185.2	-31.0	421	3.1	2
AS.104.2A	28.41	208.5	-33.0	403	5.5	2
AS.104.4A	28.41	214.8	-37.0	394	1.9	2

Corfu
lower Sidufjall reversal record
magnetite component

Sample	Level	Dec.	Inc.	Int.	Err.	Q
VA.01.1A	0.0	176.3	-28.3	194	3.0	1
VA.01.3A	0.0	181.3	-66.9	270	6.4	2
VA.03.1A	0.6	170.0	-33.4	319	3.3	1
VA.03.2A	0.6	172.5	-49.1	158	9.5	2
VA.05.1A	1.4	164.6	-42.4	248	3.2	1
VA.05.2A	1.4	203.0	-60.2	247	4.5	2
VA.07.1A	1.9	187.7	-33.6	126	1.5	1
VA.07.2A	1.9	233.9	-49.5	125	8.0	2
VA.09.1A	2.4	203.9	-41.3	214	3.0	2
VA.10.1B	2.6	116.2	-30.2	83	11.1	3
VA.11.1B	3.0	117.8	-58.6	118	6.3	2
VA.12.1B	3.1	178.1	-21.3	384	1.6	1
VA.12.2A	3.1	197.9	-31.5	286	4.3	2
VA.13.1A	3.3	156.5	37.0	48	2.3	3
VA.13.1B	3.3	130.2	-0.9	73	12.3	3
VA.13.2A	3.3	112.4	15.9	122	7.2	3
VA.15.1A	3.6	195.8	-27.1	137	5.6	2
VA.15.3A	3.6	156.4	-29.6	152	8.1	2
VA.16.1B	3.7	123.7	44.0	106	6.9	1
VA.16.2A	3.7	298.7	30.8	72	11.3	3
VA.17.1B	4.0	151.2	28.7	87	10.3	3
VA.17.2A	4.0	352.9	25.6	37	26.9	2
VA.17.3A	4.0	163.9	52.3	149	5.7	2
VA.18.1B	4.2	224.7	61.1	111	9.6	2
VA.18.2A	4.2	54.6	1.6	86	11.4	3
VA.19.1A	4.4	294.8	17.9	174	4.5	1
VA.19.1B	4.4	298.1	27.7	87	10.9	2
VA.19.2A	4.4	274.8	-6.0	41	6.4	2
VA.20.1A	4.6	347.0	28.3	46	25.9	3
VA.20.2A	4.6	263.6	-19.9	77	5.5	2
VA.20.3A	4.6	241.9	26.1	114	5.7	2
VA.21.1A	4.9	288.7	20.3	79	12.2	3
VA.21.2A	4.9	74.5	24.1	75	6.7	1
VA.21.3A	4.9	269.8	19.5	98	4.7	3
VA.22.1B	5.0	282.8	39.5	125	9.4	1
VA.22.3A	5.0	274.3	15.6	91	4.2	3
VA.23.1A	5.2	16.8	-20.6	91	13.2	2
VA.23.2A	5.2	333.0	4.5	177	5.7	2
VA.23.3A	5.2	237.9	8.9	75	9.5	2
VA.24.2A	5.4	26.6	12.9	122	8.4	2
VA.24.3A	5.4	184.4	38.8	85	12.3	3
VA.25.1A	5.7	312.7	18.5	105	7.5	2
VA.25.1C	5.7	301.2	46.8	53	11.7	3
VA.25.2A	5.7	71.0	20.8	43	17.6	2
VA.25.3A	5.7	297.4	-7.4	125	4.8	2
VA.26.2A	6.6	133.3	39.1	72	12.7	3
VA.26.3A	6.6	120.3	33.0	123	7.0	2
VA.27.3A	6.9	121.5	22.5	167	5.2	2
VA.28.1A	7.1	107.8	36.4	66	7.9	3
VA.28.3A	7.1	120.7	22.9	153	4.2	1
VA.29.1A	7.3	114.1	20.0	122	7.3	2
VA.29.2A	7.3	113.8	15.1	158	1.5	2
VA.29.3A	7.3	116.8	17.1	253	3.7	2
VA.30.3A	7.5	103.4	24.8	85	11.9	2
VA.31.3A	7.7	90.4	9.0	133	6.0	2
VA.32.1C	7.8	102.2	-11.3	94	5.4	2
VA.32.2A	7.8	128.9	20.2	171	2.2	2
VA.32.3A	7.8	119.6	-13.7	133	3.3	2
VA.33.1A	8.1	99.5	67.9	93	3.1	2
VA.33.3A	8.1	122.4	51.9	101	7.5	2
VA.34.2A	8.3	97.6	31.5	130	6.6	3
VA.34.3A	8.3	112.9	31.0	230	6.6	2
VA.35.1A	8.4	111.6	57.6	88	1.7	2
VA.35.2A	8.4	155.7	33.8	109	4.6	1
VA.35.3A	8.4	107.7	59.0	105	13.0	2
VA.36.1A	8.5	135.9	37.8	77	11.5	3
VA.36.1C	8.5	163.7	40.9	67	13.4	2
VA.36.2A	8.5	128.0	-14.0	105	7.3	2
VA.37.1A	8.7	96.7	73.2	120	6.9	2
VA.37.1C	8.7	144.1	50.2	180	6.7	2
VA.37.2A	8.7	91.8	10.3	128	11.2	2
VA.38.1C	8.9	289.6	48.0	257	3.5	2
VA.38.2A	8.9	321.6	65.2	152	4.4	2
VA.38.3A	8.9	250.6	39.7	128	9.6	2
VA.39.1A	9.1	251.6	37.4	161	5.2	3
VA.39.1C	9.1	319.0	65.6	107	22.5	3
VA.39.2A	9.1	253.1	43.7	99	9.8	2
VA.40.2A	9.5	286.7	20.8	233	5.8	2
VA.40.3A	9.5	297.8	29.6	188	11.3	2
VA.41.1A	9.7	317.7	11.6	128	14.6	3
VA.41.2A	9.7	310.8	26.8	149	6.1	2
VA.41.3A	9.7	293.4	-2.1	147	8.1	2
VA.42.1A	10.0	345.5	63.2	152	10.0	3
VA.42.1C	10.0	326.2	31.0	117	7.0	1
VA.42.2A	10.0	289.5	17.4	193	4.7	2
VA.43.1A	10.3	23.3	55.1	146	11.4	2
VA.43.2A	10.3	300.6	15.9	160	5.4	2
VA.43.3A	10.3	287.7	30.0	206	3.4	2
VA.44.2A	10.5	359.8	16.3	110	8.4	3
VA.44.3A	10.5	340.3	12.9	208	6.8	2
VA.45.1A	10.6	56.3	88.8	63	2.9	3

Sample	Level	Dec.	Inc.	Int.	Err.	Q
VA.45.2A	10.6	30.7	4.7	153	5.5	2
VA.45.3A	10.6	3.3	17.2	105	1.7	2
VA.46.2A	10.7	23.5	32.0	254	5.8	2
VA.46.3A	10.7	67.1	17.3	218	5.8	2
VA.47.1A	11.0	332.7	-5.3	152	4.9	2
VA.47.2A	11.0	348.4	0.9	165	10.2	2
VA.47.3A	11.0	30.4	26.5	156	4.4	3
VA.48.2A	11.3	349.2	26.4	124	6.0	2
VA.48.3A	11.3	354.0	35.1	178	5.3	2
VA.49.1A	11.5	52.6	28.7	177	2.9	2
VA.51.1A	11.9	32.3	39.0	297	2.1	2
VA.52.2A	12.1	47.4	55.3	214	5.5	2
VA.52.3A	12.1	75.6	53.7	192	12.3	2
VA.53.1A	12.3	26.0	63.3	331	3.6	2
VA.55.1A	12.9	47.3	37.8	222	5.5	1
VA.57.1A	13.6	18.5	51.5	180	1.5	1
VA.57.2A	13.6	25.3	49.9	183	4.0	2
VA.59.1A	14.1	23.0	44.6	277	3.0	2
VA.59.2A	14.1	45.8	54.4	193	6.4	2
VA.61.1A	14.5	34.8	37.0	267	2.5	1
VA.61.2A	14.5	23.6	41.9	118	7.7	2
VA.63.3A	15.1	343.1	66.9	141	3.2	2

CURRICULUM VITAE

Toegevoegd op verzoek van het College van Decanen van de Rijksuniversiteit Utrecht

Joannes Hubertus Linssen is geboren op 7 oktober 1959 te 's-Gravenhage. In mei 1978 behaalt hij het diploma Atheneum B aan het Vrijzinnig Christelijk Lyceum in 's-Gravenhage en begint in hetzelfde jaar met de studie Geologie aan de Rijksuniversiteit te Leiden. In mei 1985 legt hij het doktoraal examen Geochemie met groot bijvak Geofysica af aan de Rijksuniversiteit te Utrecht. Vanaf 1983 tot 1985 vervult hij student-assistentschappen bij de vakgroep Geofysica. Vanaf mei 1985 tot mei 1988 werkt hij, in dienst van de Nederlandse Organisatie voor Zuiver Wetenschappelijk Onderzoek, bij het Paleomagnetisch Laboratorium "Fort Hoofddijk" in Utrecht. Vanaf juni 1988 tot juni 1991 werkt hij voor BSO / Management Support te 's-Gravenhage. Vanaf juli 1991 zal hij als zelfstandig adviseur informatie technologie werkzaam zijn.